

DEVELOPMENT OF HIGHLY STRUCTURED NON-HEME IRON CATALYSTS FOR SELECTIVE C-H GROUP OXIDATIONS

Mercè CANTA i ROLDÓS

Dipòsit legal: Gi. 1372-2014
<http://hdl.handle.net/10803/275978>

ADVERTIMENT. L'accés als continguts d'aquesta tesi doctoral i la seva utilització ha de respectar els drets de la persona autora. Pot ser utilitzada per a consulta o estudi personal, així com en activitats o materials d'investigació i docència en els termes establerts a l'art. 32 del Text Refós de la Llei de Propietat Intel·lectual (RDL 1/1996). Per altres utilitzacions es requereix l'autorització prèvia i expressa de la persona autora. En qualsevol cas, en la utilització dels seus continguts caldrà indicar de forma clara el nom i cognoms de la persona autora i el títol de la tesi doctoral. No s'autoritza la seva reproducció o altres formes d'explotació efectuades amb finalitats de lucre ni la seva comunicació pública des d'un lloc aliè al servei TDX. Tampoc s'autoritza la presentació del seu contingut en una finestra o marc aliè a TDX (framing). Aquesta reserva de drets afecta tant als continguts de la tesi com als seus resums i índexs.

ADVERTENCIA. El acceso a los contenidos de esta tesis doctoral y su utilización debe respetar los derechos de la persona autora. Puede ser utilizada para consulta o estudio personal, así como en actividades o materiales de investigación y docencia en los términos establecidos en el art. 32 del Texto Refundido de la Ley de Propiedad Intelectual (RDL 1/1996). Para otros usos se requiere la autorización previa y expresa de la persona autora. En cualquier caso, en la utilización de sus contenidos se deberá indicar de forma clara el nombre y apellidos de la persona autora y el título de la tesis doctoral. No se autoriza su reproducción u otras formas de explotación efectuadas con fines lucrativos ni su comunicación pública desde un sitio ajeno al servicio TDR. Tampoco se autoriza la presentación de su contenido en una ventana o marco ajeno a TDR (framing). Esta reserva de derechos afecta tanto al contenido de la tesis como a sus resúmenes e índices.

WARNING. Access to the contents of this doctoral thesis and its use must respect the rights of the author. It can be used for reference or private study, as well as research and learning activities or materials in the terms established by the 32nd article of the Spanish Consolidated Copyright Act (RDL 1/1996). Express and previous authorization of the author is required for any other uses. In any case, when using its content, full name of the author and title of the thesis must be clearly indicated. Reproduction or other forms of for profit use or public communication from outside TDX service is not allowed. Presentation of its content in a window or frame external to TDX (framing) is not authorized either. These rights affect both the content of the thesis and its abstracts and indexes.



Universitat de Girona

Doctoral Thesis

**Development of Highly Structured Non-Heme
Iron Catalysts for Selective C—H Group
Oxidations**

Mercè Canta i Roldós

2014

Doctoral Programme in Experimental Sciences and Sustainability

Supervised by: Dr. Miquel Costas Salgueiro and Dr. Xavi Ribas Salamaña

This manuscript has been presented to opt for the **Doctoral Degree** from the
Universitat de Girona



Universitat de Girona

Dr. Miquel Costas Salgueiro and Dr. Xavi Ribas Salamaña, of Universitat de Girona,

WE DECLARE:

That the thesis entitled “Development of Highly Structured Non-Heme Iron Catalysts for Selective C—H Group Oxidations”, presented by Mercè Canta i Roldós to obtain a doctoral degree, has been completed under our supervision and meets the requirements to opt for an International Doctorate.

For all intents and purposes, we hereby sign this document.

Dr. Miquel Costas Salgueiro

Dr. Xavi Ribas Salamaña

Girona, 26 / 06 / 2014

GRAPHICAL ABSTRACT

Abstract (p. 7)

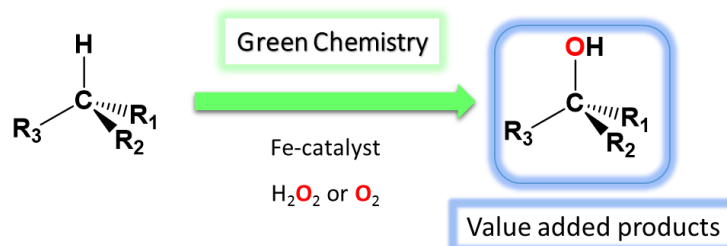
Full List of Publications (p. 10)

Glossary of Abbreviations (p. 11)

List of Figures, Tables and Schemes (p. 16)

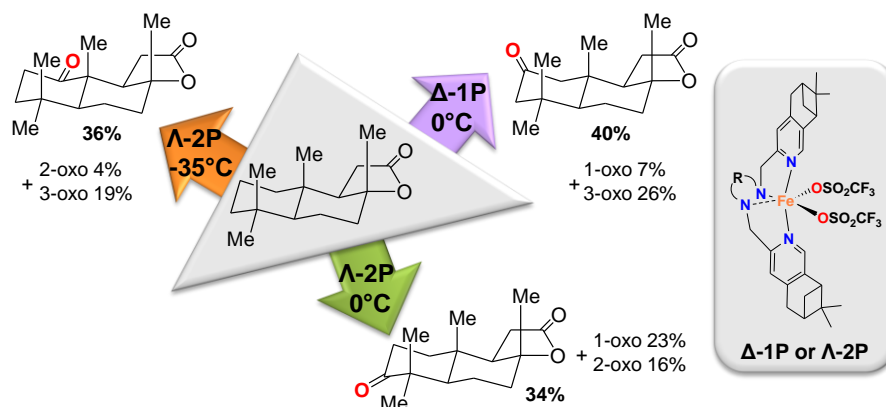
Acknowledgements (p. 26)

Chapter I. General Introduction (p. 33)

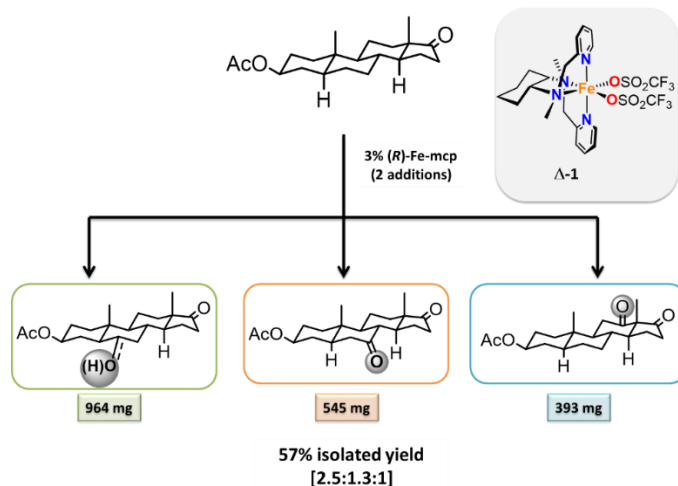


Chapter II. Main Objectives (p. 93)

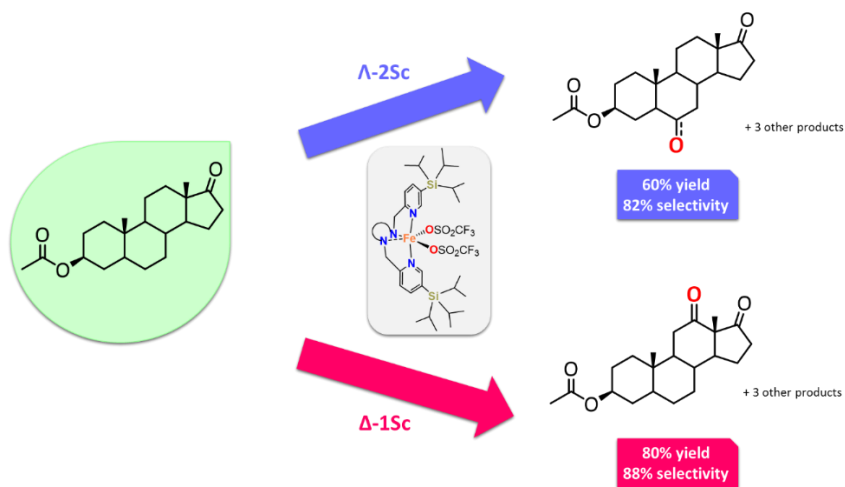
Chapter III. Regioselective Oxidation of Nonactivated Alkyl C—H Groups Using Highly Structured Non-Heme Iron Catalysts (p. 97)



Chapter IV. The Iron(II) Complex $[\text{Fe}(\text{CF}_3\text{SO}_3)_2(\text{mcp})]$ as a Convenient, Readily Available Catalyst for the Selective Oxidation of Methylenic Sites in Alkanes (p. 145)



Chapter V. A New Family of Iron Catalysts Incorporating Bulky Silyl Groups for Efficient and Regioselective Oxidation of Alkanes (p. 181)



Chapter VI. General Discussion (p. 223)

Chapter VII. General Conclusions (p. 239)

ABSTRACT

Catalytic oxidation reactions of hydrocarbons that occur in the active site of metalloenzymes exhibit high efficiency and exquisite regio- and stereoselectivity under very mild experimental conditions. However, the discovery of synthetic systems that can perform these oxidation reactions in such a manner still remains a challenge in organic chemistry. Toward this end, in this thesis we describe low molecular weight non-heme iron catalysts as functional models of the active center of these enzymes. These complexes are studied as catalysts for the selective oxidation of alkanes using a green oxidant such as hydrogen peroxide.

In the first place, we describe the highly efficient and selective oxidation of alkanes using a family of highly structured non-heme iron catalysts that introduce sterically bulky pinene groups at the 4th-5th position of the pyridine rings of a series of nitrogen-based tetradentate ligands. With these toolbox of catalysts we study the selectivity bases exhibited in the oxidation of simple alkanes, which is maintained in the oxidation of more complex molecules, such as natural products. In this way, it is possible to modulate or even alter the selectivity, which depends on the combination of the chirality of the catalyst, the nature of the diamine backbone and the presence of a cavity-like site surrounding the metal center.

In the second part, we present an optimized reaction protocol for efficient oxidation of alkanes with the readily available $[\text{Fe}(\text{CF}_3\text{SO}_3)_2(\text{mcp})]$ (mcp = *N,N'*-dimethyl-*N,N'*-bis(2-pyridylmethyl)cyclohexane-*trans*-1,2-diamine) catalyst, which turn out to show an enhanced selectivity toward methylenic site oxidation. Less sterically encumbered methylenic sites are preferentially oxidized, leading to a selectivity which is complementary to that attained with previously described oxidizing reagents. Moreover, gram-scale oxidations of steroids and terpenes can be efficiently performed, and the selectivity is satisfactorily translated from small scale reactions.

Finally, we describe a new family of iron catalysts to systematically study the steric influence of the ligand in the regioselectivity of C—H group oxidation reactions. We modify the ligand by introducing different silyl groups at the pyridine moieties. The corresponding iron(II) complexes are prepared, spectroscopically and structurally characterized, and studied in catalytic alkane oxidation reactions. We observe a strong relationship between the bulk of the silyl substituent and the regioselectivity offered by the catalyst, showing preference for the least sterically encumbered C—H groups.

RESUM

Les reaccions catalítiques d'oxidació d'hidrocarburs que ocorren al centre actiu dels metal·loenzims són altament eficients, regio- i estereoselectives en condicions experimentals molt suaus. Tot i això, el descobriment de sistemes sintètics capaços de realitzar aquestes transformacions és un dels grans reptes de la química orgànica. Treballant en aquest sentit, en aquesta tesi es descriuen catalitzadors de ferro no-hemo de baix pes molecular com a models funcionals del centre actiu d'aquests enzims. Aquests complexos s'estudien com a catalitzadors per a l'oxidació selectiva d'alcans utilitzant un oxidant benigne com el peròxid d'hidrogen.

En primer lloc, es descriu l'oxidació eficient i selectiva d'alcans utilitzant una família de catalitzadors de ferro no-hemo altament estructurats que incorporen grups pinè voluminosos a les posicions 4-5 dels anells de piridina d'una sèrie de lligands tetradentats basats en nitrogen. Amb aquest ventall de catalitzadors s'estudia les bases de la selectivitat que mostren les oxidacions d'alcans simples, que es manté en l'oxidació de molècules més complexes, com els productes naturals. D'aquesta manera és possible modular o fins i tot alterar la selectivitat, que depèn de la combinació de la quiralitat del catalitzador, la natura de la diamina pont i la presència d'una cavitat al voltat del centre metàl·lic.

En la segona part, es presenta un protocol de reacció optimitzat per l'oxidació eficient d'alcans amb el catalitzador disponible $[\text{Fe}(\text{CF}_3\text{SO}_3)_2(\text{mcp})]$ ($\text{mcp} = N,N'$ -dimetil- N,N' -bis(2-piridilmetil)ciclohexà-*trans*-1,2-diamina), que mostra una millor selectivitat per a l'oxidació de posicions metilèniques. Les posicions metilèniques menys estèricament impedides són les que s'oxiden preferentment, de manera que s'obté una selectivitat complementària a la que ofereixen els reactius d'oxidació prèviament descrits. A més, aquest catalitzador permet oxidar eficientment terpens i esteroides a l'escala de grams, i la selectivitat es manté respecte les reaccions a menor escala.

Finalment, es descriu una nova família de catalitzadors de ferro per estudiar sistemàticament la influència estèrica del lligand en la regioselectivitat de les reaccions d'oxidació de grups C—H. Per fer-ho, es modifica el lligand introduint diferents grups silil a les piridines. Es preparen els corresponents complexos de ferro(II), es caracteritzen espectroscòpicament i estructuralment i s'estudien en reaccions catalítiques d'oxidació d'alcans. S'observa una forta relació entre l'impediment imposat pel substituent silil i la regioselectivitat mostrada pel catalitzador, de manera que s'exhibeix preferència pels grups C—H menys estèricament impedits.

RESUMEN

Las reacciones catalíticas de oxidación de hidrocarburos que ocurren en el centro activo de las metaloenzimas son altamente eficientes, regio- y estereoselectivas en condiciones experimentales muy suaves. Sin embargo, el descubrimiento de sistemas sintéticos capaces de realizar estas transformaciones es uno de los grandes retos de la química orgánica. En este sentido, en esta tesis se describen catalizadores de hierro no-hemo de bajo peso molecular como modelos funcionales del centro activo de estas enzimas. Estos complejos se estudian como catalizadores para la oxidación selectiva de alcanos utilizando un oxidante benigno como el peróxido de hidrógeno.

En primer lugar, se describe la oxidación eficiente y selectiva de alcanos usando una familia de catalizadores de hierro no-hemo altamente estructurados que incorporan grupos pineno voluminosos en las posiciones 4-5 de los anillos de piridina de una serie de ligandos tetradentados basados en nitrógeno. Con estos catalizadores se estudian las bases de la selectividad en oxidaciones de alcanos simples, que se mantiene en la oxidación de moléculas más complejas, como son los productos naturales. Así es posible modular o hasta alterar la selectividad, que depende de la combinación de quiralidad del catalizador, la naturaleza de la diamina puente y la presencia de una cavidad bien definida alrededor del centro metálico.

En la segunda parte, se presenta un protocolo de reacción optimizado para la oxidación eficiente de alcanos con el catalizador disponible $[\text{Fe}(\text{CF}_3\text{SO}_3)_2(\text{mcp})]$ ($\text{mcp} = N,N'$ -dimetil- N,N' -bis(2-piridilmetil)ciclohexano-*trans*-1,2-diamina), que muestra una mejor selectividad para la oxidación de posiciones metilénicas. Las posiciones metilénicas menos impedidas estéricamente son las preferentemente oxidadas, de modo que se obtiene una selectividad complementaria a la que ofrecen los reactivos de oxidación descritos previamente. Además, permite oxidar eficientemente terpenos y esteroides en la escala de gramos, y la selectividad se mantiene respecto a las reacciones de menor escala.

Finalmente, se describe una nueva familia de catalizadores de hierro para el estudio sistemático de la influencia estérica del ligando en la regioselectividad de las reacciones de oxidación de grupos C—H. Para ello, se modifica el ligando introduciendo diferentes grupos silil en las piridinas. Se preparan los correspondientes complejos de hierro(II), se caracterizan espectroscópicamente y estructuralmente y se estudian en las reacciones catalíticas de oxidación de alcanos. Se observa una fuerte relación entre el impedimento impuesto por el sustituyente silil y la regioselectividad mostrada por el catalizador, de modo que se exhibe preferencia por los grupos C—H menos estéricamente impedidos.

FULL LIST OF PUBLICATIONS

Publications derived from this thesis:

Chapter III

Regioselective oxidation of nonactivated alkyl C—H groups using highly structured non-heme iron catalysts. L. Gómez,[†] M. Canta,[†] D. Font, I. Prat, X. Ribas, M. Costas. *J. Org. Chem.* **2013**, *78*, 1421-1433.

[†]Authors contributed equally to this work

Chapter IV

The iron(II) complex [Fe(CF₃SO₃)₂(mcp)] as a convenient, readily available catalyst for the selective oxidation of methylenic sites in alkanes. M. Canta, D. Font, L. Gómez, X. Ribas, M. Costas. *Adv. Synth. Catal.* **2014**, *356*, 818-830.

These papers have been published in journals that belong to the first quartile according to JRC.

Other publications not included in this thesis are listed in Appendix.

GLOSSARY OF ABBREVIATIONS

[O]: oxidant

2°: secondary

3°: tertiary

A/K: alcohol/ketone ratio

AcOEt: ethyl acetate

AcOH: acetic acid

bbpc: *N,N'*-di(phenylmethyl)-*N,N'*-bis(2-pyridinylmethyl)-1,2-cyclohexanediamine

cat: catalyst

CF₃-pdp: *N,N'*-bis(5-(2,6-di-(trifluoro)-methyl-phenyl)-2-pyridylmethyl)-2,2'-bipyrrolidine

conv: conversion

Cyt P450: Cytochrome P450

DCM: dichloromethane

DFT: density functional theory

DMCH: dimethylcyclohexane

DMF: dimethyl formamide

dpaq: 2-[bis-(pyridine)-2-ylmethyl]amino-*N*-quinolin-8-yl-acetamidate

e⁻: electrons

EAG: electron-activating group

equiv: equivalents

ESI-MS: electrospray ionization mass spectrometry

Et₂O: diethyl ether

EWG: electron-withdrawing group

GC: gas chromatography

His: Histidine

HOMO: highest occupied molecular orbital

kcal: kilocalorie

KIE: kinetic isotope effect

LUMO: lowest unoccupied molecular orbital

mcp: *N,N'*-dimethyl-*N,N'*-bis(2-pyridylmethyl)-cyclohexane-1,2-diamine

mcpp: *N,N'*-dimethyl-*N,N'*-bis{[(*R*)-4,5-pinenepyridin-2-yl]-methyl}-cyclohexane-1,2-diamine

Me₂BzImtacn: 1-(*N*-methylbenzimidazolyl)-4,7-dimethyl-1,4,7-triazacyclononane

MeCN: acetonitrile

mep: *N,N'*-dimethyl-*N,N'*-bis{[(*R*)-4,5-pinenepyridin-2-yl]-methyl}-ethane-1,2-diamine

mepp: *N,N'*-dimethyl-*N,N'*-bis(2-pyridylmethyl)-ethane-1,2-diamine

N4Py: *N,N'*-bis(2-pyridylmethyl)-*N*-bis(2-pyridyl)methyl-amine

NAD(P)H: Nicotinamide adenine dinucleotide(phosphate)

NDO: Naphtalene 1,2-dioxygenase

NMR: nuclear magnetic resonance

nwa: non-water-assisted

OAc: acetate group

OPiv: pivalate group

OTf: trifluoromethanesulfonate anion

pdp: *N,N'*-bis(2-pyridylmethyl)-2,2'-bipyrrolidine

Ph: phenyl group

PhIO: iodozylbenzene

Por•: porphyrin radical

PPh₃: triphenyl phosphine

py: pyridine

Pytacn: *N*-methyl-2-pyridyl *N',N''*-dialkylsubstituted triazacyclononane

qpy: 2, 2' : 6', 2'' : 6'', 2''' : 6''', 2''''-quinquepyridine

RC: retention of the configuration

rt: room temperature

TBHP: *tert*-butyl hydroperoxide

terpy: 2,2':6',2''-terpyridine

THF: tetrahydrofuran

TM: Toluene monooxygenase

tbdms: *tert*-butyl dimethyl silyl group
tips: triisopropyl silyl group
tms: trimethyl silyl group
TN: turnover number
tpa: tris-(2-pyridylmethyl)amine
triflate: trifluoromethanesulfonate
Ts: toluenesulfonate group
VT-MS: variable-temperature mass spectrometry
wa: water-assisted

Abbreviations of catalysts employed in this thesis

Abbreviations of catalysts are given in **bold**.

The number **1** or **2** refers to the nature of the diamine backbone:

1 refers to diaminocyclohexane-based catalysts

2 refers to bipyrrrolidine-based catalysts

The letter **P** or **S** after the number refers to the modifications at the pyridine moieties of the ligand. No letter indicates no substitution at the pyridines.

P indicates pinene-modified ligands

S indicates silyl-modified ligands

Sa indicates that the pyridine is substituted with a trimethyl silyl (tms) group

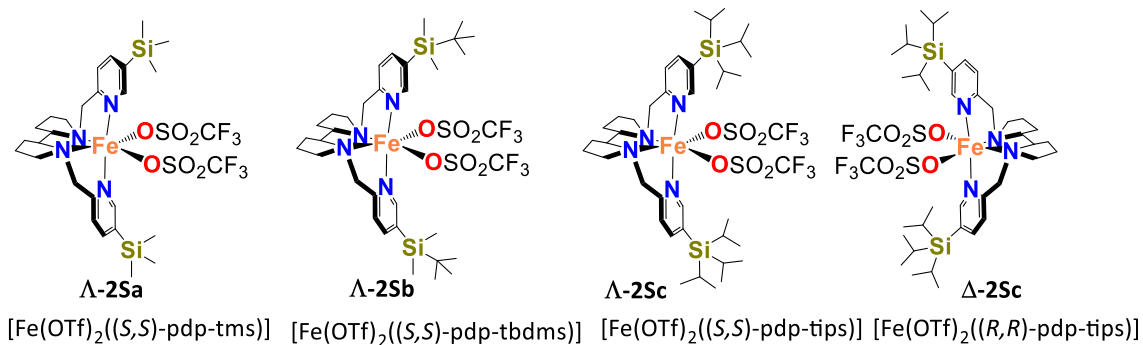
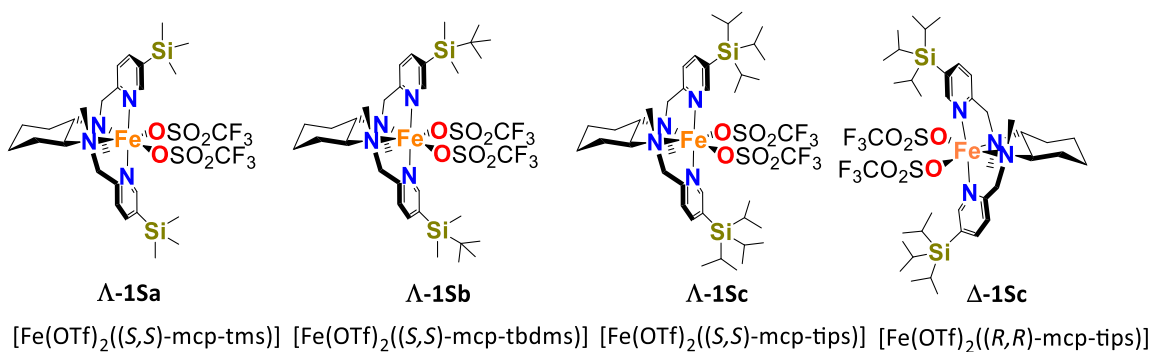
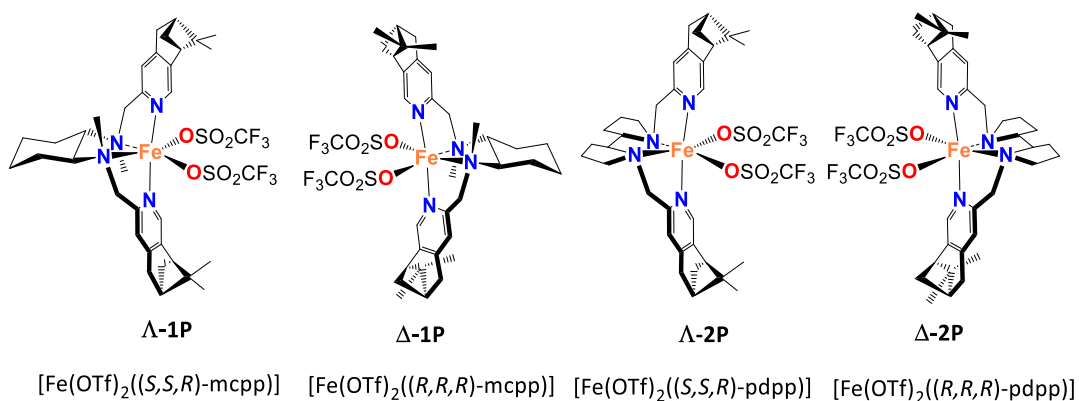
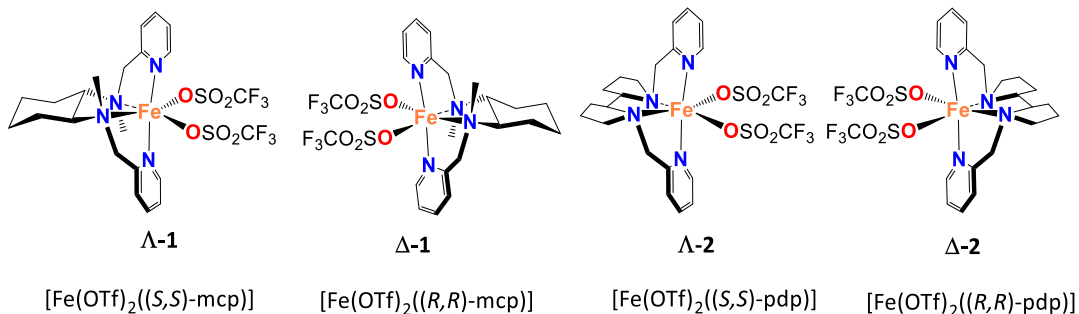
Sb indicates that the pyridine is substituted with a *tert*-butyl dimethyl silyl (tbdms) group

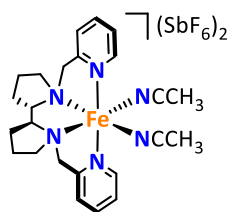
Sc indicates that the pyridine is substituted with a triisopropyl silyl (tips) group

The symbol **Λ** or **Δ** before the number indicates the chirality at the metal of the catalysts.

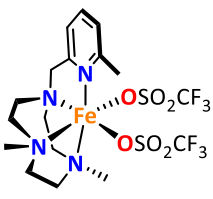
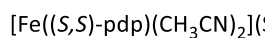
Note that the same nomenclature is maintained for the ligands, which are indicated with the letter L and regular font style. In this case, the chirality is given by (*R*) or (*S*).

Structures of the catalysts employed

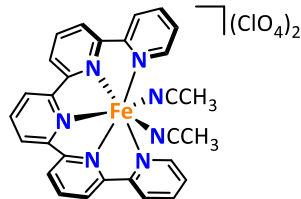
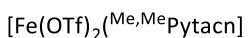




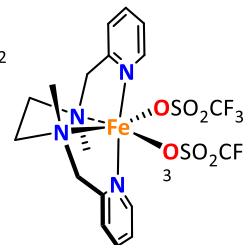
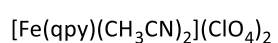
Λ-2SbF₆



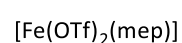
3



4



5



Abbreviations of substrates and products employed in this thesis

Abbreviations of substrates and products are numbers displayed in *italics*. They are numbered in order of appearance and maintained along the chapters. The specific number assigned to each of them is given the first time they are mentioned in the body of the thesis.

LIST OF FIGURES

Chapter I:

- Figure I.1.** X-Ray structure for the active site of Cyt-P450-camphor from *Pseudomonas putida*.....39
- Figure I.2.** X-Ray structure for the active center of Rieske dioxygenase showing the reductase and oxygenase components, with the 2-His-1-carboxylate facial triad motif in the latter.....42

Chapter III:

- Figure III.1.** 3D chemical diagrams of catalysts, Λ -1, Λ -2, Λ -2SbF₆, Λ -1P, Δ -1P, Λ -2P, and Δ -2P.....101
- Figure III.2.** Space filling diagrams of Λ -1P, Δ -1P, Λ -2P, Δ -2P, Δ -1⁵⁷ and Δ -2.⁵⁸ Counterions and solvent of crystallization have been omitted for clarity.....101
- Figure III.3.** Oxidation of (-)-menthyl acetate (3). Formation of 4 in the hydroxylation of 3 represented *versus* time in two-step addition of H₂O₂.....103
- Figure III.4.** Oxidation of *cis*-1,2-dimethylcyclohexane (5). Formation of 6 in the hydroxylation of 5 represented *versus* time in two-step addition of H₂O₂.....103
- Figure III.5.** Chair conformation structure of 1,2-dimethylcyclohexanes and decalines.....107
- Figure III.6.** Chair representations of menthyl acetate derivatives.....112
- Figure III.7.** X-Ray structures Δ -1P, Λ -2P and Δ -2P. Hydrogen atoms and solvents of crystallization are omitted for clarity.....125

Chapter IV:

- Figure IV.1.** Iron catalysts for methylenic site oxidations.....149
- Figure IV.2.** Catalysts studied in this work: Δ -1 and Λ -1.....150
- Figure IV.3.** Oxidation of *cis*-DMCH and *cis*-decalin with Λ -1, Λ -2, and 3^{47} using 3 mol% cat.....159
- Figure IV.4.** Oxidation of *trans*-DMCH and *trans*-decalin with Λ -1, Λ -2, and 3^{47} using 3 mol% cat.....160
- Figure IV.5.** Gram scale oxidation of (+)-sclareolide (50).....164
- Figure IV.6.** Gram scale oxidation of *trans*-androsterone acetate (82).....165

Chapter V:

Figure V.1. Recently reported non-heme iron catalysts for the effective oxidation of methylenic sites. ⁸⁻¹⁰	183
Figure V.2. Recently reported non-heme catalysts bearing bulky ligand architectures. ^{6,12}	184
Figure V.3. X-Ray structures of Λ-1Sa , Λ-1Sb , Λ-1Sc , Λ-2Sa , Λ-2Sb , and Λ-2Sc . Hydrogen atoms, triflate moieties (except for the atom directly bound to the iron center), and solvents of crystallization are omitted for clarity.....	188
Figure V.4. Space-filling diagrams of Λ-1Sa – Λ-2Sc . Solvent of crystallization, hydrogen atoms and CF ₃ SO ₃ molecules have been omitted for clarity.....	191
Figure V.5. ¹ H-NMR spectra of mcp-based triflate complexes Λ-1Sa – Λ-1Sc in CD ₂ Cl ₂ at 300K.....	192
Figure V.6. ¹ H-NMR spectra of pdp-based triflate complexes Λ-2Sa – Λ-2Sc in CD ₂ Cl ₂ at 300K.....	193
Figure V.7. Oxidation of (+)-neomenthyl pivalate using Λ-2Sc and 4 equiv of oxidant. Results indicate isolated yields.....	200

Chapter VI:

Figure VI.1. Pinene-substituted catalysts employed in Chapter III.....	226
Figure VI.2. Related complexes lacking the pinene rings utilized in Chapter III.....	228
Figure VI.3. Influence of chair conformation orientation in C—H group oxidations of cyclohexane-based substrates.....	229
Figure VI.4. Structure of sesquiterpenes 49 and 51 oxidized in Chapter III.....	230
Figure VI.5. Catalyst-based diverted selectivity. a) Oxidation of 75 . b) Oxidation of 50	231
Figure VI.6. Structurally simple catalysts for efficient oxidation of methylenic sites.....	232
Figure VI.7. New family of silyl-based catalysts employed in Chapter V.....	234
Figure VI.8. Structure of substrate 82 (<i>trans</i> -androsterone acetate).....	236

LIST OF TABLES

Chapter I:

- Table I.1.** Iron proteins involved in oxidative reactions by oxygen activation.^{10,17,18}38
- Table I.2.** Comparison of percentage of ¹⁸O incorporation into alcohol products in the oxidation of secondary and tertiary C—H groups by tacn-based catalysts using H₂¹⁸O.....62

Chapter III:

- Table III.1.** Oxidation of cyclohexane and *cis*- and *trans*-4-methylcyclohexyl pivalate.....105
- Table III.2.** Evaluation of electronic effects in the oxidation of tertiary C—H bonds.....106
- Table III.3.** Evaluation of electronic effects in the oxidation of secondary C—H bonds.....106
- Table III.4.** Oxidation of *cis* isomers of 1,2-dimethylcyclohexane and decalin.....108
- Table III.5.** Oxidation of *trans* isomers of 1,2-dimethylcyclohexane and decalin.....108
- Table III.6.** Steric and electronic factors in the oxidation of cycloalkanes.....109
- Table III.7.** Oxidation of ambroxide.....110
- Table III.8.** Oxidation of (+)-cedryl acetate.....111
- Table III.9.** Oxidation of menthol derivatives.....113
- Table III.10.** Oxidation of (+)-isomenthol derivatives.....114
- Table III.11.** Oxidation of neomenthol derivatives.....115
- Table III.12.** Diverting selectivity in the oxidation of **75** as substrate.....117
- Table III.13.** Oxidation of (+)-sclareolide.....118
- Table III.14.** Temperature dependence on **Λ-2P** catalytic activity in the oxidation of **50**....119
- Table III.15.** Diverting selectivity in the oxidation of **50** as substrate.....119
- Table III.16.** Crystal data and refinement details for **Δ-1P**, **Λ-2P**, and **Δ-2P**.....124
- Table III.17.** Selected bond lengths [Å] and angles [°] for **Δ-1P**, **Λ-2P** and **Δ-2P**.....125
- Table III.18.** Conditions for the oxidation of several substrates.....132
- Table III.19.** Conditions to favor the formation of **76**. Catalyst **Λ-1P**, at 0 °C.....140
- Table III.20.** Conditions to favor the formation of **77**. Catalyst **Δ-1P**, at 0 °C.....140
- Table III.21.** Conditions to favor the formation of **78**. Catalyst **Λ-2P**, at -35 °C.....141

Table III.22. Conditions to favor the formation of 79 . Catalyst Λ-1P , at 0 °C.....	141
Table III.23. Conditions to favor the formation of 80 . Catalyst Λ-2P , at 0 °C.....	141

Chapter IV:

Table IV.1. Optimization of reaction for tertiary C–H bond oxidation with Λ-1	151
Table IV.2. Optimization of reaction for secondary C–H bond oxidation with Λ-1	152
Table IV.3. Comparison of oxidation of 7 of 45 in presence or absence of PPh ₃ using Λ-1 ...154	
Table IV.4. Oxidation of tertiary and secondary C–H bonds with Λ-1	156
Table IV.5. Oxidation of cyclohexane derivatives with Λ-1	158
Table IV.6. Oxidation of androsterone derivatives with different iron catalysts.....	161
Table IV.7. Oxidation of 3-17-androstanedione (84) with 1 -based catalysts using the iterative addition protocol.....	163
Table IV.8. Amounts of reagents employed in Table IV.1 and Table IV.2 using the single addition protocol.....	169
Table IV.9. Amounts of reagents employed in Table IV.1 and Table IV.2 using the iterative addition protocol.....	171

Chapter V:

Table V.1. Selected bond lengths [Å] and angles [°] for mcp-based complexes Λ-1Sa , Λ-1Sb , and Λ-1Sc	189
Table V.2. Selected bond lengths [Å] and angles [°] for pdp-based complexes Λ-2Sa , Λ-2Sb , and Λ-2Sc	190
Table V.3. Oxidation of <i>trans</i> -1,2-DMCH by various catalysts.....	194
Table V.4. Oxidation of <i>trans</i> -decalin by various catalysts.....	195
Table V.5. Oxidation of simple substrates by various catalysts.....	197
Table V.6. Oxidation of (+)-neomenthyl pivalate by various catalysts.....	199
Table V.7. Oxidation of <i>trans</i> -androsterone acetate with various catalysts.....	201

Table V.8. Crystal data and structure refinement details for complexes Λ-1Sa – Λ-1Sc	216
Table V.9. Crystal data and structure refinement details for complexes Λ-2Sa – Λ-2Sc	217
Table V.10. Conditions for the oxidation of substrates.....	219

LIST OF SCHEMES

Chapter I:

Scheme I.1. Oxidation of alkane hydrocarbons into value added product through Fe-catalyzed reactions as example of a challenging efficient, selective, and environmentally sustainable transformation.....	35
Scheme I.2. Relevant oxidation reactions catalyzed by Cyt P450 enzymes.....	38
Scheme I.3. Established catalytic cycle for alkane hydroxylation performed by Cyt P450.....	40
Scheme I.4. Benzylic hydroxylation and aromatic <i>cis</i> -dihydroxylation reactions catalyzed by Rieske oxygenases (toluene monooxygenase and naptalene-1,2-dioxygenase, respectively).....	41
Scheme I.5. Established catalytic cycle for <i>cis</i> -dihydroxylation performed by Rieske dioxygenases.....	42
Scheme I.6. Tpa-based ligands employed to prepare Fe ^{II} complexes.....	44
Scheme I.7. Representation of N ₄ -tetradentate iron complexes with two <i>cis</i> coordination positions occupied by labile ligands (X).....	46
Scheme I.8. Tpa-based ligands introducing aliphatic amines used for the preparation of Fe ^{II} complexes.....	46
Scheme I.9. Structure of [Fe(OTf ₂)(mep)] catalyst.....	47
Scheme I.10. Structure of relevant Pytacn-based complexes for C—H oxidation reactions....	47
Scheme I.11. [Fe(pdp)(CH ₃ CN) ₂](SbF ₆) ₂ catalyst reported for predictable C—H group oxidations.....	48
Scheme I.12. Bispidine-based catalysts, where X is solvent molecule or oxo group.....	48
Scheme I.13. Structure of [Fe(qpy)](ClO ₄) ₂ catalyst reported for the oxidation of cyclohexane.....	49
Scheme I.14. Structure of [Fe ^{III} (dpaq)(H ₂ O)] ²⁺ catalyst.....	49
Scheme I.15. Proposed mechanistic scenario for [Fe(OTf) ₂ (mep)]-catalyzed oxidations.....	50
Scheme I.16. Proposed mechanism for C—H oxidations performed by tpa-based iron catalysts.....	52

Scheme I.17. Proposed mechanism for the O—O bond cleavage mechanism in tpa-based iron system.....	53
Scheme I.18. Proposed mechanisms for epoxidation and <i>cis</i> -dihydroxylation in non-water assisted (<i>nwa</i>) and water-assisted (<i>wa</i>) mechanisms.....	54
Scheme I.19. Mass peaks obtained for putative $[\text{Fe}^{\text{V}}(\text{O})(\text{OH})(\text{OTf})(^{\text{Me,H}}\text{Pytacn})]^+$ species in labeling experiments.....	55
Scheme I.20. Mass peaks obtained for putative $[\text{Fe}^{\text{III}}(\text{OTf})(\text{C}_8\text{H}_{14}(\text{O})(\text{OH})(^{\text{Me,H}}\text{Pytacn}))]^+$ species in labeling experiments.....	56
Scheme I.21. Proposed O—O bond heterolysis mechanism facilitated by protons to form a putative $[\text{Fe}^{\text{V}}(\text{dpaq})(\text{O})]^{2+}$ intermediate.....	56
Scheme I.22. Proposed mechanism of olefin oxidation by $[\text{Fe}(\text{tpa})(\text{CH}_3\text{CN})_2](\text{ClO}_4)_2$ that accounts for the observed O-atom incorporation pattern.....	58
Scheme I.23. Family of Pytacn complexes studied in C—H group oxidation labeling studies..	59
Scheme I.24. Mechanism of cyclohexane hydroxylation by Pytacn-based iron complexes proposed from DFT calculations and isotopic labeling studies.....	60
Scheme I.25. Postulated structure for the $[\text{Fe}^{\text{V}}(\text{O})(\text{OH})(^{\text{Me,Me}}\text{BzImtacn})]$ active species (a) and oxo-hydroxo tautomerism proposed for Pytacn-based and BzImtacn-based catalysts (b).....	62
Scheme I.26. Proposed mechanism for dual hydroxylase/desaturase activity in oxidation reactions catalyzed by $[\text{Fe}(\text{pdp})(\text{CH}_3\text{CN})_2](\text{SbF}_6)_2$	63
Scheme I.27. Taxane-based radical trap: rearrangement of taxane A to <i>nortaxane</i> B	64
Scheme I.28. Oxidation of a tertiary C—H bond with complete stereoretention as a radical clock.....	64
Scheme I.29. C—H group oxidation in presence of a cyclopropane ring, showing no ring-opened products.....	65
Scheme I.30. Oxidation of substrates with electronically different groups by $[\text{Fe}(\text{pdp})(\text{CH}_3\text{CN})_2](\text{SbF}_6)_2$	66
Scheme I.31. Selective oxidation of (–)-menthyl acetate with $[\text{Fe}(\text{pdp})(\text{CH}_3\text{CN})_2](\text{SbF}_6)_2$ as catalyst.....	66
Scheme I.32. Oxidation of complex molecules by $[\text{Fe}(\text{pdp})(\text{CH}_3\text{CN})_2](\text{SbF}_6)_2$	67

Scheme I.33. Electronic effects on C—H group oxidation by [Fe(pdp)(CH ₃ CN) ₂](SbF ₆) ₂	67
Scheme I.34. Chemoselectivity of secondary vs tertiary –H bonds in <i>cis</i> - and <i>trans</i> -1,2-DMCH oxidation by [Fe(pdp)(CH ₃ CN) ₂](SbF ₆) ₂	68
Scheme I.35. Combination of stereoelectronic factors in the oxidation of terpenes by [Fe(pdp)(CH ₃ CN) ₂](SbF ₆) ₂	68
Scheme I.36. Structure of pinene-based iron catalysts reported by Gómez et al.....	69
Scheme I.37. Oxidation of substrates with electronically different groups by [Fe(OTf) ₂ ((<i>S,S,R</i>)-mcpp)]......	69
Scheme I.38. Selective oxidation of (–)-menthyl acetate with [Fe(OTf) ₂ ((<i>S,S,R</i>)-mcpp)] as catalyst.....	70
Scheme I.39. Chemoselectivity of secondary vs tertiary C–H bonds oxidation by [Fe(qpy)](ClO ₄) ₂	71
Scheme I.40. Directed oxidation of a carboxylic acid-containing substrate with [Fe(pdp)(CH ₃ CN) ₂](SbF ₆) ₂	72
Scheme I.41. Oxidation of a tetrahydrogibberellic acid analog with [Fe(pdp)(CH ₃ CN) ₂](SbF ₆) ₂	73
Scheme I.42. Lactonization reactions of ester- and carboxylic acid-based substrates with [Fe(pdp)(CH ₃ CN) ₂](SbF ₆) ₂	73
Scheme I.43. Proposed mechanism for [Fe(pdp)(CH ₃ CN) ₂](SbF ₆) ₂ -catalyzed C–H lactonization reactions.....	74
Scheme I.44. Directed oxidation of a taxane-based substrate to its lactone product with [Fe(pdp)(CH ₃ CN) ₂](SbF ₆) ₂	74
Scheme I.45. Benzyl-modified mcp iron catalysts for efficient alkane oxidation reactions....	75
Scheme I.46. Oxidation of substrates with electronically different groups by [Fe(OTf) ₂ (^{Me,H} Pytacn)].....	76
Scheme I.47. Oxidation of (–)-menthyl acetate with various catalysts described in the literature.....	77

Scheme I.48. Oxidation of (+)-neomenthyl pivalate with various catalysts described in the literature. Numbers indicate normalized ratio of products arising from oxidation at the tertiary and the secondary C—H bond position.	77
Scheme I.49. Resorcinarene-based cavitands used as catalysts for fluorene oxidation.	78
Scheme I.50. Regioselectivity in the oxidation of <i>cis</i> - and <i>trans</i> -decaline by 6Fex and structure of the catalyst.	79
Scheme I.51. Structure of trajectory restrictive catalyst $[\text{Fe}(\text{CF}_3\text{-pdp})(\text{CH}_3\text{CN})_2](\text{SbF}_6)_2$ for catalyst-controlled site-selectivity.	79
Scheme I.52. Difference in regioselectivity attained with catalysts $[\text{Fe}(\text{pdp})(\text{CH}_3\text{CN})_2](\text{SbF}_6)_2$ and $[\text{Fe}(\text{CF}_3\text{-pdp})(\text{CH}_3\text{CN})_2](\text{SbF}_6)_2$	80
Scheme I.53. Oxidation of artemisinin with $[\text{Fe}(\text{pdp})(\text{CH}_3\text{CN})_2](\text{SbF}_6)_2$ and $[\text{Fe}(\text{CF}_3\text{-pdp})(\text{CH}_3\text{CN})_2](\text{SbF}_6)_2$	81
Scheme I.54. Proposed catalytic cycle for iron-catalyzed nitrene C—H insertion reactions.	82
Scheme I.55. Amination of menthyl sulfamate ester by $[\text{Fe}(\text{qpy})(\text{CH}_3\text{CN})_2]^{2+}$	83
Scheme I.56. Structure for the proposed iron—imide/nitrene intermediate involved in amination reactions mediated by $[\text{Fe}(\text{qpy})(\text{MeCN})_2]^{2+}$	84
Scheme I.57. Structure of catalyst $[\text{Fe}(\text{L})]\text{Cl}$ (L = adamantyl-dipyrromethene-2,6- $\text{Cl}_2\text{C}_6\text{H}_3$).	84
Scheme I.58. Proposed mechanism for N-heterocycle formation with $[\text{Fe}(\text{L})]\text{Cl}$ (L = adamantyl-dipyrromethene-2,6- $\text{Cl}_2\text{C}_6\text{H}_3$).	85

Chapter III:

Scheme III.1. Synthesis of pinene-containing complexes.....	122
Scheme III.2. Synthesis of menthyl derivatives.....	127
Scheme III.3. Catalytic oxidation of methyl hexanoate.....	133
Scheme III.4. Catalytic oxidation of <i>trans</i> -dimethylcyclohexane.....	133
Scheme III.5. Catalytic oxidation of (+)-cedryl acetate.	134
Scheme III.6. Catalytic oxidation of menthol derivatives.....	134
Scheme III.7. Catalytic oxidation of isomenthol derivatives.....	135
Scheme III.8. Catalytic oxidation of neomenthol derivatives.	136
Scheme III.9. Catalytic oxidation of (+)-sclareolide.....	138

Scheme III.10. Catalytic oxidation of (+)-neomenthyl pivalate at mmol scale.....	140
Scheme III.11. Catalytic oxidation of (+)-sclareolide at mmol scale.....	141

Chapter IV:

Scheme IV.1. Catalytic oxidation of 3	172
Scheme IV.2. Catalytic oxidation of 50	173
Scheme IV.3. Catalytic oxidation of 82	174
Scheme IV.4. Catalytic oxidation of 85	176
Scheme IV.5. Catalytic oxidation of 84	177

Chapter V:

Scheme V.1. Representation of the new family of silyl-derived ligands.....	185
Scheme V.2. Synthesis of the silyl-based ligands employed in this work.....	186
Scheme V.3. Preparation of complexes Λ-1Sa – Δ-2Sc	187
Scheme V.4. Synthesis of silyl-derived picolylaldehydes tms-py-CHO, tbdms-py-CHO and tips-py-CHO.	204
Scheme V.5. Schematic representation of the synthesis of the mcp-based ligands (L-S-1Sa – L-R-1Sc).	206
Scheme V.6. Schematic representation of the synthesis of the pdp-based ligands (L-S-2Sa – L-R-2Sc).	209
Scheme V.7. Catalytic oxidation of 75	219

ACKNOWLEDGEMENTS

This work would not have been possible without the following collaborations:

- Serveis Tècnics de Recerca from *Universitat de Girona* for technical support.
- Prof. Dr. Bert Klein Gebbink from *Utrecht University* for collaborative work in the development of silyl-based catalysts presented in Chapter V.
- Prof. Dr. Larry Que Jr. from *University of Minnesota* for hosting a scientific visit.
- Universitat de Girona for financial support of the aforementioned short stay.
- AGAUR of Generalitat de Catalunya for financial support through project 2009 SGR-637 and for the PhD Grant FI-DGR-2011.
- MEC of Spain for financial support through project CTQ2009-08464/BQU.
- European Research Foundation for ERC-2009-Starting Grant 239910.

TABLE OF CONTENTS

CHAPTER I. GENERAL INTRODUCTION.....	33
I.1 IMPORTANCE AND SCOPE OF ALKYL C—H OXIDATION REACTIONS	35
I.2 PRECEDENTS FOR SELECTIVE C—H HYDROXYLATIONS AT NON—HEME IRON-DEPENDENT ENZYMES. 37	
I.2.1 Biological Precedents	37
I.2.1.1 <i>Oxidative iron proteins</i>	37
1.2.1.1.1 Cytochrome P450.....	37
1.2.1.1.2 Rieske oxygenases.....	41
I.2.2 Relevance of Synthetic Model Systems.....	43
I.3 MECHANISTIC CLARIFICATION ON CATALYTIC ALKANE OXIDATION REACTIONS	43
I.3.1 Catalysts for Efficient C—H Bond Oxidation	45
I.3.2 Clarification of Species Involved in Alkane Oxidation.....	50
I.3.2.1 <i>Isotopic labeling studies performed on catalyst [Fe(OTf)₂(mep)]</i>	50
I.3.2.2 <i>Investigation on the nature of the metal-based oxidant in tpa-based iron catalysts</i>	51
I.3.2.3 <i>DFT calculations performed on tpa-based iron catalysts</i>	52
I.3.2.4 <i>Combined experimental and theoretical studies on the oxidation of olefins by the [Fe(OTf)₂(mep)] system: a water assisted mechanism</i>	53
I.3.2.5 <i>Evidence for a Fe^V(O)(OH) species by means of mass spectrometry</i>	54
1.3.2.5.1 Variable-temperature mass spectrometry and DFT studies on Pytacn-based iron system.....	54
1.3.2.5.2 Cold-spray-ionization mass spectrometry on dpaq-based iron complex.....	56
I.3.2.6 <i>Kinetic studies on tpa iron system supporting water-assisted O—O bond cleavage</i>	57
I.3.2.7 <i>Combined isotopic labeling studies and DFT calculations on Pytacn-based iron complexes</i>	58
I.3.3 Mechanistic Substrate Probes for Stereospecific C—H Hydroxylations: Radical Clocks and Radical Rearrangements	63
I.4 TUNING THE SELECTIVITY IN ALKANE OXIDATION REACTIONS	65
I.4.1 Predictably Selective Oxidations and Selectivity Patterns.....	65
I.4.2 Novel Selectivities in Alkane Oxidation Reactions	71

1.4.2.1	<i>Novel selectivity induced by directing groups on the substrate</i>	72
1.4.2.2	<i>Novel selectivity induced by steric modifications on the catalyst architecture</i>	74
I.5	NOVEL REACTIVITY OF MONONUCLEAR NON-HEME IRON CATALYSTS: N-INSERTION REACTIONS INTO C–H BONDS FOR THE FORMATION OF AMIDES, AMINES AND N-HETEROCYCLES.....	81
I.6	FUTURE CHALLENGES IN C–H BOND OXIDATIONS CATALYZED BY NON-HEME IRON COMPLEXES	85
I.7	REFERENCES.....	86
 CHAPTER II. MAIN OBJECTIVES.....		93
 CHAPTER III. REGIOSELECTIVE OXIDATION OF NONACTIVATED ALKYL C–H BONDS USING HIGHLY STRUCTURED NON-HEME IRON CATALYSTS.....		97
III.1	INTRODUCTION	99
III.2	RESULTS AND DISCUSSION	100
III.2.1	A Family of Highly Structured Non-Heme Iron Catalysts.....	100
III.2.2	Stability Test on the Catalysts	102
III.2.3	Optimization of the Reaction Protocol	104
III.2.4	Factors Governing Selectivity in C–H Oxidation of Simple Substrates	105
III.2.5	Selective Oxidation of Complex Molecules	110
III.2.6	Chiral Matching in C–H Oxidation Reactions	112
III.2.7	Diverting Selectivity in C–H Oxidations.....	114
III.3	CONCLUDING REMARKS.....	120
III.4	EXPERIMENTAL SECTION	121
III.4.1	Materials	121
III.4.2	Instrumentation	121
III.4.3	Synthesis of Complexes	121
III.4.4	Solid State Characterization of Complexes.....	124
III.4.5	Synthesis of Substrates.....	126
III.4.6	Reaction Conditions for Catalysis.....	130
III.4.6.1	<i>Sample analysis</i>	130
III.4.6.2	<i>Kinetic studies</i>	130
III.4.6.3	<i>Iterative addition protocol</i>	130
III.4.6.4	<i>Single addition protocol</i>	131

III.4.7 Procedure for Product Isolation	132
III.4.8 Catalytic Oxidation Reaction at mmol Scale.....	139
III.5 REFERENCES	142

CHAPTER IV. THE IRON(II) COMPLEX [Fe(CF₃SO₃)₂(MCP)] AS A CONVENIENT, READILY AVAILABLE CATALYST FOR THE SELECTIVE OXIDATION OF METHYLENIC SITES IN ALKANES..... 145

IV.1 INTRODUCTION	147
IV.2 RESULTS AND DISCUSSION.....	149
IV.2.1 Multigram Scale Preparation of the Fe-mcp Catalyst.....	149
IV.2.2 Optimization of Catalytic C—H Oxidation Reactions.....	150
IV.2.3 Scope and Selectivity Bases for C—H Oxidation	154
IV.2.4 Comparative Regioselectivity among Iron Catalysts in C—H Oxidation Reactions...157	
IV.2.5 Oxidation of Elaborated Substrates	160
IV.2.6 Multigram Scale Oxidation of Elaborated Molecules	163
IV.3 CONCLUDING REMARKS	165
IV.4 EXPERIMENTAL SECTION	166
IV.4.1 Materials	166
IV.4.2 Instrumentation.....	166
IV.4.3 Synthesis of Substrates.....	167
IV.4.4 Sample Analysis.....	168
IV.4.5 Catalytic Conditions	168
IV.4.5.1 <i>Single addition protocol</i>	168
IV.4.5.2 <i>Slow addition protocol</i>	169
IV.4.5.3 <i>Iterative addition protocol</i>	170
IV.4.6 Procedure for Gram Scale Oxidations	171
IV.4.7 Procedure for Product Isolation.....	172
IV.5 REFERENCES	178

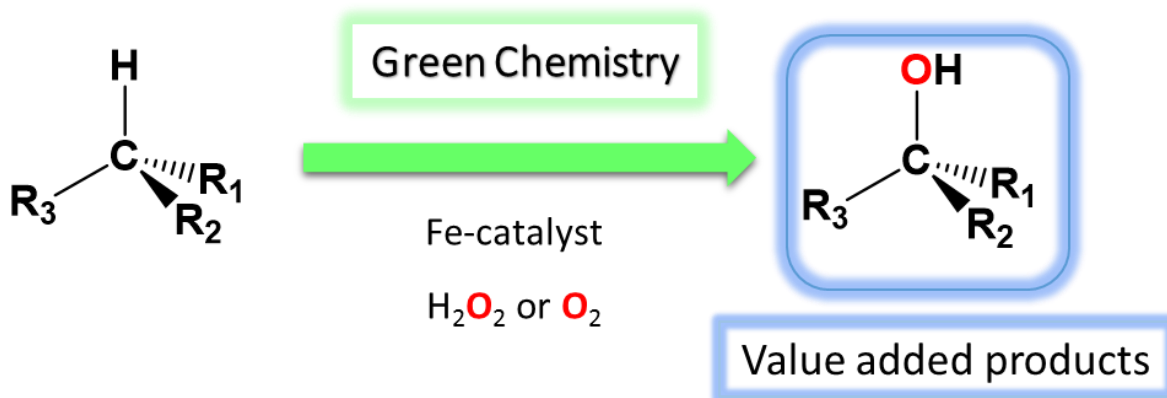
CHAPTER V. A NEW FAMILY OF IRON CATALYSTS INCORPORATING BULKY SILYL GROUPS FOR EFFICIENT AND REGIOSELECTIVE OXIDATION OF ALKANES.....	181
V.1 INTRODUCTION	183
V.2 RESULTS AND DISCUSSION	184
V.2.1 Synthesis of Ligands and Iron Complexes.....	184
V.2.2 Characterization of Complexes	187
V.2.2.1 <i>Solid state structures</i>	187
V.2.2.2 <i>Solution behavior</i>	192
V.2.3 Catalytic Studies.....	193
V.2.3.1 <i>Establishing selectivity bases on simple substrates</i>	193
V.2.3.2 <i>Application to natural product oxidations</i>	199
V.3 CONCLUDING REMARKS.....	203
V.4 EXPERIMENTAL SECTION	203
V.4.1 Materials	203
V.4.2 Instrumentation	204
V.4.3 Synthesis of Ligands.....	204
V.4.4 Synthesis of Complexes	213
V.4.5 Crystal Data	215
V.4.6 Synthesis of Substrates.....	217
V.4.7 Reaction Conditions for Catalysis.....	218
V.4.7.1 <i>Sample analysis</i>	218
V.4.7.2 <i>Reaction protocol for catalysis</i>	218
V.4.8 Procedure for Product Isolation.....	219
V.5 REFERENCES.....	220
CHAPTER VI. GENERAL DISCUSSION.....	223
VI.1 REGIOSELECTIVE OXIDATION OF NONACTIVATED ALKYL C—H GROUPS USING HIGHLY STRUCTURED NON-HEME IRON CATALYSTS	226
VI.1.1 Catalyst Design and Catalyst Highly Ordered Structures.....	226
VI.1.2 Optimization of the Catalytic Reactions	227
VI.1.3 Investigation on the Factors governing selectivity in C—H oxidations.....	228

VI.1.4 Catalytic Application to the Oxidation of Complex Organic Molecules	229
VI.2 THE IRON(II) COMPLEX [Fe(CF ₃ SO ₃) ₂ (MCP)] AS A CONVENIENT, READILY AVAILABLE CATALYST FOR THE SELECTIVE OXIDATION OF METHYLENIC SITES IN ALKANES	231
VI.2.1 Optimization of the Catalytic Protocol for Oxidation Reactions	232
VI.2.2 Substrate Scope and Selectivity Bases in C—H Oxidations	232
VI.2.3 Oxidation of Natural Products and Multigram Scale Oxidations.....	233
VI.3 A NEW FAMILY OF IRON CATALYSTS INCORPORATING BULKY SILYL GROUPS FOR EFFICIENT AND REGIOSELECTIVE OXIDATION OF ALKANES.....	233
VI.3.1 Ligand Syntheses and Complex Characterization	234
VI.3.2 Comparative Oxidation Catalysis with Simple Substrates	235
VI.3.3 Application to the Oxidation of Complex Molecules	235
VI.4 REFERENCES	237
CHAPTER VII. GENERAL CONCLUSIONS.....	239
APPENDIX.....	245

SUPPLEMENTARY DIGITAL INFORMATION

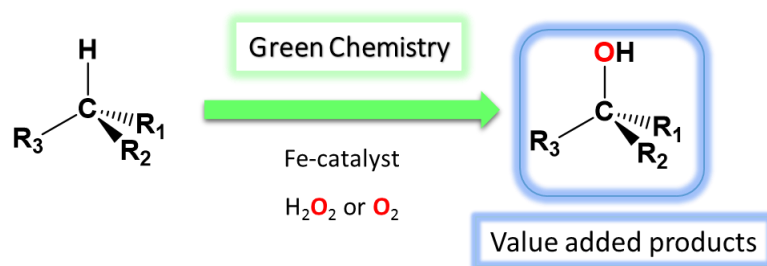
- pdf file of the manuscript
- cif files for crystal structures presented in this thesis
- pdf files containing NMR spectra for substrates and products in Chapters III - V

GENERAL INTRODUCTION



I.1 IMPORTANCE AND SCOPE OF ALKYL C—H OXIDATION REACTIONS

The functionalization of nonactivated alkyl C—H groups is a reaction of general interest and significance. Alkanes are convenient feedstocks because they are abundant and can be extracted from crude oil and natural gas.^{1–3} The catalytic oxidation of alkyl C—H groups is also highly important in bulk chemical industry, because oxidized alkane frameworks are ubiquitous in organic molecules of industrial and biological relevance. Therefore the construction of such structures is at the fundamental interest of modern organic synthesis. However, selective oxidation of alkyl C—H bonds in an environmentally sustainable manner remains as one of the main current challenges in organic synthetic chemistry (Scheme I).



Scheme I.1. Oxidation of alkane hydrocarbons into value added product through Fe-catalyzed reactions as example of a challenging efficient, selective, and environmentally sustainable transformation.

Even though the oxidation of C—H groups is thermodynamically favorable, it also has large activation barriers that translate into their characteristic inert nature against most reagents. This lack of reactivity is due to the fact that C—H bonds are strong, non-polarized, and localized, with a highly stabilized HOMO orbital a high lying LUMO orbital. Therefore highly reactive-oxidizing reagents are required to overcome these barriers, and this most commonly compromises selectivity.^{4,5} The main difficulties are (i) to control chemoselectivity, that is, to direct the oxidation toward C—H groups in the presence of other functionalities in the molecule, usually more reactive; (ii) to avoid undesired over-oxidized products; and (iii) to discriminate among the various C—H groups present in a substrate, because most organic molecules contain multiple C—H sites with only slight electronic and structural differences. Given these difficulties, even though oxygenated alkyl frameworks are basic constituents of

the majority of organic molecules, selective C—H oxidation is very rarely considered in synthetic planning. Instead, already oxygenated small molecules are employed in the building up of more complex structures, relying in protecting and deprotecting sequences.^{4–6}

On top of that, it is highly desirable that such transformations are carried out in a sustainable manner, using non-toxic, and available reagents that could generate minimum waste (Scheme I.1). In this regard, selective C—H oxidation is envisioned as a very powerful tool in organic synthesis because it will convert ubiquitous alkyl moieties into functional groups, allowing the rapid built-up of molecular complexity from inert functionalities, limiting the use of protecting groups, and enabling new and shorter synthetic strategies.^{7–9}

The development of catalysts for C—H oxidation is regarded as a highly appealing approach. These catalysts are expected to enable mild reaction conditions and introduce distinct chemo and regioselectivities based in their electronic and steric properties, as well as their ability to engage in weak and reversible noncovalent interactions with the substrate. Toward this endeavor, nature constitutes an excellent inspirational source. A number of metalloenzymes exist that perform selective C—H oxidation with high levels of chemo, regio and stereoselectivity, and iron constitutes the most common metal source found in these metalloenzymes. This prominent role of iron in biological C—H oxidative transformations in combination with the availability and lack of toxicity of this element, has made this metal very attractive toward synthetic catalyst development. Iron porphyrins have been traditionally regarded as powerful oxidation catalysts but most recently iron coordination complexes have emerged as promising and convenient alternatives with improved catalytic performance in terms of product yields and selectivities.¹⁰ Major findings and challenges of the topic are discussed in this introduction.

I.2 PRECEDENTS FOR SELECTIVE C—H HYDROXYLATIONS AT NON-HEME IRON-DEPENDENT ENZYMES

I.2.1 BIOLOGICAL PRECEDENTS

Iron is the metal ion of choice for many biological oxidations because of its natural abundance in the geosphere, its inherent electronic properties and its accessible redox potentials.¹¹ It is a ubiquitous element in living systems and its versatility is unique. The high availability of this metal and its various attainable oxidation states have led to the evolutionary selection of iron in many life processes. Iron-containing biological molecules play important roles in biologically essential transformations, such as biological oxidations and oxygen transport.¹² There is a myriad of remarkable transition-metal-dependent oxidative enzymes capable of activating dioxygen and catalyzing the selective oxidation of C—H bonds (alkane hydroxylation) or C=C groups (olefin epoxidation or *cis*-dihydroxylation).^{13–16}

I.2.1.1 *Oxidative iron proteins*

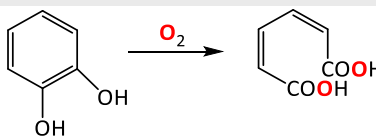
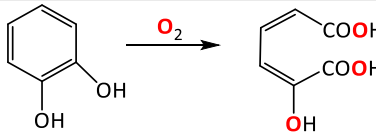
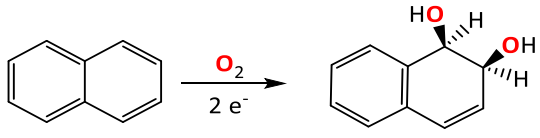
Iron proteins responsible for dioxygen activation can be found in a wide range of configurations. Depending on the nature of their active site, they can be classified in heme proteins (*e.g.* Cytochrome P450), mononuclear non-heme systems (*e.g.* Rieske dioxygenases) and dinuclear non-heme enzymes (*e.g.* soluble Methane monooxygenase) (Table I.1).^{10,17,18}

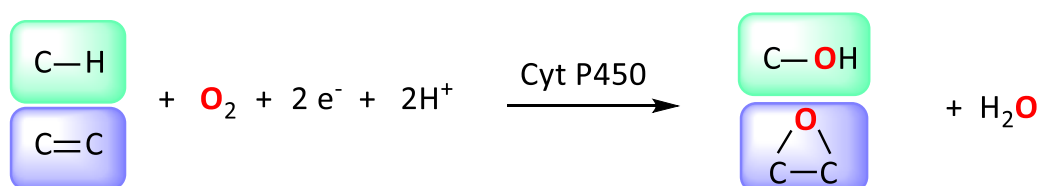
1.2.1.1.1 Cytochrome P450

Cytochrome P450 (Cyt P450) constitutes a large family of iron enzymes that is ubiquitous in all forms of life, from bacteria to mammals.^{13–15} These enzymes are involved in a great variety of vital processes, such as drug metabolism, biosynthesis of steroids, and the detoxification of xenobiotic substances. Moreover, they catalyze several biological substrates *via* oxygen activation and act as monooxygenases, inserting one oxygen atom concomitantly with a two-electron reduction of the other oxygen atom to form a water molecule. Hydroxylation of aliphatic C—H groups and epoxidation of C=C bonds are among the most

relevant reactions (Scheme I.2), but they also catalyze N-, S- and O-dealkylation, N-oxidation, sulfoxidation, and dehalogenation reactions. Not only are they highly efficient and versatile enzymes, but also highly regioselective and stereospecific.

Table I.1. Iron proteins involved in oxidative reactions by oxygen activation.^{10,17,18}

IRON-CONTAINING PROTEINS	CATALYTIC REACTION
Heme Proteins	
Cytochrome P450	$\text{C-H or C=C} \xrightarrow[2 e^-, 2H^+]{O_2} \text{C-OH or } \begin{array}{c} \text{O} \\ \diagup \quad \diagdown \\ \text{C-C} \end{array} + \text{H}_2\text{O}$
Non-Heme Proteins with a Mononuclear Iron Center	
<i>Iron(III) Dioxygenases</i>	
Intradiol-cleaving catechol dioxygenases	
<i>Iron enzymes with the 2-His-1-carboxylate facial triad motif</i>	
Extradiol-cleaving catechol dioxygenases	
α -Ketoglutarate dependent hydroxylases	$\text{R-H} + \text{R}'\text{COCO}_2\text{H} \xrightarrow{O_2} \text{R-OH} + \text{R}'\text{CO}_2\text{H} + \text{CO}_2$
Rieske dioxygenases	
Non-Heme Proteins with a Dinuclear Iron Center	
soluble-Methane Monooxygenase	$\text{CH}_4 \xrightarrow[2 e^-, 2H^+]{O_2} \text{CH}_3\text{OH} + \text{H}_2\text{O}$



Scheme I.2. Relevant oxidation reactions catalyzed by Cyt P450 enzymes.

Based on different X-Ray crystal structures characterized over the past 20 years, it has been established that Cyt P450 active site consists of a single ferric heme coordinated to a cysteinate sulfur residue of the protein at one of the axial positions of the iron ion, and the sixth coordination site is occupied by either a water molecule or a hydroxide ligand.¹⁶ As an example, the active site of Cyt P450-camphor adduct is displayed in Figure I.1, where the C—H group to be cleaved is highlighted in green.

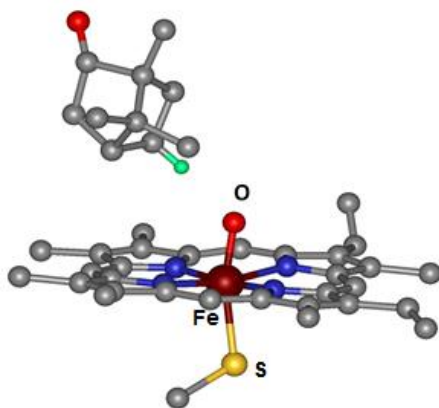
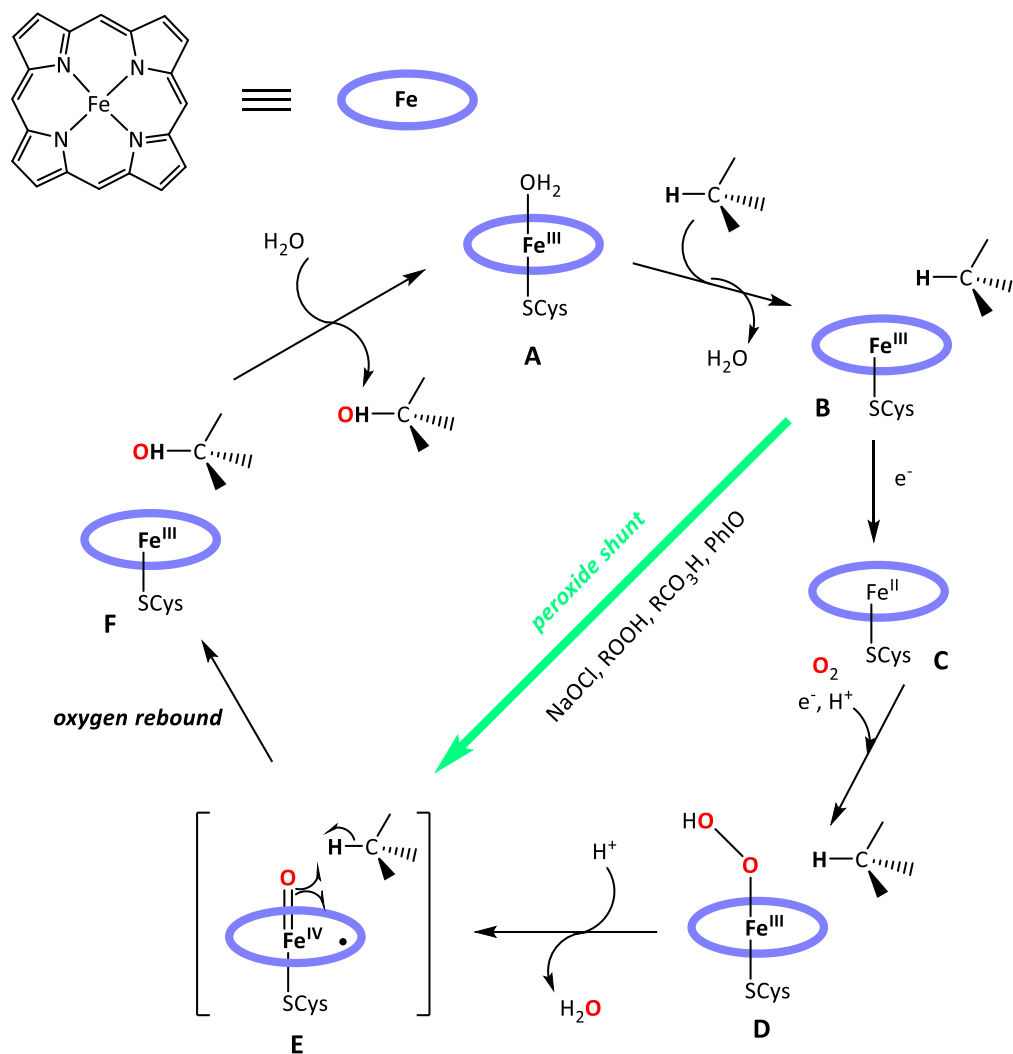


Figure I.1. X-Ray structure for the active site of Cyt P450-camphor from *Pseudomonas putida*.

In terms of reactivity, this family of enzymes is regarded as the heme paradigm for oxygen activation and alkane hydroxylation reactions performed by a single iron site, mainly due to its efficiency and versatility. Given the high interest in understanding its catalytic mechanism, several studies have addressed this issue during the last 3 decades, and its catalytic cycle is now well-established (Scheme I.3).^{14–16} In the initial step, the substrate approaches the metal site causing extrusion of a water ligand (**A**→**B**). This five-coordinated iron site undergoes a spin state change, thus increasing the $\text{Fe}^{\text{III}}/\text{Fe}^{\text{II}}$ oxidation potential, which in turn triggers the injection of one electron from the electronic transport chain of the enzyme and reduces the iron center by one electron (**C**). At this point, molecular oxygen enters the catalytic cycle and binds to the ferrous center, thus generating a ferric-superoxide complex. This species rapidly traps one proton and one electron from the enzyme to afford an iron(III)-hydroperoxo complex (**D**, Cpd 0), which undergoes proton-assisted O—O heterolytic cleavage to form a high-valent oxo- Fe^{IV} -porphyrin radical cation (**E**, Cpd I), concomitant with the formation of a water molecule. This highly oxidizing species transfers

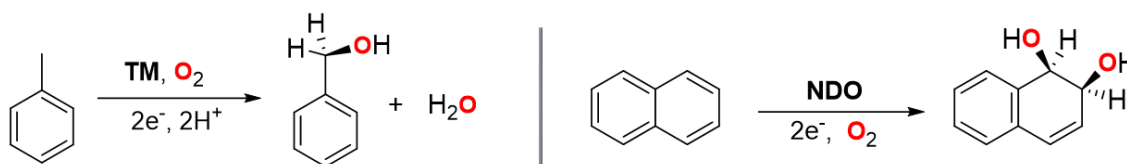
its oxygen atom into the C—H group of the nearby substrate by a two-step process known as *oxygen rebound*, thus generating the reduced iron(III) complex (**F**).^{19,20} Finally, in the last step of the catalytic cycle the oxidized product completely dissociates from the active site. The direct cycling of the ferric resting state (**B**) to the high-valent oxidant species (**E**) has proven possible using hydro and alkylperoxides, NaOCl, PhIO and peracids as oxidants, the so-called peroxide shunt (Scheme I.3, green pathway), which receives use in catalysis.^{21,22}



Scheme I.3. Established catalytic cycle for alkane hydroxylation performed by Cyt P450.

1.2.1.1.2 Rieske oxygenases

In the past 15-20 years, several studies have been performed on the understanding of mononuclear non-heme iron(II) enzymes. Among them, Rieske oxygenases constitute a relevant and paradigmatic example of mononuclear non-heme iron(II) proteins involved in O₂ activation reactions. Their efficiency and versatility are even greater than those of the related heme-containing Cyt P450, being able to catalyze benzylic hydroxylation and *cis*-dihydroxylation reactions (Scheme I.4). Therefore Rieske oxygenases are considered its non-heme analogue. Besides, they are the only among both heme and non-heme iron enzymes capable of stereospecific and enantioselective *cis*-dihydroxylation of arene and olefin double bonds, which are reactions of high biotechnological interest as they initiate the biodegradation of aromatics in the soil.^{10,23–28}



Scheme I.4. Benzylic hydroxylation and aromatic *cis*-dihydroxylation reactions catalyzed by Rieske oxygenases (toluene monooxygenase and naphthalene-1,2-dioxygenase, respectively).

Rieske oxygenases are part of a superfamily of enzymes that share a characteristic structure that consists of an oxygenase component (a mononuclear non-heme iron(II) high spin center containing a 2-His-1-carboxylate facial triad motif in the active site)^{23,29,30} and a reductase component (an Fe₂-S₂ Rieske center) that delivers electrons from NAD(P)H to the oxygenase center (Figure I.2).³¹

Naphthalene-1,2-dioxygenase (NDO) is one of the best studied examples of the Rieske dioxygenases family, and a catalytic cycle has been proposed (Scheme I.5).^{25,31} Studies on crystals of NDO exposed to O₂ indicate that a side-on-bound peroxo (or hydroperoxo)-iron(III) species (**C**) is the last detectable intermediate before substrate oxidation occurs.³² In this reaction, both O₂ atoms are incorporated in the *syn*-diol product. Interestingly, labeling studies also show H₂¹⁸O incorporation into the *syn*-diol product, suggesting that the O–O bond heterolytic cleavage can generate a putative Fe^V=O species prior to substrate attack,

although direct evidence for this high-valent oxo species has yet to be obtained.^{25,31,33} Moreover, recent experiments also reveal that phtalase dioxygenase can elicit catalytic chemistry when H_2O_2 is used as oxidant thus resembling the peroxide shunt of Cyt P450.³⁴

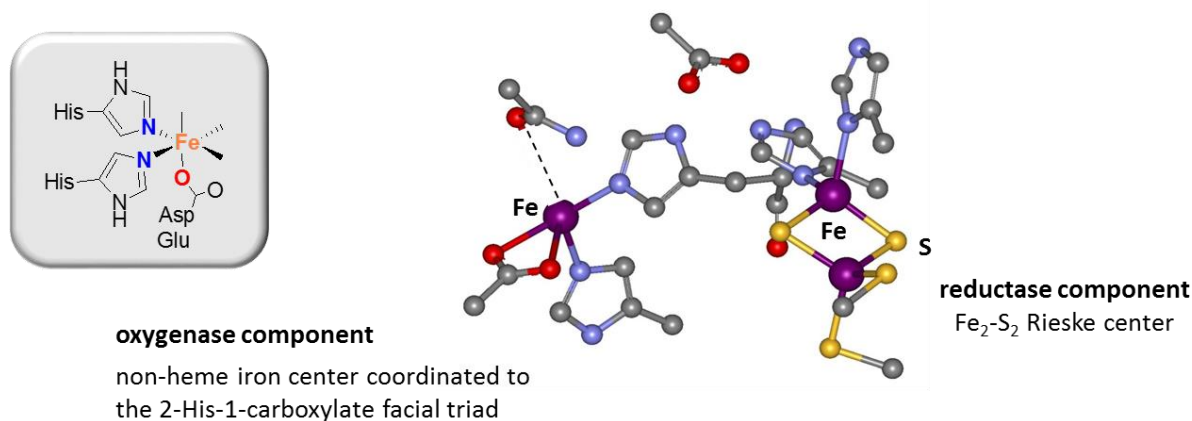
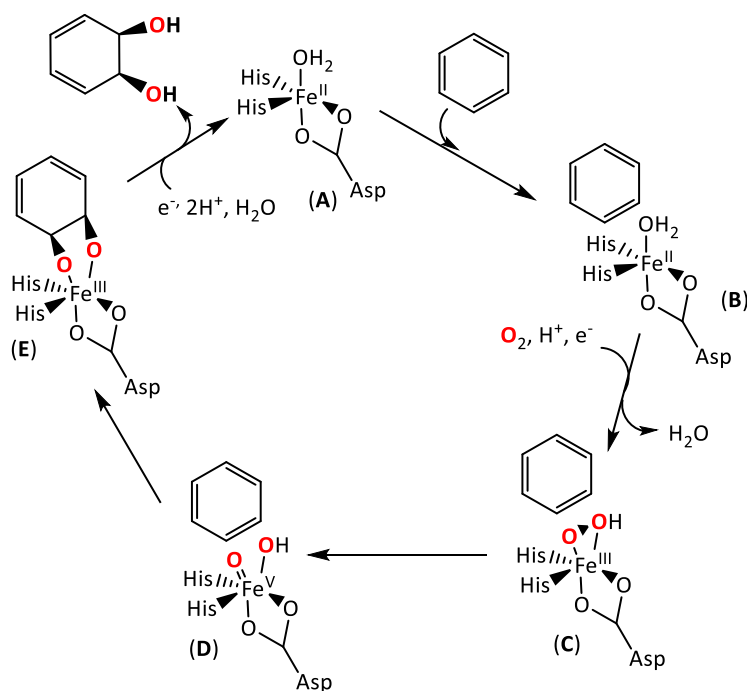


Figure I.2. X-Ray structure for the active center of Rieske dioxygenase showing the reductase and oxygenase components, with the 2-His-1-carboxylate facial triad motif in the latter.



Scheme I.5. Established catalytic cycle for *cis*-dihydroxylation performed by Rieske dioxygenases.

Finally, experiments with radical clock substrates have shown that oxidation of norcarane with NDO enzyme occurs through the intermediacy of a short-lived carbon-centered radical,³⁵ strongly suggesting that a rebound-like mechanism as in Cyt P450 is operative. Overall, evidences point toward a common mechanistic landscape operating in Cyt P450 and Rieske oxygenases, suggesting that high-valent iron species are responsible for the catalysis.

1.2.2 RELEVANCE OF SYNTHETIC MODEL SYSTEMS

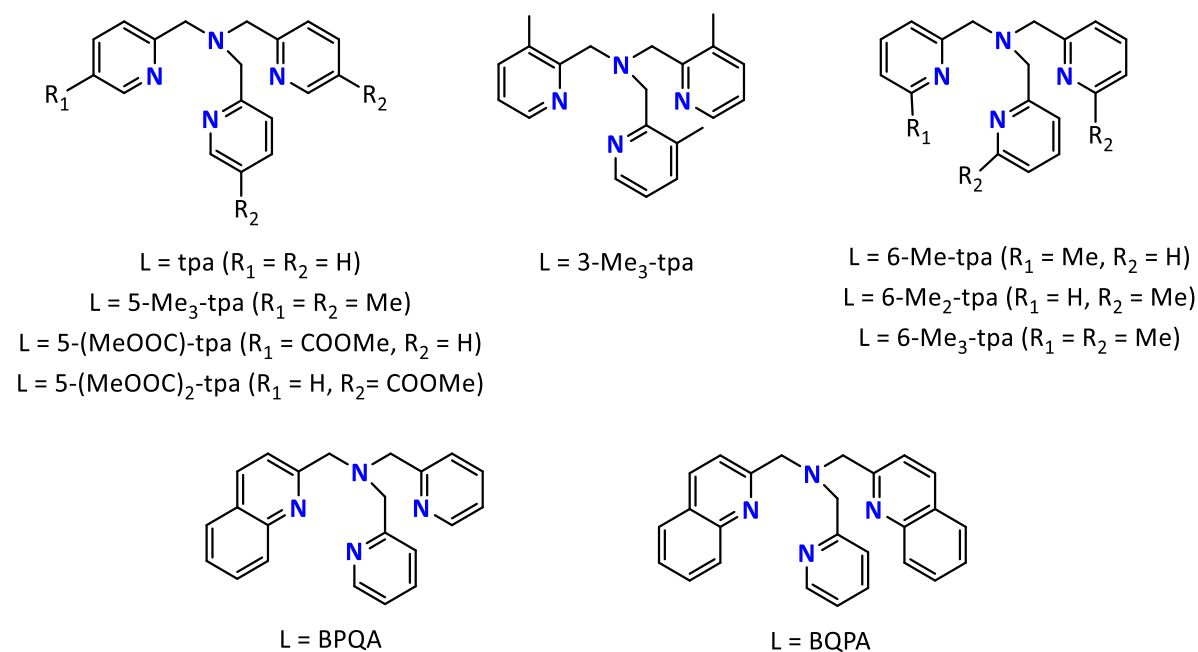
Knowledge on the metalloenzymes structures and functions is relevant to its potential application in synthetic catalysts design. Synthetic model systems present some advantages over metalloenzymes, being the formers capable of expanding the scope of possible substrates, increasing the scale of production and tuning the selectivity and/or the specificity of the processes.³⁶ Moreover, they would be valuable for environmentally friendly catalytic chemistry, where it is important to avoid the use of toxic or expensive metal reagents and oxidant, energy-consuming processing steps and undesirable reaction media.³⁷ Most importantly, mechanistic insight in biomimetic catalysts will provide insight into biological pathways and new understanding of the fundamental reaction steps and reactive intermediates relevant to metalloenzymes, and lead to practical applications.¹¹

1.3 MECHANISTIC CLARIFICATION ON CATALYTIC ALKANE OXIDATION REACTIONS

Reaction mechanisms operating in C—H oxidation reactions mediated by non-heme iron compounds were very actively explored since the 80's. Arguably, the most relevant examples are Fenton reagents and Gif chemistry³⁸⁻⁴¹ which were initially proposed to involve metal centered C—H functionalization reactions where carbon centered free diffusing radicals did not form. However, critical scrutiny of these reactions demonstrated otherwise, as it also occurred for C—H oxidation reactions with *tert*-butyl hydroperoxide (TBHP) catalyzed by well-defined coordination complexes.⁴²⁻⁴⁴ At this point it was unclear if metal-based oxidation

mechanism analogous to heme-catalyzed hydroxylations, devoid of free diffusing radicals, could be attained with non-heme iron catalysts.

Convincing evidence for a metal-based mechanism in non-heme catalyzed C—H oxidation reactions appeared in 2001 in a work by Que and co-workers⁴⁵ where a family of tpa-based (tpa = tris-(2-pyridylmethyl)amine) iron (II) complexes (Scheme I.6) were investigated as C—H oxidation catalysts using H₂O₂ as oxidant. High alcohol/ketone (A/K) product ratios were obtained in the oxidation of cyclic alkanes, and isotopic labelling experiments showed that O₂, a particularly fast and efficient carbon centered radical trap, did not play a significant role in the reaction (less than 3% ¹⁸O₂ incorporation into cyclohexanol product was measured and the A/K ratio was unaffected).



Scheme I.6. Tpa-based ligands employed to prepare Fe^{II} complexes.

Furthermore, the results of competitive oxidations of C—H bonds with different strengths indicated the involvement of a rather selective oxidant, inconsistent with a free hydroxyl radical. However, the most significant result to favor a metal-based oxidation is the stereospecificity of these oxidation reactions, showing no epimerization of the products, thus hydroxylation must proceed with retention of configuration. This reactivity pattern resembles that associated with iron porphyrin catalysts operating via high-valent metal-oxo oxidants.⁴⁶⁻

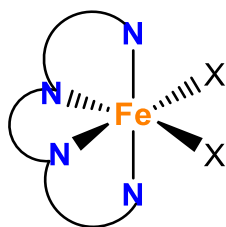
⁴⁹ Low temperature monitoring of the reaction of H₂O₂ with the iron catalysts lead to the identification of [Fe^{III}(OOH)(tpa)]²⁺ as a reaction intermediate. Isotopic labelling experiments also showed that substantial amounts of oxygen atoms from water are incorporated in the oxidized products. These findings supported the involvement of a high-valent iron-oxo species, [Fe^V(O)(OH)(tpa)]²⁺ that incorporates water into the oxo ligand via a prototypic oxo-hydroxo tautomerism akin iron-oxo porphyrins. This Fe^V(O) species was also proposed to oxidize hydrocarbons in a P450-like rebound mechanism that entails initial C—H abstraction followed by rapid hydroxyl ligand transfer.

Beyond their mechanistic significance, these findings were key for the future development of this chemistry with synthetic aim, because a metal-based mechanism bears implicitly the possibility of modulating the reactivity and thus the selectivity of the iron-oxo species that attack the C—H bond by means of ligand design. Instead, C—H breaking reactions initiated by hydroxyl or alkoxy radicals are devoid of this control. Therefore, the *bona fide* settling on an iron based C—H functionalization mechanism fundamentals the following past and present efforts to develop non-heme iron complexes as selective C—H oxidation catalysts.^{50,51}

1.3.1 CATALYSTS FOR EFFICIENT C—H BOND OXIDATION

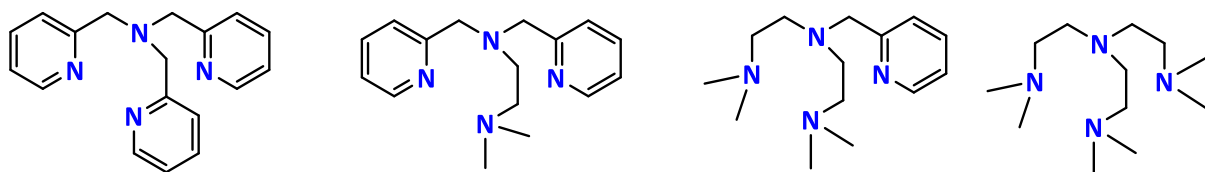
Mononuclear non-heme iron (II) complexes containing N-based ligands, especially those containing pyridine heterocycles, have been extensively explored in metal-catalyzed transformations during the last decade.^{11,51} A particularly relevant aspect of the use of N-based ligands is that they led to the discovery of very selective C—H and C=C oxidation iron catalysts, and synthetically useful methodologies have also emerged from the use of these complexes. A very challenging aspect of this chemistry is that the catalytic activity of a complex is dramatically dependent on its ligand structure; therefore accurate design of the ligand is necessary, yet not obvious. The vast majority of iron complexes that can mediate stereospecific hydroxylation of alkanes contain a Fe^{II} center and tetradentate N-based ligands that leave two coordination positions vacant in a *cis* relative position that are occupied by weakly bound ligands (Scheme 1.7). The lability of these positions is a key aspect to ensure a

fast reaction with the oxidant. Tripodal and linear families of complexes bearing tetradentate ligands have most been studied in the oxidation of alkanes that use H_2O_2 as oxidant.



Scheme I.7. Representation of N_4 -tetradentate iron complexes with two *cis* coordination positions occupied by labile ligands (X).

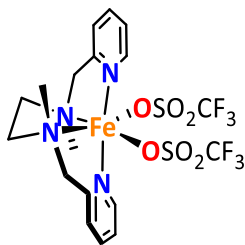
An illustrative example of tripodal ligand is tpa. As previously mentioned, the combination of $[\text{Fe}(\text{tpa})(\text{CH}_3\text{CN})_2](\text{ClO}_4)_2$ with H_2O_2 proved to effectively oxidize alkanes. The oxidation was reported to be highly stereospecific (>99% retention of configuration for the oxidation of *cis*- and *trans*-1,2-dimethylcyclohexane (DMCH)), being the first example of non-heme iron catalysts capable of stereospecific alkane oxidation.^{52,53} Studies with $[\text{Fe}(\text{OTf})_2(\text{tpa})]$ (OTf = trifluoromethylsulfonate) and derivatives where pyridine heterocycles were systematically replaced by aliphatic amines (Scheme I.8) were performed by Britovsek and coworkers⁵⁴. These studies showed that at least two pyridine donors were needed in the ligand to show reactivity distinct from Fenton-type chemistry, and are essential for high catalytic activity and selectivity in these systems.



Scheme I.8. Tpa-based ligands introducing aliphatic amines used for the preparation of Fe^{II} complexes.

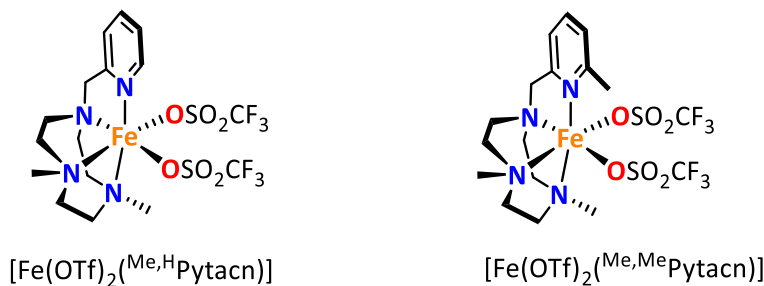
A more interesting catalyst is $[\text{Fe}(\text{OTf})_2(\text{mep})]$ (mep = *N,N'*-dimethyl-*N,N'*-bis(2-pyridylmethyl)-ethane-1,2-diamine, Scheme I.9),^{53,55,56} which proved to be more efficient in stereospecific alkane hydroxylation than its tpa analogue, but still worked under conditions of large excess of substrate.^{54,57,58} Interestingly, Bermejo and coworkers⁵⁹ recently reported

the stereoselective oxidation of steroid ketones using $[\text{Fe}(\text{OTf})_2(\text{mep})]$. In this case, substrate limiting conditions were employed, and synthetically useful yields (up to 70%) were achieved.



Scheme I.9. Structure of $[\text{Fe}(\text{OTf})_2(\text{mep})]$ catalyst.

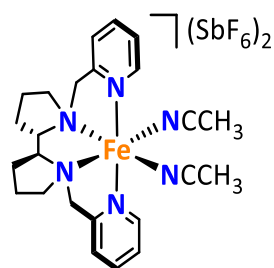
Another interesting ligand platform that has been extensively studied is the Pytacn (Pytacn = *N*-methyl-2-pyridyl *N,N'*-dialkylsubstituted triazacyclononane) family (Scheme I.10).⁵⁰ $[\text{Fe}(\text{OTf})_2(\text{Me,HPytacn})]$ proved to be capable of mediating the hydroxylation of alkanes with retention of configuration.⁶⁰ Substitution on the N atoms of the triazamacrocycle and on the pyridine 6th position were studied in order to explore steric effects, in catalytic oxidations. The 6-methyl pyridine substituted $[\text{Fe}(\text{OTf})_2(\text{Me,MePytacn})]$ showed unprecedented efficiency in the stereospecific oxidation of alkanes and alkenes with H_2O_2 to that date. This catalyst was also described to mediate the oxidation of alkyl C—H bonds with product yields that may be amenable for synthetic purposes.⁶¹ Besides its high activity, this catalyst exhibits enhanced selectivity toward methylene sites, while operating under mild experimental conditions.



Scheme I.10. Structure of relevant Pytacn-based complexes for C—H oxidation reactions.

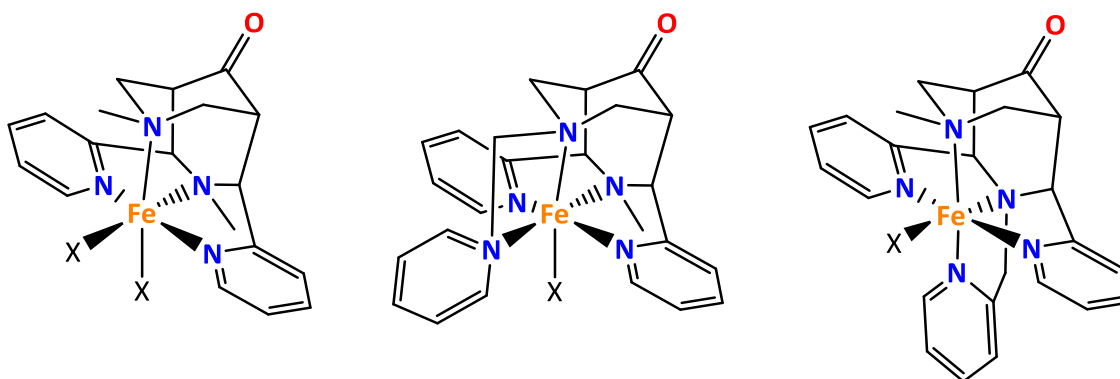
A major breakthrough was introduced by White and coworkers⁶² in 2007, when they reported the predictably selective oxidation of C—H bonds for the synthesis of complex molecules employing H_2O_2 as oxidant and a non-heme iron catalyst. In this case the catalyst employed was $[\text{Fe}(\text{pdp})(\text{CH}_3\text{CN})_2](\text{SbF}_6)_2$ (pdp = *N,N'*-bis(2-pyridylmethyl)-2,2'-bipyrrolidine), a coordination complex that bears a relatively bulky tetradentate ligand framework (Scheme

I.11). In substrates with distinct C—H bonds, the preferential oxidation site of this system could be predicted on the basis of the electronic and steric environment of the C—H bonds. Additionally, when carboxylate functionality was present, it could direct oxidations toward five-membered ring lactone formation. Three years later, these authors used the same catalyst to study the effect of the combination of different effects on dictating selectivity in methylene oxidations.⁶³ The authors reported the site-selective oxidation of isolated, nonactivated secondary C—H bonds to afford monooxygenated products in preparative useful yields without the use of directing or activating groups. In the oxidation of natural products, useful levels of chemo-, site- and diastereoselective methylene oxidations were obtained.



Scheme I.11. $[\text{Fe}(\text{pdp})(\text{CH}_3\text{CN})_2](\text{SbF}_6)_2$ catalyst reported for predictable C—H group oxidations.

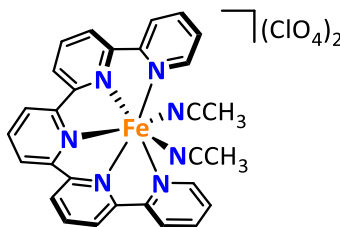
Comba and coworkers⁶⁴ described a set of rigid pentadentate iron complexes based on bispidine derivatives (Scheme I.12) for the catalytic oxidation of cyclohexane, obtaining reasonably good turnover numbers (TON) (up to 34 TON).



Scheme I.12. Bispidine-based catalysts, where X is solvent molecule or oxo group.

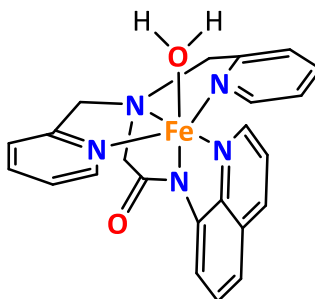
A different approach was proposed by Che and coworkers,⁶⁵ who used $[\text{Fe}(\text{qpy})](\text{ClO}_4)_2$ (qpy = 2, 2' : 6', 2'' : 6'', 2''' : 6''', 2''''-quinquepyridine, Scheme I.13) in combination with

Oxone for the oxidation of cyclohexane, obtaining modest TON of products. Substrates with activated C—H bonds (benzylics) were tested affording up to 85% yield for the oxidation of xanthene.



Scheme I.13. Structure of $[\text{Fe}(\text{qpy})](\text{ClO}_4)_2$ catalyst reported for the oxidation of cyclohexane.

Finally, Hitomi *et al* recently presented catalytic system based on the pentadentate H-dpaq ligand (dpaq = 2-[bis-(pyridine)-2-ylmethyl]amino-*N*-quinolin-8-yl-acetamidate, Scheme I.14).⁶⁶ The complex $[\text{Fe}^{\text{III}}(\text{dpaq})(\text{H}_2\text{O})]^{2+}$ was used in combination with various oxidants to show a metal-based oxidation mechanism suggested by the high alcohol/ketone (A/K) ratios obtained in the oxidation of cyclohexane regardless of the oxidant employed. This catalyst presented virtually identical performance as $[\text{Fe}(\text{pdp})(\text{CH}_3\text{CN})_2](\text{SbF}_6)_2$ in the oxidation of *cis*-4-methylcyclohexyl-1-pivalate and 1-substituted 3,7-dimethyl-octane without the addition of acetic acid.

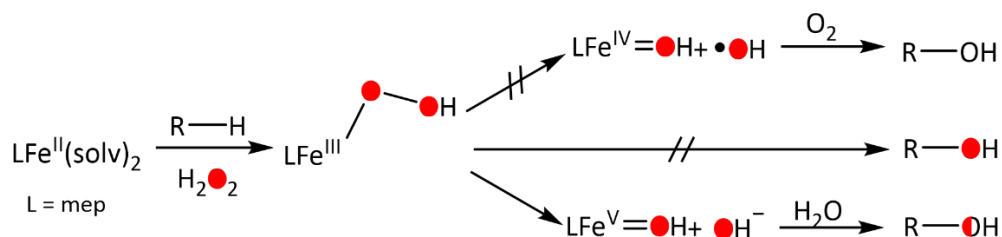


Scheme I.14. Structure of $[\text{Fe}^{\text{III}}(\text{dpaq})(\text{H}_2\text{O})]^{2+}$ catalyst.

I.3.2 CLARIFICATION OF SPECIES INVOLVED IN ALKANE OXIDATION

I.3.2.1 Isotopic labeling studies performed on catalyst $[Fe(OTf)_2(mep)]$

The first evidence for the participation of a high-valent iron-oxo species in stereospecific alkane hydroxylation by a non-heme iron catalysts appeared in 1999 in a work from Chen and Que,⁵³ where $[Fe(OTf)_2(mep)]$ was used to show the incorporation of $H_2^{18}O$ into the oxidation products. The first suggestion for the participation of a metal-based oxidant was the high A/K ratio obtained for this catalyst under air, which contrasted the much smaller ratios diagnostic of radical chain terminations. More interesting were the ^{18}O -labeling experiments using $H_2^{18}O$ in the hydroxylation of cyclohexane, which showed 18(3)% of ^{18}O -labeled cyclohexanol product. Besides, the complementary experiment using $H_2^{18}O_2$ afforded 84(4)% ^{18}O -labeled alcohol. All together, these results demonstrated that O_2 was not involved in the reaction. Furthermore, ^{18}O -incorporation was significantly dependent on the amount of $H_2^{18}O$ used in the reaction, suggesting that the mechanism of alkane hydroxylation by the $[Fe(OTf)_2(mep)]$ - H_2O_2 system involves an oxidant capable of oxygen atom exchange with H_2O in competition with C–O bond formation. Taking into account the stereospecificity of this system in the oxidation of *cis*-1,2-DMCH and the 26(1)% of ^{18}O -incorporation into the *cis*-alcohol product when $H_2^{18}O$ was used, the authors proposed ^{18}O -exchange to happen prior to the interaction of the iron-based oxidant and the alkane C–H bond. The proposed mechanistic scenario involved the heterolysis of the O–O bond of a Fe–OOH intermediate to form a formally $Fe^V=O$ species, capable of solvent exchange (Scheme I.15).

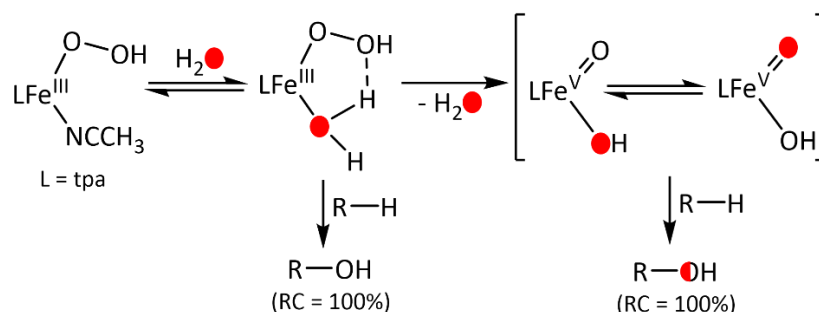


Scheme I.15. Proposed mechanistic scenario for $[Fe(OTf)_2(mep)]$ -catalyzed oxidations.

1.3.2.2 Investigation on the nature of the metal-based oxidant in tpa-based iron catalysts

An analogous study was performed in 2001 with the structurally related $[\text{Fe}(\text{tpa})(\text{CH}_3\text{CN})_2](\text{ClO}_4)_2$ complex.⁴⁵ It was shown that the A/K ratio remained unaffected by the presence of O_2 , showing again that the cleavage of alkane C—H bonds does not generate long-lived alkyl radicals susceptible to react with O_2 . Furthermore, this catalyst afforded stereospecific oxidations. The reaction of $[\text{Fe}(\text{tpa})(\text{CH}_3\text{CN})_2](\text{ClO}_4)_2$ with excess H_2O_2 generates a low-spin $[\text{Fe}^{\text{III}}(\text{OOH})(\text{tpa})]^{2+}$ intermediate that had been successfully characterized spectroscopically.^{52,67} Moreover, its mass spectrum was not affected by the addition of H_2^{18}O , demonstrating that peroxy oxygen atoms do not exchange with solvent H_2^{18}O .⁶⁸ However, experiments with cyclohexane and H_2O_2 in the presence of H_2^{18}O gave cyclohexanol with 27(2)% ^{18}O -incorporation, and the complementary experiment with $\text{H}_2^{18}\text{O}_2$ afforded 70(5)% ^{18}O -cyclohexanol.⁴⁵ These results exclude the direct insertion of a $\text{Fe}^{\text{III}}\text{-OOH}$ peroxy oxygen into the alkane C—H bond as the sole mechanism for alkane hydroxylation and require a mechanism involving a species that allows an oxygen atom from solvent H_2^{18}O to be incorporated. This water exchange process could in principle occur at the $\text{Fe}^{\text{V}}=\text{O}$ stage prior to C—H bond cleavage or at the $\text{Fe}^{\text{IV}}=\text{O}$ stage after C—H bond cleavage. The latter case is excluded due to the correlation observed between C—H bond strength and ^{18}O -incorporation; in fact more ^{18}O -incorporation in the cleavage of stronger C—H bonds was obtained. This trend was also observed in the oxidation of alkanes by $[(\text{Por}\bullet)\text{Fe}^{\text{IV}}=\text{O}]$ ($\text{Por}\bullet =$ porphyrin radical) in the presence of H_2^{18}O ,⁶⁹ thus water exchange must occur within the $\text{Fe}^{\text{V}}=\text{O}$ species prior to C—H bond cleavage. By analogy to heme systems,⁷⁰ oxo-hydroxo tautomerization of the high-valent species is proposed to transfer ^{18}O from H_2^{18}O into the terminal oxo, which is then incorporated into the alcohol product. Two key features were proposed for the special reactivity of the $[\text{Fe}^{\text{III}}(\text{OOH})(\text{tpa})]^{2+}$ intermediate: the low-spin nature of the iron(III) center and an available coordination site *cis* to the $\eta^1\text{-OOH}$ for water to bind. The coordination of a hydroperoxide to a low-spin Fe(III) center strengthens the Fe—O bond and weakens the O—O bond, thereby promoting the prospects for O—O lysis. In this case, the authors proposed that the adjacent water ligand directs the cleavage toward O—O bond

heterolysis, acting as an acid whose acidity is enhanced by coordination to the metal center. An intramolecular hydrogen bond between the water ligand and the terminal oxygen of the adjacent HOO^- forms a five-membered ring, and subsequent O–O bond heterolysis is facilitated by the release of a water molecule to afford the *cis*- $\text{HO-Fe}^{\text{V}}=\text{O}$ (Scheme I.16).

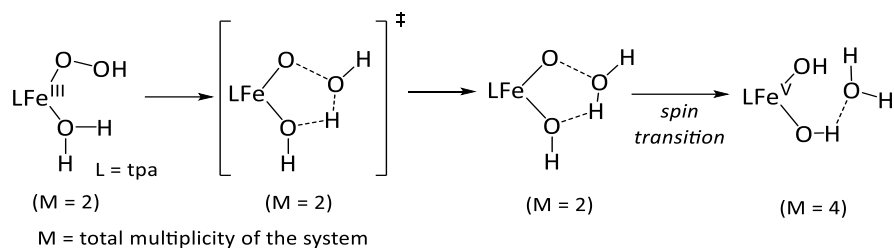


Scheme I.16. Proposed mechanism for C–H oxidations performed by tpa-based iron catalysts.

1.3.2.3 DFT calculations performed on tpa-based iron catalysts

The viability of an $\text{Fe}^{\text{V}}=\text{O}$ oxidant in a tpa ligand environment and its role in catalysis was explored by means of DFT calculations in a work performed by Bassan and coworkers.⁷¹ Quantum mechanical calculations predicted the $[\text{Fe}(\text{OOH})(\text{tpa})]^{2+}$ complex to be low-spin in the ground state, in agreement with the aforementioned experimental data, being more stable when the HOO^- ligand is in *trans* orientation with respect to the sp^3 amine ligand site. This complex was found to have a transition state for the O–O heterolytic cleavage at 19.2 kcal/mol. At this point, a spin-crossing must occur to yield the product of the O–O bond heterolysis, *cis*- $\text{HO-Fe}^{\text{V}}=\text{O}$, in the quartet ground state, which was found to be more favorable in energy. Although spin-forbidden, this transition is favored by the large spin–orbit coupling at the iron center. The overall O–O bond cleavage reaction was found to be endergonic by 5.1 kcal/mol. Furthermore, a water molecule was calculated to the O–O bond cleavage through hydrogen bonding rearrangement, acting as proton acceptor, to form the final iron-oxo product. The viability of O–O homolysis was also evaluated. Although homolytic and heterolytic pathways are computed to occur with similar energy barriers, they showed significant differences in the relative energies of the iron-oxo product of the O–O cleavage, being the homolytic pathway too endergonic to occur. Hence, supporting the experimental

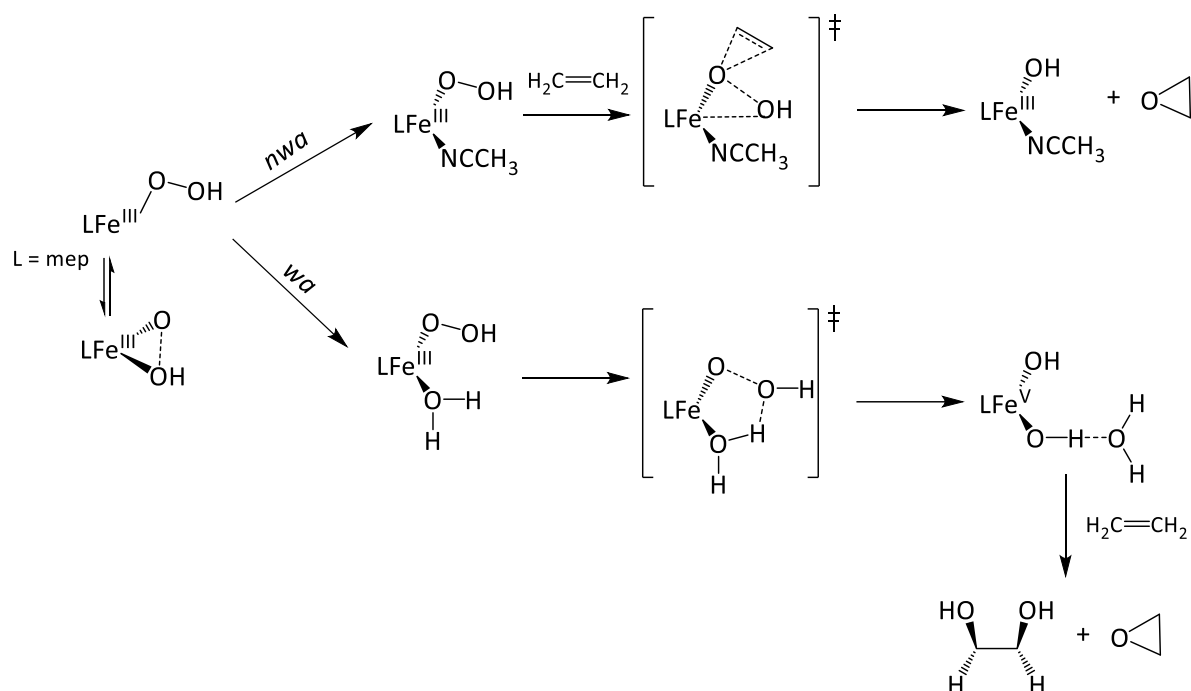
evidence, DFT calculations suggest that the oxidizing species in stereospecific alkane oxidation is best described as a high-valent $\text{Fe}^{\text{V}}=\text{O}$ compound (Scheme I.17).



Scheme I.17. Proposed mechanism for the O—O bond cleavage mechanism in tpa-based iron system.

I.3.2.4 Combined experimental and theoretical studies on the oxidation of olefins by the $[\text{Fe}(\text{OTf})_2(\text{mep})]$ system: a water assisted mechanism

In order to further study the role of the H_2O molecule in the proposed water-assisted mechanism for the generation of the *cis*-HO- $\text{Fe}^{\text{V}}=\text{O}$ species, the $[\text{Fe}(\text{OTf})_2(\text{mep})]$ complex was chosen to perform a combined experimental and theoretical analysis.⁷² Two different scenarios were considered for the epoxidation of olefins: water-assisted (*wa*) vs non-water-assisted (*nwa*). In the absence of water (*nwa*), DFT calculations strongly favor the direct attack of the $[\text{Fe}^{\text{III}}(\text{OOH})(\text{mep})]^{2+}$ intermediate to the olefin, leading exclusively to the epoxide product, as indeed observed experimentally (Scheme I.18, *nwa*).⁶⁵ In presence of water (*wa*), the oxidation is proposed to occur via a OH- $\text{Fe}^{\text{V}}=\text{O}$ species instead, which leads to both epoxide and *syn*-diol products (Scheme I.18, *wa*). The two oxidizing iron species are found to have comparable activation barriers. These theoretical findings were tested experimentally, observing an increased diol/epoxide ratio in the oxidation of cyclooctene when excess of water was added. Moreover, ^{18}O -labeling experiments were performed, showing 30% incorporation of labeled oxygen in the epoxide product in presence of H_2^{18}O . However, these results suggest that about 40% of the product arises from the *nwa* mechanism.



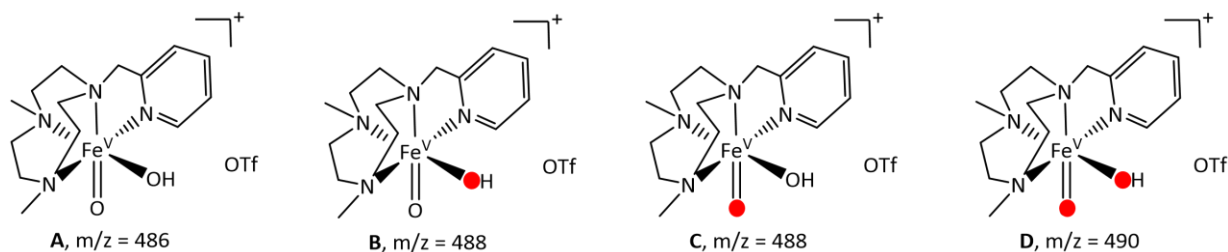
Scheme 1.18. Proposed mechanisms for epoxidation and *cis*-dihydroxylation in non-water assisted (*nwa*) and water-assisted (*wa*) mechanisms.

1.3.2.5 Evidence for a $\text{Fe}^{\text{V}}(\text{O})(\text{OH})$ species by means of mass spectrometry

1.3.2.5.1 Variable-temperature mass spectrometry and DFT studies on Pytacn-based iron system

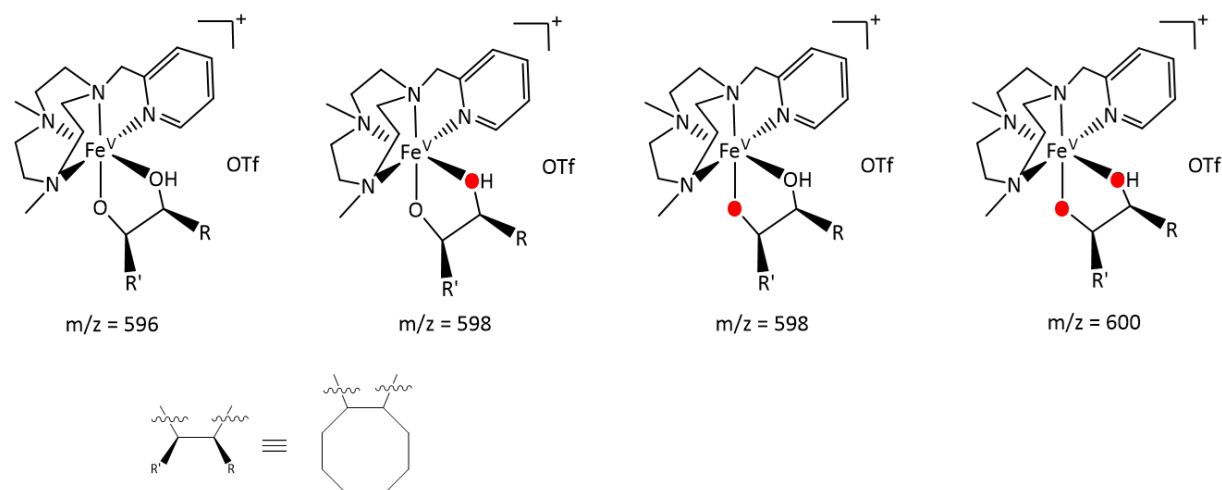
Further experimental evidence for the implication of a high-valent iron-oxo intermediate in catalytic C—H oxidation reactions were gathered for the $[\text{Fe}(\text{OTf})_2(\text{Me,HPytacn})]$ catalyst.⁷³ Variable-temperature mass spectrometry (VT-MS) technique was employed to trap and characterize a $\text{Fe}^{\text{V}}=\text{O}$ species involved in C—H and C=C oxidation reactions. Isotopic labeling studies in combination with DFT methods led to the proposal of an $\text{OH}-\text{Fe}^{\text{V}}=\text{O}$ species as responsible for the C—H and C=C oxidation events. $[\text{Fe}(\text{OTf})_2(\text{Me,HPytacn})]$ in combination with H_2O_2 was studied by means of VT-MS between 20°C and -40 °C, obtaining a prominent peak at $m/z = 470.1$ assigned to $[\text{Fe}^{\text{III}}(\text{OH})(\text{OTf})(\text{Me,HPytacn})]^+$ and a second, less intense peak at $m/z = 486.1$ (M) that could be formulated as either $[\text{Fe}^{\text{III}}(\text{OOH})(\text{OTf})(\text{Me,HPytacn})]^+$ or $[\text{Fe}^{\text{V}}(\text{O})(\text{OH})(\text{OTf})(\text{Me,HPytacn})]^+$, being the latter only observed at low temperatures (Scheme 1.19, **A**). Isotopic labeling studies were conducted to distinguish between the two putative

metastable species. Reaction of the iron complex with $\text{H}_2^{16}\text{O}_2$ in the presence of H_2^{18}O showed a new peak assigned to $M+2$ (Scheme I.19, **B**). The complementary experiment using $\text{H}_2^{18}\text{O}_2$ in the presence of H_2^{16}O afforded the same peak $M+2$ (Scheme I.19, **C**). Finally, when the experiment was performed with $\text{H}_2^{18}\text{O}_2$ and H_2^{18}O , the peak $M+2$ continued to be the major species, but a peak $M+4$ appeared as the second most intense component of the spectrum (Scheme I.19, **D**).



Scheme I.19. Mass peaks obtained for putative $[\text{Fe}^{\text{V}}(\text{O})(\text{OH})(\text{OTf})(^{\text{Me,H}}\text{Pytcn})]^+$ species in labeling experiments.

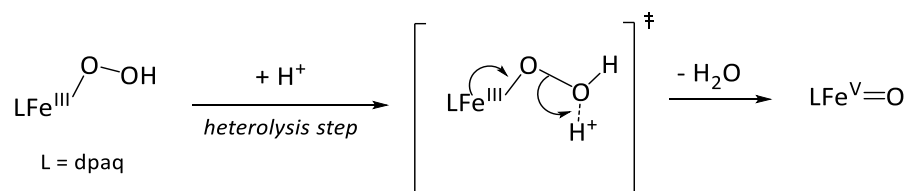
Since peroxide-type species do not exchange their oxygen atoms with water, the isotopic labeling experiments provided strong indication that the metastable intermediate should be assigned as $[\text{Fe}^{\text{V}}(\text{O})(\text{OH})(\text{OTf})(^{\text{Me,H}}\text{Pytcn})]^+$, in which one oxygen atom derived from H_2O_2 and another derived from H_2O , presumably via a water-assisted heterolytic O–O bond cleavage in the hydroxide species (*vide supra*). Regarding the reactivity of such species, experiments in the presence of cyclooctene were performed, affording the kinetically stable iron–(hydrogen)glycolate species. In this case, the peak assigned to $[\text{Fe}^{\text{V}}(\text{O})(\text{OH})(\text{OTf})(^{\text{Me,H}}\text{Pytcn})]^+$ disappeared to form two new peaks associated to the glycolate species $[\text{Fe}^{\text{III}}(\text{C}_8\text{H}_{14}\text{O}_2)(^{\text{Me,H}}\text{Pytcn})]^+$ and the hydrogenglycolate species $[\text{Fe}^{\text{III}}(\text{C}_8\text{H}_{14}(\text{O})(\text{OH}))(\text{OTf})(^{\text{Me,H}}\text{Pytcn})]^+$. Isotopic labeling experiments were also performed in the presence of an olefin, showing again the expected 2-mass unit displacement of the peaks, when either H_2^{18}O or $\text{H}_2^{18}\text{O}_2$ were used in the reactions (Scheme I.20). DFT calculations support the fact that $[\text{Fe}^{\text{V}}(\text{O})(\text{OH})(\text{OTf})(^{\text{Me,H}}\text{Pytcn})]^+$ is capable of dihydroxylating *trans*-2-butene (used as model substrate) with a very small energy barrier (3.3 kcal/mol), being the overall reaction highly exergonic (70 kcal/mol).



Scheme I.20. Mass peaks obtained for putative $[\text{Fe}^{\text{III}}(\text{OTf})(\text{C}_8\text{H}_{14}(\text{O})(\text{OH})(^{\text{Me,H}}\text{Pytacn}))]^+$ species in labeling experiments.

I.3.2.5.2 Cold-spray-ionization mass spectrometry on dpaq-based iron complex

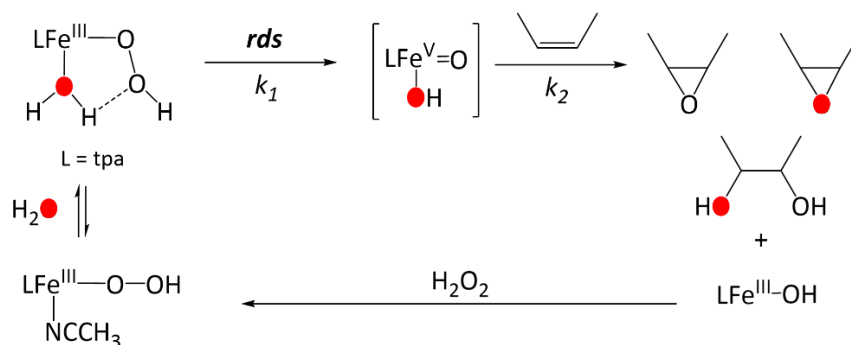
$\text{Fe}^{\text{V}}=\text{O}$ species responsible for alkane oxidation was also supported in the case of a complex in an anionic amidate ligand environment, as presented by Hitomi and coworkers.⁶⁶ In this case, cold-spray-ionization mass spectrometry (CSI-MS) technique was employed to study the reaction of $[\text{Fe}^{\text{III}}(\text{dpaq})(\text{H}_2\text{O})]^{2+}$ with H_2O_2 . The spectrum showed primarily the formation of $[\text{Fe}^{\text{III}}(\text{dpaq})(\text{OOH})]^+$, a peak that was 4 mass units shifted when $\text{H}_2^{18}\text{O}_2$ was used. Interestingly, a weak ion signal also appeared, assigned to a $[\text{Fe}^{\text{V}}(\text{dpaq})(\text{O})](\text{ClO}_4)^+$ intermediate, which shifted 2 mass units when generated with $\text{H}_2^{18}\text{O}_2$. O–O bond heterolysis was proposed to be facilitated by protons (Scheme I.21), since in the presence of a strong base the A/K ratio of cyclohexane products is substantially reduced.



Scheme I.21. Proposed O–O bond heterolysis mechanism facilitated by protons to form a putative $[\text{Fe}^{\text{V}}(\text{dpaq})(\text{O})]^{2+}$ intermediate.

1.3.2.6 Kinetic studies on tpa iron system supporting water-assisted O—O bond cleavage

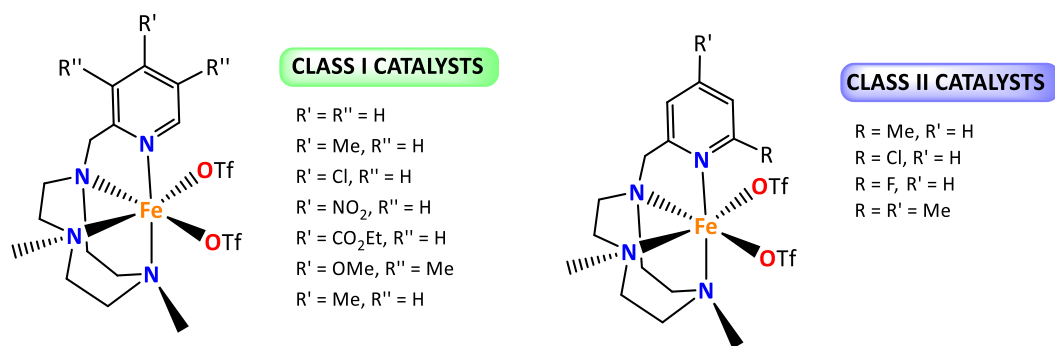
Very recently, it has been reported the first kinetic evidence that supports the water-assisted mechanism for the O—O bond cleavage step of $[\text{Fe}^{\text{III}}(\text{OOH})(\text{tpa})]^{2+}$ to generate the $[\text{Fe}^{\text{V}}(\text{O})(\text{OH})(\text{tpa})]^{2+}$ oxidant.⁷⁴ When $[\text{Fe}(\text{tpa})(\text{CH}_3\text{CN})_2](\text{ClO}_4)_2$ was reacted with excess of H_2O_2 in the presence of 1-octene, an $\text{Fe}^{\text{III}}\text{-OOH}$ intermediate was rapidly formed. A steady-state phase appeared, suggesting that the decay rate of the intermediate was comparable to that of its re-formation as long as excess H_2O_2 was present. There was a second phase entailing a first-order decay of the $\text{Fe}^{\text{III}}\text{-OOH}$ concentration attributed to the depletion of H_2O_2 , which was independent of the concentration of 1-octene, indicating that this intermediate is not directly involved in substrate oxidation. However, oxidation products were formed during the same time period as the formation and decay of $\text{Fe}^{\text{III}}\text{-OOH}$, suggesting that this species is required for olefin oxidation and corresponds to the rate-determining step (rds) of the reaction. Considering these observations and ^{18}O -labeling studies, it can be concluded that $\text{Fe}^{\text{III}}\text{-OOH}$ is not the oxidant itself but a precursor to the actual oxidant that must incorporate an O atom from water (*vide supra*). Such incorporation was proposed to come from ligand exchange of water into $[\text{Fe}^{\text{III}}(\text{tpa})(\text{OOH})(\text{NCCH}_3)]^{2+}$, forming $[\text{Fe}^{\text{III}}(\text{tpa})(\text{OOH})(\text{OH}_2)]^{2+}$. This is in agreement with the sensitivity of the decay rate to the concentration of water present in solution, *i.e.*, increasing the water concentration shortened the steady-state phase and enhanced the rates of $\text{Fe}^{\text{III}}\text{-OOH}$ decay and product formation. A rapid pre-equilibrium binding of H_2O onto the iron center was proposed, previous to the decay of the water adduct, which accelerated the O—O bond cleavage. Moreover, a KIE of 2.5 was observed for the decay and for the product formation, which demonstrated the role of a proton in the rds that in turn facilitates the O—O bond heterolysis. This cleavage pathway would generate a $\text{HO-Fe}^{\text{V}}=\text{O}$ species, which is proposed to be responsible for olefin oxidation (Scheme I.22).



Scheme 1.22. Proposed mechanism of olefin oxidation by $[\text{Fe}(\text{tpa})(\text{CH}_3\text{CN})_2](\text{ClO}_4)_2$ that accounts for the observed O-atom incorporation pattern.

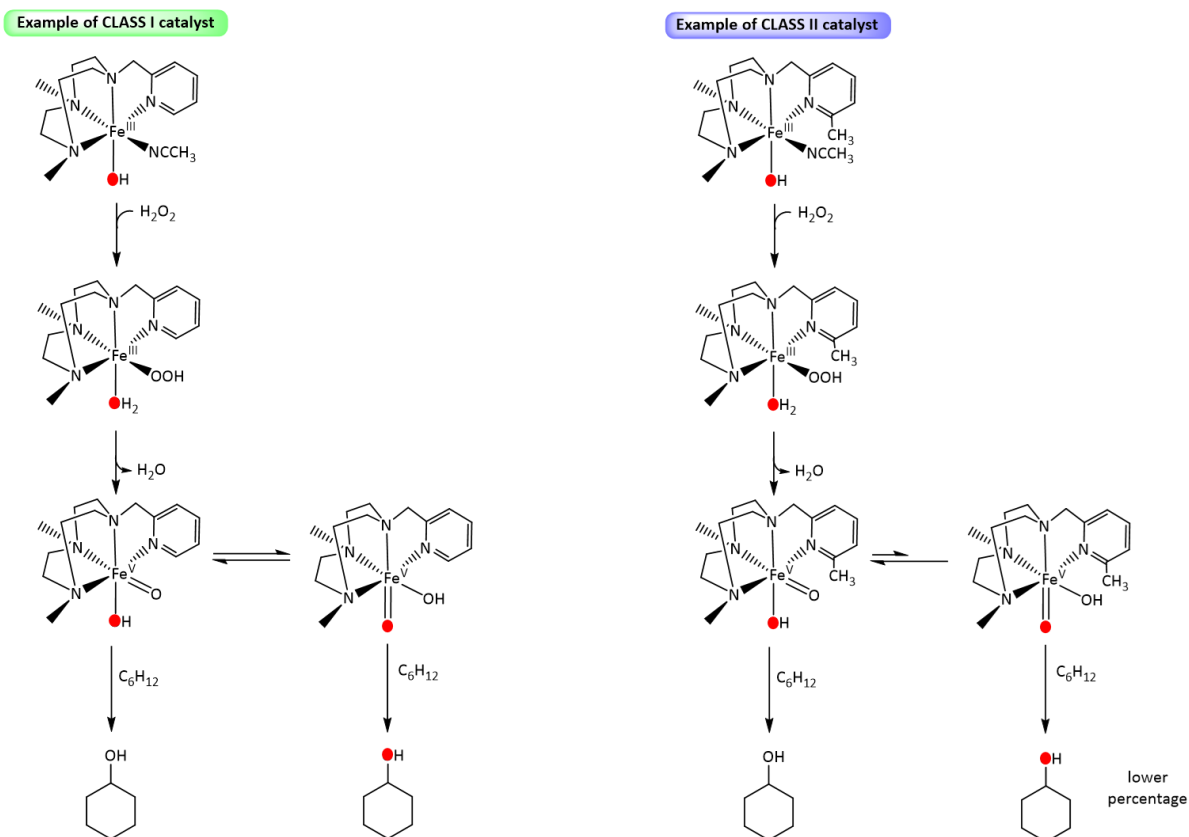
1.3.2.7 Combined isotopic labeling studies and DFT calculations on Pytacn-based iron complexes

A family of Pytacn-based complexes have been very recently studied by means of isotopic labeling experiments in combination with DFT calculations to get insight into the mechanism by which $[\text{Fe}^{\text{V}}(\text{O})(\text{OH})(\text{Pytacn})]^{2+}$ reacts with alkanes.⁷⁵ Systematic modifications were introduced in the pyridine ring of the ligand in order to analyze electronic and steric parameters. The isotopic labeling studies showed that there was a pre-equilibrium involving reversible water-binding at the iron center, plus water incorporation was independent on the concentration of substrate. Cyclohexane and adamantane were tested as examples of secondary and tertiary C—H bonds, respectively. The results showed that the level of water incorporation in tertiary sites was significantly more sensitive to the nature of the catalyst than in secondary sites. Moreover, no competition between water exchange and substrate oxidation was observed. Taking all these results into account, the family of catalysts was classified into two categories: class I, catalysts with no substituent in the α -position of the pyridine ring, and class II, with a substituent in the 6th position of the pyridine ring (Scheme 1.23).



Scheme I.23. Family of Pytacn complexes studied in C—H group oxidation labeling studies.

Modification of the electronic properties of the catalysts (Scheme I.23) did not have a significant influence either in the catalytic activity or in the isotopic patterns. However, steric modifications at the α -position of the pyridine yielded a great impact in the labeling results: class I catalysts showed a larger amount of water incorporation in tertiary C—H bonds than in secondary ones, while class II catalysts incorporated much less oxygen from water and the extent of water incorporation into tertiary sites was smaller than in secondary ones. Oxidation of alkenes was also tested, and the isotopic pattern of the corresponding diols confirmed that in the whole family of catalysts a HO-Fe^V=O species containing one oxygen atom from water and another from H₂O₂ is responsible for the oxidation events. According to ESI-MS analyses, the resting state was assigned to a [Fe^{III}(OH)(^{Me,H}Pytacn)(L)]²⁺ or [Fe^{III}(OH)(^{Me,Me}Pytacn)(L)]²⁺ species, respectively, where L is a solvent molecule, presumably acetonitrile. Overall, the involvement of a common HO-Fe^V=O active species in the hydroxylation of alkanes could be deduced from the alkene *cis*-dihydroxylation reactions, however fundamental differences exist in the exact details of the C—H cleavage and/or the C—O formation event, as isotopic pattern in C—H oxidized products, unlike in the syn-diols, are catalyst dependent. In contrast to [Fe(mep)] and [Fe(tpa)] (*vide supra*), [Fe(Pytacn)]-based catalysts present important differences with respect to the mechanism proposed for heme systems. For class I catalysts, water is the main source of oxygen atoms that end up in tertiary sites, and the percentage of water incorporation is larger for substrates with weaker C—H bonds. No competition between substrate attack and oxo-hydroxo tautomerism was detected, indicating that the C—H bond activation mechanism was somewhat dependent on the nature of the C—H bond itself.



Scheme 1.24. Mechanism of cyclohexane hydroxylation by Pytacn-based iron complexes proposed from DFT calculations and isotopic labeling studies.

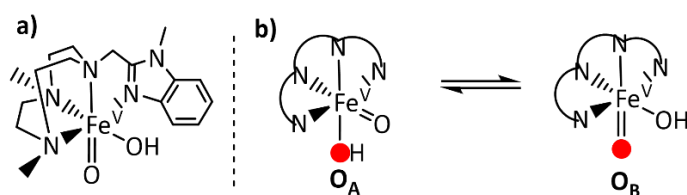
DFT calculations were undertaken to address these results. It was found that both class I and class II complexes follow an identical mechanism until the formation of the HO-Fe^V=O active species, which undergoes rapid oxo-hydroxo tautomerism assisted by water. However, due to the unsymmetrical nature of the ligand, the two *cis*-exchangeable sites are not equivalent. For class I catalysts, both tautomers were found virtually equally reactive, yielding the corresponding alcohol products in comparable amounts of ¹⁶O- and ¹⁸O-labeled alcohols in the presence of H₂¹⁸O. In contrast, for class II catalysts, reaction of the substrate with the tautomer in which the oxo moiety derives from H₂O₂ was energetically more favored and dominated the overall reaction. This fact explained the minimal ¹⁸O-incorporation using H₂¹⁶O₂ in the presence of H₂¹⁸O, and can be rationalized in terms of the steric hindrance offered by the α -substituents of the pyridine ring. The tautomer where the oxo group derives from H₂¹⁸O placed the pyridine moiety in parallel position with respect to the Fe–O vector, thus the α -substituent stayed in close position to the oxygen atom hindering the Fe=O unit

from substrate approach and therefore limits its reactivity (Scheme I.24). Furthermore, for all the family of catalysts it was found that the C—H abstraction step and the C—OH bond formation occurred in an asynchronous concerted mechanism, *i.e.*, the alkyl radical has no life time, leading to stereospecific oxidation reactions. The oxo ligand that initiates the attack is in fact the same that ends up in the newly formed C—OH bond.

Further confirmation of the steric discrimination was confirmed by Mitra et al⁷⁶ using a new tacn-based complex $[\text{Fe}(\text{OTf})_2(\text{Me,MeBzImtacn})]$ ($\text{Me,MeBzImtacn} = 1-(N\text{-methylbenzimidazolyl})\text{-}4,7\text{-dimethyl-}1,4,7\text{-triazacyclononane}$). In this complex, the pyridyl arm of the Pytacn scaffold was replaced by an *N*-methyl benzimidazolyl substituent, whose sp^2 character and rigidity should provide a well-defined steric demand, intermediate between that attained with $[\text{Fe}(\text{OTf})_2(\text{Me,HPytacn})]$ and $[\text{Fe}(\text{OTf})_2(\text{Me,MePytacn})]$. Moreover, since the relative donor capacities of pyridine and benzimidazole are estimated to be very similar, differences in reactivity among this set of catalysts can be traced to steric factors.

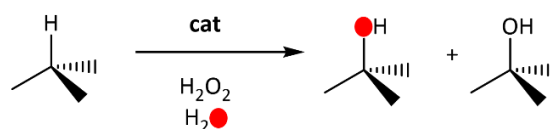
$[\text{Fe}(\text{OTf})_2(\text{Me,MeBzImtacn})]$ was found capable of efficiently oxidizing cyclohexane in the presence of large excess of substrate. Under these conditions, cyclohexanol was the major product ($A/K = 10.6$), and this was postulated to be the exclusive primary product since the A/K ratio observed at the early stage of the reaction was substantially higher. Mechanistic probes (KIE, $3^\circ/2^\circ$ ratio, stereoretention) pointed toward the implication of a selective oxidant whose relative reactivity against C—H groups can be modulated by their bond strengths and steric properties. Since these are in accordance with that described for iron catalysts that mediate stereospecific C—H hydroxylations, including the Pytacn-based family, the analogous active species $[\text{Fe}^{\text{V}}(\text{O})(\text{OH})(\text{Me,MeBzImtacn})]$ was tentatively inferred (Scheme I.25, a). This fact was supported by the *syn*-diol/epoxide ratio observed in the oxidation of cyclooctene (3.5), and most importantly in the *syn*-diol being 98% $^{16}\text{O}^{18}\text{O}$ labeled in presence of H_2^{18}O . The relative reactivity of the putative \mathbf{O}_A and \mathbf{O}_B tautomers, analogous to those proposed for Pytacn-based complexes (Scheme I.25, b) was also investigated. The unusually high level of water incorporation into alcohol products in the oxidation of cyclohexane (45%) indicated that both tautomers are equally reactive against secondary C—H groups. However,

the level of water incorporation in the oxidation of tertiary sites was significantly lower, indicating a preference for the active species \mathbf{O}_A . Illustrative examples are shown in Table I.2.



Scheme I.25. Postulated structure for the $[\text{Fe}^{\text{V}}(\text{O})(\text{OH})(\text{Me,MeBzImtacn})]$ active species (a) and oxo-hydroxo tautomerism proposed for Pytacn-based and BzImtacn-based catalysts (b).

Table I.2. Comparison of percentage of ^{18}O incorporation into alcohol products in the oxidation of secondary and tertiary C—H groups by tacn-based catalysts using H_2^{18}O .



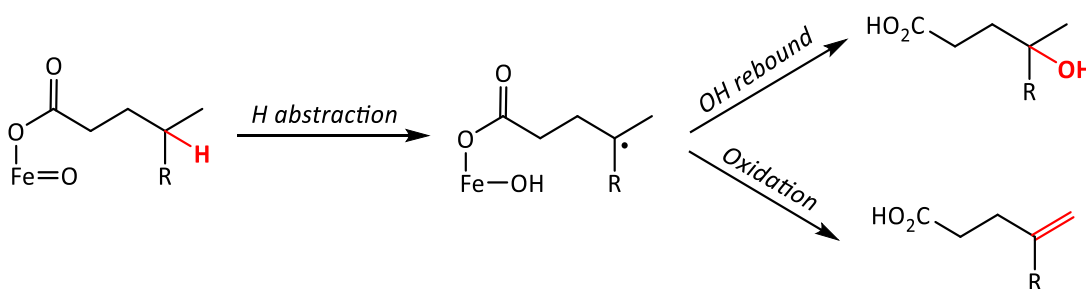
Substrate	% of H_2^{18}O incorporation using:		
	$[\text{Fe}(\text{OTf})_2(\text{Me,MeBzImtacn})]$	$[\text{Fe}(\text{OTf})_2(\text{Me,HPytacn})]$	$[\text{Fe}(\text{OTf})_2(\text{Me,MePytacn})]$
Cyclohexane	48	45	11
<i>cis</i> -1,2-DMCH	26	79	2

As exemplified in Table I.2, catalyst $[\text{Fe}(\text{OTf})_2(\text{Me,MePytacn})]$ showed very little water incorporation percentage into the alcohol products, indicating that the tautomer \mathbf{O}_A was much more reactive than \mathbf{O}_B , being the latter almost negligible. On the other hand, $[\text{Fe}(\text{OTf})_2(\text{Me,MeBzImtacn})]$ showed a different behavior in the oxidation of secondary and tertiary C—H groups. While $\sim 50\%$ of water incorporation was attained for the oxidation of secondary sites, indicative of \mathbf{O}_A and \mathbf{O}_B being virtually equally reactive, the oxidation of tertiary C—H bonds occurred with low levels of incorporation of water ($\sim 25\%$) into the alcohol products, pointing toward a more reactive \mathbf{O}_A tautomer than \mathbf{O}_B . This was interpreted as an intermediate behavior between $[\text{Fe}(\text{OTf})_2(\text{Me,MePytacn})]$ and $[\text{Fe}(\text{OTf})_2(\text{Me,HPytacn})]$, the latter showing $\sim 50\%$ of water incorporation into secondary site oxidized products and $\sim 80\%$ into tertiary sites, which indicates that \mathbf{O}_A and \mathbf{O}_B tautomers are almost equally reactive in the oxidation of secondary C—H bonds but \mathbf{O}_B stands as the most reactive tautomer toward tertiary sites.

This reactivity can be rationalized in terms of steric hindrance at the proximity of the reactive oxo moiety of the Fe^{V} intermediate combined with steric bulk offered by the substrates. The benzimidazole ring introduces steric bulk at the proximity of the axial position at the iron center intermediate between that set by pyridine and 6-Me-pyridine arms. Therefore, $[\text{Fe}(\text{OTf})_2(\text{Me},\text{MeBzImtacn})]$ reacts as $[\text{Fe}(\text{OTf})_2(\text{Me},\text{H}^{\text{Pytacn}})]$ toward more sterically exposed secondary C—H groups. In contrast, the reactivity of $[\text{Fe}(\text{OTf})_2(\text{Me},\text{MeBzImtacn})]$ toward bulkier tertiary sites resembles that of the more sterically demanding $[\text{Fe}(\text{Me},\text{MePytacn})(\text{OTf})_2]$ catalyst. With these results, strong evidence was provided that the reactivity of the $\text{O}_\text{A}/\text{O}_\text{B}$ tautomers could be tuned by modifying the steric properties of the catalysts.

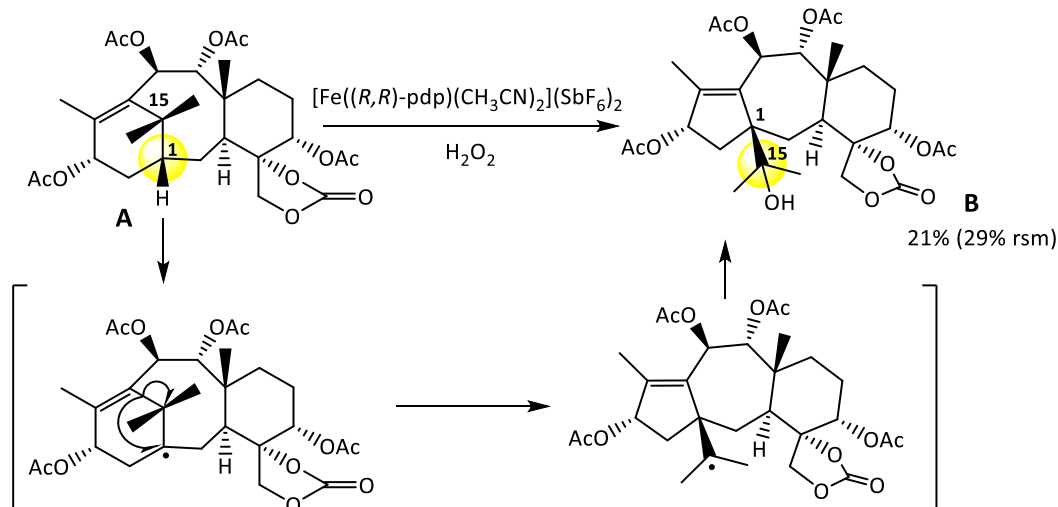
1.3.3 MECHANISTIC SUBSTRATE PROBES FOR STEREOSPECIFIC C—H HYDROXYLATIONS: RADICAL CLOCKS AND RADICAL REARRANGEMENTS

In 2011, White and coworkers showed that $[\text{Fe}(\text{pdp})(\text{CH}_3\text{CN})_2](\text{SbF}_6)_2$ catalyst was capable of mixed hydroxylase/desaturase activity on aliphatic substrates containing carboxylic acids.⁷⁷ Mechanistic studies suggested that both products arose from a common pathway *via* a very short-lived carbon centered radical substrate intermediate (Scheme I.26).



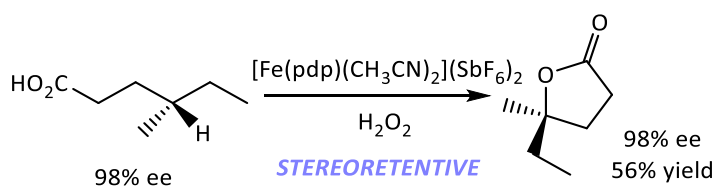
Scheme I.26. Proposed mechanism for dual hydroxylase/desaturase activity in oxidation reactions catalyzed by $[\text{Fe}(\text{pdp})(\text{CH}_3\text{CN})_2](\text{SbF}_6)_2$.

Evidence for a carbon-centered substrate radical was provided through a taxane-based radical trap that rearranged under oxidation with $[\text{Fe}(\text{pdp})(\text{CH}_3\text{CN})_2](\text{SbF}_6)_2$ catalyst to yield a *nortaxane*-based structure as the major product. It was proposed that the rearrangement occurred *via* hydrogen abstraction, followed by a Wagner–Meerwein-type rearrangement, and finally hydroxyl rebound to form the *nortaxane* product (Scheme I.27).



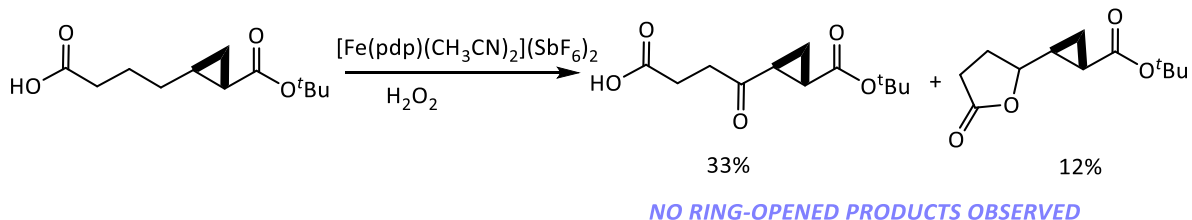
Scheme I.27. Taxane-based radical trap: rearrangement of taxane **A** to *nortaxane* **B**.

Intermolecular hydroxylations with this catalyst proceed with complete stereoretention, suggesting that the carbon-centered radical that forms after initial H-atom abstraction must have a life-time shorter than 10^{-10} s. Further insight into the short life-time of such radical was gained by studying the hydroxylation of alkanolic acids. In these reactions, an intramolecular lactonization rapidly follows the initial hydroxylation. An enantioenriched alkanolic acid was oxidized and shown to proceed with complete retention of stereochemistry, indicating that the intramolecular system does not generate longer-lived alkyl radicals susceptible to epimerize (Scheme I.28).



Scheme I.28. Oxidation of a tertiary C—H bond with complete stereoretention as a radical clock.

Besides, an ester-substituted cyclopropane was used as a substrate probe, and its oxidation did not generate detectable amounts of ring-opened products (ring-opening rate constant of $\sim 10^{11} \text{ s}^{-1}$, Scheme I.29). This result suggests that the hydroxyl rebound is extremely rapid, and is in line with the recently proposed asynchronous concerted mechanism for alkane hydroxylation.⁷⁵



Scheme 1.29. C—H group oxidation in presence of a cyclopropane ring, showing no ring-opened products.

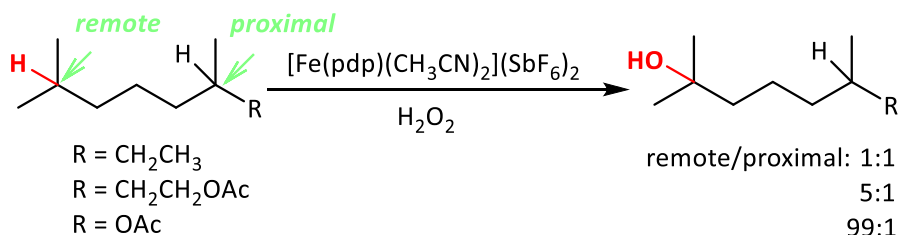
1.4 TUNING THE SELECTIVITY IN ALKANE OXIDATION REACTIONS

One of the major subjects of interest over the last decade in metal-catalyzed alkane oxidation reactions has been the understanding of the factors determining the C—H site selectivity of such processes. This knowledge is necessary to face the challenge of devising chemical tools for overcoming the innate reactivity of C—H bonds, introducing novel selectivities in these reactions.

1.4.1 PREDICTABLY SELECTIVE OXIDATIONS AND SELECTIVITY PATTERNS

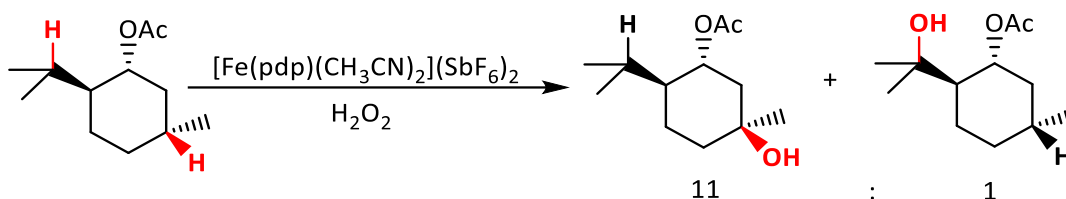
A major breakthrough in predictably selective aliphatic C—H oxidation reactions was introduced by White and Chen in 2007.⁶² In this landmark work, predictable selectivity was achieved on the basis of the electronic and steric properties of the C—H bonds, without the need for directing groups. Very interestingly, this predictability could also be applied to selectively oxidize complex natural products at specific C—H bonds in preparative useful yields. Selectivity could be achieved by introducing directing groups (*vide infra*, section 1.4.2.1), or by controlling the sterics and electronics of the substrate. The iron catalyst $[\text{Fe}(\text{pdp})(\text{CH}_3\text{CN})_2](\text{SbF}_6)_2$ (15 mol%), together with H_2O_2 as oxidant and acetic acid as additive, was capable of performing selective oxidations of nonactivated C—H bonds for a broad range of substrates. Hydroxylation occurred preferentially at the most electron-rich tertiary C—H bond, despite the significant statistical advantage of secondary ones, with complete retention of stereochemistry (provided that tertiary site was part of a stereogenic center). In order to test the site selectivity among different tertiary C—H bonds, small molecules with two tertiary sites were oxidized, obtaining always preferential oxidation at the more remote

tertiary C—H bond from electron-withdrawing groups (EWGs). The selectivity between the two tertiary sites ranges from 5:1 (remote:proximal, R:P) to 99:1 (R:P), depending on the substrate. However, when no EWGs were present in the molecule, no selectivity was obtained, affording ratios of 1:1 (R:P) (Scheme I.30).



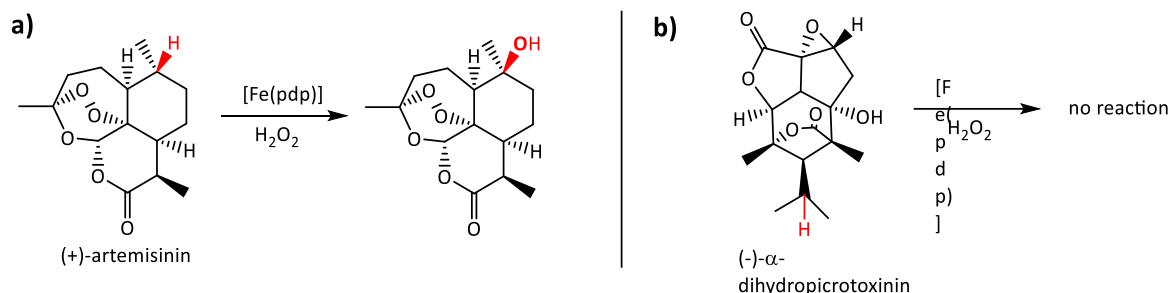
Scheme I.30. Oxidation of substrates with electronically different groups by $[\text{Fe}(\text{pdp})(\text{CH}_3\text{CN})_2](\text{SbF}_6)_2$.

Regarding the steric effects, (–)-menthyl acetate was chosen as substrate, in which two of the three tertiary sites are virtually equivalent in terms of electronics. Oxidation occurred preferentially at the less hindered tertiary C—H bond, with 11:1 (accessible:hindered) selectivity and 55% combined yield (Scheme I.31).



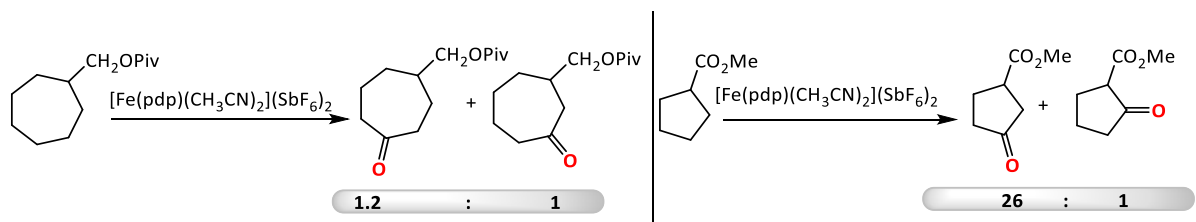
Scheme I.31. Selective oxidation of (–)-menthyl acetate with $[\text{Fe}(\text{pdp})(\text{CH}_3\text{CN})_2](\text{SbF}_6)_2$ as catalyst.

When steric and electronic effects were interplaying in a single substrate, experiments showed that the steric effects could override the electronic ones in site selectivities. The oxidation of the complex molecule (+)-artemisinin took place preferentially at the more electron-rich and less encumbered tertiary site with moderate yield (34%), that could be risen to 54% by recycling the starting material twice (Scheme I.32, a). This result has however been corrected by the same authors in a more recent paper showing also formation of a second product arising from oxidation at a methylene site (see Scheme I.53).⁷⁸ On the other hand, in the highly hindered environment of (–)- α -dihydropicrotoxinin, no oxidation was attained, and 92% of the starting material was recovered after the oxidation process (Scheme 32, b).



Scheme I.32. Oxidation of complex molecules by $[\text{Fe}(\text{pdp})(\text{CH}_3\text{CN})_2](\text{SbF}_6)_2$.

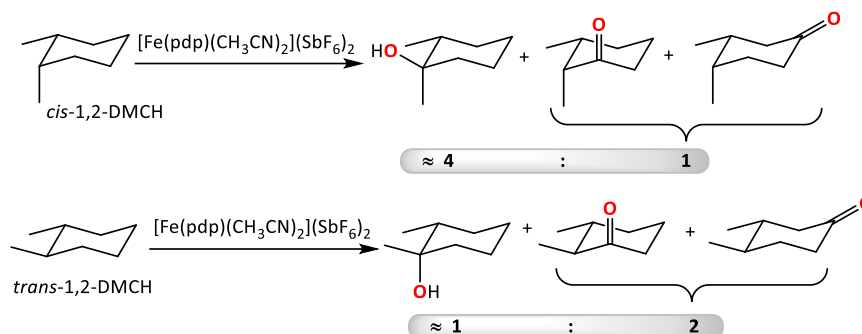
A study on methylene oxidation was presented by the same authors in 2010, using again the $[\text{Fe}(\text{pdp})(\text{CH}_3\text{CN})_2](\text{SbF}_6)_2$ catalyst.⁶³ Secondary C–H bonds have intermediate bond strength and steric properties between tertiary and primary sites. Nonactivated secondary C–H bonds could be site-selectively oxidized to afford mono-oxygenated products in preparative useful yields. In substrates with no electronic biasing elements, such as *n*-hexane, no site selectivity was attained. However, when EWGs were present in the substrate (inductive effects), the oxidation is biased towards the more remote site of the EWG, with selectivities ranging from 1.2:1 (R:P) to 26:1 (R:P), depending on the substrate and on the electronwithdrawing substituent in the ring (Scheme I.33). Proximity of the oxidized hydrogen atoms with respect to the EWG is key to determine the extent of the selectivity. Substrates where all protons are close to the EWG, such as cyclopentanone, showed poor conversion.



Scheme I.33. Electronic effects on secondary C–H group oxidation by $[\text{Fe}(\text{pdp})(\text{CH}_3\text{CN})_2](\text{SbF}_6)_2$.

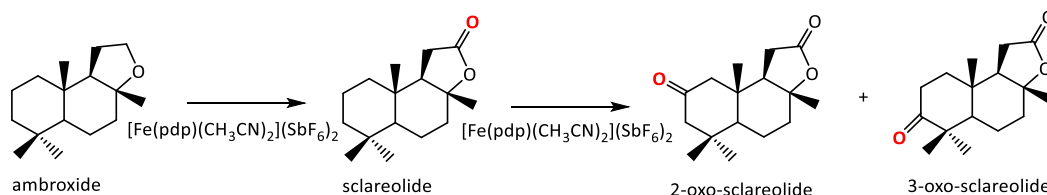
Interestingly, it was pointed out that stereoelectronic parameters based on conformational effects are also strong contributing factors to the product distribution in six-membered ring oxidations. Besides, methylene sites adjacent to bulky groups were disfavored. However, the catalyst allows for subtle steric influence to have significant effects on the chemoselectivity of secondary vs tertiary C–H bonds. In the oxidation of *cis*-1,2-DMCH,

the tertiary:secondary (3°:2°) ratio of products is 4:1, however, for *trans*-1,2-DMCH the 3°:2° ratio is reversed to 1:2, favoring the oxidation at secondary sites (Scheme I.34). The latter case might be explained because of the axial disposition of the tertiary sites,⁷⁹ which are disfavored and thus predominantly secondary site oxidation was attained.



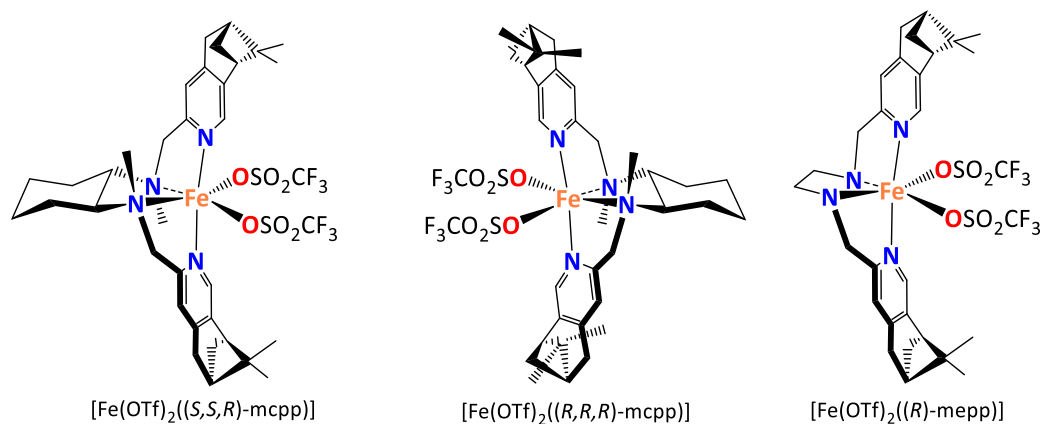
Scheme I.34. Chemoselectivity of secondary vs tertiary –H bonds in *cis*- and *trans*-1,2-DMCH oxidation by $[\text{Fe}(\text{pdp})(\text{CH}_3\text{CN})_2](\text{SbF}_6)_2$.

On the other hand, electron-activating groups (EAGs) were used to achieve orthogonal site selectivity to inductive or steric effects by means of hyperconjugation. For example, when a cyclopropane ring was fused to a cyclohexane ring, oxidation occurred preferentially at the more proximal position to the cyclopropane ring (1:5.2 R:P). Moreover, steric, electronic and stereoelectronic factors can be synergistically combined in the oxidation of complex natural products, resulting in useful levels of chemo-, site-, and even diastereoselective methylene oxidations. For the oxidation of complex natural products, terpenoids were chosen as appropriate substrate platforms to study the predictability of the oxidations. An interesting example of hyperconjugative effects was the oxidation of (–)-ambroxide, which selectively afforded (+)-sclareolide in very high yield (80%). (+)-Sclareolide contains a lactone deactivating group, therefore further oxidation of this molecule yielded a mixture of (+)-2-oxo-sclareolide and (+)-3-oxo-sclareolide (1.4:1), thus oxidizing the more distal secondary sites from the EWG (Scheme I.35).



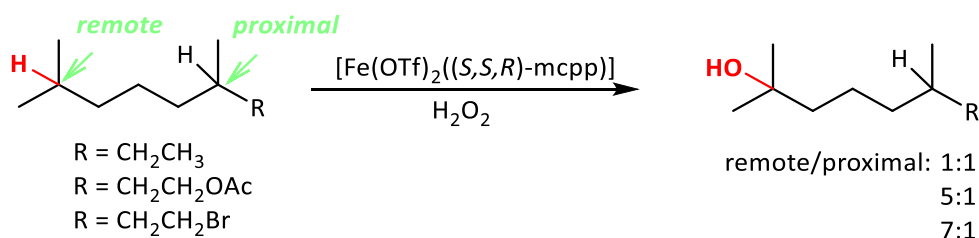
Scheme I.35. Combination of stereoelectronic factors in the oxidation of terpenes by $[\text{Fe}(\text{pdp})(\text{CH}_3\text{CN})_2](\text{SbF}_6)_2$.

Inspired by the well-established principles in oxidation catalysis with heme complexes, Gómez et al designed a new catalyst platform based on modifications at well-known mep and mcp ligands (mcp = *N,N'*-dimethyl-*N,N'*-bis(2-pyridylmethyl)-cyclohexane-1,2-diamine) by introducing bulky pinene groups at the 4th and 5th position of the pyridine rings.⁸⁰ By doing so, [Fe(OTf)₂((*S,S,R*)-mcpp)], [Fe(OTf)₂((*R,R,R*)-mcpp)] (mcpp = *N,N'*-dimethyl-*N,N'*-bis[[(*R*)-4,5-pinenepyridin-2-yl]-methyl]-cyclohexane-1,2-diamine), and [Fe(OTf)₂((*R*)-mepp)] (mepp = *N,N'*-dimethyl-*N,N'*-bis(2-pyridylmethyl)-ethane-1,2-diamine) complexes were synthesized (Scheme I.36).



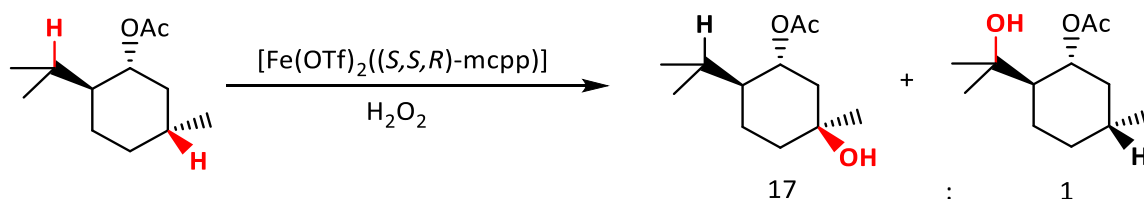
Scheme I.36. Structure of pinene-based iron catalysts reported by Gómez et al.

The catalyst [Fe(OTf)₂((*S,S,R*)-mcpp)] stood as the most efficient of the series using very low catalyst loadings (1 mol%), even more efficient than [Fe(pdp)(CH₃CN)₂](SbF₆)₂ under these catalytic conditions, for the oxidation of *cis*-1,2-DMCH. This catalyst was shown also capable of cyclohexane oxidation in 70% yield using 2 mol % catalyst. Under these conditions, electronic effects were studied with 2,7-dimethyl-octane derivatives (Scheme I.37), affording yields and selectivities very similar to those previously reported by White and coworkers (compare with Scheme I.30).⁶²



Scheme I.37. Oxidation of substrates with electronically different groups by [Fe(OTf)₂((*S,S,R*)-mcpp)].

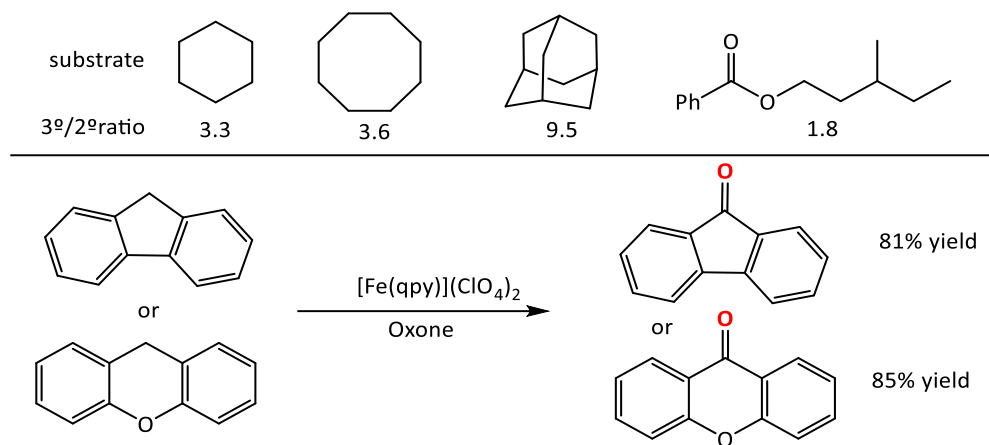
Furthermore, (-)-menthyl acetate was also tested using 3 mol% catalyst, obtaining 62% combined yield of oxidation at the tertiary sites with 17:1 selectivity (accessible:hindered) (Scheme I.38). This efficient selectivity was even more remarkable to that obtained with 15 mol% $[\text{Fe}(\text{pdp})(\text{CH}_3\text{CN})_2](\text{SbF}_6)_2$,⁶² (compare with Scheme I.32) most likely due to the well-defined chiral cavity around the metal center, which provides robustness by protecting the iron site against catalyst deactivation, and enhances the selectivity of the catalyst. The effect of the pinene ring in terms of catalyst efficiency and stability were demonstrated by performing a time-profile analysis of the oxidation of (-)-menthyl acetate catalyzed by $[\text{Fe}(\text{OTf})_2((S,S,R)\text{-mcpp})]$ and $[\text{Fe}(\text{OTf})_2((S,S)\text{-mcp})]$. These results indicated that H_2O_2 was more rapidly and efficiently consumed by the pinene-containing catalyst, which was not substantially deactivated during the course of the reaction. After a second addition of oxidant and substrate, $[\text{Fe}(\text{OTf})_2((S,S,R)\text{-mcpp})]$ was the only catalyst still active, capable of efficiently continue oxidizing the substrate into the desired alcohol product.



Scheme I.38. Selective oxidation of (-)-menthyl acetate with $[\text{Fe}(\text{OTf})_2((S,S,R)\text{-mcpp})]$ as catalyst.

A different approach was presented by Che and coworkers using $[\text{Fe}(\text{qpy})](\text{ClO}_4)_2$ (5 mol%) with Oxone.⁶⁵ High temperatures (80 °C) were required in this methodology. First of all, simple cyclic alkanes with no electronic effects interplaying were tested. Oxidation of cyclohexane yielded 15.6 TON and 3.3 A/K ratio, while cyclooctane afforded 50% combined yield and 3.6 A/K ratio (Scheme I.39). On the other hand, in the oxidation of adamantane 42% yield was obtained, with a $3^\circ/2^\circ$ ratio of 9.5. Hyperconjugation effects were used to direct the oxidation to the most proximal position to the electronactivating groups. Interestingly, this catalyst supports aromatic groups on the substrate, and fluorene and xanthene were the most effectively and selectively oxidized, obtaining up to 85% yield of the ketone product (the sole product observed for these two substrates). Ester moieties were also employed as

EWGs, as in the case of 3-methylpentyl benzoate, where the tertiary alcohol was obtained in 33% yield, and 18% of oxidation at the secondary most remote site ($3^\circ/2^\circ = 1.8$).



Scheme I.39. Chemoselectivity of secondary vs tertiary C–H bonds oxidation by [Fe(qpy)](ClO₄)₂.

This type of oxidations proved to be stereospecific, as shown in the oxidation of *cis*- and *trans*-4-methylcyclohexyl benzoate, which occurred with retention of the configuration. In terms of yields, the former was more efficiently oxidized to the corresponding tertiary alcohol (45% yield) than the latter (19% yield). Finally, mmol scale oxidations of xanthene and tetrahydronaphthalene were performed, showing the practicability of this methodology. Xanthone was obtained as a sole product in 83% yield in the oxidation of xanthene, whereas the products of tetrahydronaphthalene oxidation were a mixture of ketone (49%), secondary alcohol (12%) and overoxidized product (26%).

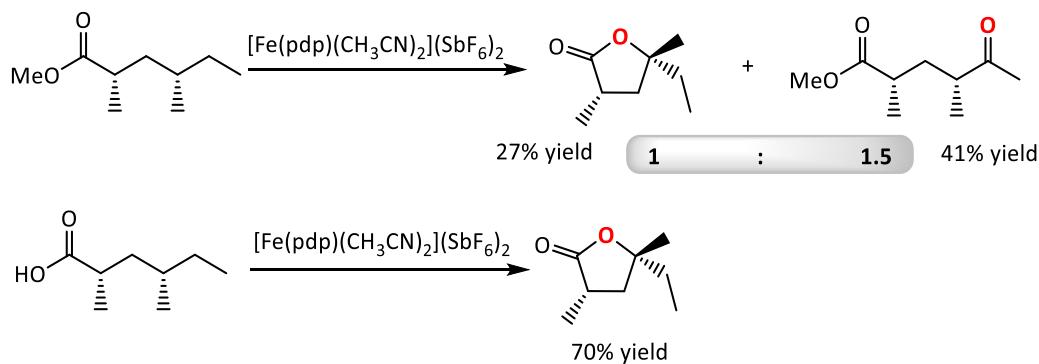
I.4.2 NOVEL SELECTIVITIES IN ALKANE OXIDATION REACTIONS

The factors that govern selectivity in C–H oxidation reactions by traditional organic reagents are determined by the innate nature of the C–H bonds of the substrates.⁸¹ The [Fe(pdp)(CH₃CN)₂](SbF₆)₂ catalyst appears to obey the same rules, and offer little versatility. Overriding these intrinsic bias imposed by the general reactivity of the substrate is particularly valuable, because it can complement current methodologies and open novel synthetic pathways. Towards this end, two different approaches can be undertaken: the introduction of directing groups on the substrate and modifications on the catalyst

architecture introducing structural aspects that condition substrate access to the catalyst active site. Both strategies are described in the following lines.

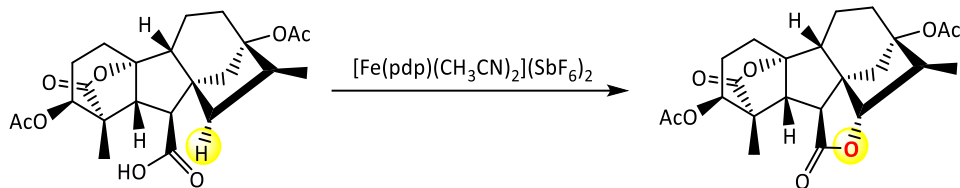
1.4.2.1 Novel selectivity induced by directing groups on the substrate

The use of directing groups on the substrate has been the most successful strategy to divert C–H regioselectivity in alkane oxidations.^{82–86} In the particular case of non-heme iron-catalyzed oxidations, White and Chen described the directed oxidation of carboxylic acid-containing substrates.⁶² They postulated that a carboxylate group on the substrate could be used to direct the site of C–H oxidation, based on the role of carboxylates as ligands for non-heme iron complexes and the beneficial role of acetic acid on the catalytic activity of $[\text{Fe}(\text{pdp})(\text{CH}_3\text{CN})_2](\text{SbF}_6)_2$. Diastereoselective lactonizations at secondary C–H sites were achieved with this methodology. For example, (+)-2,4-dimethyl-hexanoic acid was oxidized using $[\text{Fe}(\text{pdp})(\text{CH}_3\text{CN})_2](\text{SbF}_6)_2$ (15 mol%) and H_2O_2 , furnishing a five-membered ring lactone in 70% yield; whereas the oxidation of the analogous methyl ester gave a methyl ketone as the major product (Scheme I.40).



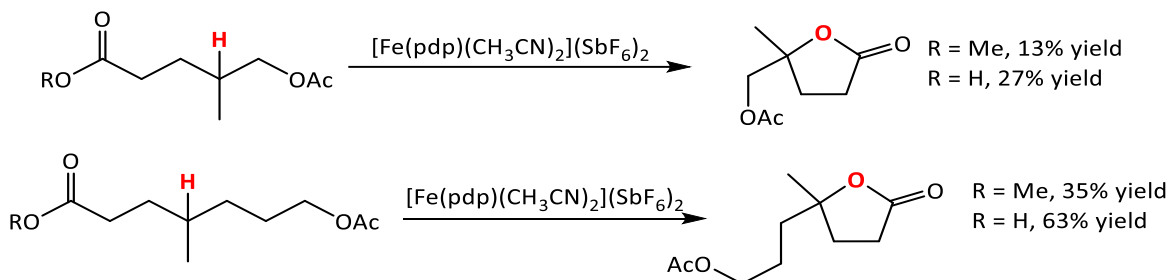
Scheme I.40. Directed oxidation of a carboxylic acid-containing substrate with $[\text{Fe}(\text{pdp})(\text{CH}_3\text{CN})_2](\text{SbF}_6)_2$.

On the other hand, this methodology was evaluated with a tetrahydrogibberellic acid analog, which yielded the corresponding five-membered ring lactone as a single diastereoisomer in 52% yield (recycling the substrate once) (Scheme I.41). In contrast, oxidation of the corresponding methyl ester resulted in mostly recovered starting material and mixtures of undefined oxidation products.



Scheme I.41. Oxidation of a tetrahydrogibberellic acid analog with $[\text{Fe}(\text{pdp})(\text{CH}_3\text{CN})_2](\text{SbF}_6)_2$.

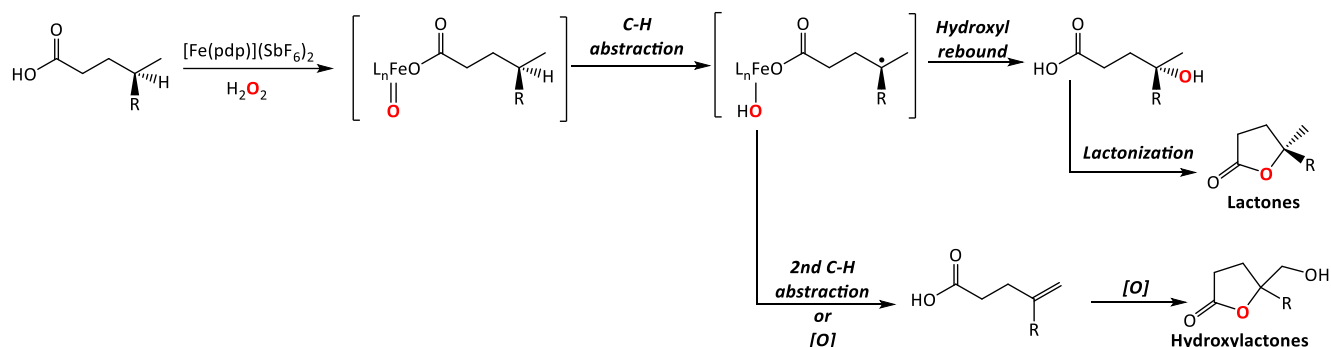
The same authors presented a more thorough study on the evaluation of the selectivity rules governing C–H oxidation of carboxylic acid-containing substrates in 2012.⁸⁷ In this work it was shown that carboxylic acids not only controlled the site selectivity, but they were also capable of overcoming unfavorable electronic, steric, and stereoelectronic effects within the substrate by rendering the oxidation reaction intramolecular. Linear methyl esters with EWGs were tested, showing that the substrate became more reactive as the EWGs were shifted away from the tertiary center, but poor yields were obtained. However, analogous carboxylic acid substrates were significantly more reactive, affording moderate yields of the corresponding lactones (Scheme I.42).



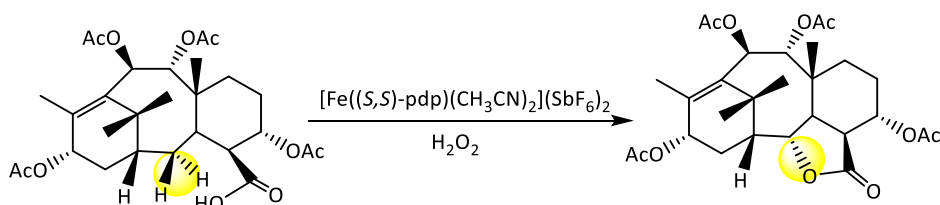
Scheme I.42. Lactonization reactions of ester- and carboxylic acid-based substrates with $[\text{Fe}(\text{pdp})(\text{CH}_3\text{CN})_2](\text{SbF}_6)_2$.

Moreover, a matched/mismatched behavior with the chiral $[\text{Fe}(\text{pdp})(\text{CH}_3\text{CN})_2](\text{SbF}_6)_2$ catalyst was detected when a chiral carboxylic acid was employed, while this behavior was not detected with analogous chiral methyl esters. This observation supported the proposal of carboxylic acid acting as ligand for the metal center. Enantiomeric enrichment of racemic carboxylic acid and lactone product was possible upon reaction with the chiral catalyst. In terms of steric effects, it was shown that lactone products arising from oxidation of cyclohexane-derivatized carboxylic acids was virtually unaffected by the axial or equatorial disposition of the C–H bond to be oxidized, a very different behavior from methyl ester substrates. From a mechanistic point of view, it is proposed that, analogously to C–H

hydroxylation, the iron catalyst reacts with H_2O_2 and carboxylic acid substrate to generate an iron-oxo carboxylate as the active oxidant species, capable of engaging in intramolecular hydrogen atom abstraction to afford a short-lived carbon-centered substrate radical. This radical can proceed via two different rebound pathways to furnish the lactone product: (i) carboxylate rebound to form lactone directly, or (ii) hydroxyl rebound followed by lactonization (Scheme I.43). The latter pathway is favored according to labeling studies, which showed that doubly ^{18}O -labeled carboxylic acid led to predominantly singly labeled lactone. Alternatively, the carbon-centered radical can undergo a second hydrogen abstraction to furnish an olefin intermediate, and further oxidation to yield hydroxylactones. Very interestingly, this strategy was employed in the directed, stereoselective oxidation of a taxane, obtaining moderate yield (49%) of the desired lactone (Scheme I.44).



Scheme I.43. Proposed mechanism for $[\text{Fe}(\text{pdp})(\text{CH}_3\text{CN})_2](\text{SbF}_6)_2$ -catalyzed C—H lactonization reactions.



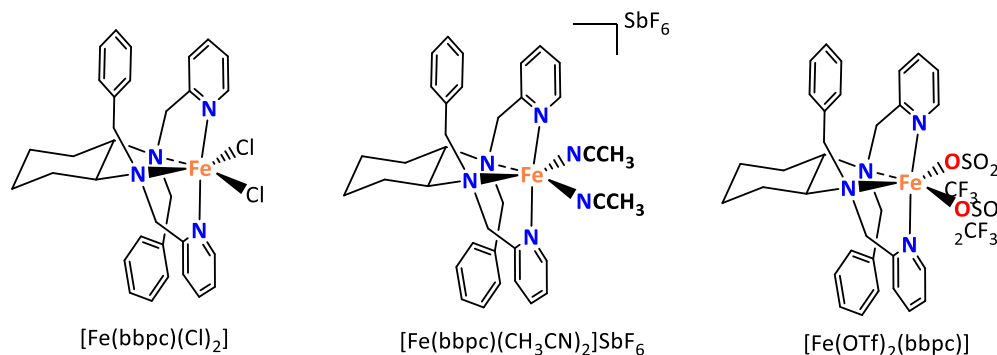
Scheme I.44. Directed oxidation of a taxane-based substrate to its lactone product with $[\text{Fe}(\text{pdp})(\text{CH}_3\text{CN})_2](\text{SbF}_6)_2$.

1.4.2.2 Novel selectivity induced by steric modifications on the catalyst architecture

A more subtle and elaborated approach exploited by enzymes relies on the use of highly spatially structured oxidizing sites that could regulate selectivity by controlling access and

orientation of the substrate in its approach toward the oxidizing unit. Pursuing this strategy, new bioinspired iron catalysts have been designed introducing steric modifications on the catalyst architecture.

In an attempt to alter the regioselectivity of non-heme iron catalysis, Goldsmith and coworkers⁸⁸ described a new mcp-modified ligand framework, where methyl groups on the aliphatic amine nitrogen atoms were replaced with benzyl groups. Three iron complexes were synthesized, $[\text{FeCl}_2(\text{bbpc})]$, $[\text{Fe}(\text{OTf})(\text{bbpc})_2]$, and $[\text{Fe}(\text{bbpc})(\text{CH}_3\text{CN})_2](\text{SbF}_6)_2$, (bbpc = *N,N'*-di(phenylmethyl)-*N,N'*-bis(2-pyridinylmethyl)-1,2-cyclohexanediamine) (Scheme 1.45), and appeared to catalyze the oxidation of alkanes by H_2O_2 , being the hexafluoroantimonate complex the most active and selective of the series for alkane hydroxylation.



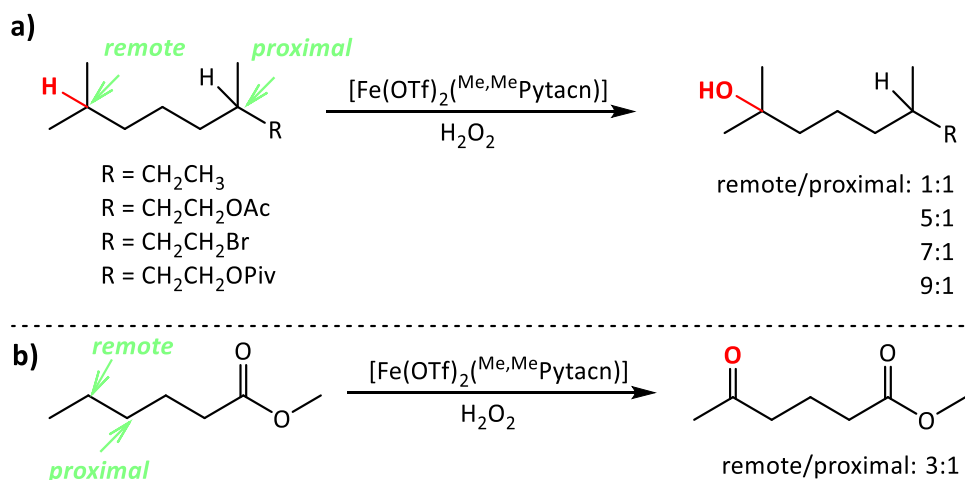
Scheme 1.45. Benzyl-modified mcp iron catalysts for efficient alkane oxidation reactions.

Interestingly, the bulk installed on the ligand architecture happened to direct the oxidation toward the less sterically hindered positions of alkane substrates. Upon reaction of $[\text{Fe}(\text{bbpc})(\text{CH}_3\text{CN})_2](\text{SbF}_6)_2$ (15 mol%) with *cis*- and *trans*-1,2-DMCH preferential oxidation for tertiary and secondary sites was observed, respectively. As previously mentioned, this can be explained in terms of strain release of 1,3-diaxial interactions. Interestingly, when comparing these results with previously described catalysts under the same catalytic conditions, a clear preference for oxidation at the secondary position was observed for both substrates. Despite the high catalyst loading employed, yields obtained are modest (~ 30%). This effect might be attributed to the steric hindrance offered by *N*-benzyl group.

In a recent work by Prat et al,⁶¹ $[\text{Fe}(\text{OTf})_2(\text{Me,MePytacn})]$ (Me,MePytacn = 1-(6-methyl-2-pyridylmethyl)-4,7-dimethyl-1,4,7-triazacylononane) was described as an efficient catalyst

with enhanced preference for oxidizing methylenic sites. Interestingly, low catalyst loadings (3 mol%) were used in this protocol, and the addition of acetic acid appeared not to be strictly required for efficient catalysis, indicating the remarkably facile O–O lysis for this catalyst.

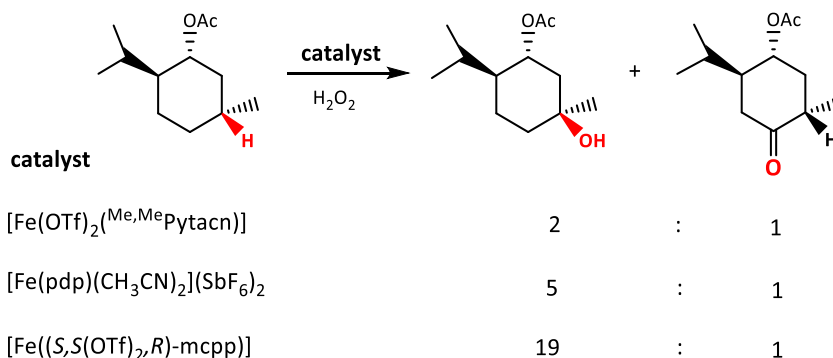
Following the same trend as the previously mentioned catalysts, alkane C–H oxidation with $[\text{Fe}(\text{OTf})_2(\text{Me},\text{MePytacn})]$ occurred preferentially at remote positions from EWGs, indicating its electrophilic nature (Scheme I.46, a). The obtained remote/proximal ratios were virtually the same as those attained with catalysts $[\text{Fe}(\text{pdp})(\text{CH}_3\text{CN})_2](\text{SbF}_6)_2$ and $[\text{Fe}(\text{OTf})_2(\text{S},\text{S},\text{R})\text{-mcpp}]$ (for comparison see Scheme I.30 and Scheme I.37, respectively). However, using $[\text{Fe}(\text{OTf})_2(\text{Me},\text{MePytacn})]$ significant amount of secondary site oxidation (ketone formation) was observed. Moreover, methylene oxidation was also sensitive to the electronic properties of the C–H bonds, as shown in the oxidation of methyl hexanoate (Scheme I.46, b).



Scheme I.46. Oxidation of substrates with electronically different groups by $[\text{Fe}(\text{OTf})_2(\text{Me},\text{MePytacn})]$.

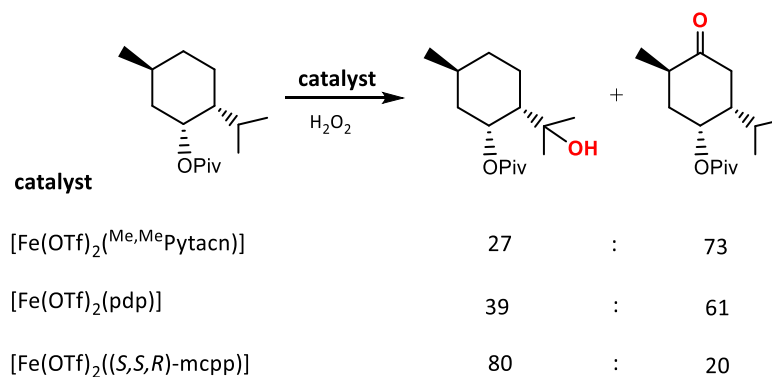
Steric effects on the substrate also appeared to play a role in the oxidation reactions. An interesting example is 1,1-DMCH, which oxidation indicated that oxidation at adjacent position to the methyl groups was disfavored because of steric encumbrance, and the other two methylenic sites were thus favored. The enhanced selectivity for secondary sites was best illustrated in the oxidation of (–)-menthyl acetate, which furnished a ~ 2:1 mixture of tertiary alcohol:ketone resulting from selective oxidation at a methylenic site. This behavior was in stark contrast with that offered by $[\text{Fe}(\text{pdp})(\text{CH}_3\text{CN})_2](\text{SbF}_6)_2$ ^{62,63} and $[\text{Fe}(\text{OTf})_2(\text{S},\text{S},\text{R})\text{-mcpp}]$.

mcpp)]⁸⁰ under analogous conditions, which fairly selectively hydroxylate the most sterically exposed tertiary C–H bond (5:1 A/K and 19:1 A/K, respectively, Scheme I.47).



Scheme I.47. Oxidation of (–)-menthyl acetate with various catalysts described in the literature.

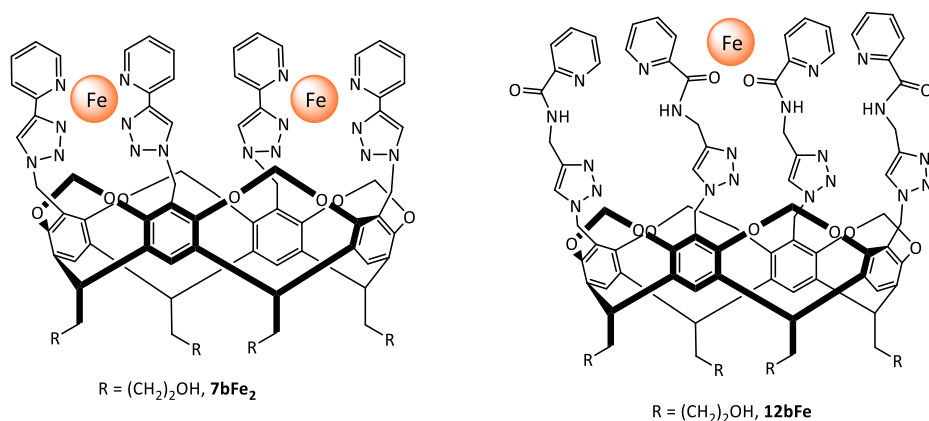
On the other hand, in the oxidation of *trans*-cyclohexane-based substrates, oxidation at methylenic positions was found to be in competition with that of tertiary C–H bonds. *trans*-1,2-DMCH yielded a normalized 24:76 3^o/2^o ratio, and this trend was even more significant in the oxidation of *trans*-decaline (4:96), indicating that products arising from methylene oxidation are largely dominant. The rationale for this behavior lies on the steric demand exerted by the methyl group in the α -position of the pyridine, which stayed in close proximity to the iron site. This fact favors preferential oxidation at the spatially more accessible methylenic sites in contrast to the more embedded tertiary C–H bonds. More importantly, this could be applied to divert regioselectivity in the C–H oxidation of (+)-neomenthyl esters (Scheme I.48).



Scheme I.48. Oxidation of (+)-neomenthyl pivalate with various catalysts described in the literature. Numbers indicate normalized ratio of products arising from oxidation at the tertiary and the secondary C–H bond position.

While $[\text{Fe}(\text{OTf})_2(\text{pdp})]$ offered poor discrimination between secondary and tertiary C–H bonds, $[\text{Fe}(\text{OTf})_2((S,S,R)\text{-mcpp})]$ and $[\text{Fe}(\text{OTf})_2(\text{Me,MePytacn})]$ were found to be complementary, the former yielding the tertiary alcohol as the major product (up to 80:20 normalized $3^\circ/2^\circ$ ratio), and the latter affording preferential oxidation at the methylenic site (up to 27:73 normalized $3^\circ/2^\circ$ ratio).

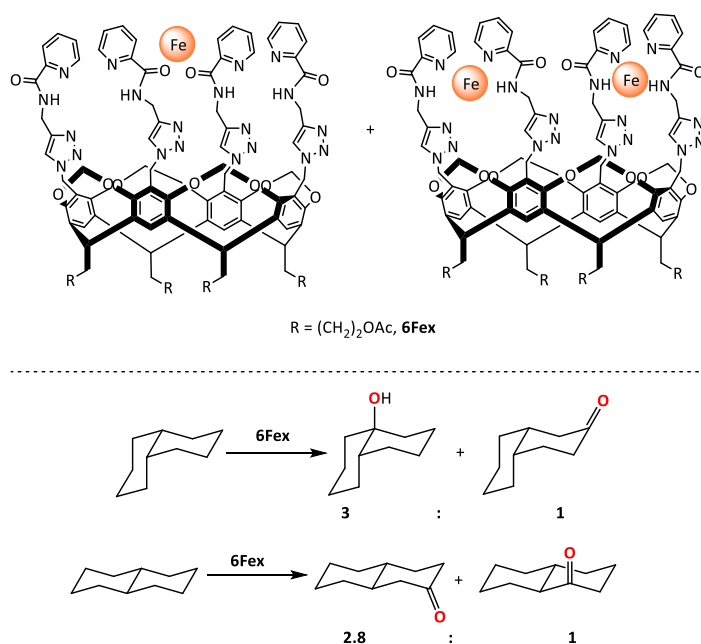
A different approach was proposed by Hooley and coworkers.⁸⁹ In this study resorcinarene-based cavitands were used as catalysts, which allow for binding of iron(II) by bidentate ligands, leaving empty sites for further reactivity at the metal sites. The iron-coordinated cavitands **7bFe₂** and **12bFe** (Scheme I.49) bore free coordination sites, thus they were envisioned to perform C–H oxidation reactions under mild conditions, inspired by the mode of action of the Rieske oxygenases. However, these catalysts proved inactive towards cyclohexane and methylcyclohexane oxidations. In contrast, they were able to smoothly convert fluorene to fluorenone using TBHP as oxidant.



Scheme I.49. Resorcinarene-based cavitands used as catalysts for fluorene oxidation.

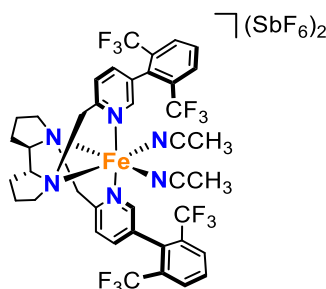
In a later study,⁹⁰ the authors showed that **6Fex** (Scheme I.50) was able of efficiently oxidizing *cis*-decaline to the tertiary alcohol (*cis*-1-decalol) and the ketone product (*cis*-3-decalone) (up to 69% yield) using TBHP. (Cautious note should be made at this point. *cis*-decaline bears a hydrogen in axial position and one in equatorial position. Although authors have no positive evidence of which of them is being oxidized, one could think that in this particular case the oxidation of the axial site is favored, due to the great steric hinderance offered by such catalysts). Interestingly, the addition of acetic acid was not strictly required for the outcome of the reaction, however large reaction times (24 hours) and high

temperature (60 °C) were needed. Good selectivity for the tertiary alcohol was obtained (up to 75% normalized regioselectivity). On the other hand, *trans*-decaline afforded *trans*-2-decalone and *trans*-3-decalone as oxidized products in a 2.8:1 ratio with 46% overall yield. Interestingly, these catalysts were also able to oxidize benzylic methylenic sites very efficiently (up to 88% yield for the oxidation of 1-ethyl-4-methyl benzene).

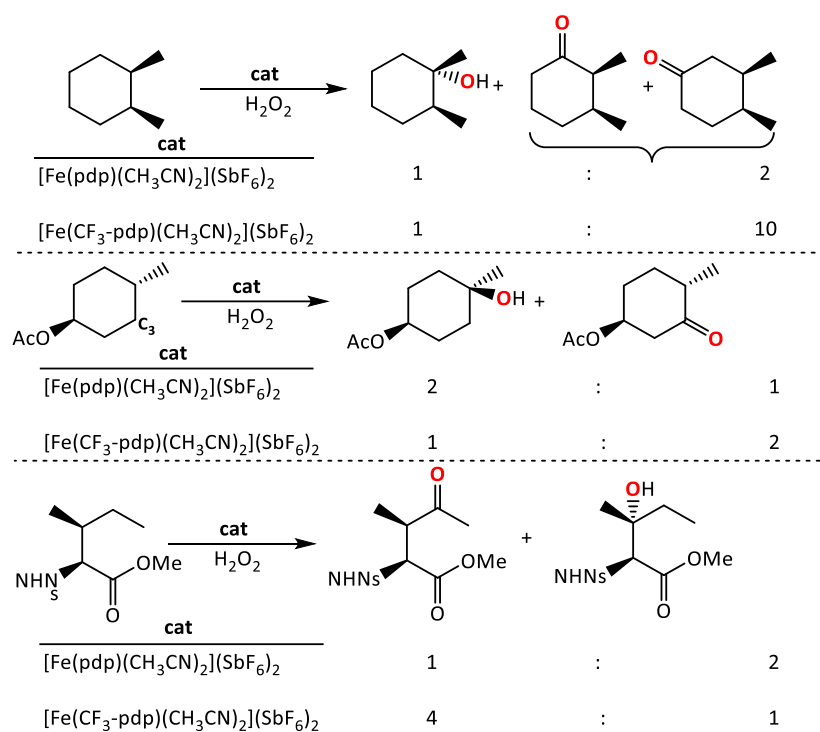


Scheme I.50. Regioselectivity in the oxidation of *cis*- and *trans*-decaline by **6Fex** and structure of the catalyst.

Finally, very recently White and coworkers⁷⁸ designed a new catalyst [Fe(CF₃-pdp)(CH₃CN)₂](SbF₆)₂, (CF₃-pdp = *N,N'*-bis(5-(2,6-di-(trifluoro)-methyl-phenyl)-2-pyridylmethyl)-2,2'-bipyrrolidine) that was proposed to use a trajectory restriction strategy to achieve predictable, catalyst-controlled site-selectivity (Scheme I.51).



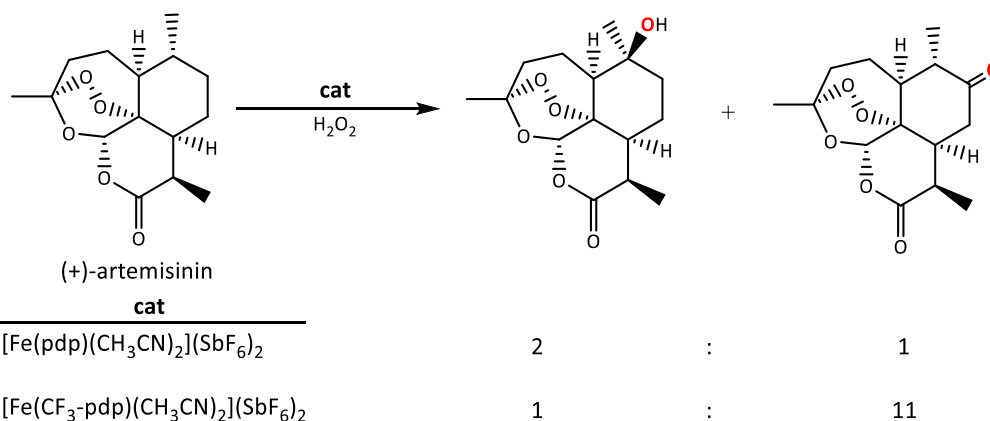
Scheme I.51. Structure of trajectory restrictive catalyst [Fe(CF₃-pdp)(CH₃CN)₂](SbF₆)₂ for catalyst-controlled site-selectivity.



Scheme I.52. Difference in regioselectivity attained with catalysts $[\text{Fe}(\text{pdp})(\text{CH}_3\text{CN})_2](\text{SbF}_6)_2$ and $[\text{Fe}(\text{CF}_3\text{-pdp})(\text{CH}_3\text{CN})_2](\text{SbF}_6)_2$.

In the oxidation of *trans*-1,2-DMCH, this catalyst exhibited enhanced selectivity towards secondary sites (10:1 2°/3° ratio), while the structurally related $[\text{Fe}(\text{pdp})(\text{CH}_3\text{CN})_2](\text{SbF}_6)_2$ catalyst provided 2:1 2°/3° ratio (Scheme I.52). On the other hand, this catalyst was able to nicely overturn the inherent reactivity of the substrates. This was the case of *trans*-4-methylcyclohexyl acetate, which gave the tertiary alcohol as major product when $[\text{Fe}(\text{pdp})(\text{CH}_3\text{CN})_2](\text{SbF}_6)_2$ was used (1:2 2°/3° ratio) but the C₃-ketone was the major product when $[\text{Fe}(\text{CF}_3\text{-pdp})(\text{CH}_3\text{CN})_2](\text{SbF}_6)_2$ was employed (2:1 2°/3° ratio). Also, the protected (+)-isoleucine changed from 1:2 to 4:1 2°/3° ratio when the sterically encumbered catalyst was used to oxidize this substrate.

This strategy was further investigated in the oxidation of complex molecules such as (+)-artemisinin, where 2 products are yielded: (+)-10 β -hydroxy-artemisinin (3° site) and (+)-9-oxo-artemisinin (2° site). While $[\text{Fe}(\text{pdp})(\text{CH}_3\text{CN})_2](\text{SbF}_6)_2$ catalyst afforded 2:1 2°/3° ratio, $[\text{Fe}(\text{CF}_3\text{-pdp})(\text{CH}_3\text{CN})_2](\text{SbF}_6)_2$ yielded 11:1 2°/3° ratio, the latter being able to override a strong electronic substrate bias (Scheme I.53).

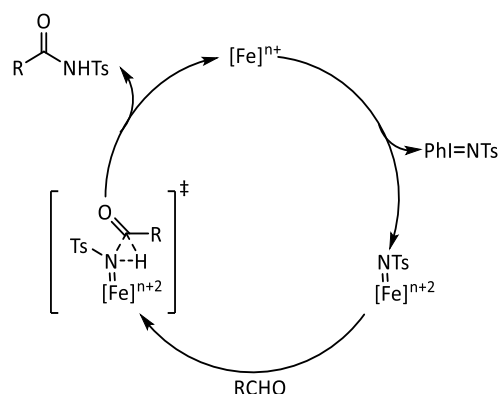


Scheme I.53. Oxidation of artemisinin with $[\text{Fe}(\text{pdp})(\text{CH}_3\text{CN})_2](\text{SbF}_6)_2$ and $[\text{Fe}(\text{CF}_3\text{-pdp})(\text{CH}_3\text{CN})_2](\text{SbF}_6)_2$.

I.5 NOVEL REACTIVITY OF MONONUCLEAR NON-HEME IRON CATALYSTS: N-INSERTION REACTIONS INTO C–H BONDS FOR THE FORMATION OF AMIDES, AMINES AND N-HETEROCYCLES

Catalytic N-insertion into C–H bonds using mononuclear iron complexes has been explored for more than 30 years. However, in these pioneer reports the reactivity was limited to intramolecular insertions or intermolecular insertions into weak C–H bonds.^{91–96} The topic has however experienced very remarkable accomplishments during the last three years.

In 2011, Che and coworkers reported the nitrene insertion reaction into benzaldehydes, and linear and cyclic alkylic aldehydes for the construction of amide compounds using FeCl_2 , terpyridine as ligand and $\text{PhI}=\text{NTs}$ ($\text{Ts} = \text{tosyl}$) as oxidant, under mild conditions.⁹⁷ In this work the authors showed that this methodology smoothly worked for differently substituted benzaldehydes. Interestingly, the system seemed to be more efficient for preparing amides from aliphatic aldehydes than from aryl aldehydes, yielding the insertion products up to 89% yield in the case of isopropyl aldehyde. Moreover, they proposed a high valent iron imido complex $[\text{Fe}(\text{terpy})_2(\text{NTs})]^{2+}$ as active species (Scheme I.54), as observed by ESI-MS studies.

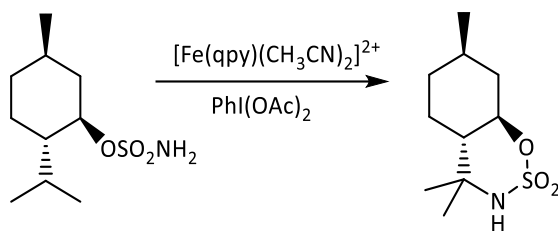


Scheme I.54. Proposed catalytic cycle for iron-catalyzed nitrene C—H insertion reactions.

Iron-catalyzed intramolecular allylic C—H amination was reported by White and coworkers using $[\text{Fe}(\text{Pc})]^+$ (Pc = phthalocyanine).⁹⁸ Silver salt as additive, toluene:acetonitrile solvent mixture and $\text{PhI}(\text{OPiv})_2$ as oxidant were found as key factors for the optimal allylic amination of sulfamate esters. This methodology was effective not only for the amination of styrenyl, trisubstituted, terminal and cyclic allylic C—H bonds, but also for benzylic and tertiary alkylic sites, which occurred with retention of the configuration. Good to moderate yields were obtained for this type of reactions, and high ratio insertion product/aziridination was achieved. In a competitive study with substrates bearing more than one site susceptible to be aminated, the authors demonstrated that allylic C—H bonds were more reactive than benzylic, which were in turn more easily aminated than alkylic sites. Mechanistic probes showed modest KIE values and stereoretention in amination of tertiary C—H centers. However, scrambling of the double bond geometry occurred during allylic amination.

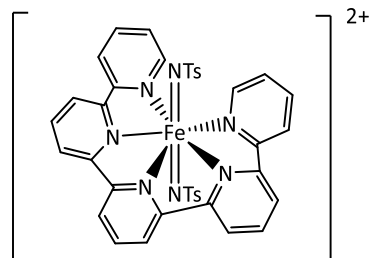
Very recently, Che and coworkers have described the catalytic amination of C—H bonds using $[\text{Fe}(\text{qpy})(\text{CH}_3\text{CN})_2]^{2+}$ as catalyst.⁹⁹ Very good yields were achieved for the intramolecular amination of benzylic and allylic sulfamate esters, up to 92% yield in presence of electron donating groups in the aryl moiety. In a competitive study with substrates with more than one possible C—H to be aminated the authors demonstrated that benzylic sites were more easily aminated than allylic, and allylic C—H bonds were more reactive than aliphatic sites. Very interestingly, they applied this methodology to the amination of natural products derivatized with sulfamate ester groups, such as terpenes and steroids. By doing so, for

example, a menthyl sulfamate ester was exclusively aminated at the tertiary alkylic C–H bond in 93% yield (Scheme I.55). Intermolecular amination of benzylic and allylic C–H bonds was also performed obtaining very good yields for activated benzylic sites, good yields for non-activated benzylic C–H bonds and moderate to good yields for the amination of allylic sites. C–H bonds of cyclohexanes were also effectively aminated with this protocol, either by using $\text{PhI}=\text{NTs}$ or a more convenient *in-situ* generated oxidant $\text{PhI}(\text{OAc})_2 + \text{H}_2\text{NTs}$ without much loss of activity.



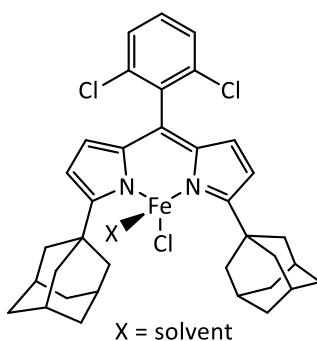
Scheme I.55. Amination of menthyl sulfamate ester by $[\text{Fe}(\text{qpy})(\text{CH}_3\text{CN})_2]^{2+}$.

In order to shed light in the species involved in this reaction, the authors performed high resolution-ESI-MS studies on this catalytic system, where they observed a peak corresponding to the mass of the $[\text{Fe}(\text{qpy})(\text{NTs})_2]^{2+}$ species (Scheme I.56). Such an analogous peak could not be found when the less active $[\text{Fe}(\text{N4Py})(\text{MeCN})](\text{ClO}_4)_2$ ($\text{N4Py} = N,N'$ -bis(2-pyridylmethyl)- N -bis(2-pyridyl)methyl-amine) or $[\text{Fe}(\text{Cl}_3\text{terpy})_2](\text{ClO}_4)_2$ ($\text{terpy} = 2,2':6',2''$ -terpyridine) were used as catalysts, which might explain their difference in reactivity. Kinetic isotopic effect was investigated for the amination of cyclohexane with $\text{PhI}=\text{NTs}$ using catalyst $[\text{Fe}(\text{qpy})(\text{MeCN})_2]^{2+}$, and was determined to be 4.0 at 25 °C. The Hammett plot for the reaction of *para*-substituted ethylbenzenes with $\text{PhI}=\text{NTs}$ showed a negative slope ($\rho = -0.55$), while the plot for the reaction of ethylbenzene and *para*-substituted oxidants showed a positive slope ($\rho = 1.14$). In addition, the C–H bond dissociation energy (BDE) of different substrates correlated well with their relative amination rate. All this data together point towards an electrophilic oxidant that operates *via* hydrogen atom abstraction.



Scheme I.56. Structure for the proposed iron—imide/nitrene intermediate involved in amination reactions mediated by $[\text{Fe}(\text{qpy})(\text{MeCN})_2]^{2+}$.

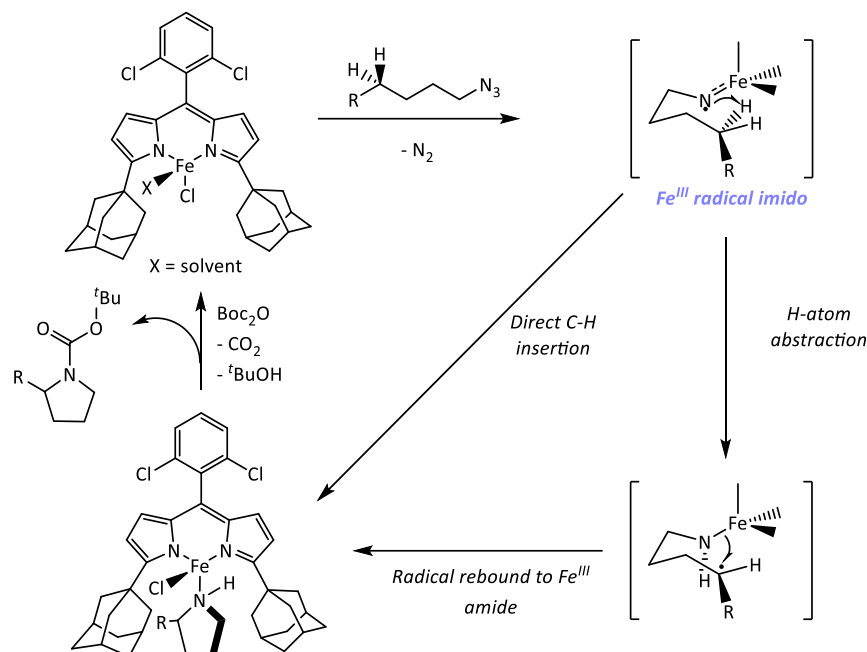
Finally, also in 2013, Betley and coworkers reported the synthesis of complex N-heterocycles via iron-catalyzed, direct C–H bond amination.¹⁰⁰ A ferrous dipyrinato complex $[\text{Fe}(\text{L})]\text{Cl}$ (L = adamantyl-dipyrromethene-2,6- $\text{Cl}_2\text{C}_6\text{H}_3$) (Scheme I.57) was used to catalyze the intramolecular C–H amination of various azides, which required *in-situ* protection of the final product. Exposure of substrates containing allylic, benzylic, or tertiary C–H bonds to this reaction protocol provided the corresponding protected pyrrolidine in good isolated yields (up to 75%).



Scheme I.57. Structure of catalyst $[\text{Fe}(\text{L})]\text{Cl}$ (L = adamantyl-dipyrromethene-2,6- $\text{Cl}_2\text{C}_6\text{H}_3$).

The authors also investigated the potential of this methodology to generate N-heterocycles of various ring sizes, and were able to synthesize pyrrolidines, piperidines and azetidines. The C–H bond functionalization was proposed to occur through oxidation of the Fe^{II} catalyst to a Fe^{III} imido radical by the alkyl azide substrate, followed by the intramolecular hydrogen atom abstraction to generate an alkyl radical and a Fe^{III} amide (Scheme I.58). Finally, a radical recombination would take place to render the observed N-heterocyclic product. The H-atom abstraction pathway was favored in front of a possible direct N-insertion alternative due to the KIE of 5.3 found for the cyclization of 1-azido-4-deutero-phenylbutane, although the carbon radical must be very short-lived because no radical rearrangement is observed

for the addition of the radical clock substrate (2-(4-azidobutyl)cyclopropyl)benzene (recombination rate $> 10^{11} \text{ s}^{-1}$).



Scheme 1.58. Proposed mechanism for N-heterocycle formation with $[\text{Fe}(\text{L})\text{Cl}]$ (L = adamantyl-dipyrromethene-2,6- $\text{Cl}_2\text{C}_6\text{H}_3$).

I.6 FUTURE CHALLENGES IN C–H BOND OXIDATIONS CATALYZED BY NON-HEME IRON COMPLEXES

Although many efforts have been devoted to clarify the nature of the active species involved in non-heme iron catalyzed C–H bond functionalization reactions, most specially in C–H oxidations, a complete characterization of such species is still lacking. This is due to the fact that high-valent iron species capable of attacking strong C–H bonds are extremely reactive, and thus it is particularly difficult that they could accumulate in solution in amounts that could sustain a proper spectroscopic characterization. Cryogenic techniques, novel ligand platforms that could provide enhanced stability to these species as well as innovative methods for generating and accumulating these species are needed and will represent very valuable steps towards understanding and mastering of this chemistry.

Moreover, selectivity patterns are still often dictated by the nature of the C–H bonds in the substrate. Some advances have been achieved in the field; however a tool-box of catalysts

that allow for a completely alternative selectivity in a broad range of substrates is yet to be reported.

Finally, the chiral nature of the catalysts could be applied to induce stereoselectivity via C—H functionalization of non-chiral substrates. Asymmetric C—H functionalization of alkyl C—H bonds remains as one of the holy grails of modern chemistry, but the findings that selected iron catalyzed C—H bond functionalization reactions are metal based devoid of free radical processes has opened a promising path towards this goal.

Summarizing, as our knowledge on iron based enzymatic catalysis grows, novel reactions are being incorporated into the “wishful thinking” of future bioinspired oxidation catalysts. For example, alkyl C—H desaturation,⁷⁷ halogenation,¹⁰¹ and oxidative carbocyclization reactions¹⁰² constitute remarkable examples of this flourishing field.

I.7 REFERENCES

- (1) Sheldon, R. A.; Kochi, J. A. *Metal-Catalyzed Oxidations of Organic Compounds*; Academic Press: New York, 1981.
- (2) Dyker, G. *Handbook of C-H Transformations*; Wiley-VCH: Weinheim, 2005; Vol. 1-2.
- (3) Shilov, A. E.; Shul'pin, G. B. *Activation and Catalytic Reactions of Saturated Hydrocarbons in the Presence of Metal Complexes*; Verlag, S.-, Ed.; Boston, 2000.
- (4) Gutekunst, W. R.; Baran, P. S. *Chem. Soc. Rev.* **2011**, *40*, 1976.
- (5) McMurray, L.; O'Hara, F.; Gaunt, M. J. *Chem. Soc. Rev.* **2011**, *40*, 1885.
- (6) Che, C.-M.; Lo, V. K.-Y.; Zhou, C.-Y.; Huang, J.-S. *Chem. Soc. Rev.* **2011**, *40*, 1950.
- (7) Labinger, J. A.; Bercaw, J. E. *Nature* **2002**, *417*, 507.
- (8) Godula, K.; Sames, D. *Science* **2006**, *312*, 67.
- (9) Chen, K.; Baran, P. S. *Nature* **2009**, *459*, 824.
- (10) Costas, M.; Mehn, M. P.; Jensen, M. P.; Que Jr., L. *Chem. Rev.* **2004**, *104*, 939.
- (11) Que Jr., L.; Tolman, W. B. *Nature* **2008**, *455*, 333.

-
- (12) Cotton, F. A.; Wilkinson, G.; Murillo, C. A.; Bochmann, M. In *Advanced Inorganic Chemistry*; John Wiley & Sons: New York, 1999.
- (13) Meunier, B.; Bernadou, J. *Struct. Bond.* **2000**, *97*, 1.
- (14) Meunier, B.; de Visser, S. P.; Shaik, S. *Chem. Rev.* **2004**, *104*, 3947.
- (15) Montellano, P. O. de. *Cytochrome P450 : Structure, Mechanism, and Biochemistry*, 3rd edition; Springer, 2004.
- (16) Schlichting, I.; Berendzen, J.; Chu, K.; Stock, A. M.; Maves, S. A.; Benson, D. E.; Sweet, R. M.; Ringe, D.; Petsko, G. A.; Sligar, S. G. *Science* **2000**, *287*, 1615.
- (17) Kraatz, H.-B.; Metzler-Nolte, N. *Concepts and Models in Bioinorganic Chemistry*; Wiley-VCH: Weinheim, 2006.
- (18) Wallar, B. J.; Lipscomb, J. D. *Chem. Rev.* **1996**, *96*, 2625.
- (19) Groves, J. T.; McCluskey, G. A. *J. Am. Chem. Soc.* **1976**, *98*, 859.
- (20) Aldrich-Wright, J. R.; Vagg, R. S.; Williams, P. A. *Coord. Chem. Rev.* **1997**, *166*, 361.
- (21) Knof, U.; von Zelewsky, A. *Angew. Chem. Int. Ed.* **1999**, *38*, 302.
- (22) Sono, M.; Roach, M. P.; Coulter, E. D.; Dawson, J. H. *Chem. Rev.* **1996**, *96*, 2841.
- (23) Bruijninx, P. C. A.; van Koten, G.; Klein Gebbink, R. J. M. *Chem. Soc. Rev.* **2008**, *37*, 2716.
- (24) Gibson, D. T.; Subramanian, V. In *Microbial Degradation of Aromatic Hydrocarbons*; Gibson, D. T., Ed.; Marcel Dekker: New York, 1984; p. 535.
- (25) Gibson, D. T.; Resnick, S. M.; Lee, K.; Brand, J. M.; Torok, D. S.; Wackett, L. P.; Schocken, M. J.; Haigler, B. E. *J. Bacteriol.* **1995**, *177*, 2615.
- (26) Wolfe, M. D.; Parales, J. V.; Gibson, D. T.; Lipscomb, J. D. *J. Biol. Chem.* **2001**, *276*, 1945.
- (27) Gibson, D. T.; Parales, R. E. *Curr. Opin. Biotechnol.* **2000**, *11*, 236.
- (28) Hudlicky, T.; Gonzalez, D.; Gibson, D. T. *Aldrichimica Acta* **1999**, *32*, 35.
- (29) Hegg, E. L.; Que Jr., L. *Eur. J. Biochem.* **1997**, *250*, 625.
- (30) Koehntop D., K.; Emerson, J. P.; Que Jr., L. *J. Biol. Inorg. Chem.* **2005**, *10*, 87.
- (31) Kauppi, B.; Lee, K.; Carredano, E.; Parales, R. E.; Gibson, D. T.; Eklund, H.; Ramaswamy, S. *Structure* **1998**, *6*, 571.

-
- (32) Karlsson, A.; Parales, J. V.; Parales, R. E.; Gibson, D. T.; Eklund, H.; Ramaswamy, S. *Science* **2003**, *299*, 1039.
- (33) Wolfe, M. D.; Altier, D. J.; Stubna, A.; Popescu, C. V.; Münck, E.; Lipscomb, J. D. *Biochemistry* **2002**, *41*, 9611.
- (34) Wolfe, M. D.; Lipscomb, J. D. *J. Biol. Chem.* **2003**, *278*, 829.
- (35) Chakrabarty, S.; Austin, R. N.; Deng, D.; Groves, J. T.; Lipscomb, J. D. *J. Am. Chem. Soc.* **2007**, *129*, 3514.
- (36) Meunier, B. *Biomimetic Oxidations Catalyzed by Transition Metal Complexes*; Meunier, B., Ed.; Imperial College Press: London, 2000.
- (37) Sheldon, R. A.; Arends, I. W. C. E.; Hanefeld, U. *Green Chemistry and Catalysis*; WILEY-VCH Verlag GmbH, 2007.
- (38) Walling, C. *Acc. Chem. Res.* **1998**, *31*, 155.
- (39) Stavropoulos, P.; Celenligil-Cetin, R.; Tapper, A. E. *Acc. Chem. Res.* **2001**, *34*, 745.
- (40) Curci, R.; d'Accolti, L.; Fusco, C. *Acc. Chem. Res.* **2006**, *39*, 1.
- (41) Fokin, A. A.; Schreiner, P. R. *Chem. Rev.* **2002**, *102*, 1551.
- (42) Kim, J.; Harrison, R. G.; Kim, C.; Que Jr., L. *J. Am. Chem. Soc.* **1996**, *118*, 4373.
- (43) Arends, I. W. C. E.; Ingold, K. U.; Wayner, D. D. M. *J. Am. Chem. Soc.* **1995**, *117*, 4710.
- (44) MacFaul, P. A.; Ingold, K. U.; Wayner, D. D. M.; Que Jr., L. *J. Am. Chem. Soc.* **1997**, *119*, 10594.
- (45) Chen, K.; Que Jr., L. *J. Am. Chem. Soc.* **2001**, *123*, 6327.
- (46) Groves, J. T.; Nemo, T. E. *J. Am. Chem. Soc.* **1983**, *105*, 6243.
- (47) Khenkin, A. M.; Shilov, A. E. *New J. Chem.* **1989**, *13*, 659.
- (48) Sorokin, A. B.; Khenkin, A. M. *New J. Chem.* **1990**, *14*, 63.
- (49) Dores Assis, M.; Lindsay Smith, J. R. *J. Chem. Soc., Perkin Trans. 2* **1998**, 2221.
- (50) Company, A.; Gómez, L.; Güell, M.; Ribas, X.; Luis, J. M.; Que, L.; Costas, M. *J. Am. Chem. Soc.* **2007**, *129*, 15766.
- (51) Costas, M.; Chen, K.; Que Jr., L. *Coord. Chem. Rev.* **2000**, *200-202*, 517.
- (52) Kim, C.; Chen, K.; Kim, J.; Que Jr., L. *J. Am. Chem. Soc.* **1997**, *119*, 5964.
- (53) Chen, K.; Que Jr., L. *Chem. Commun.* **1999**, 1375.

-
- (54) Britovsek, G. J. P.; England, J.; White, A. J. P. *Inorg. Chem.* **2005**, *44*, 8125.
- (55) Toftlund, H.; Pedersen, E.; Yde-Adersen, S. *Acta Chem. Scand., Ser. A* **1984**, *38*, 693.
- (56) Okuno, T.; Ito, S.; Ohba, S.; Nishida, Y. *J. Chem. Soc., Dalton Trans.* **1997**, 3547.
- (57) England, J.; Davies, C. R.; Banaru, M.; White, A. J. P.; Britovsek, G. J. P. *Adv. Synth. Catal.* **2008**, *350*, 883.
- (58) England, J.; Gondhia, R.; Bigorra-Lopez, L.; Petersen, A. R.; White, A. J. P.; Britovsek, G. J. P. *Dalton Trans.* **2009**, *27*, 5319.
- (59) Clemente-Tejeda, D.; López-Moreno, A.; Bermejo, F. A. *Tetrahedron* **2012**, *68*, 9249.
- (60) Company, A.; Gómez, L.; Fontrodona, X.; Ribas, X.; Costas, M. *Chem. Eur. J.* **2008**, *14*, 5727.
- (61) Prat, I.; Gómez, L.; Canta, M.; Ribas, X.; Costas, M. *Chem. Eur. J.* **2013**, *19*, 1908.
- (62) Chen, M. S.; White, M. C. *Science* **2007**, *318*, 783.
- (63) Chen, M. S.; White, M. C. *Science* **2010**, *327*, 566.
- (64) Comba, P.; Maurer, M.; Vadivelu, P. *Inorg. Chem.* **2009**, *48*, 10389.
- (65) Liu, P.; Liu, Y.; Wong, E.; Xiang, S.; Che, C.-M. *Chem. Sci.* **2011**, *2*, 2187.
- (66) Hitomi, Y.; Arakawa, K.; Funabiki, T.; Kodera, M. *Angew. Chem. Int. Ed.* **2012**, *51*, 3448.
- (67) Ho, R. Y. N.; Roelfes, G.; Feringa, B. L.; Que Jr., L. *J. Am. Chem. Soc.* **1999**, *121*, 264.
- (68) Kim, J. Mechanistic studies of oxygen atom transfer at nonheme iron centers, Univ. of Minnesota: Minneapolis, 1995, p. 135.
- (69) Goh, Y. M.; Nam, W. *Inorg. Chem.* **1999**, *38*, 914.
- (70) Bernadou, J.; Meunier, B. *Chem. Commun.* **1998**, 2167.
- (71) Bassan, A.; Blomberg, M. R. A.; Siegbahn, P. E. M.; Que Jr., L. *J. Am. Chem. Soc.* **2002**, *124*, 11056.
- (72) Quiñonero, D.; Morokuma, K.; Musaev, D. G.; Mas-Balleste, R.; Que Jr., L. *J. Am. Chem. Soc.* **2005**, *127*, 6548.
- (73) Prat, I.; Mathieson, J. S.; Güell, M.; Ribas, X.; Luis, J. M.; Cronin, L.; Costas, M. *Nat. Chem.* **2011**, *3*, 788.
- (74) Oloo, W. N.; Fielding, A. J.; Que, L. *J. Am. Chem. Soc.* **2013**, *135*, 6438.

-
- (75) Prat, I.; Company, A.; Postils, V.; Ribas, X.; Que Jr, L.; Luis, J. M.; Costas, M. *Chem. Eur. J.* **2013**, *19*, 6724.
- (76) Mitra, M.; Lloret-Fillol, J.; Haukka, M.; Costas, M.; Nordlander, E. *Chem. Commun.* **2014**, *50*, 1408.
- (77) Bigi, M. A.; Reed, S. A.; White, M. C. *Nat. Chem.* **2011**, *3*, 216.
- (78) Gormisky, P. E.; White, M. C. *J. Am. Chem. Soc.* **2013**, *135*, 14052.
- (79) Chen, K.; Eschenmoser, A.; Baran, P. S. *Angew. Chem. Int. Ed.* **2009**, *48*, 9705.
- (80) Gómez, L.; Garcia-Bosch, I.; Company, A.; Benet-Buchholz, J.; Polo, A.; Sala, X.; Ribas, X.; Costas, M. *Angew. Chem. Int. Ed.* **2009**, *48*, 5720.
- (81) Newhouse, T.; Baran, P. S. *Angew. Chem. Int. Ed.* **2011**, *50*, 3362.
- (82) Chen, K.; Richter, J. M.; Baran, P. S. *J. Am. Chem. Soc.* **2008**, *130*, 7247.
- (83) Kasuya, S.; Kamijo, S.; Inoue, M. *Org. Lett.* **2009**, *11*, 3630.
- (84) Simmons J. F., Hsrtwig, E. M. *Nature* **2012**, *483*, 70.
- (85) Zhang, S.-Y.; He, G.; Zhao, Y.; Wright, K.; Nack, W. A.; Chen, G. *J. Am. Chem. Soc.* **2012**, *134*, 7313.
- (86) Wang, Y.-F.; Chen, H.; Zhu, X.; Chiba, S. *J. Am. Chem. Soc.* **2012**, *134*, 11980.
- (87) Bigi, M. A.; Reed, S. A.; White, M. C. *J. Am. Chem. Soc.* **2012**, *134*, 9721.
- (88) He, Y.; Gorden, J. D.; Goldsmith, C. R. *Inorg. Chem.* **2011**, *50*, 7431.
- (89) Djernes, K. E.; Moshe, O.; Mettry, M.; Richards, D. D.; Hooley, R. J. *Org. Lett.* **2012**, *14*, 788.
- (90) Djernes, K. E.; Padilla, M.; Mettry, M.; Young, M. C.; Hooley, R. J. *Chem. Commun.* **2012**, *48*, 11576.
- (91) Svastits, E. W.; Dawson, J. H.; Breslow, R.; Gellman, S. H. *J. Am. Chem. Soc.* **1985**, *107*, 6427.
- (92) Breslow, R.; Gellman, S. H. *J. Am. Chem. Soc.* **1983**, *105*, 6728.
- (93) Wang, Z.; Zhang, Y.; Fu, H.; Jiang, Y.; Zhao, Y. *Org. Lett.* **2008**, *10*, 1863.
- (94) Breslow, R.; Gellman, S. H. *J. Chem. Soc. Chem. Commun.* **1982**, 1400.
- (95) Yan, S.-Y.; Wang, Y.; Shu, Y.-J.; Liu, H.-H.; Zhou, X.-G. *J. Mol. Catal. A Chem.* **2006**, *248*, 148.

- (96) King, E. R.; Hennessy, E. T.; Betley, T. A. *J. Am. Chem. Soc.* **2011**, *133*, 4917.
- (97) Liu, Y.; Guan, X.; Wong, E. L.-M.; Liu, P.; Huang, J.-S.; Che, C.-M. *Synlett* **2011**, *8*, 1174.
- (98) Paradine, S. M.; White, M. C. *J. Am. Chem. Soc.* **2012**, *134*, 2036.
- (99) Liu, Y.; Guan, X.; Wong, E. L.-M.; Liu, P.; Huang, J.-S.; Che, C.-M. *J. Am. Chem. Soc.* **2013**, *135*, 7194.
- (100) Hennessy, E. T.; Betley, T. A. *Science*. **2013**, *340*, 591.
- (101) Vaillancourt, H.; Yeh, E.; Vosburg, D. A.; Garneau-Tsodikova, S.; Walsh, C. T. **2006**, 3364.
- (102) Sydor, P. K.; Barry, S. M.; Odulate, O. M.; Barona-Gomez, F.; Haynes, S. W.; Corre, C.; Song, L.; Challis, G. L. *Nat. Chem.* **2011**, *3*, 388.

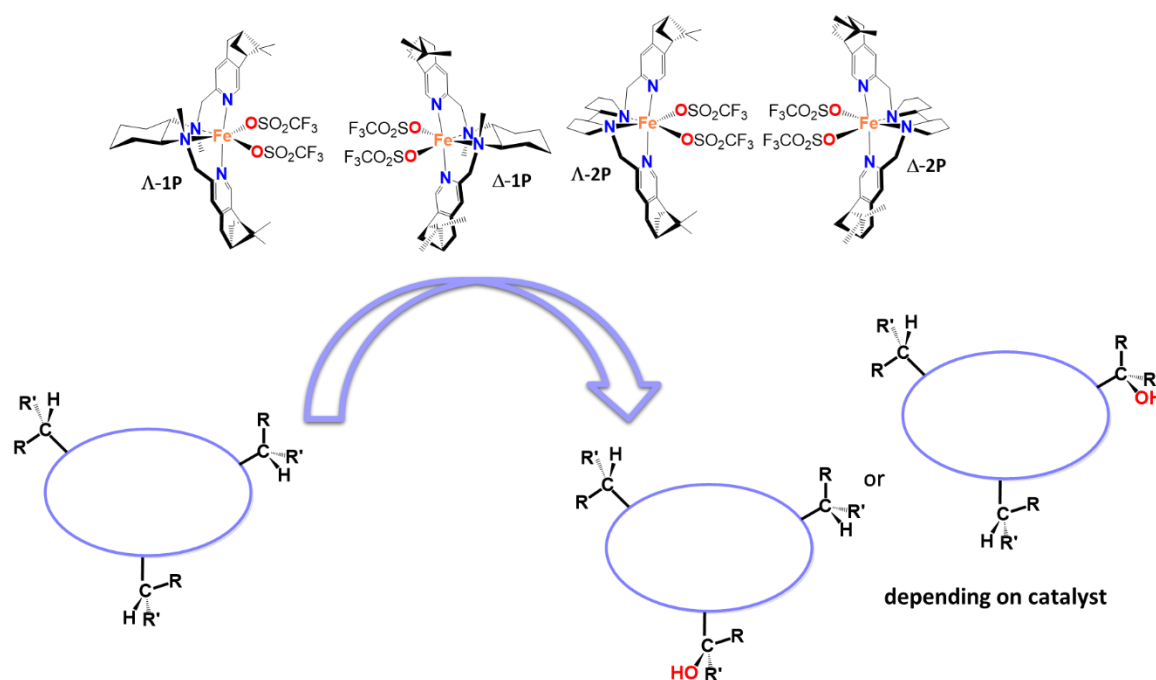
CHAPTER II

MAIN OBJECTIVES

II. MAIN OBJECTIVES

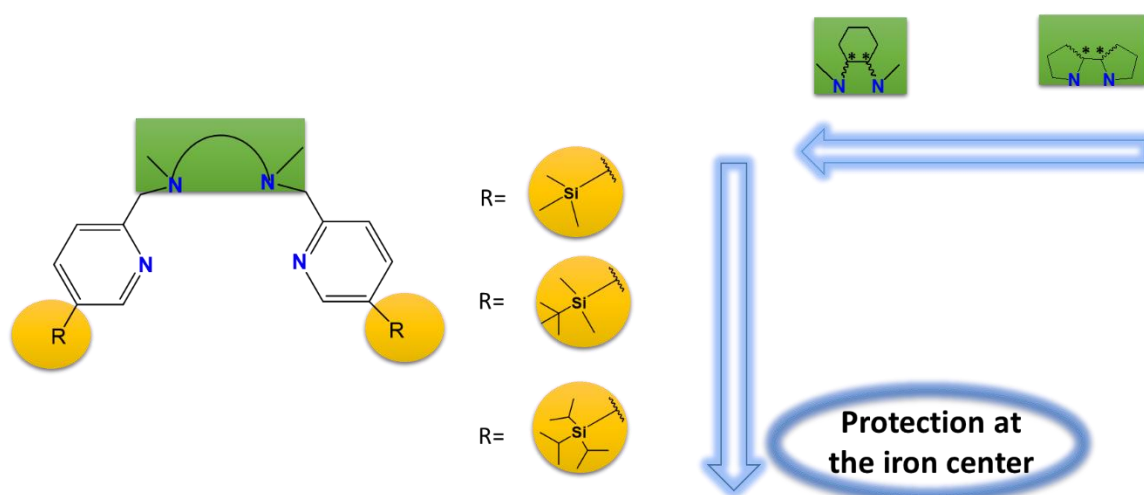
Taking as source of inspiration the highly efficient and selective oxidation reactions mediated by natural metalloenzymes, which occur under very mild conditions, in this dissertation we have explored the selectivity bases of C—H oxidation reactions attained by non-heme iron catalysts that contain structural elements that confer the metal center with a certain degree of steric hindrance.

Towards this end, a new family of non-heme iron catalysts was recently developed in our research group by introducing bulky pinene rings at the catalyst scaffold.¹ Based on this work, in the first part of this thesis (Chapter III) we aim to thoroughly study the selectivity bases in C—H oxidation reactions exhibited by this family of catalysts, and explore the role of the steric bulk around the metal center in defining the C—H selectivity. The catalytic performance and selectivity will be examined in the oxidation of tertiary and secondary C—H groups in alkanes using hydrogen peroxide as oxidant which, in combination with iron, make it an environmentally friendly oxidation system. Moreover, we seek to apply this toolbox of catalysts to override the intrinsic C—H reactivity imposed by the substrates and to divert the selectivity in the oxidation of complex molecules such as natural products.



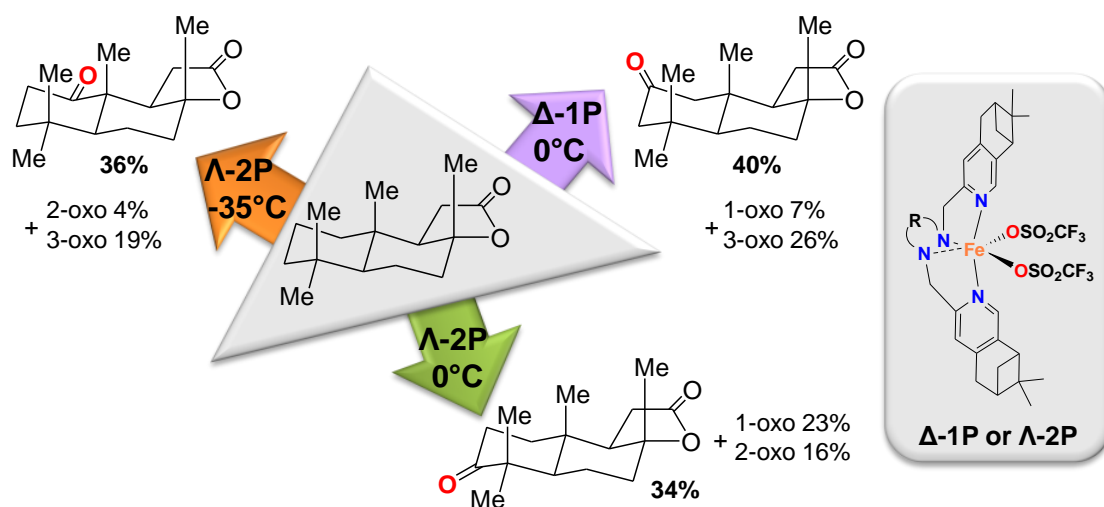
In the second part of this dissertation (Chapter IV) we seek to evaluate the catalytic activity of the readily available $[\text{Fe}(\text{CF}_3\text{SO}_3)_2(\text{mcp})]$ ($\text{mcp} = N,N'$ -dimethyl- N,N' -bis(2-pyridylmethyl) cyclohexane-*trans*-1,2-diamine) catalyst under optimized catalytic conditions using hydrogen peroxide as oxidant. Under this new reaction protocol, this catalyst is envisioned to efficiently oxidize alkanes using low catalyst loadings. Moreover, the simple structure of this catalyst makes it easily available in large quantities. Taking advantage of this, we aim to study the selectivity bases of this catalyst to be applied in the oxidation of natural products in synthetically amenable yield with a simple and convenient reaction protocol.

Finally, in Chapter V we seek to synthesize a new family of iron catalysts to systematically explore the steric influence of the ligand in the regioselectivity of C—H groups oxidation reactions. The design strategy to introduce steric bulk at the ligand architecture will be to modify the 5th position of the pyridine rings with different silyl moieties. We aim to fully characterize this new family of catalysts and evaluate their catalytic performance in the oxidation of alkanes. Moreover, we intend to establish a relationship between the steric hindrance offered by the ligand and the C—H regioselectivity offered by the catalysts. We envision that the appropriate choice of catalyst will enable the catalyst dependent site-selective oxidation of natural products.



CHAPTER III

REGIOSELECTIVE OXIDATION OF NONACTIVATED ALKYL C—H GROUPS USING HIGHLY STRUCTURED NON-HEME IRON CATALYSTS



This chapter is based on the following publication:

Laura Gómez,[†] Mercè Canta,[†] David Font, Irene Prat, Xavi Ribas, and Miquel Costas*

J. Org. Chem. **2013**, *78*, 1421-1433

[†]Authors contributed equally to this work

III.1 INTRODUCTION

Oxidized hydrocarbons constitute a basic structural motif in organic molecules. Prominent examples constitute families of natural products such as terpenes^{1,2} and steroids,³ and particularly interesting are molecules of pharmacological relevance, such as artemisin,⁴ taxanes,⁵ and briostatins⁶, to name a few representative examples. Therefore, one of the most attractive strategies in organic synthesis is the development of methodologies that allow for the site selective oxidation of alkyl sp^3 C—H groups.^{7–14} The factors that govern regioselectivity in these reactions have been actively pursued and identified.⁷ Electronic effects impact in the strength of the C—H bond, and in the absence of directing groups, they most commonly dominate selectivity. This is so because most reagents that can engage in C—H oxidation reactions have simple architectures, and do not participate in organometallic interactions.^{15–20} Consequently, in most cases, structural constraints imposed by the oxidant are not important. In addition, most oxidizing agents are limited in scope to tertiary C—H groups and activated methylene sites, and very few examples exist that can also efficiently and selectively oxidize stronger C—H groups in addition to simple cycloalkanes.^{21–26} Discovery of reagents that could bias this general reactivity are particularly valuable because they will complement current methodologies and open novel synthetic paths.

The most successful strategy to diverge C—H regioselectivity in C—H oxidations is the use of directing groups, either of covalent nature,^{27–31} or based in metal-coordination bonds.^{28,32–36} A more subtle and elaborated approach exploited by enzymes relies on employing highly spatially structured oxidizing sites that could regulate selectivity by controlling access and orientation of the substrate in its approach toward the oxidizing unit. The design of bioinspired iron catalysts is envisioned as a promising tool to pursue this strategy.^{37–41} Fe-based catalytic methods are also particularly appealing, due to the availability and the lack of toxicity of this element and because iron-based reagents are very reactive and can hydroxylate not only relatively weak 3° C—H groups but also 2° alkyl sites, thus complementing existing oxidizing technologies.^{42–55} Despite of the potential of this approach, few iron based systems provide C—H oxidized products with synthetically amenable yields, albeit with modest turnover numbers and C—H regioselectivities.

We have recently shown that a highly active non-heme iron catalyst for the selective oxidation of alkyl C—H groups with H₂O₂ is obtained by introducing steric bulk at the catalyst active site, creating a robust, well-defined cavity.⁵⁰ Herein, we show that this family of structurally elaborated catalysts imparts alternative or improved C—H site selectivities that escape from the inherent reactivity of C—H bonds, without the aid of directing groups. In addition to the steric hindrance, the chirality of the catalysts and the nature of the ligand diamine backbone are identified as additional key structural aspects of the iron catalyst active site that have an impact in C—H site selectivity. These selectivities complement those accomplished with structurally simpler oxidants, including non-heme catalysts described to date.

III.2 RESULTS AND DISCUSSION

III.2.1 A FAMILY OF HIGHLY STRUCTURED NON-HEME IRON CATALYSTS

Mononuclear iron complexes Λ -[Fe(CF₃SO₃)₂((*S,S,R*)-mcpp)], Λ -1P, Δ -[Fe(CF₃SO₃)₂((*R,R,R*)-mcpp)], Δ -1P, Λ -[Fe(CF₃SO₃)₂((*S,S,R*)-pdpp)], Λ -2P and Δ -[Fe(CF₃SO₃)₂((*R,R,R*)-pdpp)], Δ -2P (Figure III.1; Δ and Λ indicate the chirality at the metal center and the P after the number indicates that the ligand contains pinene rings fused to 4,5-positions of the pyridine) were prepared by using the two pairs of ligands (*S,S,R*)-mcpp, (*R,R,R*)-mcpp, and (*S,S,R*)-pdpp, (*R,R,R*)-pdpp, differing in the nature and chirality of the aliphatic diamine backbone.

Complexes Λ -1P, Δ -1P, Λ -2P, and Δ -2P present chirality at the metal, which in turn is determined by the chirality of the diamine backbone.⁵⁶ (*S,S*)- and (*R,R*)-diamines predetermine generation of complexes with Λ and Δ chirality at the metal, respectively. The combination of the chirality of the aliphatic diamine (*S,S* or *R,R*), with that of the (+)-pinene group allows control over the relative orientation of the methyl groups of the pinene with respect to the *cis*-exchangeable sites at the iron center. This structural feature provides a certain degree of control over the space around the metal site, where the oxidant presumably binds and substrate oxidation takes place.

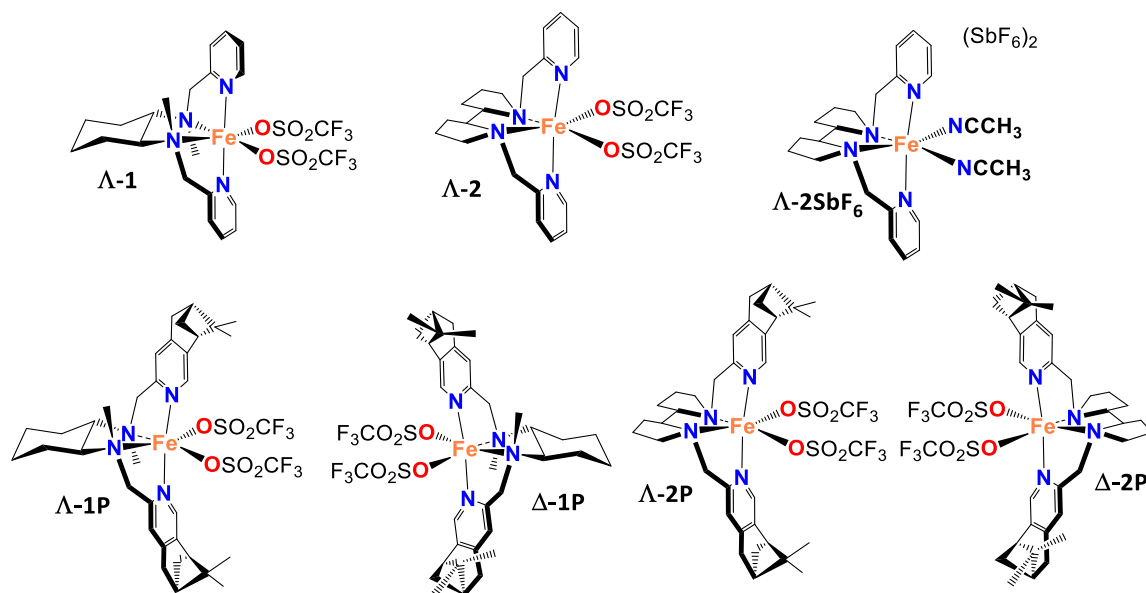


Figure III.1. 3D chemical diagrams of catalysts, Λ -1, Λ -2, Λ -2SbF₆, Λ -1P, Δ -1P, Λ -2P, and Δ -2P.

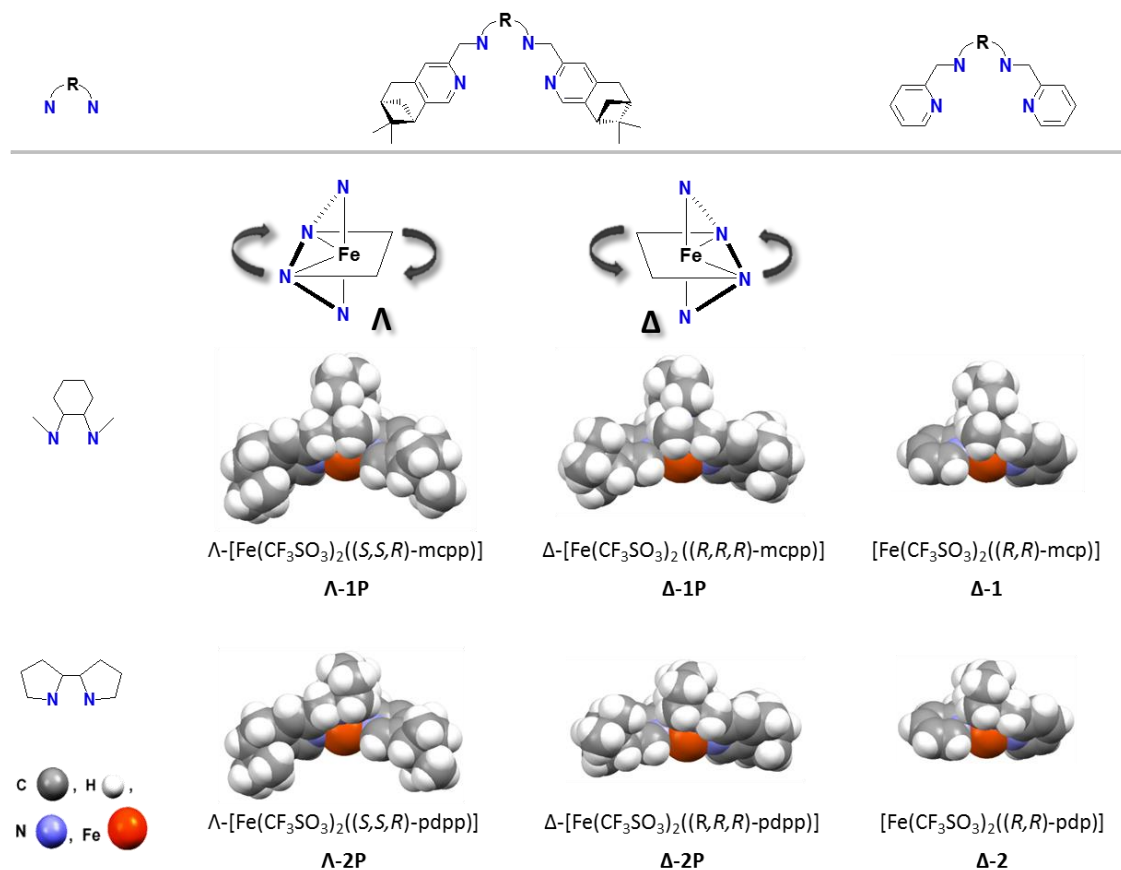


Figure III.2. Space filling diagrams of Λ -1P, Δ -1P, Λ -2P, Δ -2P, Δ -1⁵⁷ and Δ -2.⁵⁸ Counterions and solvent of crystallization have been omitted for clarity.

The space-filling analysis (Figure III.2) shows that in Λ -1P and Λ -2P the iron site is surrounded by a well-defined cavity-like space. Instead in all other complexes, the two

exchangeable *cis* coordination sites are sterically exposed. $^1\text{H-NMR}$ analyses indicate that the C_2 -symmetric structure of the solid state is retained in solution. We envisioned that the differential spatial structures of the complexes, and especially the chirality at the metal and the cavity-like architecture of **Λ -1P** and **Λ -2P** surrounding iron labile sites will have an impact in the selectivity of the catalysts in C—H oxidation reactions by regulating access of the substrate to the active site on the basis of its size, chirality, and shape.

III.2.2 STABILITY TEST ON THE CATALYSTS

In order to test the influence of the pinene group and the nature of the diamine backbone on the oxidation activity of these catalysts in C—H oxidation reactions, a time profile of product formation in the oxidation of (–)-menthyl acetate (**3**) with H_2O_2 mediated by **Λ -1P**, **Δ -1P**, **Λ -2P**, **Δ -2P**, and structurally simpler catalysts **Λ -[Fe(CF₃SO₃)₂((*S,S*)-mcp)] **Λ -1** and **Λ -[Fe(CF₃SO₃)₂((*S,S*)-pdp)] **Λ -2** (1 mol%) was monitored (Figure III.3, see Figure III.1 for catalyst structures). Irrespective of the catalyst, oxidation of **3** produces tertiary alcohol **4** with high selectivity (77–90% selectivity depending on the catalyst, see Table III.9). Reactions were fast and were finished immediately after H_2O_2 addition was complete. The structure of the aliphatic diamine plays a crucial role in the efficiency of the reactions. Complex **Λ -1**, with a cyclohexane diamine backbone,⁵⁹ is less efficient than the bipyrrolidine based complex **Λ -2**.⁵⁸ The introduction of the pinene ring in complexes with Δ topology does not have much of an influence on the outcome efficiency of the catalysts (compare **Λ -1** vs **Δ -1P** and **Λ -2** vs **Δ -2P**). On the other hand, Λ complexes containing pinene groups (**Λ -1P** and **Λ -2P**), exhibit substantially better efficiency than analogous **Λ -1** and **Λ -2**, which lack this group. Moreover, the presence of a well-defined ligand cavity around the iron ion in complexes **Λ -1P** and **Λ -2P** increases the stability of the catalysts resting state, since only these complexes maintain their activity after the first H_2O_2 addition. Indeed, for the particular case of **Λ -1P**, the number of turnovers (TN) of alcohol product **4** obtained in the first and second H_2O_2 additions are comparable (50 and 45 TN, respectively; **Λ -2P** provides 39 TN and 28 TN, respectively). Finally, the activity of **Λ -2** and **Λ -2SbF₆** appeared to be nearly identical, suggesting that triflate and SbF₆ anions have no influence on the relative activities of the two catalysts.****

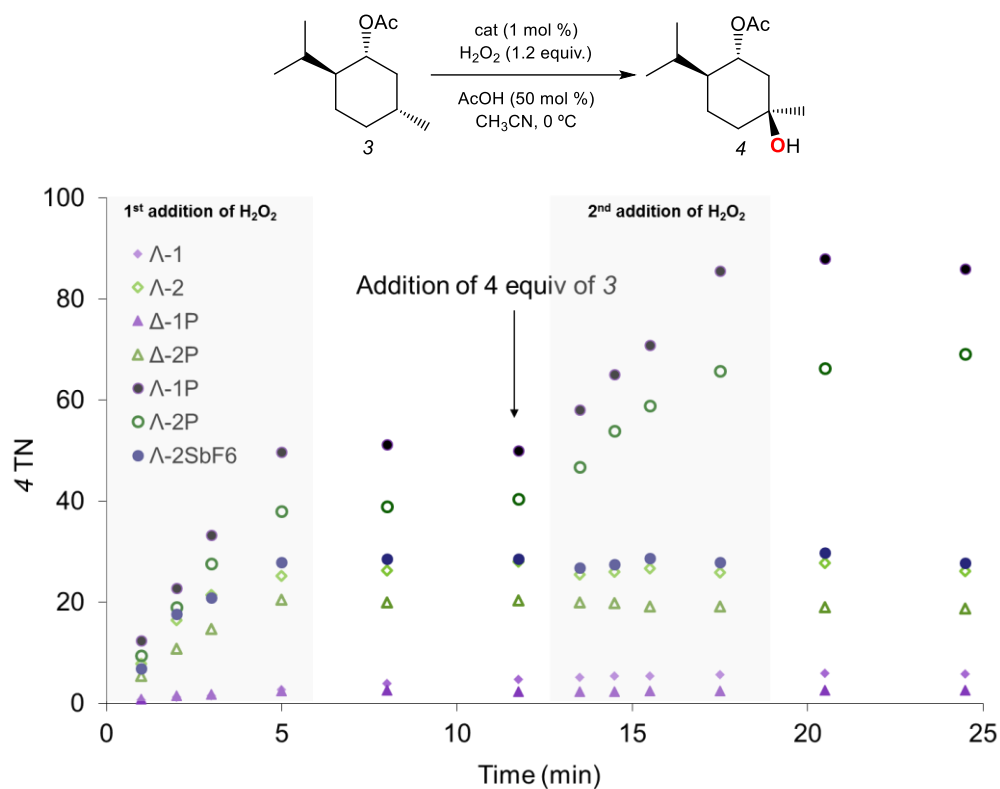


Figure III.3. Oxidation of (-)-menthyl acetate (3). Formation of 4 in the hydroxylation of 3 represented *versus* time in two-step addition of H₂O₂.

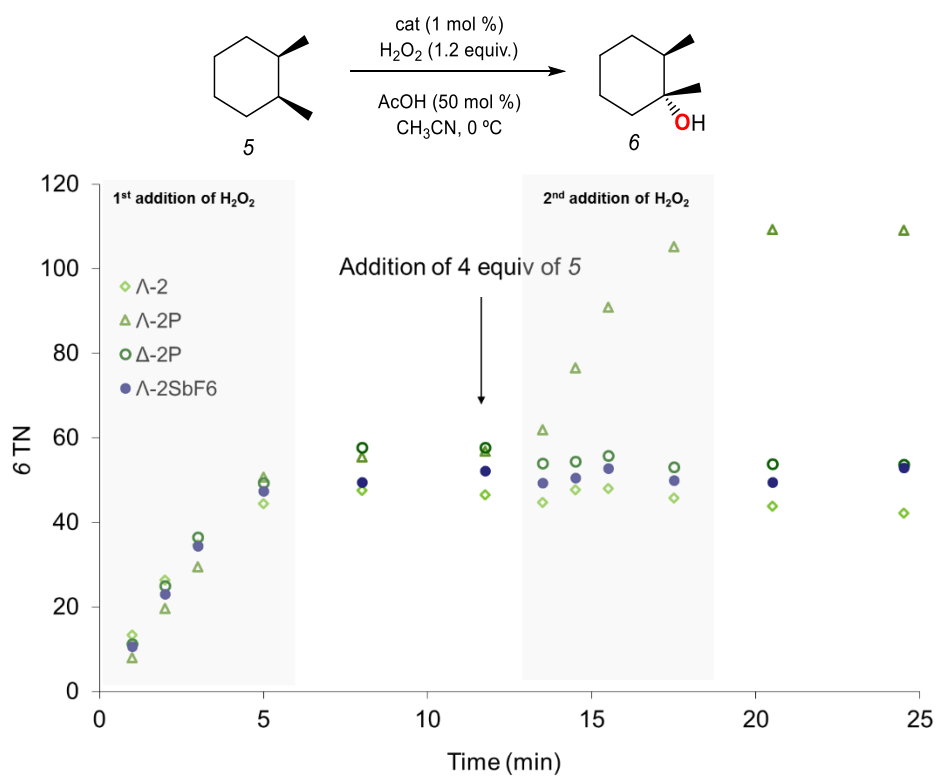


Figure III.4. Oxidation of *cis*-1,2-dimethylcyclohexane (5). Formation of 6 in the hydroxylation of 5 represented *versus* time in two-step addition of H₂O₂.

The conclusions arising from the time profile analysis of the oxidation of (–)-menthyl acetate (**3**) were further confirmed by performing analogous experiments in the oxidation of *cis*-1,2-dimethylcyclohexane (**5**) (see Figure III.4).

These observations thus demonstrate that both the presence of the pinene rings and the proper combination of the chirality at the metal (Λ/Δ), with the chirality of the pinene rings, exert a profound influence on the efficiency and stability of the catalysts. Specifically, the presence of a well-defined ligand cavity around the iron ion in complexes **Λ -1P** and **Λ -2P** increases their robustness, most likely by providing protection against bimolecular deactivation pathways leading to the formation of catalytically inactive oxo-bridged ferric oligomeric species.⁵⁰

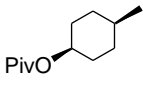
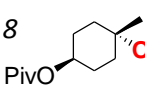

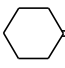
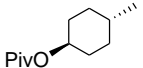
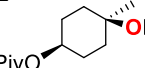
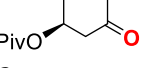
III.2.3 OPTIMIZATION OF THE REACTION PROTOCOL

Our previous experimental conditions allowed high conversion of substrate to product but they involved several subsequent additions of catalyst and H₂O₂.⁵⁰ Depending on the substrate, up to three were necessary. For convenience, a simpler protocol was evaluated, which consisted in a single syringe pump addition of H₂O₂ (17 min) over a CH₃CN solution containing the catalyst (3 mol%), AcOH (1.5 equiv) and substrate at 0 °C. *cis*-4-methyl-1-cyclohexylpivalate (**7**) and cyclohexane (**9**) were taken as model substrates for optimization because the results from these reactions allow a straightforward comparison with the literature. Table III.1 shows that this simpler set of conditions, which do not involve the most common use of excess of substrate, provides preparative useful yields based on product converted into oxidation products (51-75%) using low catalyst loadings (3 mol%) of pinene-containing complexes **Λ -1P**, **Δ -1P**, **Λ -2P** and **Δ -2P**.

Most significantly, with the single exception of **Δ -1P**, yields attained with the pinene-containing catalysts are substantially higher than those obtained with **Λ -1** and **Λ -2** both in the oxidation of secondary (*trans*-4-methyl-1-cyclohexylpivalate, **11**) and tertiary (**7**) C—H bonds. It is also interesting to notice that higher differences among catalysts efficiencies arise when using the iterative protocol. **Λ -1P** is the only complex that provides better yields when the iterative protocol is employed. Instead, all other complexes performed better with the simpler protocol. Particularly remarkable is that in the case of **Δ -1P**, the new synthesis of the complex in combination with this new protocol increased

substantially the efficiency of the catalyst in comparison with the previously reported one.¹⁰ In conclusion, the advantage of this new protocol is not only its simplicity, but also that it allows better performance of most catalysts.

Table III.1. Oxidation of cyclohexane and *cis*- and *trans*-4-methylcyclohexyl pivalate.^a

Substrate	Products	Protocol	Product yield % ^b (substrate conversion) [12/13] ^c					
			Λ -1P	Δ -1P	Λ -2P	Δ -2P	Λ -1	Λ -2
		Iterative ^d	57 ^h (75)	9 ^j (19)	62 (92)	52 (75)	20 (33)	43 (45)
		Single ^e	51 (70)	53 (65)	65 ⁱ (87)	57 (70)	38 (53)	53 (69)
		Iterative ^f	67 (92)	21 (48)	64 (91)	56 (84)	47 (77)	47 (79)
		Single ^g	72 (93)	75 (87)	71 (92)	67 (87)	61 (79)	61 (79)
	 	Single ^e	60 (67) [71/29]	58 (60) [69/31]	61 (80) [80/20]	57 (71) [77/23]	-	-

^a Except otherwise indicated for oxidation at tertiary C–H bonds RC>95% (RC = retention of configuration in the oxidation of the tertiary C–H bonds, expressed as the ratio of the tertiary alcohols: $|[(trans - cis) / (trans + cis)] \times 100|$). ^b % GC yield based on product formed. ^c Normalized (100) ratio of products. ^d Conditions: Cat:H₂O₂:substrate:AcOH; 1x3:120x3:100:50x3; ^e 3:200:100:50; ^f 1x2:120x2:100:50x2; ^g 3:280:100:150. ^h Isolated by flash chromatography. ⁱ 55% isolated by flash chromatography. ^j 82% RC.

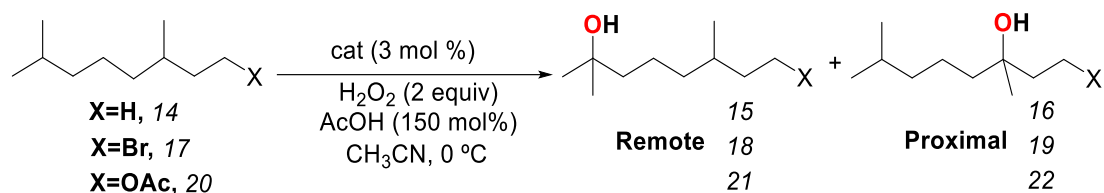
III.2.4 FACTORS GOVERNING SELECTIVITY IN C–H OXIDATION OF SIMPLE SUBSTRATES

Complexes Λ -1P, Δ -1P, Λ -2P, Δ -2P, Λ -1, and Λ -2, were compared as catalysts in the oxidation of tertiary and secondary C–H bonds (Table III.1). The standard oxidation protocol employed consisted in a single syringe pump addition of H₂O₂ over a CH₃CN solution containing the catalyst (3 mol%), AcOH (1.5 equiv) and substrate at 0 °C. This higher level of catalyst loading with regard to Figure III.3 and Figure III.4, and to our previously reported procedure⁵⁰ suffices to obtain moderate to good product yields for all the catalysts using a very simple protocol (Table III.1). Interestingly, yields attained with the pinene-containing catalysts are substantially higher (up to 65% for 7 and 75% for 9) than those obtained with their respective analogues lacking the pinene ring (Λ -1 and Λ -2).

Despite being traditionally considered as inert, it is now recognized that alkyl C–H groups have distinct inherent relative reactivity in C–H functionalization reactions.⁷

Selectivity patterns exhibited by this family of catalysts were studied. In general 3° C—H groups are preferentially oxidized in the presence of statistically more important 2° C—H sites (Table III.1, substrates 7 and 11; and Table III.2). These reactions take place with stereoretention (retention of configuration (RC) > 95%). This is indicative of a metal-centered transformation where long lived carbon centered radicals are not involved.^{45,47}

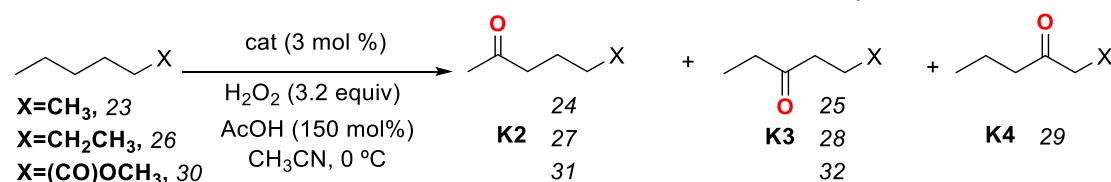
Table III.2. Evaluation of electronic effects in the oxidation of tertiary C—H bonds.



Substrate	Yield ^a % (conversion %) [Remote/Proximal]			
	Λ -1P	Δ -1P	Λ -2P	Δ -2P
14 ^b	31 (78) [55/45]	13 (54) [57/43]	32 (75) [51/49]	20 (44) [54/46]
14 ^c	32 (86) [55/45]	31 (72) [55/45]	31 (82) [48/52]	29 (64) [51/49]
17 ^c	48 (83) [88/12]	41 (66) [90/10]	43 (78) [85/15]	29 (44) [85/15]
20 ^c	49 (68) [79/21]	44 (65) [81/19]	44 (69) [77/23]	33 (51) [76/24]

^a GC yield based on product formed. ^b Cat:H₂O₂:substrate:AcOH 1:180:100:50. ^c 3:200:100:150.

Table III.3. Evaluation of electronic effects in the oxidation of secondary C—H bonds.



Substrate:	23	26	30
Yield ^a % (conversion %)			
Catalyst	[K2/K3] ^b	[K2/K3/K4] ^b	[K2/K3] ^b
Λ -1P	50 (94) [57/43]	57 (79) [51/35/14]	55 (62) [76/24]
Δ -1P	46 (72) [59/41]	53 (72) [47/36/17]	26 (36) [74/26]
Λ -2P	51 (94) [50/50]	56 (71) [42/40/18]	56 (66) [63/37]
Δ -2P	44 (74) [50/50]	50 (56) [40/40/20]	31 (34) [63/37]
Λ -2	50 (69) [53/47]	41 (61) [43/39/18]	-

^a GC yield based on product formed. ^b Normalized (100) ratio of products.

Ketones are the main products obtained in the oxidation of methylene sites (Table III.3 and III.6), presumably via a two-step oxidation of the C–H bond into the corresponding alcohol, which is rapidly further oxidized to the corresponding ketone. Consistent with this scenario, submitting cyclohexanol to the standard reaction conditions using **A-1P** as catalyst provides quantitative conversion into cyclohexanone.

Electronic effects in the regioselective oxidation of 3° (Table III.2, substrates 17 and 20) and 2° (Table III.3, substrate 30) C–H groups showed the characteristic pattern of an electrophilic active species, preferentially oxidizing remote, most electron rich C–H sites.

Cyclohexanes constitute common basic frameworks in organic molecules and may be regarded as informative substrate probes. When they are subjected to the standard oxidation procedure, cyclohexane derivatives provide moderate to good product yields (43%-75%; Table III.4-Table III.6). In cyclohexane derivatives the orientation of the C–H group to be oxidized is determinant for the regioselective outcome of the oxidation reaction.⁶⁰ Tertiary C–H groups in equatorial position are more prone to oxidation, because they are spatially more accessible and because a strain release of the 1,3-diaxial interactions occurs in the rate determining C–H bond-breaking step. Instead, breakage of tertiary C–H bonds in axial positions is not facilitated by strain release, and competitive oxidation between 3° and 2° sites can occur, because the latter are also spatially more accessible (Figure III.5).

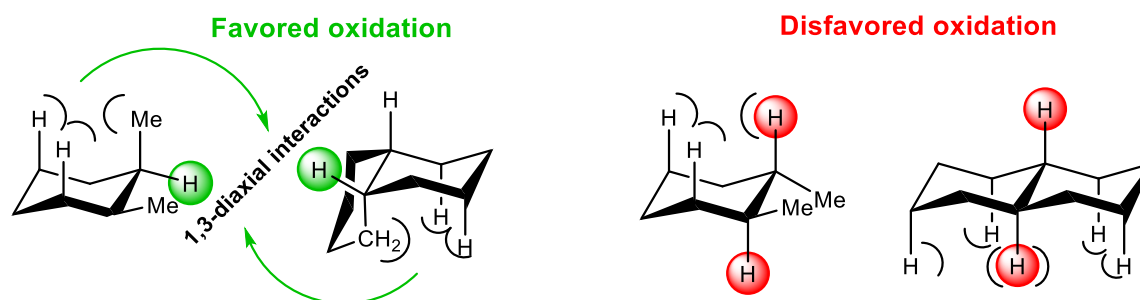
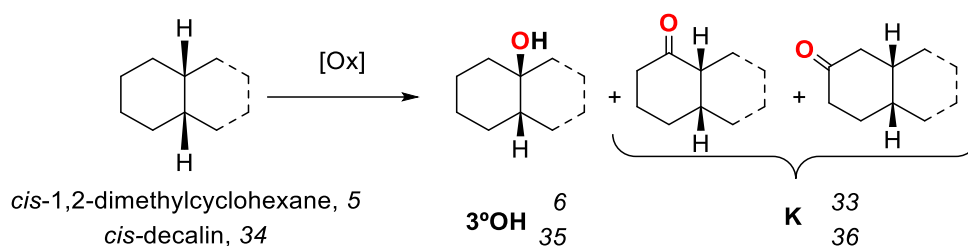
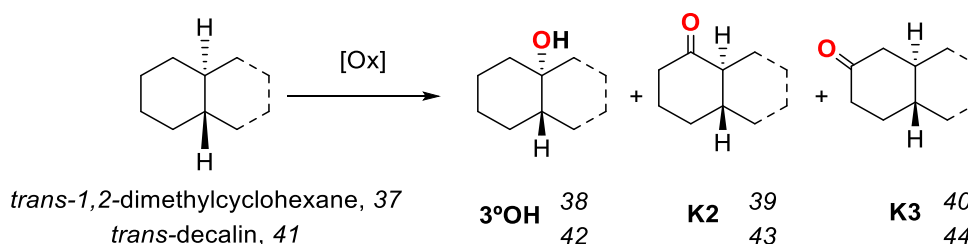


Figure III.5. Chair conformation structure of 1,2-dimethylcyclohexanes and decalines.

Table III.4. Oxidation of *cis* isomers of 1,2-dimethylcyclohexane and decalin.

Catalyst	Substrate					
	5 ^a			34 ^b		
	Yield ^c % (conversion)	[6/33] ^d	RC ^e	Yield ^c % (conversion)	[35/36] ^d	RC ^e
Λ -1P	57 (80)	[84/16]	99	46 (86)	[69/31]	99
Δ -1P	58 (81)	[83/17]	99	51 (88)	[71/29]	99
Λ -2P	58 (80)	[88/12]	99	48 (82)	[77/23]	99
Δ -2P	55 (72)	[86/14]	99	47 (91)	[74/26]	99

^a Cat:H₂O₂:substrate:AcOH 1:120:100:50. ^b Cat:H₂O₂:substrate:AcOH 3:200:100:150 ^c GC yield based on product formed. ^d Normalized (100) ratio of products. ^e RC = retention of configuration in the oxidation of the tertiary C-H bonds, expressed as the ratio of the tertiary alcohols: $[(trans - cis) / (trans + cis)] \times 100$.

Table III.5. Oxidation of *trans* isomers of 1,2-dimethylcyclohexane and decalin.

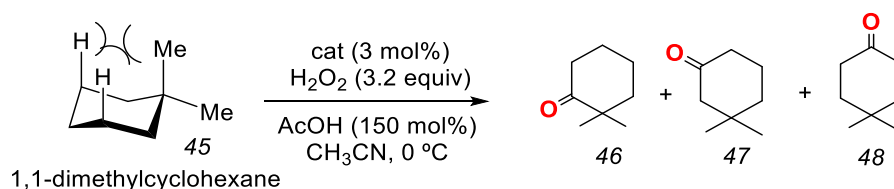
Catalyst	Substrate					
	37 ^a			41 ^b		
	Yield ^c % (conversion)	[38/39/40] ^d	RC ^e	Yield ^c % (conversion)	[42/43/44] ^d	RC ^e
Λ -1P	47 (77)	[26/29/45]	99	47 (85)	[4/37/59]	99
Δ -1P	52 (74)	[28/26/46]	98	50 (70)	[7/37/56]	98
Λ -2P	49 (87)	[48/24/28]	99	48 (83)	[14/41/45]	99
Δ -2P	43 (77)	[50/21/29]	99	52 (88)	[16/40/44]	99
Λ -2	36 (65)	[48/22/30]	99	48 (88)	[15/38/46]	99

^a Cat:H₂O₂:substrate:AcOH 3:200:100:150. ^b Cat:H₂O₂:substrate:AcOH 3:280:100:150 ^c GC yield based on product formed. ^d Normalized (100) ratio of products. ^e RC = retention of configuration in the oxidation of the tertiary C-H bonds, expressed as the ratio of the tertiary alcohols: $[(trans - cis) / (trans + cis)] \times 100$.

As predicted from this analysis, in substrates where at least one tertiary C–H is in equatorial disposition (e.g., **5**, **7**, and **34**), the corresponding tertiary alcohol (**6**, **8** and **35** respectively), is obtained with high selectivity, good yield (up to 65%), and high retention of configuration (>95%). Instead, oxidation of the corresponding *trans* isomers (compare **5** vs **37**, **34** vs **41** and **7** vs **11**; Table III.1, Table III.4, and Table III.5) occurs preferentially at 2° C–H sites in comparison to *cis* isomers.

In *cis*- and *trans*- isomers the regioselectivity towards the tertiary C–H is also influenced by steric constraint around this bond. For example, the bicyclic nature of decalines (**34** and **41**) accounts for a more efficient shielding of the tertiary C–H bond than in single cyclohexane rings, which translates in an increased preference for the oxidation of the 2° sites (compare **34** vs **5** and **7**; or **41** vs **11** and **37**, respectively). Most interestingly, however, selectivity also depends on the structure of the catalysts. The best selectivities toward oxidation of methylene sites are attained when using catalysts **Λ-1P** and **Δ-1P**, and this selectivity is remarkably acute in the oxidation of *trans*-decaline (**41**; 96% and 93%, respectively). To the best of our knowledge, such a level of selectivity has only been previously documented for Mizuno's polyoxometalates.²⁴

Table III.6. Steric and electronic factors in the oxidation of cycloalkanes.



Catalyst	Yield ^a % (conversion)	[46/47/48] ^b
Λ-1P	67 (94)	[23/54/23]
Δ-1P	66 (90)	[21/57/22]
Λ-2P	68 (81)	[37/44/19]
Δ-2P	69 (92)	[32/47/21]
Λ-2	58 (68)	[36/43/21]

^a GC yield based on product formed. ^b Normalized (100) ratio of products

Moreover, catalysts **Λ-1P** and **Δ-1P** exhibit remarkable discrimination between methylene position 2 (ketone **K2** formed) and position 3 (**K3** formed), in favor of the latter,

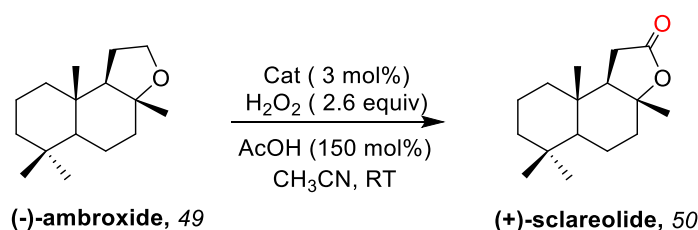
which is the least sterically hindered (Table III.5). Instead, catalysts **Λ -2P**, **Δ -2P** and **Λ -2** show almost no discrimination between the two methylene sites. This is also observed in the oxidation of **45** (Table III.6) and in the significant (albeit modest) regioselectivity observed in oxidation of simple alkanes such as *n*-hexane or *n*-heptane (Table III.3, substrates **23** and **26**).^{61,62} Therefore, for these simple substrates the nature of the diamine backbone has a more decisive role than the cavity created by the relative orientation of the pinene rings in defining C—H regioselectivity on the basis of sterics. We conclude that the cyclohexyl *N*-methyl groups in **Λ -1P** and **Δ -1P** result in more effective steric constraints in close proximity to the iron site than those exerted by the bipyrrolidine (**Λ -2P** and **Δ -2P**).

In conclusion, the combination of observations points out **Λ -1P** and **Δ -1P** as very unique catalysts that sensitively respond to steric properties of C—H groups in these simple hydrocarbons, while providing good yields of alkyl C—H oxidized products.

III.2.5 SELECTIVE OXIDATION OF COMPLEX MOLECULES

The potential utility of this family of catalysts in organic synthesis is best illustrated in the oxidation of structurally more complex substrates. The structurally rich nature of the complexes was envisioned to most sensitively affect yields and/or selectivities in the oxidation of these non-trivial molecules.

Table III.7. Oxidation of ambroxide.



Catalyst	Λ-1P	Δ-1P	Λ-2P	Δ-2P	Λ-2	Δ-2	Δ-2SbF₆
Product yield %^a	73 (70) ^b	73	60	72	58	66	57

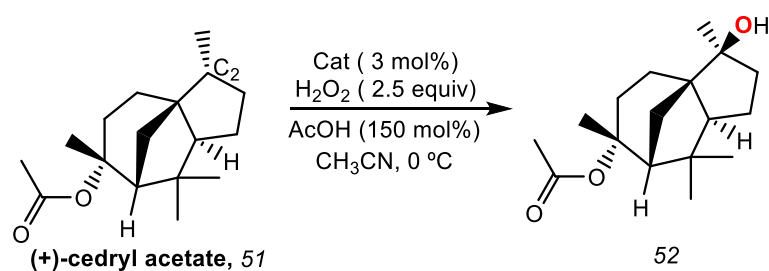
^a GC yield based on product formed. ^b Isolated by flash chromatography. After reaction, 1 equivalent of HCl (2M) was added and the crude mixture heated to 40°C for 4 hours to reverse partial lactone ring-opening.

The selective oxidation of (-)-ambroxide (**49**) can be regarded as a non-trivial problem. This terpenoid contains 14 methylene and 2 tertiary C—H bonds (Table III.7). It

has been recently described that (–)-ambroxide (**49**) can be selectively oxidized at the activated methylene site adjacent to the ether moiety to yield (+)-sclareolide (**50**) in 80% yield employing 15 mol% of Λ -**2SbF₆**.⁵¹ However, when submitted to oxidation under similar experimental conditions (using 3 mol% catalyst in our case) by the family of complexes Λ -**1P**, Δ -**1P**, Λ -**2P** and Δ -**2P**, selective formation of (+)-sclareolide (**50**), resulting from oxidation at the activated methylene site adjacent to the ether moiety is obtained in yields ranging from 60 to 73%. Interestingly, best product yields are obtained with pinene-containing catalysts Λ -**1P**, Δ -**1P** and Δ -**2P**, but a clear relationship between catalyst structure and catalytic activity could not be identified, suggesting that optimum product yield results from a combination of factors.

The rigid bridged tricyclic sesquiterpene (+)-cedryl acetate (**51**) does not contain a powerful electronic directing group. From the two tertiary C–H bonds present, one is in a bridgehead and a second one is situated in a ring junction. Therefore, C2–H (Table III.8) appears to be the less sterically hindered tertiary C–H site, and it is the most distant from the deactivating acetate group. When **51** was submitted to our standard experimental conditions, catalysts containing the well-defined cavity around the metal center (Λ -**1P** and Λ -**2P**) were the most efficient, furnishing hydroxylated product **52** in 56 and 57% yields, respectively. Modest yields are obtained with Λ -**2** and Δ -**2**, and for comparison, it should be noted that oxidation with Gif reagents provides the product in 1% yield.⁶³

Table III.8. Oxidation of (+)-cedryl acetate



Catalyst	Λ - 1P	Δ - 1P	Λ - 2P	Δ - 2P	Λ - 2	Δ - 2	Λ - 2SbF₆
Product yield % ^a	56 (49) ^b	32	57	21	20	17	15

^a GC yield based on product formed. ^b Isolated by flash chromatography.

III.2.6 CHIRAL MATCHING IN C—H OXIDATION REACTIONS

A set of derivatives of menthol was further identified as a test platform for studying selectivity in C-H oxidation responding to a combination of electronic, steric and chiral properties of the substrate, and the catalysts. Figure III.6 shows the most stable conformational isomers for (+)-menthyl acetate (53), (+)-isomenthyl acetate (54), and (+)-neomenthyl acetate (55).^{13,14} The conformational isomers shown in the figure are also assumed to be the most reactive (Curtin-Hammett principle) and to dominate the regioselectivity outcome of their oxidation.

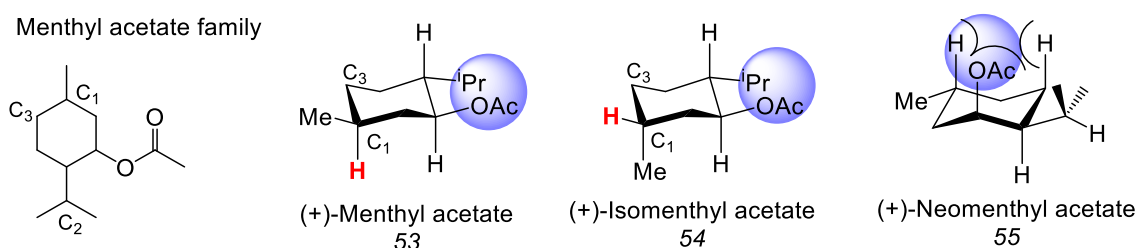
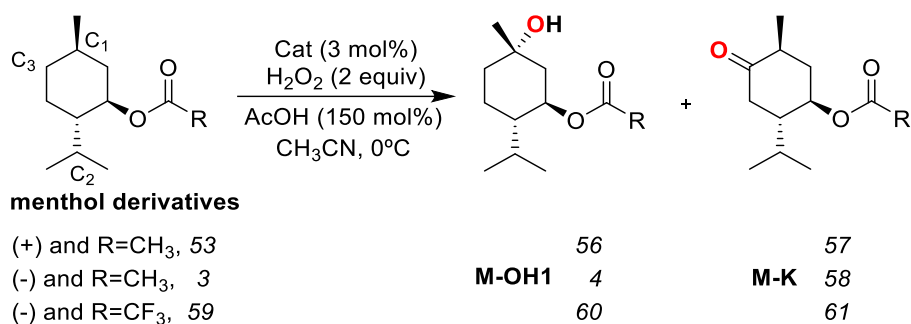


Figure III.6. Chair representations of menthyl acetate derivatives.

For menthyl and isomenthyl esters, tertiary C—H bonds at C₁ and C₂ and the CH₂ in position C₃ were identified as the electronically less deactivated positions. From the 3D chair structure (Figure III.6) it can be observed that the ester moiety is spatially close to the isopropyl group, and some steric protection of C₂—H could be predicted. Menthyl and isomenthyl acetate differ uniquely in the disposition of the C₁—H bond. In the first one, the C₁—H bond is in axial disposition, while equatorial in the second. For this reason, we envisioned that the oxidation of the C₁ position would be more efficient for isomenthyl acetate than for menthyl acetate. As expected, irrespective of the iron catalyst employed, menthyl and isomenthyl esters are oxidized preferentially in C₁—H to the corresponding tertiary alcohol (Table III.9 and Table III.10, respectively). In addition, the ketone product resulting from oxidation at C₃ is a minor product, and oxidation at C₂ is observed in only trace amounts. Also as expected, the best yields and excellent selectivity towards C₁-H were obtained in the oxidation of isomenthyl esters. For example, the oxidation of (+)-isomenthyl acetate (54) proceeds to the corresponding tertiary alcohol with better yields (up to 83% for **Δ-1P**) than the oxidation of (+)-menthyl acetate (53) (up to 58% for **Δ-1P**).

Table III.9. Oxidation of menthol derivatives.

Menthol derivatives			
	53	3	59
Catalyst	Yield % ^a [M-OH1 / M-K] ^b		
Λ-1P	37 [86/13]	63 (65) ^c [95/5]	51 [93/7]
Δ-1P	58 [90/10]	42 [76/24]	29 [73/27]
Λ-2P	47 [85/15]	59 [88/12]	53 [75/25]
Δ-2P	52 [85/15]	47 [79/21]	48 [70/30]
Λ-2SbF₆	42 [78/22]	47 [83/17]	
Λ-2	45 [77/23]	48 [83/17]	37 [69/31]
Δ-2	48 [84/16]	47 [78/22]	39 [68/32]

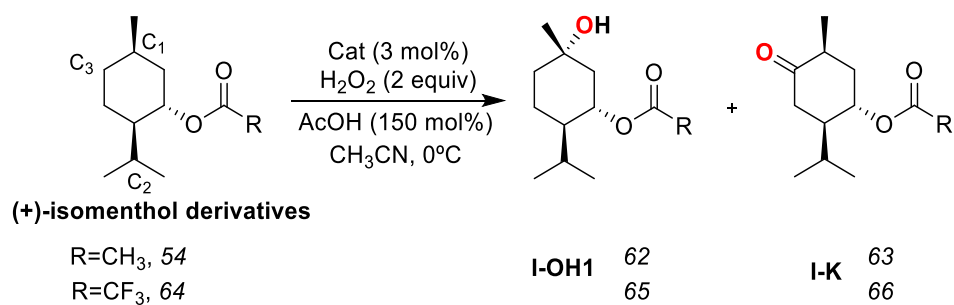
^a Combined GC yield based on product formed. ^b Normalized (100) ratio of products. ^c Isolated by flash chromatography. Arrows connecting reactions of **Λ-2** and **Δ-2** with substrates 53 and 3 correspond to enantiomerically related reactions.

Comparative oxidation of optically pure + and – enantiomers of menthyl acetate allowed us to investigate if a stereoselective match between chiral catalyst and substrate could give rise to distinct selectivities and/or improved yields.

Effectively, as a general rule, complexes presenting Λ chiral conformation such as **Λ-1P**, **Λ-2P**, and **Λ-2** showed better yields and selectivity for the tertiary alcohol at C₁ (**M-OH1**) when reacting with 3 (– isomer). Instead, 53 (+ isomer) is more conveniently oxidized with complexes possessing Δ chirality (Table III.9). Most remarkable differences are observed in the case of catalysts **Δ-1P** and **Λ-1P**. The latter is very selective and efficient in the oxidation of 3 (yield% [**M-OH1**/**M-K**], 65 [95/5]) but quite mediocre when reacting with 53 (yield% [**M-OH1**/**M-K**], 37 [86/13]). The contrary occurs with **Δ-1P** (yield% [**M-**

OH1/M-K = 42 [76/24] and 58 [90/10], respectively). On the other hand, in the oxidation of (-)-menthyl trifluoroacetate complexes **Λ -1P** and **Λ -2P** afford better yields and selectivities than **Δ -1P** and **Δ -2P**, while virtually the same results are obtained with **Λ -2** compared with **Δ -2**. Moreover, (+)-isomenthyl acetate (**54**) by **Δ -1P** provides better yield (83%) than by **Λ -1P** (75%, Table III.10).

Table III.10. Oxidation of (+)-isomenthol derivatives.



Catalyst	Substrate	
	54	64
	Yield % ^a [I-OH1 % / I-K %] ^b	
Λ-1P	75 [86/14]	68 [87/13]
Δ-1P	83 [89/11]	82 (71) ^c [91/9]
Λ-2P	70 (63) ^c [83/17]	67 [83/17]
Δ-2P	65 [85/15]	67 [86/15]

^a Combined GC yield based on product formed. ^b Normalized (100) ratio of products. ^c Combined isolated by flash chromatography.

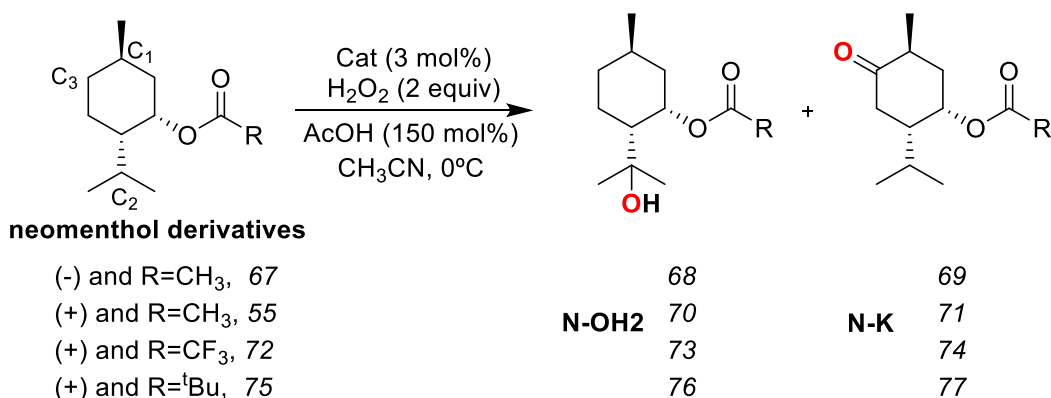
In conclusion, for each substrate a lead catalyst can be identified in terms of yields and selectivity. However, irrespective of the catalyst, the dominant regioselectivity in these substrates is dictated by the relative inherent reactivities of the different C—H bonds.

III.2.7 DIVERTING SELECTIVITY IN C—H OXIDATIONS

A more interesting case will be the oxidation of molecules where different activating-deactivating factors are in competition, and there is not only a single strongly favored C—H oxidation site. In these cases, it was envisioned that the toolset of iron catalysts could allow determination of the preferential C—H oxidation site.

Analysis of the chair-3D structure of neomenthol derivatives (55, 67, 72, 75) (Table III.11, see Figure III.3 for chair-3D structure) shows that in this case the ester group is in axial position and provides steric protection for the axial C–H bond at C₁. In addition, because of the axial orientation of the acetate group, the tertiary C–H site at C₂ is not effectively shielded and becomes spatially more accessible. This analysis predicts that two distinct sites are most prone for oxidation; these are the tertiary C–H bond at C₂ to form alcohol **N-OH2**, and methylene C–H at C₃ to yield ketone **N-K**, which are the most distant to the electron-withdrawing acetate group. Since neither of these two positions appear to be strongly favored, these substrates are a convenient platform for exploring regioselectivity tuning responding to catalyst structure.

Table III.11. Oxidation of neomenthol derivatives.



Catalyst	Substrate			
	67	55	72	75
	Yield % ^a (conversion) [N-OH2 / N-K] ^b			
Λ-1P	40, 42 ^c (53) [55/45]	43 (77) [83/17]	35, 35 ^c (64)[83/17]	54 (71) [80/20]
Δ-1P	44 (59) [64/36]	41 (51) [44/56]	34 (40) [61/39]	40 (44) [34/66]
Λ-2P	47 (72) [58/42]	43 (74) [69/31]	41 (96) [53/47]	46, 45 ^c (66) [52/48]
Δ-2P	43 (69) [48/52]	44 (68) [44/56]	34 (72) [42/58]	35 (48) [34/66]
Λ-2SbF₆	43 (70) [41/59]	46 (66) [48/52]		
Λ-2	43 (69) [42/58]	44 (66) [49/51]	33 (61) [40/60]	38 (50) [40/60]
Δ-2	44 (72) [48/52]	44 (72) [42/58]	33 (64) [37/63]	34 (43) [35/65]

^a Combined GC yield based on product formed. ^b Normalized (100) ratio of products ^c Isolated by flash chromatography.

As predicted, oxidation of these substrates with the full family of catalysts (Table III.11) yields two major oxidation products; tertiary alcohol resulting from oxidation at C₂—H, along with ketone resulting from oxidation at C₃. Interestingly, regioselectivity also depends on the relative chirality of the substrate and the catalyst. The simplest case to analyze is the oxidation of (–)-neomenthyl acetate (67) and (+)-neomenthyl acetate (55) by **Λ-2** and **Δ-2** catalysts. In all cases similar amounts of **N-OH2** and **N-K** are obtained (Table III.11), being the ketone slightly favored. This small selectivity towards **N-K** is slightly higher when (–)-neomenthyl acetate (67) is oxidized with **Λ-2**, or (+)-menthyl acetate (53) with **Δ-2**.

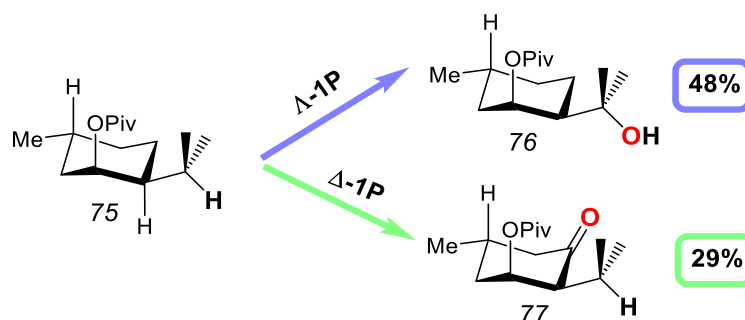
Use of the more structurally elaborated pinene-containing catalysts allows modulating selectivity in a remarkable manner (Table III.11). Most significant, pinene-containing complexes with **Λ** chirality diverge C—H regioselectivity in the oxidation of (+)-neomenthyl acetate (55) towards the tertiary C₂—H bond, and reach an excellent selectivity with **Λ-1P** (yield (%) [**N-OH2/N-K**], 43 [83/17]). Interestingly, the high regioselectivity depends on the chirality of the substrate, and oxidation of (–)-neomenthyl acetate (67) with **Λ-1P** and **Λ-2P** proceeds with substantially smaller selectivity.

In general, when the acetate group is replaced by bulkier groups such as trifluoroacetate or pivalate (72, 75, respectively), a significant increase in the relative C—H selectivity towards the ketone product is observed. In both cases, this effect probably responds to a bigger steric hindrance of these groups, which are situated in spatial proximity to the isopropyl group. On the other hand, the electron withdrawing nature of the trifluoroacetate group may exert some deactivation in the closer C₂—H site.

Therefore, the oxidation of neomenthyl esters with the family of complexes **Λ-1P/Δ-1P**, **Λ-2P/Δ-2P** serves to demonstrate the apparent ability of these highly structured catalysts to diverge regioselectivity between a tertiary and a secondary C—H site in natural product derivatives. Nevertheless, a cautious note should be made, as some of the reactions exhibit deficient mass balance and therefore overoxidation reactions may have influenced the final regioselectivities attained.

In order to further illustrate the potential synthetic utility of this selectivity, selected oxidation reactions of (+)-neomenthol derivatives were scaled up to mmol scale, with experimental conditions chosen to favor oxidation at C₂–H and C₃–H (Table III.12). (+)-Neomenthyl pivalate **75** (0.7 mmol) was oxidized using **Λ-1P** (2 x 3 mol%) yielding tertiary alcohol **76** in 48% isolated yield (along with 10% yield of ketone **77**). Alternatively, by using **Δ-1P** (3 x 3 mol%) ketone **77** was obtained as the main oxidation product in 29% isolated yield (along with 20% yield of alcohol **76**).

Table III.12. Diverting selectivity in the oxidation of **75** as substrate.



Catalyst	Yield % ^a			[76/77] ^d	Conversion (%)
	76	77	Total		
Λ-1P^b	48	10	58	83/17	91
Δ-1P^c	20	29	49	41/59	89

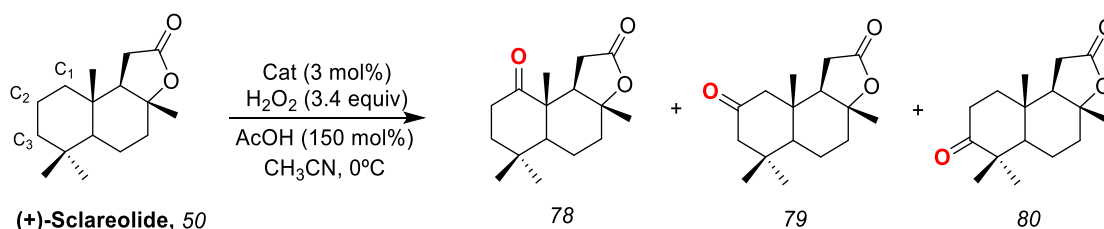
^a 0°C. Cat:H₂O₂:substrate:AcOH; ^b (3)x2:(200)x2:100:(150)x2. ^c (3)x3:(200)x3:100:(150)x3. ^d Normalized (100) ratio of products

An even more challenging possibility would be to apply these iron catalysts to direct oxidation among multiple non-activated methylene sites in complex organic molecules. Towards this end, (+)-sclareolide (**50**) was chosen as a test. In this case, the carbonyl group deactivates the surrounding C–H bonds, directing the oxidation towards the most remote cyclohexane ring, which contains three chemically distinct methylene sites (Table III.13). Preferential functionalization at C₂ was described with catalyst **Δ-2SbF₆**,⁵¹ and in rhodium catalyzed nitrene insertions.⁶⁰ Mn-porphyrin mediated halogenations of (+)-sclareolide can be preferentially directed towards C₂ and C₃ depending on the porphyrin catalyst.⁶⁴ In all these reactions, C–H selectivity among C₁, C₂, and C₃ positions has been understood to be governed by steric factors.

When (+)-sclareolide is subjected to oxidation using **Λ-1P**, **Δ-1P**, **Λ-2P**, **Δ-2P**, **Λ-2** and **Δ-2** as catalysts, ketone products (**78**, **79** and **80**, Table III.13) arising from oxidation

at three different methylene sites (C_1 , C_2 and C_3 , respectively) are obtained. Particular excellent yields (up to 89%) are furnished with catalysts **Λ -1P** and **Λ -2P**. Most surprisingly, site selectivity in the oxidation of (+)-sclareolide appears to be strongly dependent on the nature of the catalyst, and the set of pinene containing complexes (**Λ -1P**, **Δ -1P**, **Λ -2P**, **Δ -2P**) allow to discriminate and to diverge the dominant regioselectivity among multiple methylene sites. Such change in site selectivity cannot be attained with the structurally simpler catalysts **Λ -2** and **Δ -2** (Table III.13); in our conditions, **Λ -2** and **Δ -2** afford ketones (+)-2-oxo-sclareolide **79** and (+)-3-oxo-sclareolide **80** arising from preferential oxidation at C_2 and C_3 in roughly 1:1 relative ratios, accounting for more than 80% of the oxidized products obtained.

Table III.13. Oxidation of (+)-sclareolide.



		Catalyst					
Λ-1P	Δ-1P	Λ-2P	Δ-2P	Λ-2	Δ-2		
Total yield %^a [78/79^b/80]^c							
83	67	89 (78) ^d	69	64	61		
[36/37/26]	[7/63/30]	[28/25/47]	[17/42/41]	[11/45/44]	[18/43/39]		

^a GC yield based on product formed. ^b C_2 -alcohol is also included. ^c Normalized (100) ratio of products. ^d Isolated by flash chromatography.

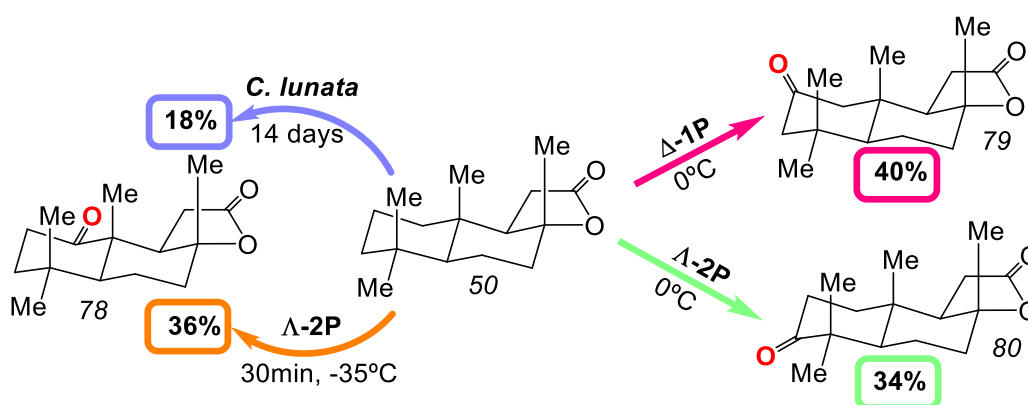
Interestingly, in the case of **Λ -2P**, the regioselectivity can be further modulated by varying the temperature from 25 °C to -35 °C (Table III.14). Upon lowering the temperature, preferential oxidation at position C_3 is gradually lost in favor of increased selectivity towards position C_1 . Indeed, when the oxidation is carried out at -35 °C, **78** becomes the main product of the reaction. Further enhancement occurs at -40°C but at this temperature reaction yield is severely lowered, possibly due to partial solvent freezing. Therefore, by choosing the proper catalyst and experimental conditions, differentiation among multiple methylene sites can be accomplished, and ketones **78**, **79** and **80** can become the dominant oxidation product in synthetically amenable yields.

Table III.14. Temperature dependence on Λ -2P catalytic activity in the oxidation of 50.

Temp (°C)	25	0	-10	-30	-35	-40
Total yield % ^a	74	89	79	65	55	10
[78/79/80] ^b	[27/27/46]	[28/25/47]	[36/25/39]	[48/24/28]	[53/23/24]	[60/20/20]

Cat:H₂O₂:substrate:AcOH 3:340:100:150. ^a GC yield based on product formed. ^b Normalized (100) ratio of products.

To probe the synthetic value of these observations, oxidation of (+)-sclareolide was scaled up to millimole scale using experimental conditions that favor ketones 78, 79 and 80 (Table III.15). These can be obtained as the main product in isolated yields of 36% (61% selectivity), 40% (55% selectivity), and 34% (47% selectivity), respectively, by choosing the appropriate experimental conditions and catalyst.

Table III.15. Diverting selectivity in the oxidation of 50 as substrate.

Catalyst (T)	Yield % ^a			Total	Conversion (%)
	78	79	80		
Λ -2P (-35°C) ^a	36	4	19	59	77
Δ -1P (0°C) ^a	7	40	26	73	89
Λ -2P (0°C) ^b	23	16	34	73	87

Cat:H₂O₂:substrate:AcOH; ^a (3)x2:(340)x2:100:(150)x2. ^b 3:340:100:150. See section III.4.8 for details.

In conclusion, this family of catalysts allows for the late-stage oxidation of a complex organic molecule toward three different ketone products by means of selective methylene oxidation. While overall yields could be regarded as modest, they are still suitable for preparative purposes and their value becomes most evident when considering that functionalization of C₁ has not been described for any synthetic catalyst. Indeed, (+)-1-oxo-sclareolide (78) is only available in low yields *via* biotransformations by filamentous

fungi (*A. niger*, *C. blackesleeana*, and *C. lunata*; 10%, 9% and 18% yield respectively),⁶⁵ and at much longer reaction times (14 days) than for our system. In addition, to the best of our knowledge, the switch in selectivity among distinct methylene sites using nonenzymatic reagents finds exclusive precedent in shape-selective oxidations with sterically hindered metalloporphyrins.^{61,66}

III.3 CONCLUDING REMARKS

Pinene-containing non-heme iron catalysts **Λ -1P**, **Δ -1P**, **Λ -2P** and **Δ -2P** mediate the fast oxidation of nonactivated tertiary and secondary alkyl moieties under mild experimental conditions in synthetically amenable yields, employing H₂O₂ as oxidant, without requiring an excess of substrate. Steric hindrance at the iron active site confers stability toward catalyst degradation pathways. This stability enables the use of low catalyst loadings. Complex organic molecules are oxidized in good yields and selectivity. Simple rules previously established for alkyl C—H functionalization with electrophilic reagents can be used to predict which C—H groups may be more prone to oxidation. Unlike most synthetic C—H oxidation reagents, the present catalysts are highly structured. Interestingly this feature allows for modulating or even altering selectivity without the use of covalent or strong supramolecular substrate–oxidant interactions. Therefore, the final selectivity outcome depends on the combination of more subtle aspects mainly affecting the spatial structure of the iron active site. The chirality of the catalysts, the nature of the ligand diamine backbone, and the presence of a cavity-like site surrounding the iron center have been identified as structural aspects that translate into C—H site selectivity.

It should be noted that the percentage conversion and percentage yield differ in some of the reactions. This fact might be due to the difficulty of this type of oxidations, where mass balance is not complete. Although the formation of significant amounts of a single nonidentified product is not observed, the formation of trace amount of multiple byproducts can not be excluded.

A cautious note must be made at this point. It is quite illustrative to remark that changes in regioselectivity dictated by the nature and chirality of the diamine, or the orientation of the pinene correspond to very modest variations in the relative energies of the paths leading to oxidation of the different C—H bonds. Therefore, interpretation

needs caution. Nevertheless, changes in selectivity ratios between tertiary and secondary C–H groups and also among multiple methylene sites are shown to be useful for providing oxidation products in synthetically valuable yields. Furthermore, regioselectivities obtained with these Fe-based catalysts are important because they are complementary to those that can be reached with other oxidizing agents.^{16–21,67,68}

III.4 EXPERIMENTAL SECTION

III.4.1 MATERIALS

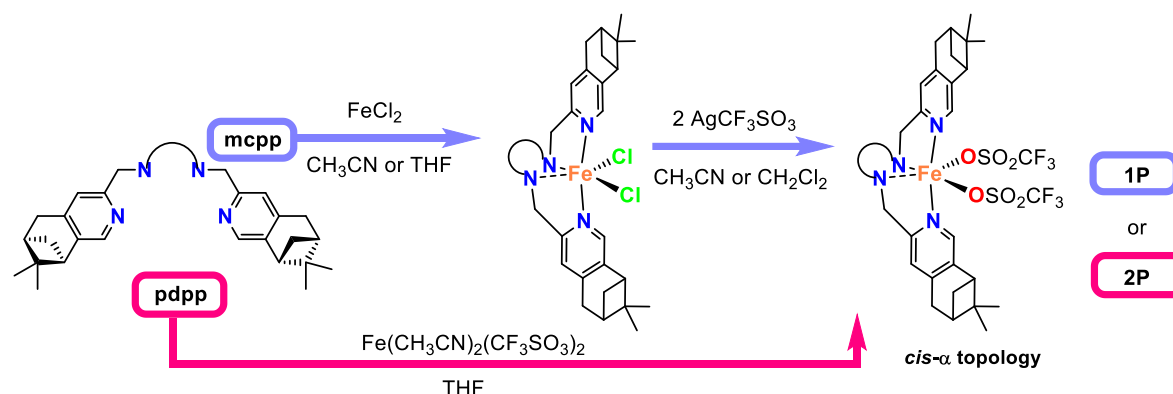
Reagents and solvents used were commercially available reagent quality unless otherwise stated. Acetonitrile for catalysis was HPLC grade. Preparation and handling of air-sensitive materials were carried out in a N₂ dry box with O₂ and H₂O concentrations < 1 ppm. **2**,⁵⁸ **2SbF₆**,⁴⁸ **1**,⁶⁹ **Λ-1P**,⁵⁰ ((*S,S,R*)-pdpp),⁷⁰ and ((*R,R,R*)-pdpp)⁷⁰ were prepared according to published procedures.

III.4.2 INSTRUMENTATION

IR spectra were taken in a FT-IR spectrophotometer using a single reflection ATR system. NMR spectra were taken on a 300 or 400 MHz spectrometer. ¹H-NMR spectra of paramagnetic compounds were performed with the following special parameters; relaxation delay = 0.03 s, acquisition time = 0.064 s, line broadening = 30 Hz, sweep width = 100–250 ppm. Spectra were referenced to the residual solvent peaks or TMS (tetramethylsilane) for ¹H. Elemental analyses were performed using a CHNS-O elemental analyzer. X-Ray diffraction analysis were carried out on a BRUKER SMART APEX CCD diffractometer using graphite-monochromated Mo K α radiation ($\lambda = 0.71073 \text{ \AA}$) from an X-Ray Tube. ESI-MS experiments were performed using methanol or acetonitrile as a mobile phase. HRMS were performed on time-of-flight mass spectrometer with an ESI source using methanol as mobile phase. Product analyses were performed on a gas chromatograph (HP5 column, 30m or Cyclosil-B column, 30 m) and a flame ionization detector. GC-MS spectral analyses were performed on an gas chromatograph interfaced with an mass spectrometer. A 50% NH₃/CH₄ mix was used as the ionization gas for chemical ionization analyses.

III.4.3 SYNTHESIS OF COMPLEXES

Complex **Δ -1P** was prepared following a two-step procedure that involves initial reaction of FeCl_2 with **(*R,R,R*)-mcpp** to yield chloride complex $[\text{Fe}(\text{Cl}_2)((\textit{R,R,R})\text{-mcpp})]$.⁵⁰ This was subsequently treated with 2 equiv of AgCF_3SO_3 to afford triflate complex $[\text{Fe}(\text{CF}_3\text{SO}_3)_2((\textit{R,R,R})\text{-mcpp})]$ that could be isolated in crystalline form by diffusion of diethyl ether to dichloromethane solution of the complex. **Λ -2P** and **Δ -2P** were prepared by direct reaction of the ligand and $[\text{Fe}(\text{CF}_3\text{SO}_3)_2(\text{CH}_3\text{CN})_2]$. Attempts to prepare **Λ -1P** and **Δ -1P** by this method yielded a mixture of products according to $^1\text{H-NMR}$ analysis, probably reflecting a mixture of topological isomeric species.^{56,59,71} For **Δ -1P**, the standard procedure described for **1** and **Λ -1P** resulted in non-crystalline material. Changing acetonitrile by THF in the reaction of **(*R,R,R*)-mcpp** with FeCl_2 and by CH_2Cl_2 in the subsequent reaction to obtain the triflate complex produced highly pure complex **Δ -1P** in crystalline form from CH_2Cl_2 /diethyl ether. A schematic representation for the synthesis of the complexes is shown in Scheme III.2.



Scheme III.1. Synthesis of pinene-containing complexes.

Δ - $[\text{FeCl}_2((\textit{R,R,R})\text{-mcpp})]$. Under a N_2 atmosphere, FeCl_2 (25 mg, 0.198 mmol) was added to a stirred solution of **(*R,R,R*)-mcpp** (100 mg, 0.198 mmol) in THF (5 mL). The reaction was stirred overnight to obtain an orange jelly. The solvent was evaporated under reduced pressure and the resulting solid was redissolved with CH_2Cl_2 and filtered. Slow diffusion of diethyl ether to the solution led to the formation of 40 mg (0.062 mmol, 63%) of orange crystals after 2 days. Anal. Calcd for $\text{C}_{34}\text{H}_{48}\text{Cl}_2\text{FeN}_4 \cdot 0.6 \text{CH}_2\text{Cl}_2$ (MW = 639.53 g/mol): N, 8.11; C, 60.19; H, 7.18. %. Found: N, 8.39; C, 59.99; H, 7.06%. FT-IR (ATR) ν , cm^{-1} : 2969 – 2867 (C-H)_{sp3}, 1736, 1616, 1560, 1489, 1473, 1454, 1422, 1356, 1270, 1253, 1107, 1020, 975, 956, 925, 873, 724. $^1\text{H-NMR}$ (400 MHz, CD_3CN , 300 K) δ , ppm: 138 (s), 107 (s), 48.4 (s), 47.5 (s), 16.8 (s), 9.98-0.89 (m), -6.0 (s), -23.5 (s). ESI-MS (m/z): 603.3

(100) $[M-Cl]^+$, 284.1 (25) $[M-2Cl]^{+2}$. UV(CH₃CN): λ_{max} , nm (ϵ , M⁻¹·cm⁻¹): 270 (5518), 330 (sh) and 419 (1114). CV: E_{1/2} (ΔE): 101 mV (106). X-Ray analysis indicates that the complex adopts a Δ topological chirality.

Δ -[Fe(CF₃SO₃)₂((*R,R,R*)-mcpp)] (Δ -1P). Under a N₂ atmosphere, to a stirred mixture of **Δ -[FeCl₂((*R,R,R*)-mcpp)]** (50 mg, 0.08 mmol) in CH₂Cl₂ (1.5 mL) was added a suspension of AgCF₃SO₃ (40.7 mg, 0.16 mmol) in CH₂Cl₂ (1.5 mL). The mixture was stirred for 3 hours and then filtered through Celite® to remove the precipitated AgCl. The solvent was removed under reduced pressure and the resulting solid dissolved in 1 mL of CH₂Cl₂. Slow diffusion of diethyl ether to the solution led to the formation of 41 mg (0.048 mmol, 60%) of yellow crystals after 2 days. Anal. Calcd for C₃₆H₄₈F₆FeN₄O₆S₂·0.15 CH₂Cl₂ (MW = 879.44 g/mol): N, 6.37; C, 49.37; H, 5.54; S, 7.29%. Found: N, 6.71; C, 49.08; H, 5.61; S, 7.04%. FT-IR (ATR) ν , cm⁻¹: 2935 - 2875 (C-H)_{sp3}, 1289 (Py), 1236, 1217, 1160, 1026, 634 (CF₃SO₃). ¹H-NMR (400 MHz, CD₂Cl₂, 300 K) δ , ppm: 167 (s), 112 (s), 66.5 (s), 50 (s), 25 (s), 19 (s), 9.7-0.1(m). ESI-MS (m/z): 717.2 (100) $[M-CF_3SO_3]^+$, 284.9 (20) $[M-2CF_3SO_3]^{+2}$. UV(CH₃CN): λ_{max} , nm (ϵ , M⁻¹·cm⁻¹): 256 (sh), 265 (sh) and 377 (5448).

Λ -[Fe(CF₃SO₃)₂((*S,S,R*)-pdpp)] (Λ -2P). A suspension of Fe(CH₃CN)₂(CF₃SO₃)₂ (130 mg, 0.30 mmol) in THF (2 mL) was added dropwise to a vigorously stirred solution of **(*S,S,R*)-pdpp** (138 mg, 0.30 mmol) in THF (1 mL). The pale yellow precipitate formed after stirring overnight was filtered. Diethyl ether was added to the resulting solution to ensure the complete precipitation of the product. This solid was added to the previously filtered, dissolved in CH₂Cl₂ (2 mL) and filtered again. Slow diethyl ether diffusion over the solution afforded, after a couple of days, the product as pale yellow crystals suitable for X-Ray diffraction (152 mg, 0.176 mmol, 59%). Anal. Calcd for C₃₆H₄₆F₆FeN₄O₆S₂·0.1 Et₂O (MW = 872.15 g/mol): N, 6.42; C, 50.13; H, 5.43; S, 7.35%. Found: N, 6.72; C, 50.36; H, 5.25; S, 7.55%. FT-IR (ATR) ν , cm⁻¹: 2990 – 2908 (C-H)_{sp3}, 1315 (Py), 1236, 1215, 1157, 1027, 632 (CF₃SO₃). ¹H-NMR (400 MHz, CD₂Cl₂, 300 K) δ , ppm: 182 (s), 117 (s), 76 (s), 51 (s), 32.3 (s), 28.8 (s), 21.8-17.4 (m), 7.9 to -6 (m), -8.3 (s), -20.6 (s). ESI-MS (m/z): 715.3 (100) $[M-CF_3SO_3]^+$, 283.1 (50) $[M-2CF_3SO_3]^{+2}$. UV(CH₃CN): λ_{max} , nm (ϵ , M⁻¹·cm⁻¹): 256 (sh), 265 (sh) and 376 (6301). X-Ray analysis indicates that the complex adopts a Λ topological chirality.

Δ -[Fe(CF₃SO₃)₂((R,R,R)-pdpp)] (Δ -2P). The same procedure as for complex Λ -2P gave Δ -2P as yellow crystals (147 mg, 0.170 mmol, 57%). Anal. Calcd for C₃₆H₄₆F₆FeN₄O₆S₂·H₂O (MW = 882.75 g/mol): N, 6.35; C, 48.99; H, 5.48; S, 7.25%. Found: N, 6.39; C, 48.88 H, 5.40; S, 7.10%. FT-IR (ATR) ν , cm⁻¹: 2987 – 2873 (C-H)_{sp3}, 1312 (Py), 1235, 1216, 1158, 1029, 630 (CF₃SO₃). ¹H-NMR (400 MHz, CD₂Cl₂, 300 K) δ , ppm: 176 (S), 118 (s), 79 (s), 49 (s), 33.7 (s), 28.3 (s), 18.3 (sa), 8.2 to -2 (m), -8.1 (s), -15.9 (s). ESI-MS (m/z): 715.3 (100) [M-CF₃SO₃]⁺, 283.1 (80) [M-2CF₃SO₃]⁺². UV(CH₃CN): λ_{\max} , nm (ϵ , M⁻¹·cm⁻¹): 257 (sh), 265 (sh) and 378 (5550). X-Ray analysis indicates that the complex adopts a Δ topological chirality.

III.4.4 SOLID STATE CHARACTERIZATION OF COMPLEXES

Table III.16. Crystal data and refinement details for Δ -1P, Λ -2P, and Δ -2P.

Compound	Δ -1P	Λ -2P	Δ -2P
Empirical formula	C ₃₆ H ₄₈ F ₆ FeN ₄ O ₆ S ₂	C ₃₆ H ₄₆ F ₆ FeN ₄ O ₆ S ₂	C ₃₆ H ₄₆ F ₆ FeN ₄ O ₆ S ₂
Formula weight	866.75	864.74	864.74
Temperature	100(2) K	300(2) K	300(2) K
Wavelength	0.71073 Å	0.71073 Å	0.71073 Å
Crystal system	Trigonal	Orthorhombic	Orthorhombic
Space group	P3121	P2(1)2(1)2(1)	P2(1)2(1)2(1)
Unit cell dimensions	a = 18.797(3) Å α = 90° b = 18.797(3) Å β = 90° c = 12.998(12) Å γ = 120°	a = 14.954(11) Å α = 90° b = 16.340(12) Å β = 90° c = 16.575(12) Å γ = 90°	a = 15.398(2) Å α = 90° b = 26.204(3) Å β = 90° c = 10.6011(14) Å γ = 90°
Volume	3977.2(16) Å ³	4050(5) Å ³	4277.4(10) Å ³
Z	3	4	4
Density (calculated)	1.271 Mg/m ³	1.418 Mg/m ³	1.610 Mg/m ³
Absorption coefficient	0.434 mm ⁻¹	0.551 mm ⁻¹	0.537 mm ⁻¹
F(000)	1608	1800	2152
Reflections collected	38824	63774	67855
Independent reflections	6235 [R(int) = 0.0581]	10101 [R(int) = 0.0808]	10554 [R(int) = 0.1084]
Final R indices	R1 = 0.0406	R1 = 0.0549	R1 = 0.0596
[I>2sigma(I)]	wR2 = 0.1029	wR2 = 0.1440	wR2 = 0.1301
R indices (all data)	R1 = 0.0450 wR2 = 0.1044	R1 = 0.0890 wR2 = 0.1610	R1 = 0.1112 wR2 = 0.1467

The solid state structure of Δ -1P, Λ -2P, and Δ -2P could be established by X-Ray diffraction analysis. Crystal data and refinement details are given in Table III.16. X-Ray structure is shown in Figure III.7, and selected bond lengths and angles are detailed in Table III.17.

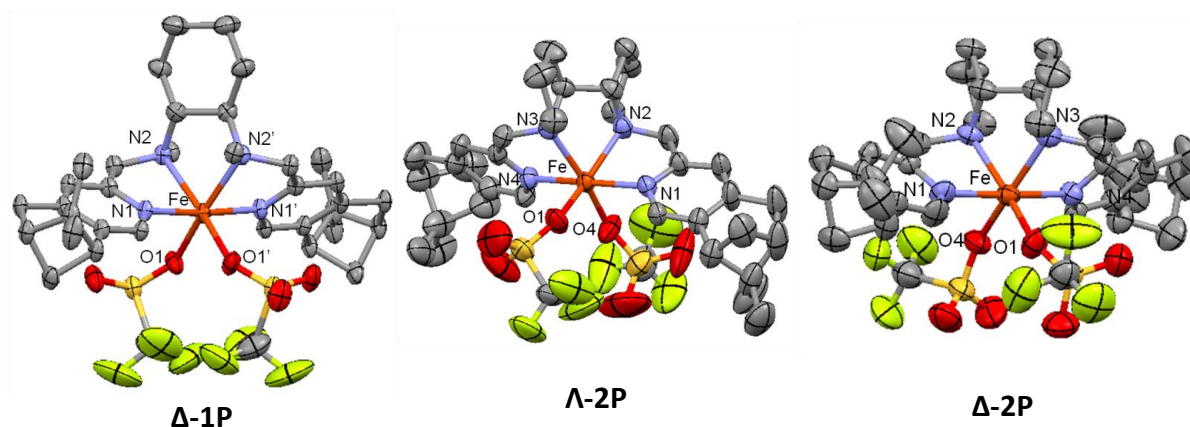


Figure III.7. X-Ray structures Δ -1P, Λ -2P and Δ -2P. Hydrogen atoms and solvents of crystallization are omitted for clarity.

Table III.17. Selected bond lengths [Å] and angles [°] for Δ -1P, Λ -2P and Δ -2P.

Δ -1P		Λ -2P		Δ -2P	
Fe1 N1'	2.1407	Fe1 N1	2.176(3)	Fe1 N1	2.180(3)
Fe1 N1	2.1407	Fe1 N2	2.220(3)	Fe1 N2	2.218(3)
Fe1 N2'	2.2335	Fe1 N3	2.210(3)	Fe1 N3	2.228(3)
Fe1 N2	2.2335	Fe1 N4	2.184(3)	Fe1 N4	2.175(3)
Fe1 O1'	2.1229	Fe1 O1A	2.132(3)	Fe1 O1	2.121(3)
Fe1 O1	2.1229	Fe1 O1B	2.116(3)	Fe1 O4	2.127(3)
N1 Fe1 N2	98.38	N1 Fe1 N2	77.49(11)	N1 Fe1 N2	77.79(12)
N1 Fe1 N2'	77.57	N1 Fe1 N3	99.18(11)	N1 Fe1 N3	98.47(11)
N1 Fe1 N1'	174.80	N1 Fe1 N4	172.96(11)	N1 Fe1 N4	175.75(12)
N2 Fe1 N2'	79.85	N2 Fe1 N3	80.80(12)	N2 Fe1 N3	79.93(12)
N2 Fe1 N1'	77.57	N2 Fe1 N4	107.20(11)	N2 Fe1 N4	102.19(13)
N2' Fe1 N1'	98.38	N3 Fe1 N4	76.75(11)	N3 Fe1 N4	77.38(11)
O1' Fe1 N1	95.16	O1B Fe1 N1	86.46(11)	N1 Fe1 O1	88.46(12)
O1' Fe1 N2	164.39	O1B Fe1 N2	162.98(11)	N2 Fe1 O1	161.73(12)
O1' Fe1 N2'	95.60	O1B Fe1 N3	96.42(14)	N3 Fe1 O1	90.42(11)
O1' Fe1 N1'	88.44	O1B Fe1 N4	88.28(11)	N4 Fe1 O1	90.64(13)
O1 Fe1 N1	88.44	O1A Fe1 N1	95.94(12)	N1 Fe1 O4	96.35(11)
O1 Fe1 N2	95.60	O1A Fe1 N2	85.23(13)	N2 Fe1 O4	92.48(13)
O1 Fe1 N2'	164.39	O1A Fe1 N3	156.62(12)	N3 Fe1 O4	161.49(11)
O1 Fe1 N1'	95.16	O1A Fe1 N4	89.75(11)	N4 Fe1 O4	87.90(12)
O1' Fe1 O1	92.48	O1B Fe1 O1A	102.24(15)	O1 Fe1 O4	101.04(13)

III.4.5 SYNTHESIS OF SUBSTRATES

(1*R*)-(-)-menthyl acetate (3), cyclohexane (9), 2,6-dimethyloctane (14), 1-bromo-3,7-dimethyloctane (17), *n*-hexane (23), *n*-heptane (26), methyl hexanoate (30), *cis*-1,2-dimethylcyclohexane (5), *cis*-decalin (34), *trans*-1,2-dimethylcyclohexane (37), *trans*-decalin (41), gem-dimethylcyclohexane (45), (-)-ambroxide (49), (3*aR*)-(+)-sclareolide (50), (1*R*)-(-)-neomenthyl acetate (67) and (1*S*)-(+)-neomenthyl acetate (55) were purchased from Aldrich or TCI America. *cis*-4-methylcyclohexanol, *trans*-4-methylcyclohexanol, 3,7-dimethyl-1-octanol, (1*S*,2*R*,5*S*)-(+)-menthol, (1*R*,2*S*,5*R*)-(-)-menthol, (1*S*,2*S*,5*R*)-(+)-neomenthol and (+)-cedrol were purchased from Aldrich or TCI America. (1*S*,2*R*,5*R*)-(+)-isomenthol was purchased from ABCR (Germany). *Cis*-4-methylcyclohexyl pivalate (7), *trans*-4-methylcyclohexyl pivalate (11) and 3,7-dimethyloctyl acetate (20) were synthesized as previously described.⁵⁰ All liquid substrates were passed through an alumina plug before being used.

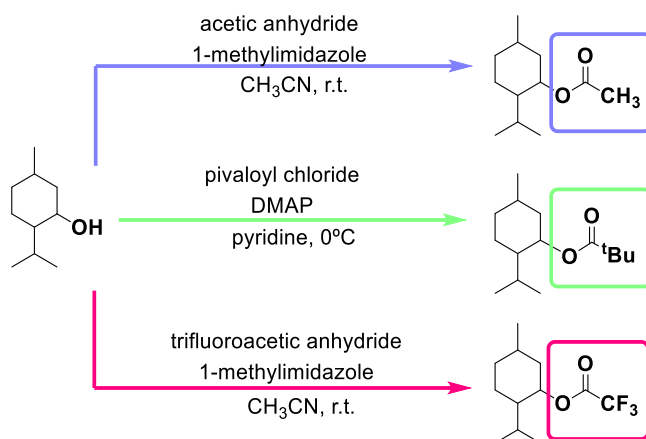
(+)-Cedryl acetate (51)

(+)-Cedryl acetate was prepared by acetylating the commercially available (+)-cedrol, following the procedure described below:

(+)-Cedrol (2.00 g, 9.0 mmol), 4-dimethylaminopyridine (DMAP, 1.32 g, 10.8 mmol) and acetic anhydride (1.0 mL, 10.8 mmol) were dissolved in dichloromethane (27 mL) and stirred for 24 h at room temperature. After this time, DMAP (0.66 g, 5.4 mmol) and acetic anhydride (0.5 mL, 5.4 mmol) were added and the mixture was further stirred for 24 h at rt. The reaction was then diluted with dichloromethane (50 mL) and washed successively with water (50 mL), saturated NaHCO₃ solution (50 mL) and brine (50 mL). The organic layer was dried over MgSO₄ and the solvent was removed under reduced pressure. The product was purified by flash chromatography over silica (hexane:diethyl ether 30:1). 1.91 g of colorless oil was obtained (76% yield). FT-IR (ATR) ν , cm⁻¹: 2991, 2901, 2872, 1723, 1486, 1373, 1242, 1117, 1086. ¹H-NMR (400 MHz, CDCl₃, 300 K) δ , ppm: 2.40 (d, *J* = 5.2 Hz, 1H), 2.1-1.8 (m, 4H), 1.95 (s, 3H), 1.7-1.6 (m, 2H), 1.54 (s, 3H), 1.45-1.2 (m, 6H), 1.17 (s, 3H), 0.98 (s, 3H), 0.83 (d, *J* = 6.8 Hz, 3H). ¹³C-NMR (100 MHz, CDCl₃, 300 K) δ , ppm: 170.3, 86.2, 56.8, 56.7, 53.9, 43.3, 41.3, 40.9, 36.9, 33.2, 31.2, 28.4, 26.9, 25.8, 25.2, 22.8, 15.5. ESI-MS (*m/z*): 287.3 [M+Na]⁺.

Menthol derivatives

(+)-Menthyl acetate (**53**) and (+)-isomenthyl acetate (**54**) were prepared by acetylating the commercially available (+)-menthol and (+)-isomenthol, respectively, following the procedure described below (Scheme III.2)



Scheme III.2. Synthesis of menthyl derivatives.

(+)-Menthol or (+)-isomenthol (5g, 30.7 mmol), 1-methylimidazole (3.5 mL) and acetic anhydride (35 mL) were dissolved in CH₃CN (60 mL) and stirred for 30 min at room temperature. Ice (50 mL) was added at this point. After stirring for 15 min, CHCl₃ (125 mL) was added. The organic layer was washed with H₂SO₄ 1 M (50 mL), saturated NaHCO₃ solution (50 mL) and water (50 mL), dried over MgSO₄ and the solvent was removed under reduced pressure.

(+)-Menthyl acetate (**53**)

Purification by flash chromatography over silica (hexane:ethyl acetate 3:1). 72% yield. ¹H-NMR (400 MHz, CDCl₃, 300 K) δ, ppm: 4.67 (td, J = 10.8, 4.4 Hz, 1H), 2.03 (s, 3H), 2.01-1.95 (m, 1H), 1.90-1.81 (m, 1H), 1.71-1.63 (m, 2H), 1.55-1.41 (m, 1H), 1.39-1.31 (m, 1H), 1.11-0.80 (m, 3H), 0.89 (d, J = 6.6 Hz, 3H), 0.88 (d, J = 7.1 Hz, 3H), 0.75 (d, J = 6.9 Hz, 3H). In agreement with that of (–)-menthyl acetate. GC-MS (m/z): 216.2 [M+NH₄]⁺.

(+)-Isomenthyl acetate (**54**)

Purification by flash chromatography over silica (hexane:ethyl acetate 2:1). 79% yield. FT-IR (ATR) ν, cm⁻¹: 2956, 2929, 2871, 1730, 1368, 1239, 1028. ¹H-NMR (400 MHz, CDCl₃, 300 K) δ, ppm: 5.03 (td, J = 6.8, 3.7 Hz, 1H), 2.03 (s, 3H), 1.89-1.86 (m, 1H), 1.76-1.71 (m, 1H), 1.60-1.54 (m, 2H), 1.52-1.43 (m, 3H), 1.32-1.22 (m, 2H), 0.93 (d, J = 6.8 Hz,

3H), 0.92 (d, $J = 6.9$ Hz, 3H), 0.85 (d, $J = 6.6$ Hz, 3H). $^{13}\text{C-NMR}$ (100 MHz, CDCl_3 , 300 K) δ , ppm: 170.6, 71.5, 45.8, 35.9, 30.0, 27.5, 26.3, 21.4, 20.9, 20.7, 20.4, 18.9. HRMS (ESI-TOF, $[\text{M} + \text{Na}]^+$): m/z calcd for $\text{C}_{12}\text{H}_{22}\text{O}_2\text{Na}$ 221.1512, found 221.1515.

(+)-Isomenthyl pivalate (64) and (+)-neomenthyl pivalate (75) were prepared by reaction of pivaloyl chloride with commercially available (+)-isomenthol and (+)-neomenthol, respectively, in presence of catalytic amounts of 4-dimethylaminopyridine following the procedure described below (Scheme III.2):

(+)-Isomenthol or (+)-neomenthol (5 g, 30.7 mmol) and 4-dimethylaminopyridine (360 mg) were dissolved in pyridine (50 mL). The resulting mixture was cooled in an ice-bath and a solution of pivaloyl chloride (4.2 mL, 33.5 mmol) in pyridine (30 mL) was added dropwise. After stirring for 24 hours, the solvent was removed under reduced pressure and the resulting residue was treated with CHCl_3 (250 mL) and washed with water (100 mL), saturated NaHCO_3 aqueous solution (100 mL) and saturated NaCl aqueous solution (100 mL). The organic phase was dried over MgSO_4 , filtered and the solvent was removed under reduced pressure to yield a colorless liquid.

(+)-Isomenthyl pivalate (64)

Purification by flash chromatography over silica (hexane:ethyl acetate 7:1) followed by flash chromatography over alumina (100% hexane). 65% yield. FT-IR (ATR) ν , cm^{-1} : 2957, 2930, 2872, 1723, 1283, 1163, 1138. $^1\text{H-NMR}$ (400 MHz, CDCl_3 , 300 K) δ , ppm: 5.01 (dt, $J = 6.2, 3.4$, 1H), 1.88-1.82 (m, 1H), 1.78-1.70 (m, 1H), 1.60-1.41 (m, 6H), 1.35-1.26 (m, 1H), 1.19 (s, 9H), 0.94 (d, $J = 6.6$ Hz, 3H), 0.91 (d, $J = 7.1$ Hz, 3H), 0.85 (d, $J = 6.7$ Hz, 3H). $^{13}\text{C-NMR}$ (100 MHz, CDCl_3 , 300 K) δ , ppm: 177.9, 71.3, 45.4, 38.8, 35.5, 29.9, 27.5, 27.1, 26.2, 21.0, 20.9, 20.8, 19.3. HRMS (ESI-TOF, $[\text{M} + \text{Na}]^+$): m/z calcd for $\text{C}_{15}\text{H}_{28}\text{O}_2\text{Na}$ 263.1981, found 263.1969.

(+)-Neomenhtyl pivalate (75)

Purification by flash chromatography over silica (hexane 100%). 75% yield. FT-IR (ATR) ν , cm^{-1} : 2954, 2920, 2870, 1723, 1478, 1284, 1164, 1142. $^1\text{H-NMR}$ (400 MHz, CDCl_3 , 300 K) δ , ppm: 5.15-5.12 (m, 1H), 1.96-1.89 (m, 1H), 1.80-1.72 (m, 2H) 1.65-1.52 (m, 1H), 1.47-1.25 (m, 2H), 1.20 (s, 9H), 1.65-0.91 (m, 3H), 0.89 (d, $J = 6.7$ Hz, 3H), 0.85 (d, $J = 6.5$

Hz, 3H), 0.84 (d, $J = 6.6$ Hz, 3H). ^{13}C -NMR (100 MHz, CDCl_3 , 300 K) δ , ppm: 177.8, 70.5, 47.0, 39.1, 39.0, 34.8, 29.3, 27.2, 26.6, 25.4, 22.2, 21.1, 20.6. HRMS (ESI-TOF, $[\text{M} + \text{Na}]^+$): m/z calcd for $\text{C}_{15}\text{H}_{28}\text{O}_2\text{Na}$ 263.1981, found 263.1967.

(–)-Menthyl trifluoroacetate (59) and (+)-neomenthyl trifluoroacetate (72) were prepared by acetylating the commercially available (–)-menthol and (+)-neomenthol, respectively, following the procedure described below (Scheme S2):

(–)-Menthol or (+)-neomenthol (2.5 g, 16.0 mmol), 1-methylimidazole (1.5 mL) and trifluoroacetic anhydride (15 mL) were dissolved in CH_3CN (30 mL) and stirred for 24 hours at room temperature. Ice (25 mL) was added at this point. After stirring for 15 min, CHCl_3 (60 mL) was added. The organic layer was washed with H_2SO_4 1 M (25 mL) and a mixture of water (23 mL) and saturated NaHCO_3 solution (2 mL) (four times, until neutral pH), dried over MgSO_4 and the solvent was removed under reduced pressure.

(–)-Menthyltrifluoroacetate (59)

Purification over silica (hexane ethyl acetate 95:5). 75% yield. FT-IR (ATR) ν , cm^{-1} : 2959, 2930, 2874, 1776, 1218, 1161, 1143, 947, 729. ^1H -NMR (400 MHz, CDCl_3 , 300 K) δ , ppm: 4.87 (td, $J = 11.0, 4.5$ Hz; 1H), 2.07-2.04 (m, 1H), 1.89-1.81 (m, 1H), 1.76-1.72 (m, 2H), 1.56-1.50 (m, 2H), 1.18-1.12 (m, 2H), 0.97-0.88 (m, 1H), 0.94 (d, $J = 6.6$ Hz, 3H), 0.92 (d, $J = 7.0$ Hz, 3H), 0.78 (d, $J = 7.0$ Hz, 3H). ^{13}C -NMR (100 MHz, CDCl_3 , 300 K) δ , ppm: 157.2, 114.7, 79.3, 46.7, 40.0, 33.9, 31.4, 26.2, 23.4, 21.8, 20.5, 16.1. HRMS (ESI-TOF, $[\text{M} + \text{Na}]^+$): m/z calcd for $\text{C}_{12}\text{H}_{19}\text{F}_3\text{O}_2\text{Na}$ 275.1223, found 275.1216.

(+)-Neomenthyltrifluoroacetate (72)

Purification over silica (hexane ethyl acetate 95:5). 73% yield. FT-IR (ATR) ν , cm^{-1} : 2955, 2929, 1778, 1331, 1217, 1160, 1137. ^1H -NMR (400 MHz, CDCl_3 , 300 K) δ , ppm: 5.41-5.40 (m, 1H), 2.05-2.00 (m, 1H), 1.81-1.77 (m, 2H), 1.65-1.59 (m, 1H), 1.48-1.33 (m, 2H), 1.2-1.04 (m, 2H), 1.12-0.95 (m, 1H), 0.92 (d, $J = 6.7$ Hz, 3H), 0.89 (d, $J = 6.6$ Hz, 3H), 0.88 (d, $J = 6.7$ Hz, 3H). ^{13}C -NMR (100 MHz, CDCl_3 , 300 K) δ , ppm: 157.0, 114.7, 76.9, 46.6, 38.6, 34.4, 29.0, 26.3, 24.7, 21.9, 20.7, 20.5. HRMS (ESI-TOF, $[\text{M} + \text{Na}]^+$): m/z calcd for $\text{C}_{12}\text{H}_{19}\text{F}_3\text{O}_2\text{Na}$ 275.1223, found 275.1199.

III.4.6 REACTION CONDITIONS FOR CATALYSIS

III.4.6.1 *Sample analysis*

GC analysis of the catalysis provided substrate conversions and product yields relative to the internal standard integration. Calibration curves were obtained from commercial products when available or from pure isolated products obtained from a catalytic reaction (*vide infra*).

Cyclohexanone, tetrahydrolinalool, tetrahydromyrcenol, *n*-hexanones, *n*-heptanones, 1-decalone, 2-decalone, *gem*-dimethylcyclohexanones were purchased from Aldrich or TCI America. For non-commercially available products, pure samples were synthesized, isolated and characterized following the experimental procedure described below or in the literature.⁵⁰

III.4.6.2 *Kinetic studies*

Profiles of the catalytic oxidation of (1R)-(-)-menthyl acetate (**3**) and *cis*-1,2-dimethylcyclohexane (**5**). Two-step addition of H₂O₂ to prove the relative stability of the catalysts in the presence of large excess of substrate. A 5 mL vial was charged with: Catalyst (7 μmol, 1 mol%), substrate (**3** or **5**) (700 μmol, 1 equiv), CH₃CN (4.7 mL) and a magnetic stir bar. The vial was placed in an ice bath and stirred. A 1.74 M CH₃CO₂H solution in CH₃CN was added (197 μL, 350 μmol, 50 mol%) and 560 μL of a 1.5 M (840 μmol, 1.2 equiv) H₂O₂ solution (diluted from a 35% H₂O₂ aqueous solution) were delivered by syringe pump over 6 min at 0°C. After syringe pump addition, the resulting solution was stirred for another 6 min. At this point 4 equiv of substrate (**3** or **5**) (2.8 mmol) were added and a second addition of H₂O₂ (560 μL of 1.5 M, 840 μmol, 1.2 equiv, starting time of second addition: 12.5 min) were delivered by syringe pump over 6 min. After syringe pump addition, the resulting solution was stirred for another 6 min. 100 μL samples of the crude reaction were taken at different times and immediately passed through a short alumina plug along with the internal standard, followed by elution with 0.5 mL of AcOEt. Finally, the solution was subjected to GC analysis.

III.4.6.3 *Iterative addition protocol*

Substrates: *cis*-4-methylcyclohexyl pivalate (**7**, 3 additions) and cyclohexane (**9**, 2 additions).

A 5 mL vial was charged with: Catalyst (1 μmol , 1 mol%), the substrate (100 μmol , 1 equiv), CH_3CN (0.67 mL) and a magnetic stir bar. The vial was placed on an ice bath and stirred. A 1.74 M $\text{CH}_3\text{CO}_2\text{H}$ solution in CH_3CN was added (29 μL , 50 μmol , 50 mol%) and 80 μL of a 1.5 M (120 μmol , 1.2 equiv) H_2O_2 solution (diluted from a 35% H_2O_2 aqueous solution) were delivered by syringe pump over 6 min at 0°C. After syringe pump addition, the solution was stirred for 10 min at 0°C and a solution of catalyst (1 μmol , 1 mol%), CH_3CN (0.67 mL) and $\text{CH}_3\text{CO}_2\text{H}$ (29 μL 1.74 M solution, 50 μmol , 50 mol%) was added simultaneously with 80 μL of a 1.5 M (120 μmol , 1.2 equiv) H_2O_2 solution via syringe pump over 6 min. After syringe pump addition the resulting solution was stirred for another 10 min.

If a third addition was required: then a solution of catalyst (1 μmol , 1 mol%), CH_3CN (0.67 mL) and $\text{CH}_3\text{CO}_2\text{H}$ (29 μL 1.74 M solution, 50 μmol , 50 mol%) was added simultaneously with 80 μL of a 1.5 M (120 μmol , 1.2 equiv) H_2O_2 solution via syringe pump over 6 min. After syringe pump addition the resulting solution was stirred for another 10 min.

An internal standard was added at this point. The iron complex was removed by passing the solution through a short path of silica followed by elution with 2 mL of AcOEt . Finally, the solution was subjected to GC analysis.

III.4.6.4 *Single addition protocol*

cis-1,2-dimethylcyclohexane (5)

A 5 mL vial was charged with: Catalyst (1.2 μmol , 1 mol%), substrate (120 μmol , 1 equiv.), CH_3CN (0.8 mL) and a magnetic stir bar. A 1.74 M $\text{CH}_3\text{CO}_2\text{H}$ solution in CH_3CN was added (35 μL , 60 μmol , 150 mol%) and the vial was placed on an ice bath and stirred. 96 μL of a 1.5 M (144 μmol 1.2 equiv) H_2O_2 solution (diluted from a 35% H_2O_2 aqueous solution) were delivered by syringe pump over 6 min at 0 °C. After syringe pump addition, the resulting solution was stirred for another 10 min. Biphenyl was added at this point as internal. The iron complex was removed by passing the solution through a short path of silica followed by elution with 2 mL of AcOEt . Finally, the solution was subjected to GC analysis.

Other substrates

A 5 mL vial was charged with: Catalyst (1.2 μmol , 3 mol%), substrate (40 μmol , 1 equiv.), CH_3CN (0.8 mL) and a magnetic stir bar. A 1.74 M $\text{CH}_3\text{CO}_2\text{H}$ solution in CH_3CN was added (35 μL , 60 μmol , 150 mol%) and the vial was placed on an ice bath and stirred. The necessary amount of a 1.5 M (X equiv, see Table III.18) H_2O_2 solution (diluted from a 35% H_2O_2 aqueous solution) was delivered by syringe pump over 17 min at 0 °C. After syringe pump addition, the resulting solution was stirred for another 10 min. Biphenyl was added at this point as internal standard. The iron complex was removed by passing the solution through a short path of silica followed by elution with 2 mL of AcOEt. Finally, the solution was subjected to GC analysis.

Table III.18. Conditions for the oxidation of several substrates.

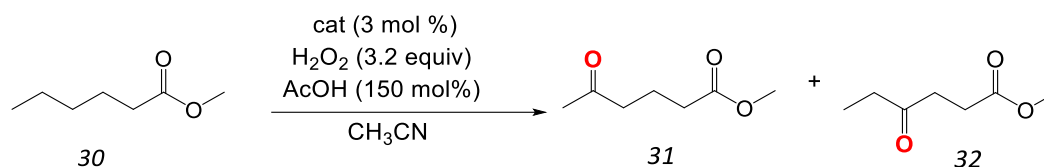
cat:H₂O₂:Substrate:AcOH (equiv of H₂O₂)	Substrates
3:200:100:150 (2)	3, 7, 11, 14, 17, 20, 34, 37, 53, 54, 55, 59, 64, 67, 72, 75
3:250:100:150 (2.5)	51
3:260:100:150 (2.6)	49 (room temperature)
3:280:100:150 (2.8)	9, 41
3:320:100:150 (3.2)	23, 26, 30, 45
3:340:100:150 (3.4)	50 (different temperatures)

III.4.7 PROCEDURE FOR PRODUCT ISOLATION

A 25 mL round bottom flask was charged with: Catalyst (12 μmol , 3 mol%), alkane (0.4 mmol, 1 equiv), CH_3CN (8 mL) and a magnetic stir bar. A 1.74 M $\text{CH}_3\text{CO}_2\text{H}$ solution in CH_3CN was added (0.35 mL, 0.6 mmol, 150 mol%) and the mixture was placed on an ice bath and stirred. The necessary amount of a 1.5 M (X equiv, Table III.18) H_2O_2 solution (diluted from a 35% H_2O_2 aqueous solution) was delivered by syringe pump over 17 min at 0 °C. After syringe pump addition, the solution was stirred for 10 min at 0 °C. The iron complex was removed by passing the solution through a short path of silica followed by elution with 2 mL of AcOEt. Solvent was removed under reduced pressure and the resulting residue was purified by flash chromatography on silica gel. Purity of obtained products was checked by $^1\text{H-NMR}$ and GC, and yields corrected based on this results.

Methylhexanoate (30):

Purification by flash chromatography over silica (100% hexane).

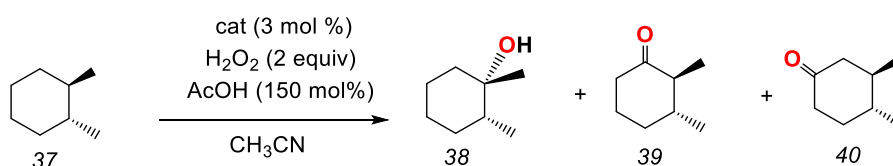
**Scheme III.3.** Catalytic oxidation of methyl hexanoate.

31. ¹H-NMR (400 MHz, CDCl₃, 300 K) δ, ppm: 3.67 (s, 3H), 2.51 (t, J = 7.2 Hz, 2H), 2.35 (t, J = 7.2 Hz, 2H), 2.14 (s, 3H), 1.90 (p, J = 7.3 Hz, 2H). In agreement with that reported in the literature.⁵¹ GC-MS (m/z): 162.1 [M+NH₄]⁺

32. ¹H-NMR (400 MHz, CDCl₃, 300 K) δ, ppm: 3.68 (s, 3H), 2.73 (t, J = 6.5 Hz, 2H), 2.60 (t, J = 6.6 Hz, 2H), 2.48 (q, J = 7.2 Hz, 2H), 1.08 (t, J = 7.2 Hz, 3H). In agreement with that reported in the literature.⁵¹ GC-MS (m/z): 162.1 [M+NH₄]⁺

***trans*-1,2-Dimethylcyclohexane (37):**

Purification by flash chromatography over silica (hexane 100%).

**Scheme III.4.** Catalytic oxidation of *trans*-dimethylcyclohexane.

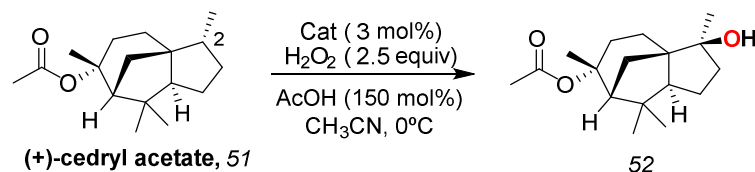
38. ¹H-NMR (400 MHz, CDCl₃, 300 K) δ, ppm: 1.69-1.63 (m, 2H), 1.54-1.48 (m, 2H), 1.46-1.20 (m, 5H), 1.18 (s, 3H), 0.90 (d, J = 6.5 Hz, 3H). In agreement with that reported in the literature.⁵⁰ GC-MS (m/z): 146.1 [M+NH₄]⁺.

39. ¹H-NMR (400 MHz, CDCl₃, 300 K) δ, ppm: 2.42-2.36 (m, 1H), 2.29 (ddt, J = 13.2, 5.9, 1.2 Hz; 1H), 2.08-1.99 (m, 2H), 1.86-1.81 (m, 1H), 1.71-1.59 (m, 1H), 1.53-1.40 (m, 2H), 1.06 (d, J = 6.1 Hz, 3H), 1.03 (d, J = 6.6 Hz, 3H). In agreement with that reported in the literature.⁷² GC-MS (m/z): 144.1 [M+NH₄]⁺.

40. ¹H-NMR (400 MHz, CDCl₃, 300 K) δ, ppm: 2.36-2.31 (m, 3H), 2.09-1.96 (m, 2H), 1.54-1.35 (m, 3H), 1.01 (d, J = 5.8 Hz, 3H), 1.00 (d, J = 6.1 Hz, 3H). In agreement with that reported in the literature.⁷² GC-MS (m/z): 144.1 [M+NH₄]⁺.

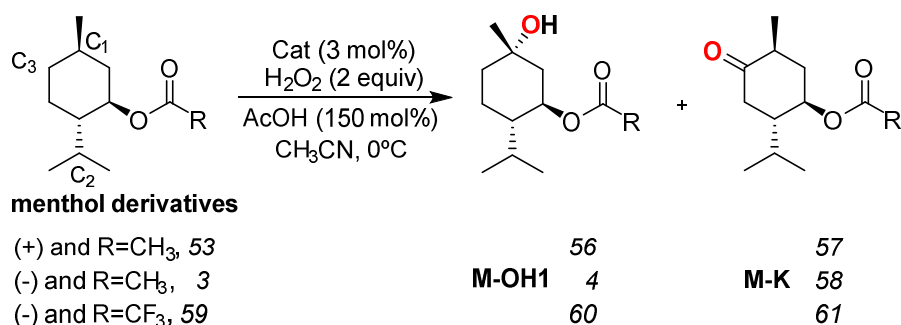
(+)-Cedryl acetate (51)

Purification by flash chromatography over silica (hexane:diethyl ether 4:1).



Scheme III.5. Catalytic oxidation of (+)-cedryl acetate.

52. FT-IR (ATR) ν , cm^{-1} : 3479, 2961, 1706, 1370, 1280, 1250, 1147, 1107, 1015. $^1\text{H-NMR}$ (400 MHz, CDCl_3 , 300 K) δ , ppm: 2.43 (d, $J = 5.6$ Hz, 1H), 2.0 (m, 1H), 1.95 (s, 3H), 1.9-1.8 (m, 4H), 1.6-1.2 (m, 6H), 1.54 (s, 3H), 1.17 (s, 3H), 1.15 (s, 3H), 1.02 (s, 3H). $^{13}\text{C-NMR}$ (75 MHz, CDCl_3 , 300 K) δ , ppm: 170.4, 85.8, 79.4, 57.3, 54.8, 53.7, 44.8, 41.2, 35.7, 33.5, 29.6, 27.9, 26.7, 25.8, 24.2, 22.7, 21.4. In agreement with that reported in the literature.^{20,73} ESI-MS (m/z): 303.2 $[\text{M}+\text{Na}]^+$.



Scheme III.6. Catalytic oxidation of menthol derivatives.

Menthyl acetate (53 or 3):

Purification by flash chromatography over silica (hexane).

56 or 4. $^1\text{H-NMR}$ (400 MHz, CDCl_3 , 300 K) δ , ppm: 5.03-4.96 (m, 1H), 2.07-2.00 (m, 1H) 2.03 (s, 3H), 1.93-1.85 (m, 1H), 1.71-1.65 (m, 1H), 1.55-1.32 (m, 5H), 1.24 (s, 3H), 0.92 (d, $J = 7.0$ Hz, 3H), 0.80 (d, $J = 7.1$ Hz, 3H). In agreement with that reported in the literature.⁵¹ GC-MS (m/z): 232.2 $[\text{M}+\text{NH}_4]^+$.

57 or 58. FT-IR (ATR) ν , cm^{-1} : 2958, 2928, 2872, 1714, 1365, 1235, 1030, 803. $^1\text{H-NMR}$ (400 MHz, CDCl_3 , 300 K) δ , ppm: 5.11-5.03 (m, 1H), 2.58-2.47 (m, 1H) 2.39-2.30 (m, 2H), 2.21-2.11 (m, 1H), 2.08 (s, 3H), 1.99-1.87 (m, 2H), 1.47-1.36 (m, 1H), 1.03 (d, $J = 6.6$ Hz, 3H), 0.89 (d, $J = 6.7$ Hz, 3H), 0.83 (d, $J = 6.7$ Hz, 3H). $^{13}\text{C-NMR}$ (100 MHz, CDCl_3 , 300 K)

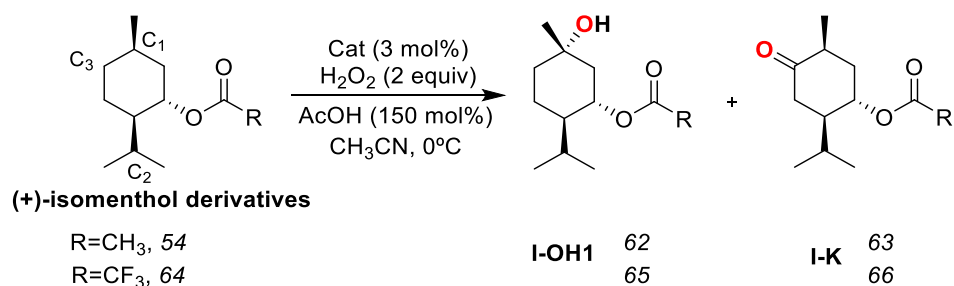
δ , ppm: 211.2, 170.6, 71.4, 47.8, 42.0, 39.2, 38.4, 26.6, 21.2, 20.3, 15.7, 14.1. HRMS (ESI-TOF, $[M + Na]^+$): m/z calcd for $C_{12}H_{20}O_3Na$ 235.1305, found 235.1297.

Menthyl trifluoroacetate (59):

Purification by flash chromatography over silica (dichloromethane 100%).

60. FT-IR (ATR) ν , cm^{-1} : 3419, 2962, 2933, 1778, 1372, 1219, 1148, 923. 1H -NMR (400 MHz, $CDCl_3$, 300 K) δ , ppm: 5.23-5.19 (m, 1H), 2.09 (ddd, $J = 12.7, 4.6, 2.7$ Hz; 1H) 1.91-1.82 (m, 1H), 1.72-1.66 (m, 1H), 1.62 - 1.46 (m, 5H), 1.28 (s, 3H), 0.94 (d, $J = 7.0$ Hz, 3H), 0.83 (d, $J = 7.0$ Hz, 3H). ^{13}C -NMR (100 MHz, $CDCl_3$, 300 K) δ , ppm: 157, 114.6, 77.4, 71.1, 46.6, 43.8, 37.7, 31.3, 26.2, 20.6, 19.2, 16.3. HRMS (ESI-TOF, $[M + Na]^+$): m/z calcd for $C_{12}H_{19}F_3O_3Na$ 291.1178, found 291.1161.

61. FT-IR (ATR) ν , cm^{-1} : 2965, 2937, 1780, 1717, 1372, 1220, 1157. 1H -NMR (400 MHz, $CDCl_3$, 300 K) δ , ppm: 5.25 (dt, $J = 10.8, 4.4$ Hz; 1H), 2.59-2.50 (m, 1H) 2.45-2.38 (m, 2H), 2.18 (dt, $J = 13.7, 1.1$ Hz; 1H), 2.12-2.02 (m, 2H), 1.95-1.88 (m, 1H), 1.07 (d, $J = 1.07$ Hz, 3H), 0.91 (d, $J = 7.0$ Hz, 3H), 0.85 (d, $J = 6.8$ Hz, 3H). ^{13}C -NMR (100 MHz, $CDCl_3$, 300 K) δ , ppm: 209.6, 157.2, 114.4, 76.0, 47.3, 41.7, 38.2, 38.0, 26.5, 20.1, 15.5, 14.0. HRMS (ESI-TOF, $[M + Na]^+$): m/z calcd for $C_{12}H_{17}F_3O_3Na$ 289.1022, found 289.1045.



Scheme III.7. Catalytic oxidation of isomenthol derivatives.

Isomenthyl acetate (54):

Purification by flash chromatography over silica (hexane:ethyl acetate 90:10).

62. FT-IR (ATR) ν , cm^{-1} : 3423, 2960, 2938, 2872, 1739, 1717, 1370, 1257, 1023, 790. 1H -NMR (400 MHz, $CDCl_3$, 300 K) δ , ppm: 4.82 (td, $J = 9.8, 4.3$ Hz, 1H), 2.05 (s, 3H), 1.98 (ddd, $J = 12.3, 4.3, 2.0$, 1H), 1.85-1.77 (m, 1H), 1.73-1.66 (m, 2H), 1.55-1.37 (m, 3H), 1.26 (s, 3H), 1.23-1.14 (m, 1H), 0.93 (d, $J = 6.7$ Hz, 3H), 0.81 (d, $J = 6.9$ Hz, 3H). ^{13}C -NMR (100

MHz, CDCl₃, 300 K) δ , ppm: 170.4, 72.0, 70.8, 46.5, 44.5, 38.5, 26.8, 26.0, 21.3, 20.8, 20.2, 17.0, HRMS (ESI-TOF, [M + Na]⁺): m/z calcd for C₁₂H₂₂O₃Na 237.1461, found 237.1466.

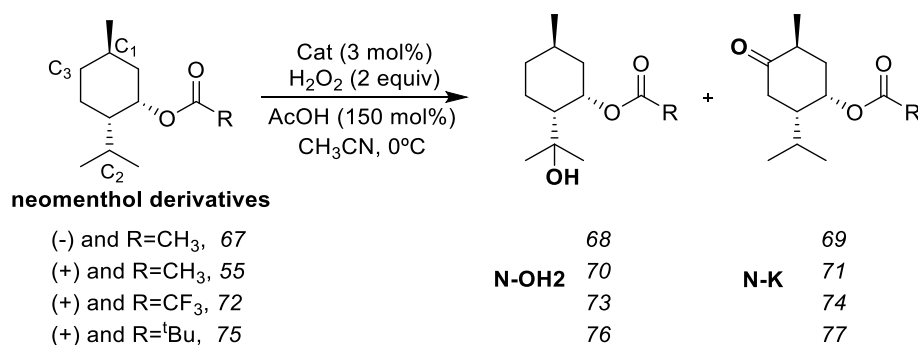
63. FT-IR (ATR) ν , cm⁻¹: 2961, 2928, 2872, 1714, 1365, 1235, 1030, 803. ¹H-NMR (400 MHz, CDCl₃, 300 K) δ , ppm: 5.23 (q, J = 3.6 Hz, 1H), 2.69-2.62 (m, 2H), 2.39 (dd, J = 14.2, 4.8 Hz, 1H), 2.12 (s, 3H), 1.92-1.88 (m, 1H), 1.74 (ddd, J = 14.7, 11.8, 3.2 Hz, 1H), 1.48-1.39 (m, 1H), 1.28-1.22 (m, 1H), 1.05 (d, J = 6.7 Hz, 3H), 0.96 (d, J = 6.8 Hz, 3H), 0.94 (d, J = 6.8 Hz, 3H). ¹³C-NMR (100 MHz, CDCl₃, 300 K) δ , ppm: 212.5, 170.4, 70.3, 48.0, 40.1, 39.1, 35.6, 28.6, 21.4, 20.3, 20.1, 14.4. HRMS (ESI-TOF, [M + Na]⁺): m/z calcd for C₁₂H₂₀O₃Na 235.1305, found 235.1309.

Isomenthyl pivalate (64):

Purification by flash chromatography over silica (hexane 100%).

65. FT-IR (ATR) ν , cm⁻¹: 3310, 2960, 2937, 2871, 1720, 1167, 1153, 1127. ¹H-NMR (400 MHz, CDCl₃, 300 K) δ , ppm: 4.81 (td, J = 9.3, 4.1 Hz, 1H), 1.98-1.92 (m, 1H), 1.87-1.77 (m, 1H), 1.75-1.64 (m, 2H), 1.55-1.39 (m, 3H), 1.28-1.22 (m, 1H), 1.25 (s, 3H), 1.19 (s, 9H), 0.94 (d, J = 6.9 Hz, 3H), 0.81 (d, J = 6.9 Hz, 3H). ¹³C-NMR (100 MHz, CDCl₃, 300 K) δ , ppm: 177.7, 71.9, 70.7, 46.3, 43.8, 38.8, 38.2, 27.2, 27.1, 26.0, 20.9, 19.9, 17.2. HRMS (ESI-TOF, [M + Na]⁺): m/z calcd for C₁₅H₂₈O₃Na 279.1931, found 279.1918.

66. FT-IR (ATR) ν , cm⁻¹: 2959, 2932, 2873, 1718, 1283, 1152, 1122. ¹H-NMR (400 MHz, CDCl₃, 300 K) δ , ppm: 5.20 (dd, J = 7.1, 3.5 Hz, 1H), 2.70-2.58 (m, 2H), 2.41 (dd, J = 14.1, 4.4 Hz, 1H), 2.15-2.09 (m, 1H), 1.93-1.71 (m, 3H), 1.25 (s, 9H), 0.96 (d, J = 6.7, 3H), 0.93 (d, J = 7.0, 3H). ¹³C-NMR (100 MHz, CDCl₃, 300 K) δ , ppm: 212.4, 177.7, 69.9, 48.0, 40.2, 39.2, 35.5, 28.7, 27.1, 27.0, 20.3, 20.2, 14.5. HRMS (ESI-TOF, [M + Na]⁺): m/z calcd for C₁₅H₂₆O₃Na 277.1474, found 277.1762.



Scheme III.8. Catalytic oxidation of neomenthol derivatives.

Neomenthyl acetate: (67 or 55)

Purification by flash chromatography over silica (hexane).

68 or 70. FT-IR (ATR) ν , cm^{-1} : 3420, 2928, 1737, 1216, 1132. $^1\text{H-NMR}$ (400 MHz, CDCl_3 , 300 K) δ , ppm: 5.39-5.35 (m, 1H), 2.07 (s, 3H), 2.00-1.92 (m, 1H) 1.86-1.79 (m, 1H), 1.77-1.57 (m, 3H), 1.42-1.37 (m, 1H), 1.20 (s, 3H), 1.16 (s, 3H), 1.11-0.91 (m, 2H), 0.87 (d, $J = 6.7$ Hz, 3H). $^{13}\text{C-NMR}$ (100 MHz, CDCl_3 , 300 K) δ , ppm: 170.7, 71.9, 71.2, 49.9, 39.4, 34.7, 28.7, 27.6, 26.6, 22.1, 22.0, 21.6. HRMS (ESI-TOF, $[\text{M} + \text{Na}]^+$): m/z calcd for $\text{C}_{12}\text{H}_{22}\text{O}_3\text{Na}$ 237.1461, found 237.1458.

69 or 71. FT-IR (ATR) ν , cm^{-1} : 2970, 2930, 1733, 1708, 1371, 1242, 1028. $^1\text{H-NMR}$ (400 MHz, CDCl_3 , 300 K) δ , ppm: 5.34-3.32 (m, 1H), 2.70-2.59 (m, 1H), 2.54-2.40 (m, 2H), 2.38-2.30 (m, 1H), 2.13 (s, 3H), 1.69-1.46 (m, 3H), 1.01 (d, $J = 6.4$ Hz, 3H), 0.93 (d, $J = 6.4$ Hz, 3H), 0.89 (d, $J = 6.5$ Hz, 3H). $^{13}\text{C-NMR}$ (100 MHz, CDCl_3 , 300 K) δ , ppm: 212.0, 170.4, 69.1, 49.0, 41.3, 38.9, 38.9, 29.6, 21.2, 20.6, 20.4, 13.7. HRMS (ESI-TOF, $[\text{M} + \text{Na}]^+$): m/z calcd for $\text{C}_{12}\text{H}_{20}\text{O}_3\text{Na}$ 235.1305, found 235.1303.

(+)-Neomenthyl trifluoroacetate (72):

Purification by flash chromatography over silica (dichloromethane 100%).

73. FT-IR (ATR) ν , cm^{-1} : 3281, 2934, 2871, 1772, 1365, 1325, 1216, 1131, 919. $^1\text{H-NMR}$ (400 MHz, CDCl_3 , 300 K) δ , ppm: 5.62-5.59 (m, 1H), 2.08-2.02 (m, 1H) 1.90-1.84 (m, 1H), 1.79-1.61 (m, 3H), 1.53-1.48 (m, 1H), 1.22 (s, 3H), 1.19 (s, 3H), 1.07-0.90 (m, 2H), 0.90 (d, $J = 6.6$ Hz, 3H). $^{13}\text{C-NMR}$ (100 MHz, CDCl_3 , 300 K) δ , ppm: 156.8, 114.6, 76.1, 71.9, 50.3, 38.9, 34.5, 28.9, 27.6, 26.4, 21.9, 21.8. HRMS (ESI-TOF, $[\text{M} + \text{Na}]^+$): m/z calcd for $\text{C}_{12}\text{H}_{19}\text{F}_3\text{O}_3\text{Na}$ 291.1178, found 291.1157.

74. FT-IR (ATR) ν , cm^{-1} : 2970, 2936, 2877, 1780, 1715, 1374, 1341, 1218, 1149, 893. $^1\text{H-NMR}$ (400 MHz, CDCl_3 , 300 K) δ , ppm: 5.54 (m, 1H), 2.68-2.54 (m, 2H), 2.49-2.39 (m, 2H), 1.71-1.58 (m, 3H), 1.05 (d, $J = 6.5$ Hz, 3H), 0.95 (d, $J = 6.4$ Hz, 3H), 0.93 (d, $J = 6.5$ Hz, 3H). $^{13}\text{C-NMR}$ (100 MHz, CDCl_3 , 300 K) δ , ppm: 210.4, 157.0, 114.6, 74.5, 48.8, 40.9, 38.6, 38.2, 29.5, 20.5, 20.3, 13.7. HRMS (ESI-TOF, $[\text{M} + \text{Na}]^+$): m/z calcd for $\text{C}_{12}\text{H}_{17}\text{F}_3\text{O}_3\text{Na}$ 289.1022, found 289.1037.

(+)-Neomenthyl pivalate (75):

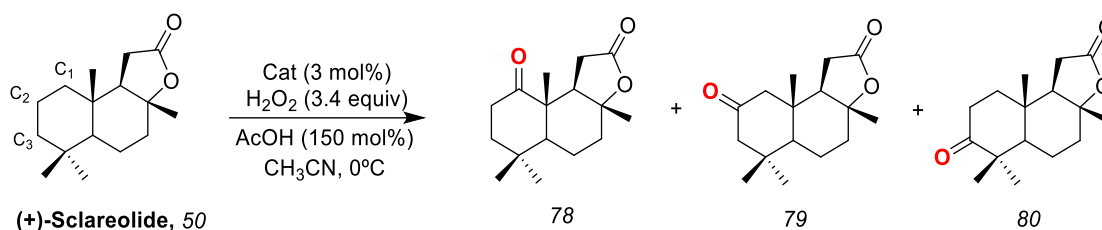
Purification by flash chromatography over silica (hexane 100%).

76. FT-IR (ATR) ν , cm^{-1} : 3340, 2948, 1717, 1478, 1283, 1140, 928, 897. $^1\text{H-NMR}$ (400 MHz, CDCl_3 , 300 K) δ , ppm: 5.36-5.35 (m, 1H), 1.95-1.89 (m, 1H), 1.87-1.81 (m, 1H), 1.78-1.60 (m, 3H), 1.44-1.39 (m, 1H), 1.22 (s, 9H), 1.20 (s, 3H), 1.16 (s, 3H), 1.11-0.91 (m, 2H), 0.88 (d, $J = 6.6$ Hz, 3H). $^{13}\text{C-NMR}$ (100 MHz, CDCl_3 , 300 K) δ , ppm: 178.0, 71.9, 71.2, 49.9, 39.5, 39.0, 34.8, 28.8, 27.6, 27.2, 26.8, 22.2, 22.1. HRMS (ESI-TOF, $[\text{M} + \text{Na}]^+$): m/z calcd for $\text{C}_{15}\text{H}_{28}\text{O}_3\text{Na}$ 279.1931, found 279.1909.

77. FT-IR (ATR) ν , cm^{-1} : 2963, 2930, 2871, 1708, 1476, 1285, 1156, 1127. $^1\text{H-NMR}$ (400 MHz, CDCl_3 , 300 K) δ , ppm: 5.27 (m, 1H), 2.62-2.49 (m, 2H), 2.44-2.30 (m, 2H), 1.60-1.50 (m, 3H), 1.25 (s, 9H), 1.01 (d, $J = 6.6$ Hz, 3H), 0.92 (d, $J = 6.9$ Hz, 3H), 0.88 (d, $J = 6.5$ Hz, 3H). $^{13}\text{C-NMR}$ (100 MHz, CDCl_3 , 300 K) δ , ppm: 212.0, 177.7, 68.7, 49.3, 41.7, 39.3, 38.9, 38.8, 29.8, 27.2, 20.6, 20.5, 13.9. HRMS (ESI-TOF, $[\text{M} + \text{Na}]^+$): m/z calcd for $\text{C}_{15}\text{H}_{26}\text{O}_3\text{Na}$ 277.1774, found 277.1758.

(+)-Sclareolide (50):

Purification by flash chromatography over silica (5% acetone/hexane).



Scheme III.9. Catalytic oxidation of (+)-sclareolide.

78: FT-IR (ATR) ν , cm^{-1} : 3014, 2952, 2924, 2854, 1772, 1695, 1182, 1020, 921. $^1\text{H-NMR}$ (400 MHz, CDCl_3 , 300 K) δ , ppm: 2.97 (dd, $J = 17.0, 6.5$ Hz, 1H), 2.68 (ddd, $J = 15.7, 9.2, 5.1$ Hz, 1H), 2.54 (dd, $J = 17.0, 14.2$ Hz, 1H), 2.29 (ddd, $J = 15.7, 8.4, 5.0$ Hz, 1H), 2.15 (dd, $J = 14.2, 6.6$ Hz, 1H), 2.09 (dd, $J = 11.1, 2.7$ Hz, 1H), 1.93-1.88 (m, 1H), 1.87-1.81 (m, 1H), 1.69 (dd, $J = 9.2, 5.0$ Hz, 1H), 1.66-1.62 (m, 1H), 1.58 (dd, $J = 13.2, 3.1$ Hz, 1H), 1.54-1.49 (m, 1H), 1.35 (s, 3H), 1.19 (s, 3H), 1.06 (s, 3H), 1.02 (s, 3H). $^{13}\text{C-NMR}$ (100 MHz, CDCl_3 , 300 K) δ , ppm: 214.2, 176.8, 85.7, 53.8, 52.0, 49.6, 39.1, 37.7, 34.5, 32.4, 31.3, 30.8, 23.2,

21.7, 21.1, 14.4. In agreement with that reported in the literature.⁶⁵ GC-MS (m/z): 282.2 [M+NH₄]⁺

79OH: FT-IR (ATR) ν , cm⁻¹: 3455, 3024, 2970, 2925, 1739, 1436, 1365, 1217. ¹H-NMR (400 MHz, CDCl₃, 300 K) δ , ppm: 4.04-3.96 (m, 1H), 2.45 (dd, *J* = 16.2, 14.7 Hz, 1H), 2.27 (dd, *J* = 16.2, 6.5 Hz, 1H), 2.10 (dt, *J* = 11.8, 3.3 Hz, 1H), 2.01 (dd, *J* = 14.8, 6.5 Hz, 1H), 1.93-1.89 (m, 1H), 1.87-1.84 (m, 1H), 1.83-1.81 (m, 1H), 1.74-1.67 (td, *J* = 12.1, 3.5 Hz, 1H), 1.58-1.52 (m, 1H), 1.43-1.40 (m, 1H), 1.39-1.35 (m, 1H), 1.34 (d, *J* = 0.92 Hz, 3H), 1.15-1.10 (m, 1H), 0.97 (s, 3H), 0.96 (s, 3H), 0.89 (s, 3H). ¹³C-NMR (100 MHz, CDCl₃, 300 K) δ , ppm: 176.0, 86.0, 64.4, 58.9, 56.2, 51.5, 48.4, 38.5, 37.4, 34.8, 33.2, 28.7, 21.8, 21.6, 20.2, 16.1. In agreement with that reported in the literature.⁷⁴ GC-MS (m/z): 284.2 [M+NH₄]⁺

79: FT-IR (ATR) ν , cm⁻¹: 2940, 1781, 1701, 1186, 1112, 1034, 915. ¹H-NMR (400 MHz, CDCl₃, 300 K) δ , ppm: 2.48-2.41 (m, 1H), 2.32-2.11 (m, 7H), 2.06-1.98 (m, 1H), 1.85-1.44 (m, 3H), 1.35 (s, 3H), 1.09 (s, 3H), 0.93 (s, 6H). ¹³C-NMR (100 MHz, CDCl₃, 300 K) δ , ppm: 209.3, 175.6, 85.6, 58.2, 56.6, 55.6, 54.9, 40.3, 38.6, 38.0, 33.3, 28.6, 22.6, 21.1, 20.7, 16.2. In agreement with that reported in the literature.⁵¹ GC-MS (m/z): 282.2 [M+NH₄]⁺

80: FT-IR (ATR) ν , cm⁻¹: 2914, 1773, 1695, 1392, 1228, 1193, 1170, 1034, 962. ¹H-NMR (400 MHz, CDCl₃, 300 K) δ , ppm: 2.63-2.40 (m, 3H), 2.29 (ddd, *J* = 16.2, 6.5, 0.4 Hz, 1H), 2.14 (dt, *J* = 11.6, 3.0 Hz, 1H), 2.01 (dd, *J* = 14.7, 6.5 Hz, 1H), 1.87-1.82 (m, 1H), 1.78-1.70 (m, 2H), 1.65-1.53 (m, 3H), 1.39 (s, 3H), 1.13 (s, 3H), 1.06 (s, 3H), 1.03 (s, 3H). ¹³C-NMR (100 MHz, CDCl₃, 300 K) δ , ppm: 215.5, 175.9, 85.6, 58.1, 54.3, 47.4, 37.73, 37.68, 35.3, 33.4, 28.6, 26.6, 21.4, 21.1, 20.7, 14.5. In agreement with that reported in the literature.⁵¹ GC-MS (m/z): 282.2 [M+NH₄]⁺

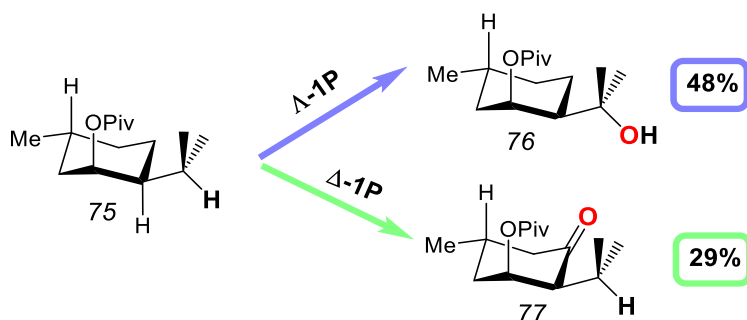
III.4.8 CATALYTIC OXIDATION REACTIONS AT MMOL SCALE

A round bottom flask was charged with: catalyst (21 μ mol, 3 mol%), alkane (0.7 mmol, 1 equiv), CH₃CN (14 mL) and a magnetic stir bar. A 1.74 M CH₃CO₂H solution in CH₃CN was added (0.6 mL, 1.05 mmol, 150 mol%) and the mixture was placed on an ice bath (for 0 °C reactions) or a CH₃CN/N₂ bath (for -35 °C reactions) and stirred. The necessary amount of a 1.5 M (*X* equiv, see Table III.18) H₂O₂ solution (diluted from a 35% H₂O₂ aqueous solution) was delivered by syringe pump over 17 min at 0 °C or -35 °C. After syringe pump addition, the solution was stirred for 10 min at 0 °C or -35 °C. Solvent was

removed under reduced pressure and the resulting residue was purified by flash chromatography on silica gel. If necessary, the recovered starting material was submitted to a second oxidation using the aforementioned procedure, and employing proportional amounts of each reactive, so the proportions stay the same. Work up was identical to the former. If necessary a third oxidation can be done in the same way. The results of each oxidation step are shown in Table III.19 and Table III.20 for (+)-neomenthyl pivalate, and Table III.21, Table III.22, and Table III.23 for (+)-sclareolide.

(+)-Neomenthyl pivalate (75):

Purification of products was done by flash chromatography over silica (Hexane: diethyl ether from 30:1 to 1:1).



Scheme III.10. Catalytic oxidation of (+)-neomenthyl pivalate at mmol scale.

Table III.19. Conditions to favor the formation of 76. Catalyst Δ -1P, at 0 °C.

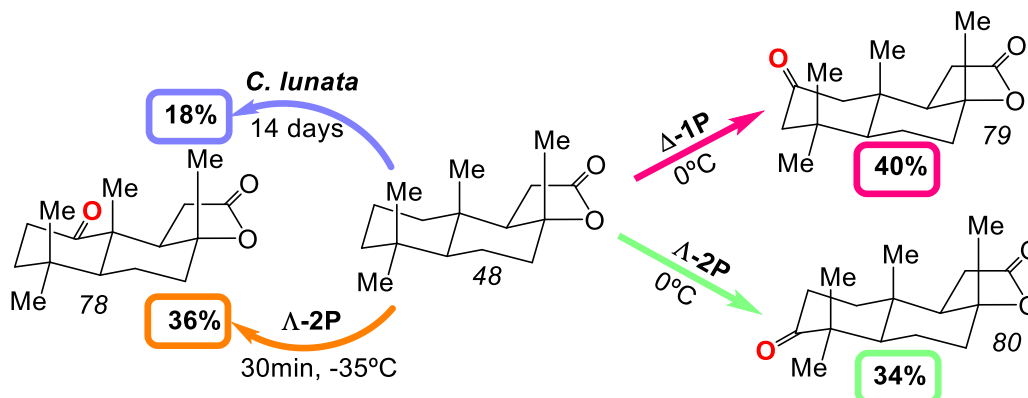
Substrate	Yield %				Conversion (%)
	76	77	Total	76/77	
672 mmol	34	7	41	83/17	64
241 mmol	38	9	47	81/19	76
TOTAL	48	10	58	83/17	91

Table III.20. Conditions to favor the formation of 77. Catalyst Δ -1P, at 0 °C.

Substrate	Yield %				Conversion (%)
	76	77	Total	76/77	
709 mmol	13	18	31	41/59	52
340 mmol	9	13	22	42/58	44
189 mmol	12	19	31	40/60	59
TOTAL	20	29	49	41/59	89

(+)-Sclareolide (48):

Product purification was done by flash chromatography over silica (Hexane: diethyl ether from 4:1 to 1:1).



Scheme III.11. Catalytic oxidation of (+)-sclareolide at mmol scale.

Table III.21. Conditions to favor the formation of 78. Catalyst Δ -2P, at -35 °C.

Substrate	Yield %			Total	Conversion (%)
	78	79	80		
627 mmol	26	4	14	44	58
252 mmol	26	-	13	39	43
TOTAL	36	4	19	59	77

Table III.22. Conditions to favor the formation of 79. Catalyst Δ -1P, at 0 °C.

Substrate	Yield %			Total	Conversion %
	78	79	80		
664 mmol	5	31	21	57	70
198 mmol	6	26	18	50	64
TOTAL	7	40	26	73	89

Table III.23. Conditions to favor the formation of 80. Catalyst Δ -2P, at 0 °C.

Substrate	Yield %			Total	Conversion %
	78	79	80		
709 mmol	23	16	34	73	87

III.5 REFERENCES

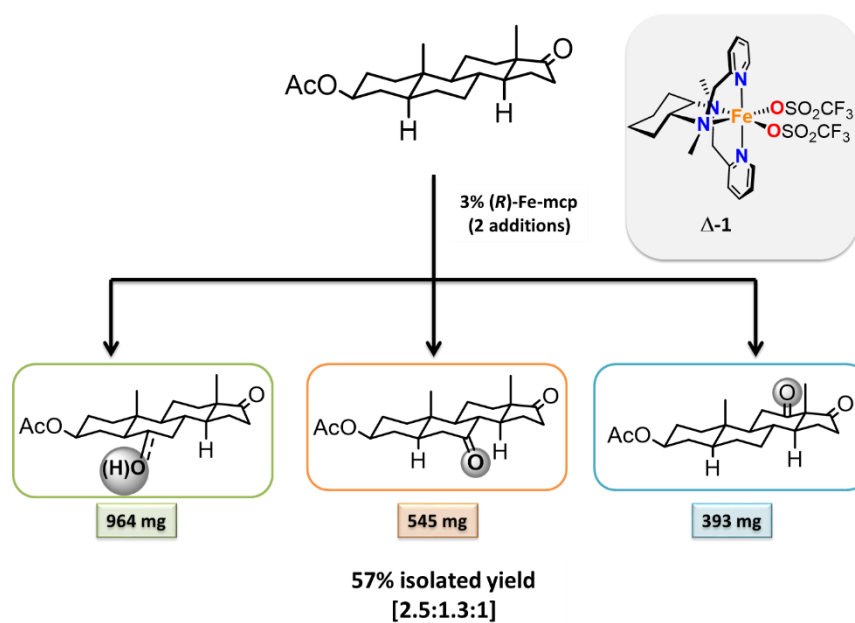
- (1) Chen, K.; Baran, P. S. *Nature* **2009**, *459*, 824.
- (2) Maimone, T. J.; Baran, P. S. *Nat Chem Biol* **2007**, *3*, 396.
- (3) Hanson, J. R. *Nat. Prod. Rep.* **2010**, *27*, 887.
- (4) Zhang, K.; Shafer, B. M.; Demars, M. D.; Stern, H. A.; Fasan, R. *J. Am. Chem. Soc.* **2012**, *134*, 18695.
- (5) Mendoza, A.; Ishihara, Y.; Baran, P. S. *Nat Chem* **2012**, *4*, 21.
- (6) Wender, P. A.; Hilinski, M. K.; Mayweg, A. V. W. *Org. Lett.* **2005**, *7*, 79.
- (7) Newhouse, T.; Baran, P. S. *Angew. Chem. Int. Ed.* **2011**, *50*, 3362.
- (8) Gutekunst, W. R.; Baran, P. S. *Chem. Soc. Rev.* **2011**, *40*, 1976.
- (9) McMurray, L.; O'Hara, F.; Gaunt, M. J. *Chem. Soc. Rev.* **2011**, *40*, 1885.
- (10) Zhou, M.; Crabtree, R. H. *Chem. Soc. Rev.* **2011**, *40*, 1875.
- (11) Lu, H.; Zhang, X. P. *Chem. Soc. Rev.* **2011**, *40*, 1899.
- (12) Company, A.; Gómez, L.; Costas, M. S. P de Visser, D. K. *Iron-Containing Enzymes, Versatile Catalysts of Hydroxylation Reactions in Nature*; RSC: Cambridge, 2011.
- (13) Shul'pin, G. B. *Org. Biomol. Chem.* **2010**, *8*, 4217.
- (14) White, M. C. *Science* **2012**, *335*, 807.
- (15) Lee, S.; Fuchs, P. L. *J. Am. Chem. Soc.* **2002**, *124*, 13978.
- (16) Brodsky, B. H.; Bois, J. Du. *J. Am. Chem. Soc.* **2005**, *127*, 15391.
- (17) Curci, R.; d'Accolti, L.; Fusco, C. *Acc. Chem. Res.* **2006**, *39*, 1.
- (18) Litvinas, N. D.; Brodsky, B. H.; Du Bois, J. *Angew. Chem. Int. Ed.* **2009**, *48*, 4513.
- (19) McNeill, E.; Du Bois, J. *Chem. Sci.* **2012**, *3*, 1810.
- (20) Tenaglia, A.; Terranova, E.; Waegell, B. *J. Org. Chem.* **1992**, *57*, 5523.
- (21) McNeill, E.; Du Bois, J. *J. Am. Chem. Soc.* **2010**, *132*, 10202.
- (22) Barton, D. H. R.; Doller, D. *Acc. Chem. Res.* **1992**, *25*, 504.
- (23) Barton, D. H. R.; Li, T.; Mackinnon, J. *Chem. Commun.* **1997**, 557.
- (24) Kamata, K.; Yonehara, K.; Nakagawa, Y.; Uehara, K.; Mizuno, N. *Nat. Chem.* **2010**, *2*, 478.
- (25) Zhao, Y.; Yim, W.-L.; Tan, C. K.; Yeung, Y.-Y. *Org. Lett.* **2011**, *13*, 4308.
- (26) Larsen, A. T.; May, E. M.; Auclair, K. *J. Am. Chem. Soc.* **2011**, *133*, 7853.
- (27) Moreira, R. F.; Wehn, P. M.; Sames, D. *Angew. Chem. Int. Ed.* **2000**, *39*, 1618.

- (28) Desai, L. V.; Hull, K. L.; Sanford, M. S. **2004**, *126*, 9542.
- (29) Chen, K.; Richter, J. M.; Baran, P. S. *J. Am. Chem. Soc.* **2008**, *130*, 7247.
- (30) Kasuya, S.; Kamijo, S.; Inoue, M. *Org. Lett.* **2009**, *11*, 3630.
- (31) Simmons J. F., E. M. . H. *Nature* **2012**, *483*, 70.
- (32) Giri, R.; Liang, J.; Lei, J.-G.; Li, J.-J.; Wang, D.-H.; Chen, X.; Naggar, I. C.; Guo, C.; Foxman, B. M.; Yu, J.-Q. *Angew. Chem. Int. Ed. Engl.* **2005**, *44*, 7420.
- (33) Das, S.; Incarvito, C. D.; Crabtree, R. H.; Brudvig, G. W. *Science (80-.)*. **2006**, *312*, 1941.
- (34) Bigi, M. A.; Reed, S. A.; White, M. C. *Nat. Chem.* **2011**, *3*, 216.
- (35) Zhang, S.-Y.; He, G.; Zhao, Y.; Wright, K.; Nack, W. A.; Chen, G. *J. Am. Chem. Soc.* **2012**, *134*, 7313.
- (36) Wang, Y.-F.; Chen, H.; Zhu, X.; Chiba, S. *J. Am. Chem. Soc.* **2012**, *134*, 11980.
- (37) Que Jr., L.; Tolman, W. B. *Nature* **2008**, *455*, 333.
- (38) Kovaleva, E. G.; Lipscomb, J. D. *Nat Chem Biol* **2008**, *4*, 186.
- (39) Bruijninx, P. C. A.; van Koten, G.; Klein Gebbink, R. J. M. *Chem. Soc. Rev.* **2008**, *37*, 2716.
- (40) Mukherjee, A.; Martinho, M.; Bominaar, E. L.; Münck, E.; Que, L. *Angew. Chem. Int. Ed. Engl.* **2009**, *48*, 1780.
- (41) Sun, C.-L.; Li, B.-J.; Shi, Z.-J. *Chem. Rev.* **2011**, *111*, 1293.
- (42) Comba, P.; Maurer, M.; Vadivelu, P. *Inorg. Chem.* **2009**, *48*, 10389.
- (43) Yoon, J.; Wilson, S. a; Jang, Y. K.; Seo, M. S.; Nehru, K.; Hedman, B.; Hodgson, K. O.; Bill, E.; Solomon, E. I.; Nam, W. *Angew. Chem. Int. Ed. Engl.* **2009**, *48*, 1257.
- (44) Liu, P.; Liu, Y.; Wong, E.; Xiang, S.; Che, C.-M. *Chem. Sci* **2011**, *2*, 2187.
- (45) Chen, K.; Que Jr., L. *J. Am. Chem. Soc.* **2001**, *123*, 6327.
- (46) Correa, A.; Mancheño, O. G.; Bolm, C. *Chem. Soc. Rev.* **2008**, *37*, 1108.
- (47) Costas, M.; Chen, K.; Que Jr., L. *Coord. Chem. Rev.* **2000**, *200-202*, 517.
- (48) Chen M. S.; White, M. C. *Science.* **2007**, *318*, 783.
- (49) Company, A.; Gómez, L.; Fontrodona, X.; Ribas, X.; Costas, M. *Chem. Eur. J.* **2008**, *14*, 5727.
- (50) Gómez, L.; Garcia-Bosch, I.; Company, A.; Benet-Buchholz, J.; Polo, A.; Sala, X.; Ribas, X.; Costas, M. *Angew. Chem. Int. Ed.* **2009**, *48*, 5720.
- (51) Chen, M. S.; White, M. C. *Science.* **2010**, *327*, 566.

-
- (52) He, Y.; Gorden, J. D.; Goldsmith, C. R. *Inorg. Chem.* **2011**, *50*, 7431.
- (53) Hitomi, Y.; Arakawa, K.; Funabiki, T.; Kodera, M. *Angew. Chem. Int. Ed.* **2012**, *51*, 3448.
- (54) Ottenbacher, R. V.; Samsonenko, D. G.; Talsi, E. P.; Bryliakov, K. P. *Org. Lett.* **2012**, *14*, 4310.
- (55) Enthaler, S.; Junge, K.; Beller, M. *Angew Chem. Int. Ed.* **2008**, *47*, 5.
- (56) Knof, U.; von Zelewsky, A. *Angew. Chem. Int. Ed.* **1999**, *38*, 302.
- (57) Costas, M.; Tipton, A. K.; Chen, K.; Jo, D.-H.; Que Jr., L. *J. Am. Chem. Soc.* **2001**, *123*, 6722.
- (58) Suzuki, K.; Oldenburg, P. D.; Que Jr., L. *Angew. Chem. Int. Ed.* **2008**, *47*, 1887.
- (59) Costas, M.; Que Jr., L. *Angew Chem. Int. Ed.* **2002**, *41*, 2179.
- (60) Chen, K.; Eschenmoser, A.; Baran, P. S. *Angew. Chem. Int. Ed.* **2009**, *48*, 9705.
- (61) Cook, B. R. .; Reinert, T. J.; Suslick, K. S. *J. Am Chem. Soc.* **1986**, *108*, 7281.
- (62) Battioni, P.; Renaud, J. P.; Bartoli, J. F.; Reina-Artiles, M.; Fort, M.; Mansuy, D. *J. Am. Chem. Soc.* **1988**, *110*, 8462.
- (63) Barton, D. H. R.; Beloeil, J.-C.; Billion, A.; Boivin, J.; Lallemand, J.-Y.; Lelandais, P.; Mergui, S. *Helv. Chim. Acta* **1987**, *70*, 2187.
- (64) Liu, W.; Groves, J. T. *J. Am. Chem. Soc.* **2010**, *132*, 12847.
- (65) Cano, A.; Ramírez-Apan, M. T.; Delgado, G. *J. Braz. Chem. Soc.* **2011**, *22*, 1177.
- (66) Bartoli, J. F.; Brigaud, O.; Battioni, P.; Mansuy, D. *J. Chem. Soc. Chem. Commun.* **1991**, 440.
- (67) Groves, J. T.; Viski, P. *J. Am. Chem. Soc.* **1989**, *111*, 8537.
- (68) Wang, C.; Shalyaev, K. V.; Bonchio, M.; Carofiglio, T.; Groves, J. T. *Inorg. Chem.* **2006**, *45*, 4769.
- (69) Kim, C.; Chen, K.; Kim, J.; Que Jr., L. *J. Am. Chem. Soc.* **1997**, *119*, 5964.
- (70) Garcia-Bosch, I.; Gómez, L.; Polo, A.; Ribas, X.; Costas, M. *Adv. Synth. Catal.* **2012**, *354*, 65.
- (71) Mas-Ballesté, R.; Costas, M.; Berg, T. v. d.; Que Jr., L. *Chem. Eur. J.* **2006**, *12*, 7489.
- (72) Pfeffer, P. E.; Osman, S. F. *J. Org. Chem.* **1972**, *37*, 2425.
- (73) Shiao, M.-J.; Luen Lin, J.; Kuo, Y.-H.; Shih, K.-S. *Tetrahedron Lett.* **1986**, *27*, 4059.
- (74) Choudhary, M. I.; Musharraf, S. G.; Sami, A.; Atta ur, R. *Helv. Chim. Acta* **2004**, *87*, 2685.

CHAPTER IV

THE IRON(II) COMPLEX $[\text{Fe}(\text{CF}_3\text{SO}_3)_2(\text{MCP})]$ AS A CONVENIENT, READILY AVAILABLE CATALYST FOR THE SELECTIVE OXIDATION OF METHYLENIC SITES IN ALKANES



This chapter is based on the following publication:

Mercè Canta, David Font, Laura Gómez, Xavi Ribas, and Miquel Costas*

Adv. Synth. Catal. **2014**, 356, 818-830

IV.1 INTRODUCTION

Oxidized hydrocarbons constitute a basic structural motif in organic molecules, and, because of that, methodologies for site selective oxidation of alkyl C–H bonds are highly desirable.^{1–12} Methods for selective late stage C–H oxidation will permit the rapid synthesis of libraries of structurally diverse compounds sharing a common structural core, especially suitable for structure-activity relationship studies, which could lead to the discovery and development of new drugs and materials.^{13,14} However, most often alkyl C–H bond functionalization occurs early within a multi-step synthesis and is applied to very simple substrates, mainly because it is one of the most difficult transformations in synthetic chemistry. This is so due to the kinetic stability of C–H bonds and their ubiquitous presence in organic molecules, which make site selectivity a formidable challenge. Oxidation of alkyl C–H bonds has traditionally required the use of highly oxidizing, non-selective reagents, which are often incompatible with other functional groups. Moreover, the reagents that perform these reactions often rely on heavy and toxic metal oxides, which exhibit poor atom economy in their reactions.^{5,6} Organic peroxides such as dioxiranes constitute valuable alternatives because they show excellent selectivity and efficiency in their reactions but present limited stability and most commonly their manipulation requires special care.^{15–18} Indeed, a general problem of alkane C–H oxidation reactions is that the scale up is not obvious because of the limited stability and high reactivity of most C–H oxidizing reagents. All of these aspects prompt for the development of novel synthetic methodologies that can target C–H bonds in a selective manner and could be suitable for practical organic synthesis.^{19–38}

Fe-based complexes represent powerful oxidants for the hydroxylation of not only tertiary but also secondary sites.^{19–22} Porphyrinic iron complexes are models of heme oxygenases and have been explored for decades.^{4,23–25} More recently, non-heme complexes have emerged as a promising alternative.^{26–30} While the combination of iron compounds and hydrogen peroxide finds wide precedent in the literature and could be dated back to Fenton chemistry,^{33–36} iron catalysts for selective alkane C–H oxidation that could yield preparative useful quantities of oxidation products have not been described until recently, and are still scarce. This class of catalysts presents very attractive features, such as the environmentally benign nature of the metal and their use of H₂O₂ as

oxidant.^{37,38} The most relevant examples in the literature are summarized in Figure IV.1. These include $[\text{Fe}(\text{pdp})(\text{CH}_3\text{CN})_2](\text{SbF}_6)_2$, **2SbF₆**, (pdp = *N,N'*-bis(2-pyridylmethyl)-2,2'-bipyrrolidine), which was described as a selective and predictable catalyst for tertiary and secondary alkyl C–H oxidation with H_2O_2 , but required the use of large 15–>25 mol% catalyst loadings.^{39–44} Improved activity was obtained with pinene-derivatized catalysts $[\text{Fe}(\text{CF}_3\text{SO}_3)_2(\text{mcpp})]$, **1P**, (mcpp = *N,N'*-dimethyl-*N,N'*-bis{[(*R*)-4,5-pinenepyridin-2-yl]-methyl}cyclohexane-1,2-diamine)⁴⁵ and $[\text{Fe}(\text{CF}_3\text{SO}_3)_2(\text{pdpp})]$, **1P**, (pdpp = *N,N'*-bis{[(*R*)-4,5-pinenepyridin-2-yl]-methyl}-2,2'-bipyrrolidine)⁴⁶, the enhanced stability of which allows for efficient operation at significantly lower catalyst loadings (1–3 mol%), and they introduce modulation of the regioselectivity on C–H oxidation of complex organic molecules. High activity has also been described with the tacn-based catalyst $[\text{Fe}(\text{CF}_3\text{SO}_3)_2(\text{Me,MePytacn})]$, **3**, (Me,MePytacn = 1-(6-methyl-2-pyridylmethyl)-4,7-dimethyl-1,4,7-triazacyclononane),⁴⁷ which shows a remarkable preference towards methylene oxidation in comparison to **2SbF₆**, **1P**, and $[\text{Fe}(\text{qpy})](\text{ClO}_4)_2$, **4**, (qpy = 2, 2' : 6', 2'' : 6'', 2''' : 6''', 2''''-quinquepyridine), which uses Oxone[®] as oxidant.⁴⁸ Nevertheless, these catalysts share a major drawback in the fact that they all contain highly elaborated and rather expensive ligands that limit scale up of the reactions. Therefore there is still a need for the development of straightforward methodologies that use simpler, readily available, non-expensive iron catalysts for performing selective C–H oxidation on a preparative scale.

Towards this end, in this work we show that the mononuclear iron complex $[\text{Fe}(\text{CF}_3\text{SO}_3)_2(\text{mcp})]$, **1**, (mcp = *N,N'*-dimethyl-*N,N'*-bis(2-pyridylmethyl) cyclohexane-*trans*-1,2-diamine, Figure IV.2) is an efficient catalyst for the oxidation of alkanes with H_2O_2 , providing oxidized products with synthetically amenable yields and exhibiting remarkable selectivity among secondary sites. This catalyst can be readily prepared in multigram amounts from inexpensive, commercially available reagents. The catalytic methodology described herein allows the performance of alkane oxidation reactions in comparable yields to those reported by more complex and expensive iron catalysts, but requires substantially lower catalyst loadings than **2SbF₆**. However, the most important aspect of the work is that reactions can be conveniently performed on a gram scale, following experimentally simple and safe protocols. These methodological aspects, in combination

with the readily accessible nature and cost of the catalyst, make it a very convenient tool for synthetic purposes.

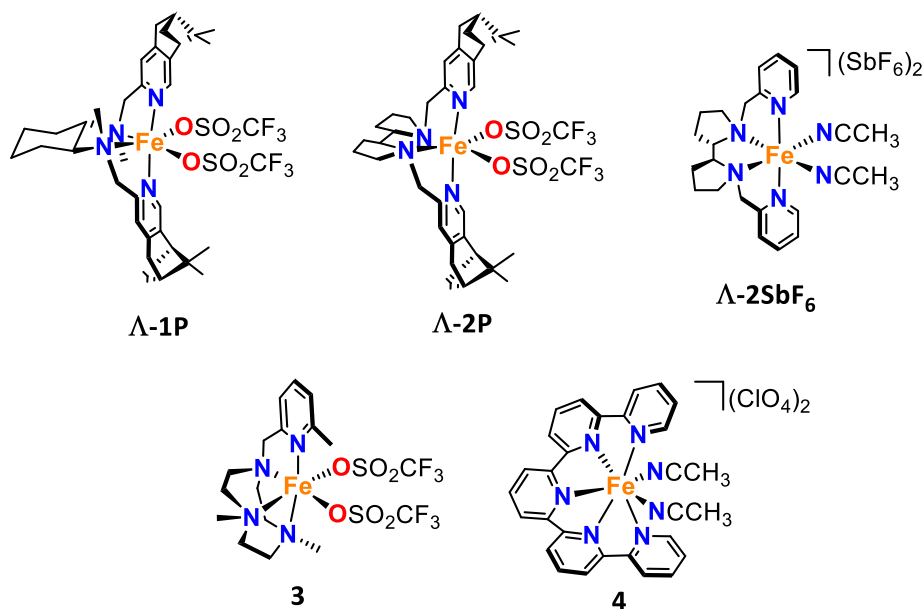


Figure IV.1. Iron catalysts for methylenic site oxidations.

IV.2 RESULTS AND DISCUSSION

IV.2.1 MULTIGRAM SCALE PREPARATION OF THE FE-MCP CATALYST

The preparation of $[\text{Fe}(\text{CF}_3\text{SO}_3)_2((S,S)\text{-mcp})]$, **Λ-1**, on the mg scale was previously described,⁴⁹ but in order to illustrate the ready accessibility of this catalyst, a multigram scale preparation was performed. Starting from 26.8 g of (+/–)-*trans*-diaminocyclohexane, the racemic diamine was resolved using (–)-*D*-tartaric acid, obtaining the desired (*S,S*)-diaminocyclohexane in 99% yield with $\geq 99\%$ enantiomeric purity as confirmed by chiral GC, without the need of recrystallization. Note that for non-chiral substrates, this step is not required and the racemic diamine can be directly used. 10 g of this diamine were used to synthesize the ligand by performing a reductive amination with 2-picolylaldehyde, followed by an Eschweiler–Clarke methylation with formaldehyde and formic acid. The ligand was purified by flash silica gel chromatography yielding 9.9 g of enantiomerically pure (*S,S*)-mcp ligand with 81% overall yield in 3 synthetic steps that can be performed in 2 days. 2.5 g of this ligand were reacted with FeCl_2 under N_2 atmosphere for 3 h and

immediately after, without any work-up, with AgOTf (2 equiv.) for another 3 h. After filtration to remove precipitated AgCl, the complex was crystallized in CH₂Cl₂/Et₂O yielding 4.2 g of bright yellow crystals (grown after 3 days of diethyl ether diffusion) corresponding to **Λ-1** (75% yield). This complex should be stored under an inert atmosphere but can be easily manipulated under air for short periods of time.

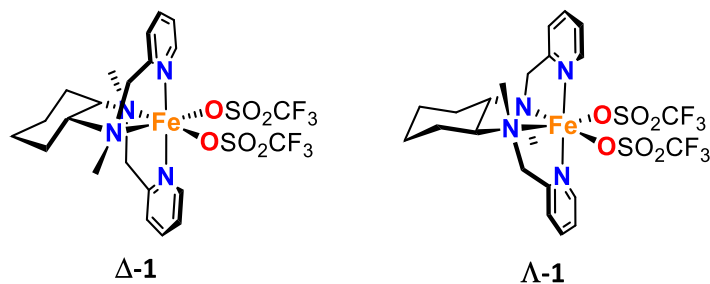


Figure IV.2. Catalysts studied in this work: **Δ-1** and **Λ-1**.

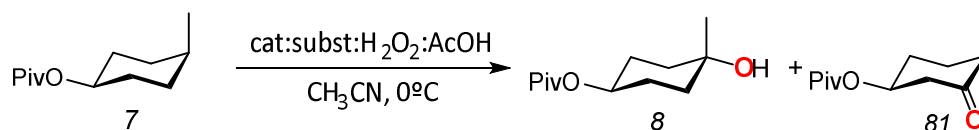
IV.2.2 OPTIMIZATION OF CATALYTIC C–H OXIDATION REACTIONS

The activity of **Λ-1** as alkane C–H oxidation catalyst employing H₂O₂ was optimized using *cis*-4-methyl-1-cyclohexylpivalate (**7**, Table IV.1) and 1,1-dimethylcyclohexane (**45**, Table IV.2), as model substrates. Oxidation of the latter was also studied with the set of catalysts [Fe(CF₃SO₃)₂(mep)],^{50,51} **5**, (mep = *N,N'*-dimethyl-*N,N'*-bis(2-pyridylmethyl) ethylenediamine) and [Fe(CF₃SO₃)₂((*R,R*)-pdp)], **Δ-2** in order to investigate possible changes in the regioselectivity of the oxidations responding to the catalyst nature. [Fe((*S,S*)-mcp)(CH₃CN)₂](SbF₆)₂, **Λ-1SbF₆** was also used to study the possible effect of the anion on the catalytic performance.

Table IV.1 and Table IV.2 collect results obtained in the optimization of the oxidation of **7** and **45**, respectively. Oxidation of **7** occurs preferentially at the tertiary C–H bond in a stereospecific manner ($\geq 96\%$), yielding the corresponding tertiary alcohol **8** with retention of the configuration. Aside from that, minor amounts ($< 6\%$) of ketone **81** were also detected. On the other hand, oxidation of **45** results in the formation of ketones **46**, **47**, and **48** (Table IV.2), which relative ratios depend on the nature of the catalyst (*vide infra*). The experimental parameters of the reactions were optimized with regard to catalyst loading (from 1 to 15%), amount of hydrogen peroxide (H₂O₂, from 2 to 4.2

equivalents), acetic acid (AcOH, as additive between 1.5 and 10 equivalents) and the number of additions of the reagents (H₂O₂, AcOH and **Λ-1**).

Table IV.1. Optimization of reaction for tertiary C–H bond oxidation with **Λ-1**.



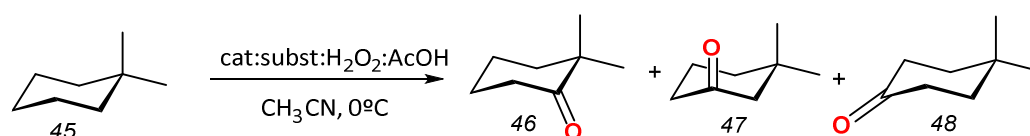
Entry	cat:subst:H ₂ O ₂ :AcOH (%)	Conversion (%) ^a	Yield (%) [8/81] ^a
1	1:100:200:150	51	36 [92/8]
2	3:100:200:150	55	41 [93/7]
3	1(×3):100:120(×3):100(×3) ^c	54	43 [91/9]
4	5:100:200:150	54	41 [93/7]
5	15:100:200:150	46	36 [92/8]
6	15:100:200:150 ^d	31	25 [92/8]
7	3:100:360:150	54	44 [89/11]
8	3:100:200:1000	68	51 [92/8]
9	3:100:360:1000	71	54 [91/9]
10	3(×2):100:200(×2):500(×2) ^e	81	57 [90/10]
11 ^b	3(×2):100:200(×2):500(×2) ^e	84	54 [90/10]
12 ^f	3(×2):100:200(×2):500(×2) ^e	62	47 [95/5]

^a Substrate conversion and product yield based on GC analysis. ^b Using **Λ-1SbF₆** as catalyst. ^c Iterative addition protocol with slow addition of catalyst. ^d Slow addition protocol. ^e Iterative addition protocol with direct addition of catalyst. (See section IV.4.5 for details). ^f Using **5** as catalyst.

Catalyst loading was first interrogated. The use of 1 mol% **Λ-1** afforded a combined 36% yield of (**8**+**81**) (entry 1, Table IV.1) and 47% yield of (**46**+**47**+**48**) (entry 1, Table IV.2). Yields were slightly increased by the use of 3 mol% catalyst (entry 2, Table IV.1 and Table IV.2), and the best results were obtained when the catalyst, acetic acid, and hydrogen peroxide were delivered to the reaction mixture in three consecutive additions. Under these conditions, **7** and **45** were oxidized in 43% and 67% respective combined yields (entry 3, Table IV.1 and Table IV.2). Further increase of the catalyst loading did not result in higher yields (entries 4-6, Table IV.1 and Table IV.2); instead, the use of 15 mol% of **Λ-1** resulted in low product yields (entry 5 in Table IV.1 and Table IV.2), and the same occurred when the catalyst was delivered *via* syringe pump (entry 6, Table IV.1 and Table IV.2). The next parameter evaluated was the amount of oxidant (H₂O₂). In this case, for simplicity

reasons, a single addition of 3 mol% catalyst was employed. Optimization was initiated by using 2 and 2.8 equivalents of H₂O₂ to oxidize **7** and **45**, respectively, because alcohols (2 e⁻ oxidation products) are mainly obtained in the oxidation of **7** and ketones (4 e⁻ oxidation products) are the products of the oxidation of **45**. Increase of the H₂O₂ loading led to a minor improvement in the oxidation of **7** (from 41% to 44% yield using 3.6 equiv., entries 2 and 7, Table IV.1), but a moderate improvement was obtained in the oxidation of **45** when increasing from 2.8 to 4.2 equiv. (from 49% to 54% yield, entries 2 and 7, Table IV.2).

Table IV.2. Optimization of reaction for secondary C–H bond oxidation with **A-1**.



Entry	cat:subst:H ₂ O ₂ :AcOH (%)	Conversion (%) ^a	Yield (%) [46/47/48] ^a
1	1:100:280:150	76	47 [21/55/24]
2	3:100:280:150	64	49 [22/53/25]
3	1(×3):100:120(×3):100(×3) ^e	94	67 [19/57/24]
4	5:100:280:150	84	52 [21/57/23]
5	15:100:280:150	71	45 [24/53/24]
6	15:100:280:150 ^{f)}	60	35 [23/51/26]
7	3:100:420:150	78	54 [20/56/24]
8	3:100:280:1000	90	59 [20/56/24]
9	3:100:420:1000	87	64 [20/56/24]
10	3(×2):100:280(×2):500(×2) ^g	95	71 [19/58/23]
11 ^b	3(×2):100:280(×2):500(×2) ^g	98	73 [20/58/22]
12 ^c	3(×2):100:280(×2):500(×2) ^g	97	65 [35/45/20]
13 ^d	3(×2):100:280(×2):500(×2) ^g	78	59 [34/46/20]

^a Based on GC analysis. ^b Using **A-1SbF₆**. ^c Using **A-2**. ^d Using **5**. ^e Iterative addition protocol with slow addition of catalyst. ^f Slow addition protocol. ^g Iterative addition protocol with direct addition of catalyst. (See section IV.4.5 for details).

Acetic acid is commonly used as a beneficial additive in iron catalyzed oxidation reactions,^{52–54} and the effect of the amount used was also studied. Increase of the amount of acetic acid from 1.5 to 10 equivalents resulted in a systematic improvement of ~ 10% in product yields both for **7** (compare entries 2 and 8, and also 7 and 9 in Table IV.1) and **45** (compare entries 2 and 8, and also 7 and 9 in Table IV.2). Finally we observed a further

improvement of the reaction yields by following an experimental protocol that involved two consecutive additions of catalyst, oxidant and acetic acid. Using this protocol, high substrate conversion was noticed and we achieved the highest yields of all tested conditions, affording 57% yield for the oxidation of **7** (entry 10, Table IV.1) and 71% yield for the oxidation of **45** (entry 10, Table IV.2).

For comparison, we performed the oxidation of **7** under optimized conditions using **5** as catalyst (entry 12, Table IV.1). Recent work by Bermejo and co-workers has shown that this simple catalyst can be used for the oxidation of organic molecules and natural products.⁵¹ However, a substantially poorer yield was obtained (47% vs 57%, compare entries 10 and 12, Table IV.1), indicating that **L-1** is a more active and suitable catalyst to perform such transformations. It is worth noticing that the selectivity patterns observed in the oxidation of **7** and **45** with catalyst **L-1** remain virtually the same regardless of the catalytic conditions used. Alcohol **8** is the major oxidation product of **7** in all cases, obtained with ~ 90% selectivity vs ketone **81** (Table IV.1). In the oxidation of **45**, ketone **47** is the major product (from 51% to 58% selectivity, entries 1-10, Table 2) being ketones **46** and **48** the minor products, obtained in ~ 20% selectivity each (note that the statistically expected selectivity ratio would be [40/40/20] according to the number of C-H bonds present in the molecule). These results indicate that **L-1** is able to discriminate among the three methylenic sites of **45**. The preferred oxidation site leading to **47** should be understood as a compromise between steric accessibility ($48 > 47 > 46$) and electron richness of the oxidized methylene site ($48 < 47 < 46$). Since the relative amount of **46**, which results from oxidation at the most sterically impeded methylene site, is substantially lower than the 40% statistically expected value, we conclude that steric interactions with **L-1** are the most decisive aspect in defining the overall regioselectivity in these reactions. This conclusion will have further support in the following lines. To further strengthen this point, the performance of **L-1** under optimized conditions was then compared with that of related catalysts that have previously proven effective in alkane oxidation, or that differ in the nature of the anion.^{42,43,51} In first place, **L-1SbF₆** and **L-1** showed virtually identical results in terms of yield and selectivity (entry 10 vs entry 11, Table IV.1 and Table IV.2), indicating that triflate and SbF₆⁻ could be indistinctly used, plus the benefit of the triflate being less expensive. On the other hand, under identical

experimental conditions, oxidation of **45** with the structurally related catalysts **A-2** and **5** proceeded with lower yields (65% for **A-2**, entry 12; and 59% for **5**, entry 13; Table IV.2), than for **A-1**. More interesting is the observation that the regioselectivity in the oxidation of **45** with **A-2** and **5** is distinct from that obtained with **A-1**, the formers being close to the statistically expected ratio on the basis of the number of C–H bonds (40/40/20). As observed for substrate **7**, the oxidation of **45** by **5** is not as efficient as when performed with **A-1** (71% vs 59% yield, compare entries 10 and 13, Table IV.2).

It is well established that the oxidation of alkanes mediated by iron catalysts in presence of H₂O₂ can give rise to formation of alkyl peroxides, which can decompose to form the corresponding ketone and alcohol products during the course of the reaction, or during GC analysis.^{55–57} In order to confirm that formation of alkyl peroxides did not occur in the course of the catalysis, the final reaction mixtures from oxidation of substrates **7** and **45** were treated with triphenylphosphine, and no changes were observed in terms of yield or alcohol/ketone ratio with respect to those determined before adding PPh₃ (see Table IV.3). These results exclude the presence of alkyl peroxides among the oxidation products.

Table IV.3. Comparison of oxidation of **7** of **45** in presence or absence of PPh₃ using **A-1**.

Substrate 7	Yield (%)	Product ratio [8/81]
Sample 1 ^a	57	[90/10]
Sample 2 ^b	56	[91/9]
Substrate 45	Yield (%)	Product ratio [46/47/48]
Sample 1 ^a	71	[19/58/23]
Sample 2 ^b	73	[19/58/23]

Cat:substrate:H₂O₂:AcOH 3x2:100:200x2:500x2 ^a Sample passed through silica plug. ^b Sample treated with PPh₃.



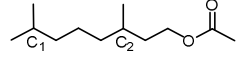

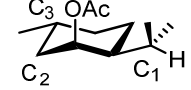
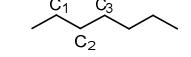
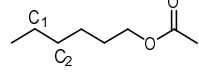
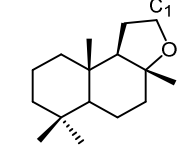
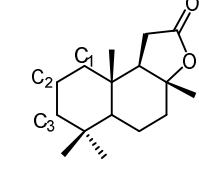
IV.2.3 SCOPE AND SELECTIVITY BASES FOR C–H OXIDATION

Once the best reaction conditions had been established, the oxidation of structurally more complex substrates containing multiple secondary and tertiary C–H bonds was evaluated. A comparison between oxidation of *cis*-4-methyl-1-cyclohexylpivalate *versus* its *trans* isomer **11** (entries 1-3, Table IV.4) is informative as it reflects the importance of subtle aspects in defining the regioselectivity of the oxidation. As already discussed, while

oxidation of **7** occurs preferentially at C₁ with high regioselectivity (91%, entry 2, Table IV.4), the oxidation of *trans*-4-methyl-1-cyclohexylpivalate exhibits a slightly different selectivity, and the corresponding ketone resulting from oxidation at C₂ is obtained in ~30% relative ratio. This difference between *cis*- and *trans*-4-methyl-1-cyclohexylpivalate arises from the position of the C–H bond to be attacked in the chair conformation. The *trans* substrate **11** has the tertiary C–H to be oxidized in axial position, but the same tertiary site in **7** is in equatorial position. Breakage of equatorial C–H bonds is facilitated in terms of stereoelectronic effects and strain release, and because of that, formation of **8** is favored.^{2,45} The importance of electronic effects in defining C–H site selectivity is evidenced in the oxidation of substrates containing electron-withdrawing moieties. For example, oxidation of 3,7-dimethyloctylacetate **20** (entries 4 and 5, Table IV.4) occurs at the more distal position from the acetate deactivating group showing that the oxidizing species have electrophilic character.

(–)-Menthyl acetate **3** and (+)-neomenthyl acetate **55** are menthol derivatives with multiple and chemically distinct C–H bonds and therefore constitute interesting, non-trivial substrate platforms to evaluate C–H regioselectivity exhibited by the catalyst. As these substrates are also chiral, matching-mismatching effects with the chirality of the catalyst can be also interrogated. Oxidation of **3** with **Λ-1** affords selectively the tertiary alcohol resulting from stereospecific oxidation at C₁, and minor amounts of ketone from oxidation at C₂ (entry 6, Table IV.4) in a combined 63% isolated yield. However, when **3** is oxidized with the other enantiomer of the catalyst [Fe(CF₃SO₃)₂((*R,R*)-mcp)], **Δ-1**, the selectivity for C₁ site is reduced (71%), and a more modest 44% combined yield is obtained (entry 7, Table IV.4). In the case of (+)-neomenthyl acetate **55**, the acetate group provides steric hindrance to the axially oriented tertiary C₃–H bond in the chair. Consequently, competitive C–H oxidation is expected to occur at the methylenic site C₂ and at the isopropyl group (C₁). Entry 8 in Table IV.4 shows that tertiary alcohol is only slightly preferred when using **Λ-1** (55% selectivity, 47% combined yield); instead, **Δ-1**, favors oxidation at C₂ yielding the ketone as major product (49% combined yield, with 62% selectivity for C₂ site; entry 9, Table IV.4). These results show that the regioselectivity in the oxidation of these chiral substrates is sensitive to the relative chirality of the catalyst.⁴⁶

Table IV.4. Oxidation of tertiary and secondary C–H bonds with **A-1**.

Substrate	Entry	Conversion (%) ^a	Yield (%) ^a	Selectivity [C ₁ /C ₂ /C ₃] ^a
7 	1	81	57	[90/10]
	2 ^b	81	53	[91/10]
11 	3	66	57	[70/30]
20 	4	74	42	[83/17]
	5 ^c	76	45	[87/13]
3 	6	86	63 ^d	[90/10]
	7 ^e	77	44	[71/29]
55 	8	79	47	[55/49]
	9 ^e	67	49	[38/62]
26 	10 ^f	67	50	[49/34/17]
30 	11 ^b	37	26	[76/24]
	12 ^{g,h}	99	37	
49 	13 ^{h,i}	87	51	
	14 ^{h,i,j}	99	60	
	15 ^{e,h}	99	41	
	16 ^{e,h,i}	99	58	
	17 ^k	86	56	[7/64/29]
	18 ^{k,l}	79	49	[8/67/25]
50 	19 ^{e,k}	74	64 (60) ^d	[6/72/22]
	20 ^{b,k}	75	55	[7/67/26]
	21 ^{k,l,m}	69	55	[7/70/23]
	22 ⁿ	96	50	[8/66/26]

Cat:substrate:H₂O₂:AcOH 3x2:100:200x2:500x2 ^a Based on GC analysis. ^b Using *rac*-**1**. ^c Using 1.5 equiv of AcOH per addition. ^d Isolated yield. ^e Using **A-1**. ^f Using 3.2 equivalents H₂O₂. ^g Using 2.6 equivalents H₂O₂. ^h Reaction at rt. ⁱ Using 1.8 equivalents H₂O₂. ^j One addition. ^k Using 3.4 equivalents H₂O₂. ^l Using 15% catalyst. ^m 4.5 mM catalyst. ⁿ Using 25% mol catalyst with protocol described by White *et al.*⁴³

Oxidation of methylene sites with **A-1** can also be accomplished in good yields, and reactions exhibit analogous selectivity patterns to those observed in the oxidation of tertiary C–H bonds. The role of steric effects in dictating regioselectivity has been already discussed in the oxidation of **45** and these effects are also shown in the oxidation of the linear alkane *n*-heptane **26**, where no major electronic effects interplay. Oxidation of *n*-heptane yielded ketones resulting from oxidation at methylene sites C₁, C₂, and C₃ (50% yield, entry 10, Table IV.4) with a modest but remarkable selectivity for the less sterically crowded site (49% selectivity, entry 10, Table IV.4. Note that the statistically expected product ratio would be [40/40/20]. On the other hand, the electrophilic nature of the oxidizing species becomes obvious when oxidizing substrates that contain electron-withdrawing groups. In this case, proximal positions are deactivated. For example, oxidation of **30** takes place at the more distal positions from the deactivating group (entry 11, Table IV.4), albeit at a reduced yield.

The hyperconjugative effect of ethers in activating adjacent C–H bonds can be also used to direct site selectivity in the oxidation of complex molecules. For example, (–)-ambroxide **49** was oxidized to (+)-sclareolide **50** in up to 60% yield (entries 12–16, Table IV.4). In this case the best results are obtained with lower amounts of hydrogen peroxide (1.8 equivalents) and a single addition of catalyst, H₂O₂ and acetic acid, to limit overoxidation of the product.

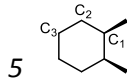
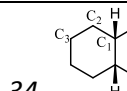
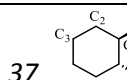
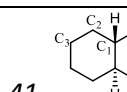
Further oxidation of (+)-sclareolide **50** can be achieved in good yields and preferential selectivity towards the less sterically hindered C₂ site (up to 64% yield and 72% selectivity, entries 17–22, Table IV.4). Use of the racemic form of the catalyst elicited lower yields (entry 20, Table IV.4), and the same occurred when catalyst loading was increased (entries 18, 19, and 22, Table IV.4). In all cases, the same selectivity pattern is maintained regardless of the protocol employed. Of particular interest is the observation that selectivity towards C₂ appears to be superior to those obtained with **A-1P**, **A-2P** and **A-2**.⁴⁶

IV.2.4 COMPARATIVE REGIOSELECTIVITY AMONG IRON CATALYSTS IN C–H OXIDATION REACTIONS

Cyclohexanes constitute common basic frameworks in organic molecules and, because of that, their selective oxidation is an interesting problem in organic synthesis. Furthermore, substituted cyclohexanes are also informative substrate probes to

interrogate C–H regioselectivity preferences between different catalysts. Results from the oxidation of cyclohexane derivatives catalyzed by **A-1** are collected in Table IV.5. *cis*-1,2-Dimethylcyclohexane **5** (*cis*-DMCH) and *cis*-decalin **34** were oxidized in good to moderate yields (68-49% respectively) and selectivity for the tertiary site (81-67% respectively) with 3 mol% **A-1** (entries 1 and 2, Table IV.5).

Table IV.5. Oxidation of cyclohexane derivatives with **A-1**.

Substrate	Entry	Conversion (%) ^a	Yield (%) ^a	Selectivity [C ₁ /C ₂ /C ₃] ^a
	1	83	68	[81/19 ^b]
	2	86	49	[67/17/16]
	3	81	46	[20/27/53]
	4	76	56	[4/37/59]

Cat:substrate:H₂O₂:AcOH 3:100:200:500 ^a Based on GC analysis. ^b C₂ + C₃ oxidation products.

Oxidations are stereospecific and only the alcohol with retention of the configuration was obtained. Preferential oxidation of these tertiary sites was indeed expected because of their equatorial position, as breakage of these bonds is facilitated by strain release. In contrast, the tertiary C–H sites in *trans*-1,2-dimethylcyclohexane **37** (*trans*-DMCH) and *trans*-decalin **41** are in axial position. Consequently, strain release is not contributing to the activation of these C–H bonds, and in addition, for **34** and **41**, their bridgehead situation confers them with some additional steric protection. Not unexpectedly, oxidation of *trans*-DMCH and *trans*-decalin occurs preferentially at the methylenic sites, providing the corresponding ketones as the major products (entries 3 and 4, Table IV.5). Most interestingly is the observation that oxidation occurs selectively at the most sterically accessible methylenic site (C₃) of both *trans*-DMCH and *trans*-decalin.

In order to substantiate this trend, regioselectivities in the oxidation of cycloalkanes obtained with **A-1** can be compared with analogous parameters obtained under analogous conditions with non-heme iron catalysts **A-2SbF₆**, **3**, **A-2P**, and **A-1P** previously described in the literature (Figure IV.3 and IV.4).

Oxidation of *cis*-DMCH and *cis*-decalin (Figure IV.3) show little differences among the series of catalysts. The tertiary alcohol is the dominant product in both cases with a selectivity that ranges from 85% with Λ -2 to 75% with **3**,⁴⁷ for *cis*-DMCH, and from 80% with Λ -2 to 67% with Λ -1 for *cis*-decalin.

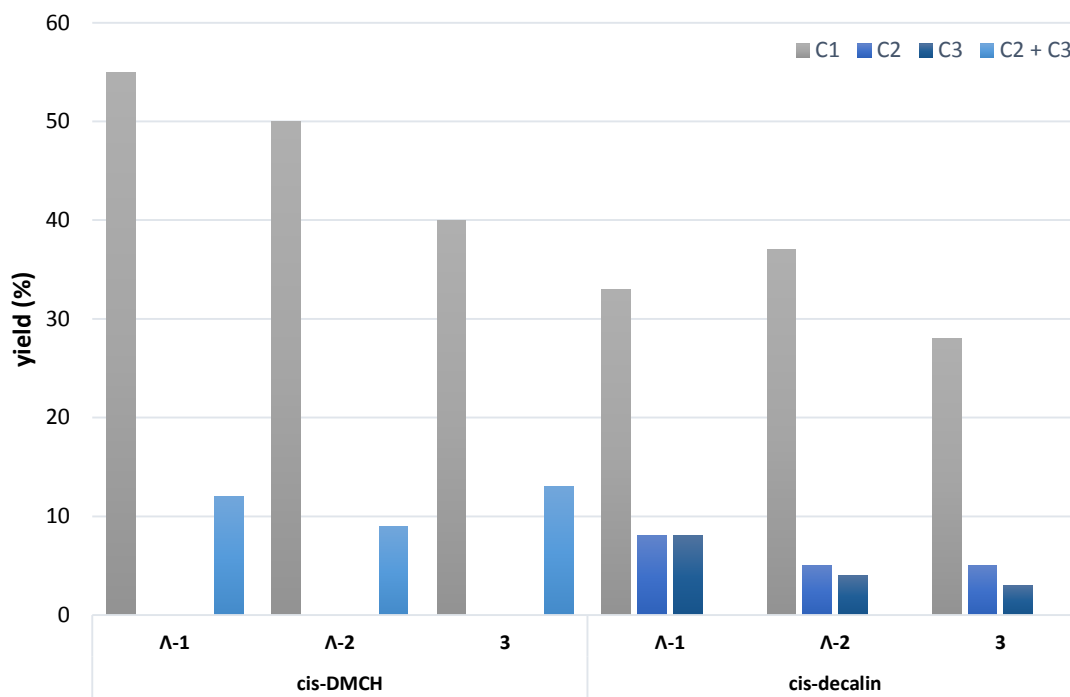


Figure IV.3. Oxidation of *cis*-DMCH and *cis*-decalin with Λ -1, Λ -2, and **3**⁴⁷ using 3 mol% cat.

More remarkable is the oxidation of *trans*-DMCH and *trans*-decalin, which is shown in a graphical manner in Figure IV.4. Irrespective of the iron catalyst employed, oxidation of these substrates occurs preferentially at the secondary sites, **3** and Λ -1 being the ones for which this selectivity is most enhanced. But the most interesting aspect is the observation that discrimination between oxidation at C₂ and C₃ sites is highly dependent on the nature of the catalyst. Thus only Λ -1P⁴⁶ and Λ -1 oxidize preferentially C₃, while the rest of the catalysts have basically no preference for any of the two sites. Considering that methylene site C₃ is the sterically least congested, we conclude that cyclohexyl-based catalysts Λ -1P and Λ -1 are the most sensitive to steric factors when the substrate contains multiple and distinct methylene sites. Indeed, this conclusion is further reinforced when the same analysis is performed in the oxidation of 1,1-dimethylcyclohexane **45** (Table IV.2). The important conclusion of this comparative analysis is that the nature of the diamine backbone in this class of catalysts appears to be more decisive than building the structure of the pyridines in order to modulate C–H selectivity among multiple methylene

sites. Therefore, a rather structurally simple catalyst such as **Λ -1** not only oxidizes alkanes in good yields but also exhibits notable regioselectivity among multiple methylenic sites on the basis of steric arguments.

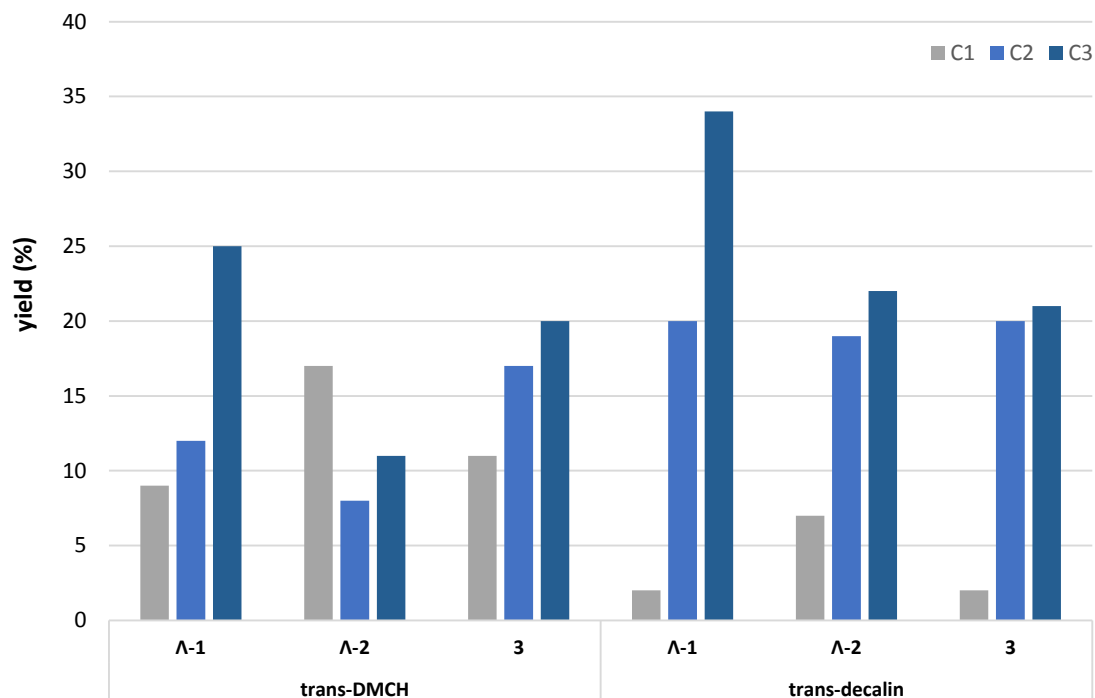
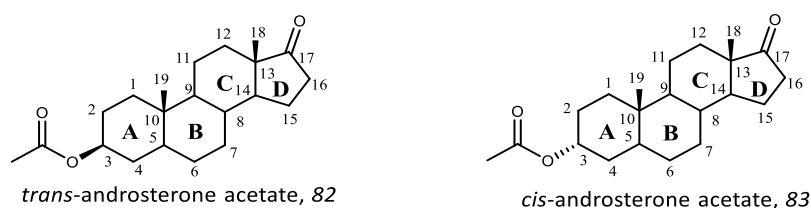


Figure IV.4. Oxidation of *trans*-DMCH and *trans*-decalin with Λ -1, Λ -2, and **3**⁴⁷ using 3 mol% cat.

IV.2.5 OXIDATION OF ELABORATED SUBSTRATES

The ability of **1** to discriminate among multiple C–H sites in simple organic molecules hints at the possibility of using this catalyst in the oxidation natural products. Towards this end, Λ -1 and Δ -1 were used in the oxidation of androsterone derivatives **82**, **83**, and **84** (see Table IV.6 and Table IV.7). These molecules are steroids, and it is well known that biosynthesis and biological degradation of steroidal hormones in living organisms involves oxidation by P450 enzymes,^{58,59} therefore their oxidation can present biological interest.⁶⁰ In addition, these substrates are structurally complex, with multiple and distinct C–H bonds, and because of that they constitute excellent platforms for studying selectivity in C–H oxidation.⁶¹

Table IV.6. Oxidation of androsterone derivatives with different iron catalysts.

Substrate	Entry	Conversion (%) ^a	Yield (%) ^a	Selectivity ^a
				[C₆^b/C₇/C₁₂/C₁₄]
	1 ^c	82	59	[50/32/17/0]
	2 ^d	85	67	[52/13/35/0]
82	3 ^e	76	45	[38/37/16/9]
	4 ^f	71	48	[32/32/13/23]
	5 ^h	73	45	[44/32/11/13]
				[C₆/C₇/C₁₂]
	6 ^c	86	52	[71/15/14]
	7 ^d	90	55	[51/11/39]
83	8 ^g	90	53 (45) ⁱ	[58/12/30]
	9 ^e	82	38	[50/20/30]
	10 ^f	84	35	[49/28/23]

Cat:substrate:H₂O₂:AcOH 3x2:100:200x2:500x2. ^a Based on GC analysis. ^b Sum of ketone and α -alcohol. ^c Using **Λ -1**. ^d Using **Δ -1**. ^e Using **Δ -2**, only 1 addition. ^f Using **Λ -2**, only 1 addition. ^g Using *rac*-**1**. ^h Using **5**. ⁱ Isolated yield.

trans- (**82**) and *cis*-androsterone acetate (**83**) contain 3 primary C–H sites, 9 secondary C–H sites and 5 tertiary C–H bonds potentially susceptible of being oxidized. Since rings A and D contain electron-withdrawing groups, it was envisioned that C–H bonds at rings B and C would be more prone to oxidation. Furthermore, considering the low reactivity of the tertiary bridgehead C–H bonds at *trans*-decaline (Table IV.5), it was also presumed that tertiary sites C₈ and C₉ would also be disfavored. Indeed, when subjected to the standard experimental conditions, oxidation of **82** and **83** proceeds with good substrate conversion (82-90%), and three major oxidation products are obtained resulting from oxidation at three different methylenic sites (C₇, C₆, and C₁₂, Table IV.6), all of them belonging to rings B and C. Although a clear rationale for the lack of oxidation at C₁₁ could not be discerned, it may be speculated that steric hindrance caused by ring A and the methyl group C₁₉ protect this site. Mass balance in these reactions ranges from 60-80%,

which should be regarded as good considering the complexity of the substrates and the difficulty of the reaction. Ketone at C₆ is the dominant product when **Λ-1** or **Δ-1** are used as catalyst, accounting for 50-52% of the products in the oxidation of **82**, and up to 71% for **83**. Ketones arising from oxidation at C₇ and C₁₂ are also obtained in the oxidation of **82**, and the relative proportion of the two products depends on the chirality of the catalyst (C₇/C₁₂; 32/17 for **Λ-1**; entry 1, Table IV.6, vs 13/35 for **Δ-1**, entry 2, Table IV.6).

Reduced product yields and a different selectivity pattern are observed for **2** catalysts in the oxidation of **82**. In this case, oxidation at C₆ and C₇ is obtained in virtually identical relative yields (38% and 37% relative selectivity, respectively, for **Δ-2** (entry 3, Table IV.6), and 32% relative selectivity for **Λ-2**, (entry 4, Table IV.6)). For **Δ-2** the ketone resulting from oxidation at C₁₂ remains as the third major product (16% normalized selectivity, entry 3, Table 5), but the alcohol resulting from hydroxylation at the tertiary position C₁₄ is detected in significant amounts (9% relative selectivity, entry 3, Table IV.6). On the other hand, the relative selectivity between C₁₂ and C₁₄ oxidation products is reverted using **Λ-2**, in favor of the C₁₄ tertiary alcohol (23% relative selectivity, entry 4, Table IV.6). This product is interesting since it is only observed when using **2**, showing again the preference of the **1**-based systems for methylenic sites.

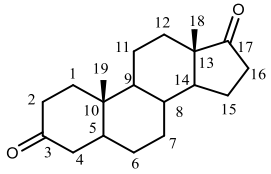
For comparison, **5** was tested under the same reaction conditions, appearing as a less active catalyst than **Δ-1** (67% vs 45% yield, compare entries 2 and 5, Table IV.6).

When the **2**-based catalysts are tested in the oxidation of **83**, product yields are again lower than the ones obtained with the **1**-based systems. Oxidation at C₆ appears as the major product for both catalyst enantiomers with ~ 50% relative selectivity (entries 9 and 10, Table IV.6). However, the second major product is dependent on the catalyst used. While **Δ-2** affords oxidation at C₁₂ with 30% relative selectivity (entry 9, Table IV.6), **Λ-2** yields C₇ oxidized product in 28% relative selectivity (entry 10, Table IV.6). Finally, by using racemic catalysts, we obtained oxidation products with intermediate product ratios between those attained with the chiral form of the catalysts. These results indicate that regioselectivity is dependent on the chirality of the catalysts, and both enantiomers have equal contribution to the overall reaction.

Substrate **84** (3,17-androstanedione) was also evaluated in the oxidation of the androsterone family (Table IV.7). In this case, there is a carbonyl group instead of an

acetate group. Oxidation at four different positions is observed (C₇, C₆, C₁₂, and C₅). Modest yields are obtained in this oxidation (up to 34% with **Λ-1**), and this fact can be rationalized in terms of the more deactivating nature of the ketone moiety. Selectivity appears to be catalyst-dependent but, interestingly, in this case it affects at the major product. Thus, **Λ-1** affords oxidation at C₇ as the major product, being C₆ and C₁₂ virtually equally oxidized. C₅ is the minor product in all cases, although a rationale for the formation of this product cannot be provided. For catalysts **Δ-1** and *rac-1* oxidation at C₁₂ is the major product. C₆ is the second preferred oxidation position for **Δ-1**, while when using *rac-1* C₇ and C₆ are virtually equally oxidized.

Table IV.7. Oxidation of 3-17-androstanedione (**84**) with **1**-based catalysts using the iterative addition protocol.

Substrate	Catalyst	Conversion (%) ^a	Yield (%) ^a	Selectivity ^a
				[C ₆ /C ₇ /C ₁₂ /C ₅]
 3,17-androstanedione, 84	Λ-1	77	34 (29) ^b	[27/41/26/6]
	Δ-1	89	28	[30/18/48/4]
	<i>rac-1</i>	82	25	[27/27/40/6]

^a Based on GC analysis. ^b Isolated yield.

IV.2.6 MULTIGRAM SCALE OXIDATION OF ELABORATED MOLECULES

Most commonly, C–H oxidation reactions are not straightforward to scale up because of the cost and sensitive nature of the reagents. In this regard, in order to illustrate the utility of the **Λ-1** catalysts in C–H oxidation reactions with preparative value, the oxidation of natural products (+)-sclareolide (**50**) and *trans*-androsterone acetate (**82**) was performed in multigram scale. Figure IV.5 collects results from the oxidation of 2.5 g (9.8 mmol) of (+)-sclareolide (**50**). The reaction was performed in acetonitrile solvent (100 mL) at 0 °C during 17 min, using 3 mol% of **Λ-1** catalyst, 5 equiv. of AcOH diluted in acetonitrile (8.7 mM) and 3.4 equiv. of H₂O₂ diluted in acetonitrile (1.8 M), that was added by syringe pump. After 10 min, a second addition of catalyst, AcOH and H₂O₂ via syringe pump over 17 min was performed. Reaction was complete in 55 min. After work-up, chromatographic separation afforded 352 mg of unreacted starting material (14%) and two major oxidation products. 865 mg of pure ketone **79** resulting from oxidation at the spatially more exposed

site were isolated (34% yield), along with 324 mg of ketone **80** (13% yield). In addition, 62 mg of **78** (2.4% yield) resulting from oxidation at C₂ is also obtained. Despite the low yield of **78**, its isolation can be regarded as significant since it had only been synthesized by means of biological methods⁶², which require high reaction times, and with **Λ-2P**⁴⁶ under very low temperature catalytic conditions.

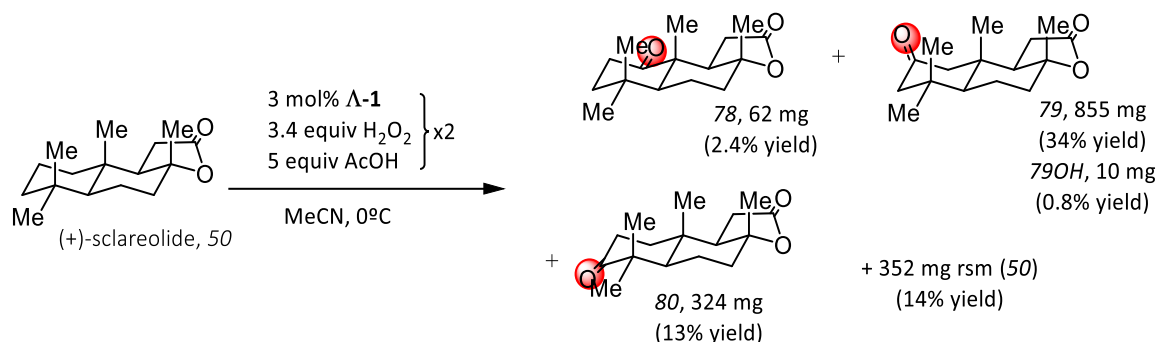


Figure IV.5. Gram scale oxidation of (+)-sclareolide (**50**).

Overall, mass balance of the reaction is moderate (~ 64%), but it should be considered as quite good for a C–H oxidation reaction of a complex molecule. Most importantly, product yields and regioselectivities obtained in this large scale reaction are in reasonably good agreement with that obtained from low scale reactions (entry 17, Table IV.4, 56% combined product yields, with normalized [C₁/C₂/C₃] = [7:64:29], compared with 50% combined yield, and normalized [C₁/C₂/C₃] = [5:69:26] for the large-scale reaction), highlighting the straightforward translation of the reaction from low to relatively large scales.

Further illustrating the practical applicability of **Λ-1** in the large scale oxidation of complex organic molecules, multigram scale oxidation of steroid **82** (Figure IV.6) was also performed with catalyst **Λ-1** following the same standard procedure employed in the oxidation of **50**. As observed in the small scale oxidations, oxidation of position 6 was largely favored, obtaining 834 mg of ketone **85**, along with 130 mg of **85-α-OH** (29% combined yield). Ketones arising from oxidation at C₇ (**86**) and C₁₂ (**87**) were also obtained in 16% (545 mg) and 12% (393 mg) respective yield, which all together account for 57% combined yield. In addition, 598 mg of unreacted starting material (18%) were recovered. Mass balance of the reaction is ~ 75% and yield and regioselectivity of the C–H oxidation reaction is also in reasonably good agreement with that obtained in analogous small scale

oxidation (compare entry 1, Table IV.6, 59% yield and normalized ratio [C₆:C₇:C₁₂] = [50:32:18], with 57% yield and normalized ratio [C₆:C₇:C₁₂] = [51:28:21] for the large scale reaction). The most important difference arises from the isolation of small amounts (4%) of alcohol *85-α-OH*, in the large scale reactions, and that was observed only in trace amounts in the small scale reactions. It is important to notice that no signs of the corresponding diastereoisomeric alcohol resulting from hydroxylation at the equatorial C₆ C–H bond could be detected. This suggests that formation of *85-α-OH* may correspond to a diastereoselective methylene hydroxylation reaction.

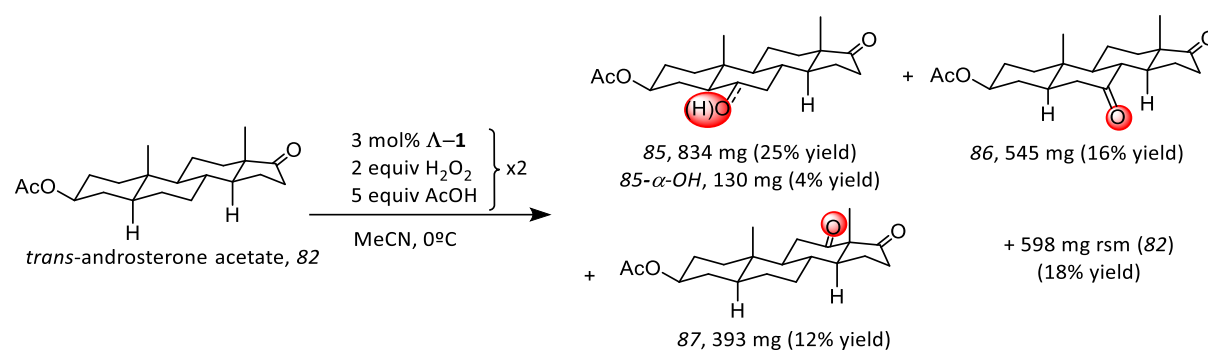


Figure IV.6. Gram scale oxidation of *trans*-androsterone acetate (**82**).

Summarizing, large-scale C–H oxidation reactions of natural products can be conveniently performed with the Λ -1 catalyst, and product yields and selectivities can be reasonably inferred from small scale reactions. Nevertheless, it should be noted that the percentage conversion and percentage yield do not match completely. This fact might be due to the difficulty of this type of oxidations, where mass balance is not complete. Although the formation of significant amounts of a single unidentified product is not observed, the formation of trace amount of multiple byproducts can not be excluded.

IV.3 CONCLUDING REMARKS

The work presented in this chapter shows that Λ -1 is a very convenient catalyst for C–H oxidation reactions employing H_2O_2 as terminal oxidant. This complex operates at low catalyst loadings (1-6 mol%) at 0 °C and short reaction times, leading to oxidation of nonactivated tertiary and secondary alkyl C–H bonds of organic molecules in preparative useful yields. Preparation of the catalyst in multigram scale can be done from simple and inexpensive reagents, which constitutes an important advantage with regard to other C–H oxidation reagents described so far, including Fe-based catalysts. The catalyst exhibits

predictable site-selectivity; it generates electrophilic species upon reaction with H₂O₂ that appear sensitive to the structural properties of the substrate, and this results in remarkable site-selectivity properties that can be used to direct oxidation in substrates where multiple methylene sites are available, obtaining remarkable selectivity for oxidation products of the less sterically hindered methylenic sites. This has been demonstrated to be useful in the oxidation of complex molecules such as natural products. Site-selectivity in these reactions is distinct from that attained with other iron catalysts previously described, offering new alternatives for selective C–H functionalization. Most remarkably, given the easy access to large amounts of catalyst, and the simplicity of the methodology, multigram scale oxidation of natural products can be conveniently performed in short reaction times, and product yields and selectivities are reliably predicted from small scale reactions.

IV.4 EXPERIMENTAL SECTION

IV.4.1 MATERIALS

Reagents and solvents used were commercially available reagent quality unless otherwise stated. Solvents were purchased from SDS and Scharlab. Solvents were purified and dried by passing through an activated alumina purification system (MBraun SPS-800). Acetonitrile for catalysis was HPLC grade. Preparation and handling of air-sensitive materials were carried out in a N₂ dry box (Braun) with O₂ and H₂O concentrations < 1 ppm. [Fe(CF₃SO₃)₂((*S,S*)-mcp)], **Λ-1**, (mcp = *N,N'*-dimethyl-*N,N'*-bis(2-pyridylmethyl)cyclohexane-*trans*-1,2-diamine), [Fe(CF₃SO₃)₂((*R,R*)-mcp)], **Δ-1**, [Fe(CF₃SO₃)₂((*rac*)-mcp)], *rac*-**1**, [Fe(CH₃CN)₂((*S,S*)-mcp)](SbF₆)₂, **Λ-1SbF₆**, [Fe(CF₃SO₃)₂(mep)] (mep = *N,N'*-dimethyl-*N,N'*-bis(2-pyridylmethyl)ethane-1,2-diamine), **5**, [Fe(CF₃SO₃)₂((*S,S*)-pdp)], **Λ-2**, (pdp = *N,N'*-bis(2-pyridylmethyl)-2,2'-bipyrrolidine), and [Fe(CF₃SO₃)₂((*R,R*)-pdp)], **Δ-1**, were prepared according to published procedures.^{46,50,63}

IV.4.2 INSTRUMENTATION

NMR spectra were taken on a Bruker DPX 300 or 400 MHz spectrometer. Spectra were referenced to the residual proton solvent peaks or TMS (tetramethylsilane) for ¹H. HRMS were performed on time-of-flight mass spectrometer with an ESI source using methanol as mobile phase. Product analyses were performed on an Agilent 7820A gas

chromatograph (HP5 column, 30m or Cyclosil-B column, 30 m) and a flame ionization detector.

IV.4.3 SYNTHESIS OF SUBSTRATES

1,1-Dimethylcyclohexane (45), (-)-menthyl acetate (3), (+)-neomenthyl acetate (55) *n*-heptane (26), methyl hexanoate (30), (-)-ambroxide (49), (+)-sclareolide (50), *cis*-1,2-dimethylcyclohexane (5), *cis*-decalin (34), *trans*-1,2-dimethylcyclohexane (37), and *trans*-decalin (41) were purchased from Aldrich or TCI America. *cis*-4-methylcyclohexanol, *trans*-4-methylcyclohexanol, 3,7-dimethyl-1-octanol, *cis*-androsterone and *trans*-androsterone were purchased from Aldrich or TCI America. All liquid substrates were passed through an alumina plug before being used.

cis-4-Methylcyclohexyl pivalate (7), *trans*-4-methylcyclohexyl pivalate (11) and 3,7-dimethyloctyl acetate (20) were synthesized as previously described.⁴⁵ *trans*-Androsterone acetate (82), *cis*-androsterone acetate (83) and 3,17-androstenedione (84) were synthesized as it follows.

trans-Androsterone acetate (82): *trans*-androsterone (2.0 mmol), DMAP (2.4 mmol) and acetic anhydride (2.4 mmol) were dissolved in DCM (8 mL) and stirred for 4 h at rt. The reaction was then diluted with DCM (25 mL) and washed successively with H₂O (20 mL), saturated NaHCO₃ solution (20 mL) and brine (20 mL). The organic layer was dried over MgSO₄ and the solvent was removed under reduced pressure. 0.610 g of a white solid were obtained (92% yield). ¹H-NMR (300 MHz, CDCl₃, 300 K) δ, ppm: 0.64-0.76 (m, 1H), 0.85 (s, 3H), 0.86 (s, 3H), 0.95-1.09 (m, 2H), 1.19-1.35 (m, 7H), 1.42-1.58 (m, 3H), 1.60-1.68 (m, 2H), 1.71-1.82 (m, 4H), 1.89-1.97 (m, 1H), 2.00-2.13 (m, 1H), 2.02 (s, 3H), 2.43 (dd, *J* = 19.0, 8.3 Hz, 1H), 4.63-4.74 (m, 1H). ¹³C-NMR (75 MHz, CDCl₃, 300 K) δ, ppm: 12.2, 13.8, 20.5, 21.4, 21.8, 27.4, 28.3, 30.8, 31.5, 33.9, 35.0, 35.6, 35.8, 36.7, 44.6, 47.8, 51.4, 54.3, 73.5, 170.7, 221.2. HRMS (ESI-TOF, [M + Na]⁺): *m/z* calcd for C₂₁H₃₂O₃Na 355.2244, found 355.2225

cis-androsterone acetate (83): The same procedure as for the synthesis of 82 was employed, using *cis*-androsterone as starting material. 0.643 g of a white solid were obtained (97% yield). ¹H-NMR (300 MHz, CDCl₃, 300 K) δ, ppm: 0.77-0.85 (m, 1H), 0.82 (s, 3H), 0.87 (s, 3H), 0.95-1.09 (m, 1H), 1.19-1.33 (m, 6H), 1.46-1.50 (m, 4H), 1.52-1.59 (m,

2H), 1.63-1.71 (m, 3H), 1.77-1.83 (m, 2H), 1.90-1.98 (m, 1H), 2.01-2.17 (m, 1H), 2.06 (s, 3H), 2.44 (dd, $J = 19.0, 8.5$ Hz, 1H), 5.01-5.03 (m, 1H). ^{13}C -NMR (75 MHz, CDCl_3 , 300 K) δ , ppm: 11.3, 13.8, 20.1, 21.5, 21.7, 26.1, 28.1, 30.8, 31.6, 31.6, 32.8, 35.0, 35.8, 36.0, 40.0, 47.8, 51.5, 54.3, 69.9, 170.7, 221.3. HRMS (ESI-TOF, $[\text{M} + \text{Na}]^+$): m/z calcd for $\text{C}_{21}\text{H}_{32}\text{O}_3\text{Na}$ 355.2244, found 355.2232

3,17-androstanedione (84): *trans*-androsterone (3.0 mmol) was dissolved in DCM (20 mL) and cooled to 0 °C. Pyridinium chlorochromate (4.5 mmol) was added and the mixture was allowed to warm to room temperature. The mixture was stirred overnight. Purification over silica (hexane:ethyl acetate 4:1 mixture) yielded 777 mg of a white solid (90% yield). ^1H -NMR (400 MHz, CDCl_3 , 300 K) δ , ppm: ^1H -NMR (400 MHz, CDCl_3 , 300 K) δ , ppm: 0.77-0.84 (m, 1H), 0.89 (s, 3H), 0.96-1.07 (m, 1H), 1.04 (s, 3H), 1.23-1.47 (m, 6H), 1.50-1.66 (m, 3H), 1.67-1.73 (m, 1H), 1.80-1.87 (m, 2H), 1.92-2.14 (m, 4H), 2.25-2.49 (m, 4H). ^{13}C -NMR (100 MHz, CDCl_3 , 300 K) δ , ppm: 11.5, 13.8, 20.7, 21.8, 28.6, 30.5, 31.5, 34.9, 35.8, 35.8, 38.1, 38.4, 44.6, 46.6, 47.7, 51.2, 53.9, 211.5, 220.9. HRMS (ESI-TOF, $[\text{M} + \text{Na}]^+$): m/z calcd for $\text{C}_{19}\text{H}_{28}\text{O}_2\text{Na}$ 311.1982, found 311.1962.

IV.4.4 SAMPLE ANALYSIS

GC analyses of the catalysis provided substrate conversions and product yields relative to the internal standard integration. Calibration curves were obtained from commercial products when available or from pure isolated samples obtained from catalytic reactions.⁴⁶

1,1-dimethylcyclohexanones, *n*-heptanones, 1-decalone, and 2-decalone were purchased from Aldrich or TCI America. For non-commercially available products, pure samples were synthesized, isolated and characterized following the experimental procedures in the literature.⁴⁵⁻⁴⁷

IV.4.5 CATALYTIC CONDITIONS

Several catalytic conditions were tested in the oxidation of *cis*-4-methyl-1-cyclohexylpivalate and 1,1-dimethylcyclohexane. In this section we describe every protocol used for each entry in the results section (IV.2).

IV.4.5.1 *Single addition protocol*

In entries 1-2, 4-5, and 7-9 from Table IV.1 and Table IV.2, the single addition protocol is used.⁴⁶ In this protocol, a 5 mL vial was charged with the proper amounts of catalyst, substrate (1 equiv) and CH₃CN to obtain a 1.5 mM solution of catalyst (see Table IV.8 for detailed amounts of reagents). The vial was placed on an ice bath and stirred. A 1.74 M CH₃COOH solution in CH₃CN was added and a 1.5 M H₂O₂ solution (diluted from a 35% H₂O₂ aqueous solution) were delivered by syringe pump over 17 min at 0 °C. After syringe pump addition, the solution was stirred for 10 minutes at 0 °C. At this point, 12.5 μmol of internal standard were added and the solution was then filtered through a silica plug to remove the catalyst and eluted with 2 mL of AcOEt. The sample was then submitted to GC analysis.

Table IV.8. Amounts of reagents employed in Table IV.1 and Table IV.2 using the single addition protocol.

Table	Entry	Catalyst	CH ₃ CN (mL)	H ₂ O ₂	CH ₃ COOH	
1	1	1 mol %, 1 μmol	0.67	2 equiv, 200 μmol	1.5 equiv, 150 μmol	
	2	3 mol %, 1 μmol	0.67	2 equiv, 67 μmol	1.5 equiv, 50 μmol	
	4	5 mol %, 2.5 μmol	1.67	2 equiv, 100 μmol	1.5 equiv, 75 μmol	
	5	15 mol %, 4 μmol	2.67	2 equiv, 53 μmol	1.5 equiv, 40 μmol	
	7	3 mol %, 1 μmol	0.67	3.6 equiv, 120 μmol	1.5 equiv, 50 μmol	
	8	3 mol %, 1 μmol	0.67	2 equiv, 67 μmol	10 equiv, 333 μmol	
	9	3 mol %, 1 μmol	0.67	3.6 equiv, 120 μmol	10 equiv, 333 μmol	
	2	1	1 mol %, 1 μmol	0.67	2.8 equiv, 280 μmol	1.5 equiv, 150 μmol
		2	3 mol %, 1 μmol	0.67	2.8 equiv, 93 μmol	1.5 equiv, 50 μmol
4		5 mol %, 2.5 μmol	1.67	2.8 equiv, 140 μmol	1.5 equiv, 75 μmol	
5		15 mol %, 4 μmol	2.67	2.8 equiv, 75 μmol	1.5 equiv, 40 μmol	
7		3 mol %, 1 μmol	0.67	4.2 equiv, 140 μmol	1.5 equiv, 50 μmol	
8		3 mol %, 1 μmol	0.67	2.8 equiv, 93 μmol	10 equiv, 333 μmol	
9		3 mol %, 1 μmol	0.67	4.2 equiv, 140 μmol	10 equiv, 333 μmol	

IV.4.5.2 *Slow addition protocol*

In entry 6 from Table IV.1 and Table IV.2, the single addition protocol is used. In this case, the catalyst is delivered via syringe pump over 17 minutes, simultaneously with the H₂O₂ solution. The substrate (1 equiv, 27 μmol) was dissolved in 250 μL of CH₃CN in a 5

mL vial and stirred in an ice bath. The catalyst (15 mol%, 4 μmol) was dissolved in 2.42 mL of CH_3CN and a 1.74 M CH_3COOH solution in CH_3CN was added (1.5 equiv, 40 μmol). This catalyst solution was delivered to the substrate solution via syringe pump over 17 minutes, simultaneously with a 1.5 M H_2O_2 solution (diluted from a 35% H_2O_2 aqueous solution, 2 equiv, 53 μmol for Table IV.1; 2.8 equiv, 75 μmol for Table IV.2). After syringe pump addition, the solution was stirred for 10 minutes at 0 $^\circ\text{C}$. At this point, 12.5 μmol of internal standard were added and the solution was then filtered through a silica plug to remove the catalyst and eluted with 2 mL of AcOEt . The sample was then submitted to GC analysis.

IV.4.5.3 *Iterative addition protocol*

In entries 3, 10, and 11 from Table IV.1 and entries 3, 10-13 from Table IV.2, the iterative addition protocol is used.⁴⁶

Iterative addition protocol with slow addition of catalyst. For the three-addition protocol (entry 3, Table IV.1 and Table IV.2), a 5 mL vial was charged with catalyst (1 μmol , 1 mol%), the substrate (100 μmol , 1 equiv) and CH_3CN (0.67 mL). The vial was placed on an ice bath and stirred. 100 μmol of CH_3COOH from a 1.74 M solution in CH_3CN were added and the proper amount of a 1.5 M H_2O_2 solution (diluted from a 35% H_2O_2 aqueous solution, 1.2 equiv, 120 μmol see Table IV.9) was delivered by syringe pump over 6 minutes at 0 $^\circ\text{C}$. After syringe pump addition, the solution was stirred for 10 min at 0 $^\circ\text{C}$. Then a solution of catalyst (1 μmol , 1 mol%), CH_3CN (0.67 mL) and CH_3COOH (100 μmol , 5 equiv) was added simultaneously with 1.2 equiv of a 1.5 M (120 μmol) H_2O_2 solution via syringe pump over 6 min. After syringe pump addition the resulting solution was stirred for another 10 min. Finally a third addition was performed by adding a solution of catalyst (1 μmol , 1 mol%), CH_3CN (0.67 mL) and CH_3COOH (100 μmol , 5 equiv) simultaneously with 1.2 equiv of a 1.5 M (120 μmol) H_2O_2 solution via syringe pump over 6 min. After syringe pump addition the resulting solution was stirred for another 10 min. At this point, 12.5 μmol of internal standard were added and the solution was then filtered through a silica plug to remove the catalyst and eluted with 2 mL of AcOEt . The sample was then submitted to GC analysis.

Iterative addition protocol with direct addition of catalyst. For the two-addition protocol (entries 10-12 in Table IV.1, entries 10-13 in Table IV.2), a 5 mL vial was charged with catalyst (1 μmol , 3 mol%), the substrate (100 μmol , 1 equiv) and CH_3CN (0.67 mL). The vial was placed on an ice bath and stirred. 167 μmol of CH_3COOH from a 1.74 M solution in CH_3CN were added and the proper amount of a 1.5 M H_2O_2 solution (diluted from a 35% H_2O_2 aqueous solution, 2 or 2.8 equiv, see Table IV.9) was delivered by syringe pump over 17 minutes at 0 $^\circ\text{C}$. After syringe pump addition, the solution was stirred for 10 min at 0 $^\circ\text{C}$ and a solution of catalyst (1 μmol , 3 mol%), CH_3CN (0.67 mL) and CH_3COOH (167 μmol , 5 equiv) were added all at once to the reaction mixture. Another addition of a 1.5 M H_2O_2 solution (2 or 2.8 equiv, see Table IV.9) was performed via syringe pump over 17 minutes at 0 $^\circ\text{C}$. After syringe pump addition, the solution was stirred for 10 minutes at 0 $^\circ\text{C}$. At this point, 12.5 μmol of internal standard were added and the solution was then filtered through a silica plug to remove the catalyst and eluted with 2 mL of AcOEt . The sample was then submitted to GC analysis.

Table IV.9. Amounts of reagents employed in Table IV.1 and Table IV.2 using the iterative addition protocol.

Table	Entry	Additions	Catalyst	CH_3CN (mL)	H_2O_2	CH_3COOH
1	3	3	1 mol%, 1 μmol	0.1	1.2 equiv, 120 μmol	1 equiv, 100 μmol
	10	2	3 mol%, 1 μmol	0.67	2 equiv, 67 μmol	5 equiv, 167 μmol
	11	2	3 mol%, 1 μmol	0.67	2 equiv, 67 μmol	5 equiv, 167 μmol
	12	2	3 mol%, 1 μmol	0.67	2 equiv, 67 μmol	5 equiv, 167 μmol
2	3	3	1 mol%, 1 μmol	0.1	1.2 equiv, 120 μmol	1 equiv, 100 μmol
	10	2	3 mol%, 1 μmol	0.67	2.8 equiv, 93 μmol	5 equiv, 167 μmol
	11	2	3 mol%, 1 μmol	0.67	2.8 equiv, 93 μmol	5 equiv, 167 μmol
	12	2	3 mol%, 1 μmol	0.67	2.8 equiv, 93 μmol	5 equiv, 167 μmol
	13	2	3 mol%, 1 μmol	0.67	2.8 equiv, 93 μmol	5 equiv, 167 μmol

IV.4.6 PROCEDURE FOR GRAM SCALE OXIDATIONS

The gram scale oxidation of (+)-sclareolide and *trans*-androsterone acetate was performed as it follows.

A 250 mL round bottom flask was charged with: **A-1** (0.29 mmol, 3 mol%), alkane (9.7 mmol, 1 equiv), CH_3CN (100 mL, 3mM solution with respect to catalyst) and a magnetic stir bar. A 8.73 M CH_3COOH solution in CH_3CN was added (48 mmol, 500 mol%)

and the mixture was placed on an ice bath and stirred. The necessary amount of a 1.5 M H₂O₂ solution (diluted from a 35% H₂O₂ aqueous solution, 3.4 equiv for (+)-sclareolide, 2 equiv for *trans*-androsterone acetate) was delivered by syringe pump over 17 min at 0 °C. After syringe pump addition, the solution was stirred for 10 min at 0 °C. A second addition was performed according to the aforementioned iterative addition protocol. When the catalysis was finished, the iron complex was removed by passing the solution through a short path of silica followed by elution with 2 mL of AcOEt. Solvent was removed under reduced pressure and the resulting residue was purified by flash chromatography on silica gel (see procedure for product isolation for details).

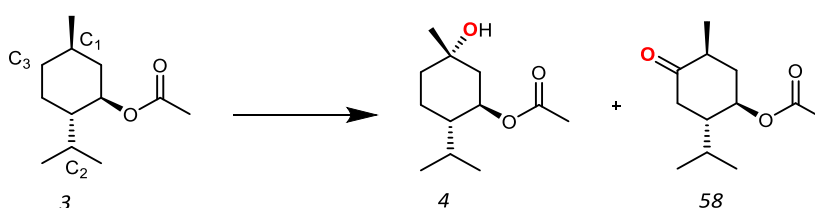
IV.4.7 PROCEDURE FOR PRODUCT ISOLATION

Isolated products were obtained following the procedure described below.⁴⁶

A 25 mL round bottom flask was charged with: catalyst (12 μmol, 3 mol%), alkane (0.4 mmol, 1 equiv), CH₃CN (8 mL) and a magnetic stir bar. A 1.74 M CH₃COOH solution in CH₃CN was added (2 mmol, 500 mol%) and the mixture was placed on an ice bath and stirred. The necessary amount of a 1.5 M H₂O₂ solution (diluted from a 35% H₂O₂ aqueous solution; 2 equiv for (-)-menthyl acetate, 2.8 equiv for (+)-sclareolide) was delivered by syringe pump over 17 min at 0 °C. After syringe pump addition, the solution was stirred for 10 min at 0 °C. A second addition was performed according to the abovementioned iterative addition protocol. When the catalysis was finished, the iron complex was removed by passing the solution through a short path of silica followed by elution with 2 mL of AcOEt. Solvent was removed under reduced pressure and the resulting residue was purified by flash chromatography on silica gel. Purity of obtained products was checked by ¹H-NMR and GC, and yields corrected based on this results.

A-1 was used for the isolation of all products, except for alcohol **88**. In the latter case **A-2** was employed, and only one addition of reagents was required.

(-)-Menthyl acetate (3):

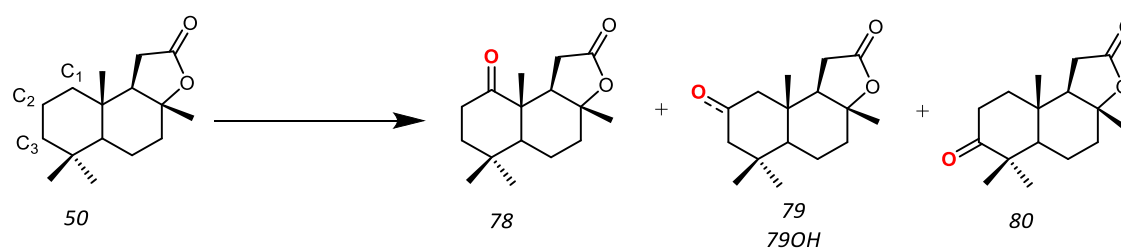


Scheme IV.1. Catalytic oxidation of 3.

4: Purification by flash chromatography over silica eluted with hexane:ethyl acetate (2:1). $^1\text{H-NMR}$ (400 MHz, CDCl_3 , 300 K) δ , ppm: 0.81 (d, $J = 7.0$ Hz, 3H), 0.92 (d, $J = 7.0$ Hz, 3H), 1.24 (s, 3H), 1.32-1.55 (m, 5H), 1.65-1.71 (m, 1H), 1.85-1.93 (m, 1H), 2.03 (s, 3H), 2.00-2.07 (m, 1H), 4.96-5.03 (m, 1H). In agreement with that reported in the literature.^{43,46}

58: Purification by flash chromatography over silica eluted with hexane:ethyl acetate (5:1). $^1\text{H-NMR}$ (400 MHz, CDCl_3 , 300 K) δ , ppm: 0.83 (d, $J = 6.8$ Hz, 3H), 0.89 (d, $J = 6.7$ Hz, 3H), 1.03 (d, $J = 6.6$ Hz, 3H), 1.36-1.46 (m, 1H), 1.89-1.98 (m, 2H), 2.08 (s, 3H), 2.12-2.19 (m, 1H), 2.31-2.37 (m, 2H), 2.47-2.57 (m, 1H), 5.05-5.11 (m, 1H). In agreement with that reported in the literature.⁴⁶

(+)-Sclareolide (50):



Scheme IV.2. Catalytic oxidation of 50.

78: Purification by flash chromatography over silica eluted with hexane:diethyl ether (1:1). $^1\text{H-NMR}$ (400 MHz, CDCl_3 , 300 K) δ , ppm: 1.02 (s, 3H), 1.06 (s, 3H), 1.19 (s, 3H), 1.35 (s, 3H), 1.49-1.54 (m, 1H), 1.58 (dd, $J = 13.2, 3.1$ Hz, 1H), 1.63-1.66 (m, 1H), 1.69 (dd, $J = 9.2, 5.0$ Hz, 1H), 1.81-1.87 (m, 1H), 1.88-1.93 (m, 1H), 2.09 (dd, $J = 11.1, 2.7$ Hz, 1H), 2.15 (dd, $J = 14.2, 6.6$ Hz, 1H), 2.29 (ddd, $J = 15.7, 8.4, 5.0$ Hz, 1H), 2.54 (dd, $J = 17.0, 14.2$ Hz, 1H), 2.68 (ddd, $J = 15.7, 9.2, 5.1$ Hz, 1H), 2.97 (dd, $J = 17.0, 6.5$ Hz, 1H). In agreement with that reported in the literature.⁶²

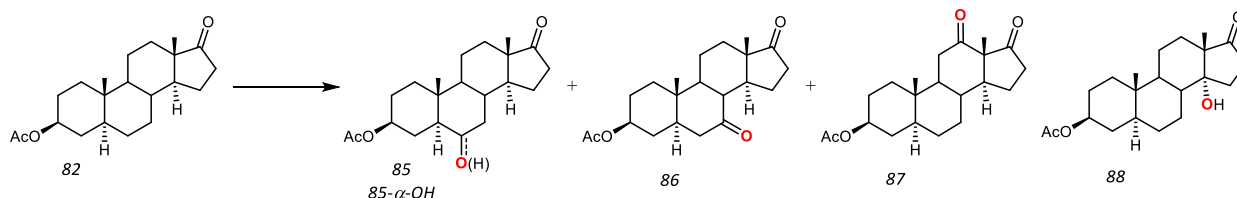
79: Purification by flash chromatography over silica eluted with hexane:diethyl ether (1:1.5). $^1\text{H-NMR}$ (400 MHz, CDCl_3 , 300 K) δ , ppm: 0.93 (s, 6H), 1.09 (s, 3H), 1.36 (s, 3H), 1.44-1.85 (m, 3H), 1.98-2.06 (m, 1H), 2.11-2.32 (m, 7H), 2.41-2.48 (m, 1H). In agreement with that reported in the literature.⁴³

79OH: Purification by flash chromatography over silica eluted with hexane:diethyl ether (1:2.5). $^1\text{H-NMR}$ (400 MHz, CDCl_3 , 300 K) δ , ppm: 0.89 (s, 3H), 0.96 (s, 3H), 0.97 (s,

3H), 1.10-1.15 (m, 1H), 1.34 (d, $J = 0.92$ Hz, 3H), 1.35-1.39 (m, 1H), 1.40-1.43 (m, 1H), 1.52-1.58 (m, 1H), 1.67-1.74 (td, $J = 12.1, 3.5$ Hz, 1H), 1.81-1.83 (m, 1H), 1.84-1.87 (m, 1H), 1.89-1.93 (m, 1H), 2.01 (dd, $J = 14.8, 6.5$ Hz, 1H), 2.10 (dt, $J = 11.8, 3.3$ Hz, 1H), 2.27 (dd, $J = 16.2, 6.5$ Hz, 1H), 2.45 (dd, $J = 16.2, 14.7$ Hz, 1H), 3.97-4.02 (m, 1H). In agreement with that reported in the literature.⁶⁴

80: Purification by flash chromatography over silica eluted with hexane:diethyl ether (1:2). ¹H-NMR (400 MHz, CDCl₃, 300 K) δ , ppm: 1.03 (s, 3H), 1.07 (s, 3H), 1.13 (s, 3H), 1.39 (s, 3H), 1.53-1.65 (m, 3H), 1.70-1.78 (m, 2H), 1.82-1.87 (m, 1H), 2.01 (dd, $J = 14.7, 6.5$ Hz, 1H), 2.14 (dt, $J = 11.6, 3.0$ Hz, 1H), 2.29 (ddd, $J = 16.2, 6.5, 0.4$ Hz, 1H), 2.40-2.63 (m, 3H). In agreement with that reported in the literature.⁴³

trans-androsterone acetate (20):



Scheme IV.3. Catalytic oxidation of **82**.

85: Purification by flash chromatography over silica eluted with hexane:ethyl acetate (2:1). ¹H-NMR (400 MHz, CDCl₃, 300 K) δ , ppm: 0.80 (s, 3H), 0.88 (s, 3H), 1.26-1.39 (m, 6H), 1.49-1.62 (m, 4H), 1.78-1.97 (m, 6H), 2.03 (s, 3H), 2.08-2.14 (m, 1H), 2.31 (dd, $J = 12.6, 2.9$ Hz, 1H), 2.43-2.47 (m, 2H), 4.63-4.71 (m, 1H). ¹³C-NMR (100 MHz, CDCl₃, 300 K) δ , ppm: 13.1, 13.8, 20.7, 21.3, 21.6, 26.1, 26.8, 31.1, 35.6, 36.4, 37.4, 40.9, 45.4, 48.1, 51.6, 53.8, 56.5, 72.6, 170.6, 209.3, 219.7. HRMS (ESI-TOF, $[M + Na]^+$): m/z calcd for C₂₁H₃₀O₄Na 369.2036, found 369.2012. In agreement with that reported in the literature.⁶⁵

85- α -OH: Purification by flash chromatography over silica eluted with hexane:ethyl acetate (1:1). ¹H-NMR (400 MHz, CDCl₃, 300 K) δ , ppm: 0.73-0.81 (m, 1H), 0.86 (s, 6H), 0.91-1.02 (m, 1H), 1.08-1.14 (m, 2H), 1.25-1.38 (m, 4H), 1.50-1.56 (m, 2H), 1.63-1.70 (m, 2H), 1.74 (dt, $J = 13.3, 3.7$ Hz, 1H), 1.80-1.86 (m, 2H), 1.96-1.99 (m, 1H), 2.01 (s, 3H), 2.10-2.16 (m, 2H), 2.22-2.26 (m, 1H), 2.46 (dd, $J = 19.4, 8.3$ Hz, 1H), 3.45 (td, $J = 10.8, 4.6$ Hz, 1H), 4.64-4.72 (m, 1H). ¹³C-NMR (100 MHz, CDCl₃, 300 K) δ , ppm: 13.3, 13.8, 20.4, 21.4, 21.8, 27.1, 28.3, 31.4, 33.9, 35.8, 36.4, 37.0, 40.4, 47.8, 51.1, 51.6, 53.7, 69.2,

73.3, 170.6, 220.8. HRMS (ESI-TOF, $[M + Na]^+$): m/z calcd for $C_{21}H_{30}O_4Na$ 371.2186, found 371.2186

In order to determine the correct configuration of the alcohol, this product was acetylated using the same conditions described for the synthesis of *trans*-androsterone acetate (**20**) (*vide supra*).

85- α -AcO: 1H -NMR (400 MHz, $CDCl_3$, 300 K) δ , ppm: 0.75-0.81 (m, 1H), 0.84 (s, 3H), 0.90 (s, 3H), 0.96-1.02 (m, 1H), 1.07-1.15 (m, 1H), 1.23-1.37 (m, 6H), 1.48-1.56 (m, 2H), 1.66-1.72 (m, 1H), 1.73-1.75 (m, 1H), 1.78-1.83 (m, 2H), 1.87-1.92 (m, 2H), 2.01 (s, 3H), 2.03 (s, 3H), 2.10-2.16 (m, 2H), 2.45 (dd, $J = 19.3, 8.6$ Hz, 1H), 4.62-4.71 (m, 2H). ^{13}C -NMR (100 MHz, $CDCl_3$, 300 K) δ , ppm: 13.2, 13.8, 20.3, 21.3, 21.4, 21.7, 27.1, 28.3, 31.3, 33.7, 35.7, 36.5, 36.7, 36.8, 47.7, 48.5, 51.1, 53.6, 71.9, 72.9, 170.6, 170.9, 220.6. In agreement with that reported in the literature.^{66,67}

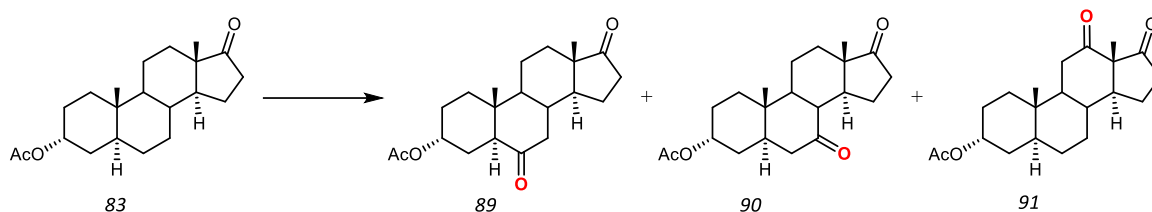
86: Purification by flash chromatography over silica eluted with hexane:ethyl acetate 2.5:1. 1H -NMR (400 MHz, $CDCl_3$, 300 K) δ , ppm: 0.87 (s, 3H), 1.05-1.13 (m, 1H), 1.12 (s, 3H), 1.17-1.22 (m, 1H), 1.46-1.77 (m, 9H), 1.79-1.84 (m, 2H), 1.89-1.93 (m, 1H), 2.03 (s, 3H), 2.08-2.20 (m, 2H), 2.34-2.53 (m, 3H), 2.58-2.65 (m, 1H), 4.64-4.72 (m, 1H). ^{13}C -NMR (100 MHz, $CDCl_3$, 300 K) δ , ppm: 11.7, 13.9, 21.2, 21.3, 22.9, 27.0, 30.7, 33.8, 35.6, 35.8, 36.0, 44.6, 45.7, 46.1, 47.4, 49.0, 55.1, 72.5, 170.5, 210.4, 220.2. HRMS (ESI-TOF, $[M + Na]^+$): m/z calcd for $C_{21}H_{30}O_4Na$ 369.2036, found 369.2013. In agreement with that reported in the literature.⁶⁸

87: Purification by flash chromatography over silica eluted with hexane:ethyl acetate 1.5:1. 1H -NMR (400 MHz, $CDCl_3$, 300 K) δ , ppm: 0.93 (s, 3H), 1.00-1.08 (m, 2H), 1.20 (s, 3H), 1.20-1.27 (m, 3H), 1.31-1.38 (m, 2H), 1.40-1.50 (m, 2H), 1.54-1.60 (m, 1H), 1.62-1.1.70 (m, 2H), 1.72-1.85 (m, 2H), 1.87-1.93 (m, 2H), 2.03 (s, 3H), 2.12-2.21 (m, 1H), 2.28-2.33 (m, 1H), 2.39-2.48 (m, 2H), 4.64-4.73 (m, 1H). ^{13}C -NMR (100 MHz, $CDCl_3$, 300 K) δ , ppm: 11.8, 14.6, 21.0, 21.4, 27.2, 28.0, 30.1, 33.7, 34.2, 36.2, 36.3, 36.8, 38.4, 44.4, 51.9, 55.4, 57.8, 73.0, 170.6, 207.0, 212.1. HRMS (ESI-TOF, $[M + Na]^+$): m/z calcd for $C_{21}H_{30}O_4Na$ 369.2036, found 369.2017.

88: Purification by flash chromatography over silica eluted with hexane:ethyl acetate 2:1. 1H -NMR (400 MHz, $CDCl_3$, 300 K) δ , ppm: 0.87 (s, 3H), 0.99 (s, 3H), 1.02-1.12

(m, 1H), 1.20-1.43 (m, 8H), 1.52-1.57 (m, 2H), 1.60-1.65 (m, 4H), 1.73-1.78 (m, 2H), 1.87-1.90 (m, 2H), 2.02 (s, 3H), 2.30-2.43 (m, 2H), 4.64-4.73 (m, 1H). ^{13}C -NMR (100 MHz, CDCl_3 , 300 K) δ , ppm: 12.1, 18.0, 19.2, 21.4, 24.8, 25.3, 27.4, 28.0, 30.1, 33.1, 33.9, 35.7, 36.8, 37.7, 44.3, 47.3, 52.6, 73.4, 81.2, 170.7, 218.8 HRMS (ESI-TOF, $[\text{M} + \text{Na}]^+$): m/z calcd for $\text{C}_{21}\text{H}_{30}\text{O}_4\text{Na}$ 371.2186, found 371.2172.

cis-androsterone acetate (83)



Scheme IV.4. Catalytic oxidation of 85.

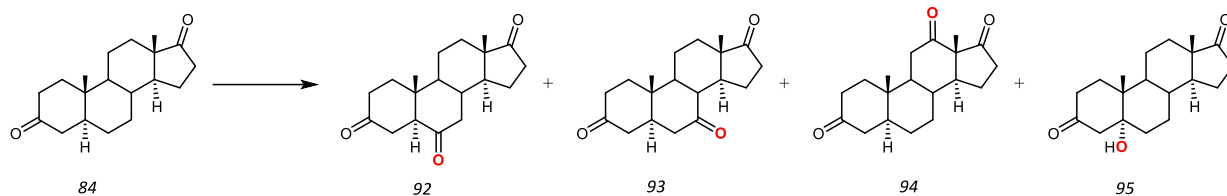
89: Purification by flash chromatography over silica eluted with hexane:ethyl acetate 2:1. ^1H -NMR (300 MHz, CDCl_3 , 300 K) δ , ppm: 0.79 (s, 3H), 0.89 (s, 3H), 1.26-1.45 (m, 4H), 1.52-1.60 (m, 5H), 1.72-1.83 (m, 4H), 1.87-1.94 (m, 2H), 2.01 (s, 3H), 2.09-2.15 (m, 2H), 2.43-2.52 (m, 2H), 2.59-2.63 (m, 1H), 5.12-5.14 (m, 1H). ^{13}C -NMR (75 MHz, CDCl_3 , 300 K) δ , ppm: 12.4, 13.8, 20.3, 21.4, 21.6, 25.0, 25.2, 31.1, 32.3, 35.6, 37.4, 41.2, 45.5, 48.1, 51.7, 52.7, 53.8, 68.6, 170.2, 210.8, 219.8. HRMS (ESI-TOF, $[\text{M} + \text{Na}]^+$): m/z calcd for $\text{C}_{21}\text{H}_{30}\text{O}_4\text{Na}$ 369.2036, found 369.2023

90: Purification by flash chromatography over silica eluted with hexane:ethyl acetate 3:1. ^1H -NMR (300 MHz, CDCl_3 , 300 K) δ , ppm: 0.87 (s, 3H), 1.09 (s, 3H), 1.20-1.37 (m, 4H), 1.43-1.63 (m, 6H), 1.68-1.85 (m, 5H), 1.87-1.98 (m, 1H), 2.05 (s, 3H), 2.07-2.32 (m, 2H), 2.40-2.65 (m, 2H), 5.04-5.06 (m, 1H). ^{13}C -NMR (75 MHz, CDCl_3 , 300 K) δ , ppm: 10.9, 13.9, 20.6, 21.4, 22.8, 25.8, 30.7, 32.6, 32.9, 35.6, 36.4, 42.1, 44.6, 45.6, 47.4, 49.2, 55.8, 69.1, 170.5, 210.9, 220.3. HRMS (ESI-TOF, $[\text{M} + \text{Na}]^+$): m/z calcd for $\text{C}_{21}\text{H}_{30}\text{O}_4\text{Na}$ 369.2036, found 369.2029.

91: Purification by flash chromatography over silica eluted with hexane:ethyl acetate 1:1. ^1H -NMR (300 MHz, CDCl_3 , 300 K) δ , ppm: 0.90 (s, 3H), 1.22 (s, 3H), 1.23-1.43 (m, 5H), 1.48-1.59 (m, 3H), 1.60-1.83 (m, 6H), 1.90-1.96 (m, 2H), 2.06 (s, 3H), 2.12-2.25 (m, 1H), 2.31-2.43 (m, 3H), 5.02 (s, 1H). ^{13}C -NMR (75 MHz, CDCl_3 , 300 K) δ , ppm: 11.0, 14.6, 20.9, 21.5, 25.9, 27.8, 30.1, 32.4, 32.6, 34.2, 36.5, 36.7, 38.1, 39.8, 52.1, 55.4, 57.8,

69.5, 170.6, 207.2, 212.2. HRMS (ESI-TOF, $[M + Na]^+$): m/z calcd for $C_{21}H_{30}O_4Na$ 369.2036, found 369.2027.

3,17-androstenedione (84)



Scheme IV.5. Catalytic oxidation of 84.

92: Purification by flash chromatography over silica eluted with hexane:ethyl acetate 1:5. 1H -NMR (300 MHz, $CDCl_3$, 300 K) δ , ppm: 0.92 (s, 3H), 1.00 (s, 3H), 1.37-1.68 (m, 8H), 1.81-1.96 (m, 3H), 2.07-2.17 (m, 4H), 2.32-2.60 (m, 5H). ^{13}C -NMR (75 MHz, $CDCl_3$, 300 K) δ , ppm: 12.6, 13.8, 20.9, 21.6, 31.1, 35.6, 36.9, 37.3, 37.4, 38.0, 41.2, 45.3, 48.1, 51.5, 53.5, 57.5, 208.1, 210.7, 219.5. HRMS (ESI-TOF, $[M + Na]^+$): m/z calcd for $C_{19}H_{26}O_4Na$ 325.1774, found 325.1763. In agreement with that reported in the literature.⁶⁹

93: Purification by flash chromatography over silica eluted with hexane:ethyl acetate 1:4. 1H -NMR (300 MHz, $CDCl_3$, 300 K) δ , ppm: 0.90 (s, 3H), 1.20-1.28 (m, 2H), 1.31 (s, 3H), 1.37-1.64 (m, 4H), 1.70-1.79 (m, 2H), 1.83-1.87 (m, 1H), 1.93-2.00 (m, 1H), 2.06-2.21 (m, 4H), 2.35-2.49 (m, 4H), 2.54-2.64 (m, 2H). ^{13}C -NMR (75 MHz, $CDCl_3$, 300 K) δ , ppm: 11.0, 13.9, 21.6, 22.8, 30.6, 35.6, 36.1, 36.9, 37.5, 44.0, 44.5, 45.5, 47.3, 47.4, 48.7, 54.3, 209.2, 209.4, 219.8. HRMS (ESI-TOF, $[M + Na]^+$): m/z calcd for $C_{19}H_{26}O_4Na$ 325.1774, found 325.1758.

94: Purification by flash chromatography over silica eluted with hexane:ethyl acetate 1:5. 1H -NMR (300 MHz, $CDCl_3$, 300 K) δ , ppm: 1.11 (s, 3H), 1.23 (s, 3H), 1.32-1.53 (m, 4H), 1.57-1.72 (m, 2H), 1.76-1.88 (m, 2H), 1.95-2.10 (m, 3H), 2.15-2.29 (m, 3H), 2.35-2.48 (m, 5H), 2.55-2.59 (m, 1H). ^{13}C -NMR (75 MHz, $CDCl_3$, 300 K) δ , ppm: 11.1, 14.6, 21.0, 28.3, 29.8, 34.1, 36.3, 36.7, 37.8, 37.8, 38.5, 44.3, 46.1, 51.7, 54.9, 57.8, 206.4, 210.5, 211.8. HRMS (ESI-TOF, $[M + Na]^+$): m/z calcd for $C_{19}H_{26}O_4Na$ 325.1774, found 325.1759.

95: Purification by flash chromatography over silica eluted with hexane/ethyl acetate 1/3. 1H -NMR (300 MHz, $CDCl_3$, 300 K) δ , ppm: 0.89 (s, 3H), 1.20 (s, 3H), 1.24-1.42 (m, 5H), 1.49-1.76 (m, 5H), 1.82-2.01 (m, 4H), 2.03-2.15 (m, 2H), 2.37-2.50 (m, 3H), 2.72

(d, $J = 15.2$ Hz, 1H). ^{13}C -NMR (75 MHz, CDCl_3 , 300 K) δ , ppm: 13.8, 15.7, 20.7, 21.8, 25.1, 30.3, 31.5, 32.7, 34.3, 34.4, 35.8, 37.8, 39.3, 45.9, 47.8, 51.0, 52.0, 210.7, 220.9. HRMS (ESI-TOF, $[\text{M} + \text{Na}]^+$): m/z calcd for $\text{C}_{19}\text{H}_{28}\text{O}_3\text{Na}$ 327.1931, found 327.1919. In agreement with that reported in the literature.⁷⁰

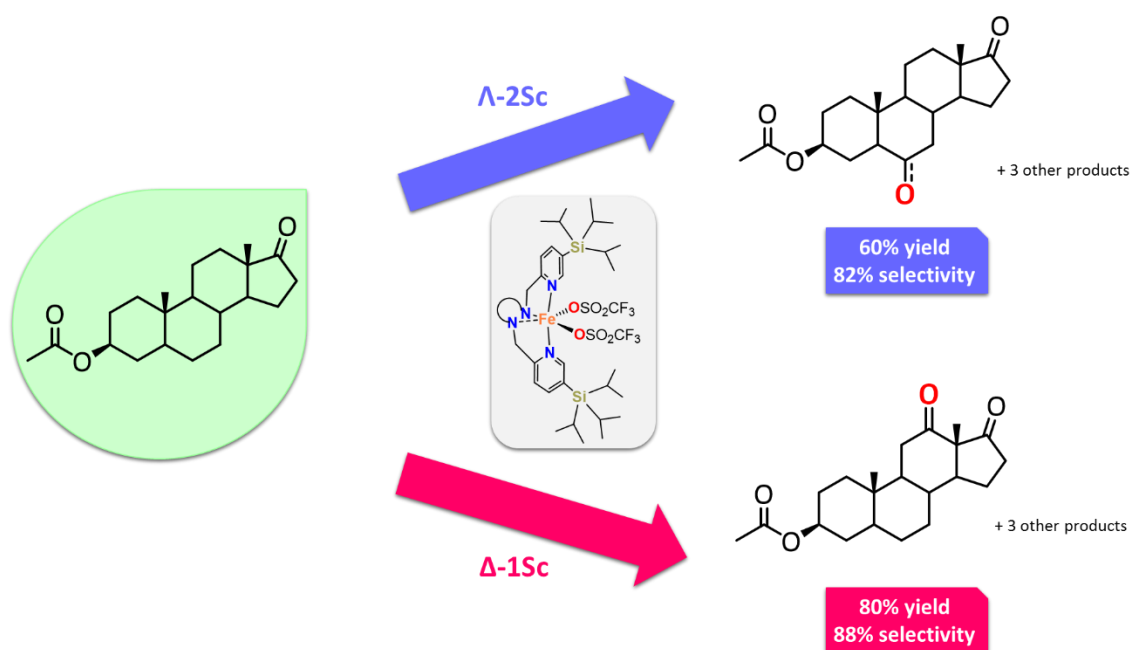
IV.5 REFERENCES

- (1) Gutekunst, W. R.; Baran, P. S. *Chem. Soc. Rev.* **2011**, *40*, 1976.
- (2) Newhouse, T.; Baran, P. S. *Angew. Chem. Int. Ed.* **2011**, *50*, 3362.
- (3) McMurray, L.; O'Hara, F.; Gaunt, M. J. *Chem. Soc. Rev.* **2011**, *40*, 1885.
- (4) Che, C.-M.; Lo, V. K.-Y.; Zhou, C.-Y.; Huang, J.-S. *Chem. Soc. Rev.* **2011**, *40*, 1950.
- (5) Dyker, G. *Handbook of C-H Transformations*; Wiley-VCH: Weinheim, 2005; Vol. 1-2.
- (6) Bordeaux, M.; Galarneau, A.; Drone, J. *Angew. Chemie Int. Ed.* **2012**, *51*, 10712.
- (7) Lloret, J.; Company, A.; Gómez, L.; Costas, M.; (Ed. Pérez, P. J.). *Alkane C-H Activation by Single-Site Metal Catalysis*; Springer: Netherlands, Dordrecht, **2013**; Vol. 38.
- (8) Kamijo, S. *J. Synth. Org. Chem. Japan* **2012**, *70*, 996.
- (9) Fokin, A. A.; Schreiner, P. R. *Adv. Synth. Catal.* **2003**, *345*, 1035.
- (10) Ishii, Y.; Sakaguchi, S.; Iwahama, T. *Adv. Synth. Catal.* **2001**, *343*, 393.
- (11) Shul'pin, G. B. *Org. Biomol. Chem.* **2010**, *8*, 4217.
- (12) Recupero, F.; Punta, C. *Chem. Rev.* **2007**, *107*, 3800.
- (13) Cusack, K. P.; Koolman, H. F.; Lange, U. E. W.; Peltier, H. M.; Piel, I.; Vasudevan, A. *Bioorg. Med. Chem. Lett.* **2013**, *23*, 5471.
- (14) Fasan, R. *ACS Catal.* **2012**, *2*, 647.
- (15) Curci, R.; d'Accolti, L.; Fusco, C. *Acc. Chem. Res.* **2006**, *39*, 1.
- (16) Mello, R.; Fiorentino, M.; Fusco, C.; Curci, R. *J. Am. Chem. Soc.* **1989**, *111*, 6749.
- (17) Kasuya, S.; Kamijo, S.; Inoue, M. *Org. Lett.* **2009**, *11*, 3630.
- (18) Murray, R. W.; Jeyaraman, R.; Mohan, L. *J. Am. Chem. Soc.* **1986**, *108*, 2470.
- (19) Sun, C.-L.; Li, B.-J.; Shi, Z.-J. *Chem. Rev.* **2011**, *111*, 1293.
- (20) Liu, L.-X. *Curr. Org. Chem.* **2010**, *14*, 1099.
- (21) Bauer, E. B. *Curr. Org. Chem.* **2008**, *12*, 1341.
- (22) Mayer, A. C.; Bolm, C.; (Ed. Plietker, B.); *Iron Catalysis in Organic Chemistry*. Wiley-VCH: Weinheim, 2008; pp. 73–92.

- (23) Costas, M. *Coord. Chem. Rev.* **2011**, *255*, 2912.
- (24) Lu, H.; Zhang, X. P. *Chem. Soc. Rev.* **2011**, *40*, 1899.
- (25) Meunier, B. *Chem. Rev.* **1992**, *92*, 1411.
- (26) Company, A.; Gómez, L.; Costas, M. S. P de Visser, D. K., Ed.; RSC: Cambridge, 2011.
- (27) Que Jr., L.; Tolman, W. B. *Nature* **2008**, *455*, 333.
- (28) Nizova, G. V.; Krebs, B.; Süß-Fink, G.; Schindler, S.; Westerheide, L.; Gonzalez Cuervo, L.; Shul'pin, G. B. *Tetrahedron* **2002**, *58*, 9231.
- (29) Romakh, V. B.; Therrien, B.; Süß-Fink, G.; Shul'pin, G. B. *Inorg. Chem.* **2007**, *46*, 3166.
- (30) Shul'pin, G. B.; Nizova, G. V.; Kozlov, Y. N.; Gonzalez Cuervo, L.; Süß-Fink, G. *Adv. Synth. Catal.* **2004**, *346*, 317.
- (31) Shul'pin, G. B.; Golfeto, C. C.; Süß-Fink, G.; Shul'pina, L. S.; Mandelli, D. *Tetrahedron Lett.* **2005**, *46*, 4563.
- (32) Nesterov, D. S.; Chygorin, E. N.; Kokozay, V. N.; Bon, V. V.; Boča, R.; Kozlov, Y. N.; Shul'pina, L. S.; Jezierska, J.; Ozarowski, A.; Pombeiro, A. J. L.; Shul'pin, G. B. *Inorg. Chem.* **2012**, *51*, 9110.
- (33) Walling, C. *Acc. Chem. Res.* **1975**, *8*, 125.
- (34) Walling, C. *Acc. Chem. Res.* **1998**, *31*, 155.
- (35) Sawyer, D. T.; Sobkowiak, A.; Matsushita, T. *Acc. Chem. Res.* **1996**, *29*, 409.
- (36) MacFaul, P. A.; Wayner, D. D. M.; Ingold, K. U. *Acc. Chem. Res.* **1998**, *31*, 159.
- (37) Enthaler, S.; Junge, K.; Beller, M. *Angew Chem. Int. Ed.* **2008**, *47*, 5.
- (38) Noyori, R.; Aoki, M.; Sato, K. *Chem. Commun.* **2003**, 1977.
- (39) Gormisky, P. E.; White, M. C. *J. Am. Chem. Soc.* **2013**, *135*, 14052.
- (40) Bigi, M. A.; Reed, S. A.; White, M. C. *J. Am. Chem. Soc.* **2012**, *134*, 9721.
- (41) Bigi, M. A.; Reed, S. A.; White, M. C. *Nat. Chem.* **2011**, *3*, 216.
- (42) Chen, M. S.; White, M. C. *Science*. **2007**, *318*, 783.
- (43) Chen, M. S.; White, M. C. *Science*. **2010**, *327*, 566.
- (44) Vermeulen, N. A.; Chen, M. S.; White, M. C. *Tetrahedron* **2009**, *65*, 3078.
- (45) Gómez, L.; Garcia-Bosch, I.; Company, A.; Benet-Buchholz, J.; Polo, A.; Sala, X.; Ribas, X.; Costas, M. *Angew. Chem. Int. Ed.* **2009**, *48*, 5720.
- (46) Gómez, L.; Canta, M.; Font, D.; Prat, I.; Ribas, X.; Costas, M. *J. Org. Chem.* **2013**, *78*, 1421.

- (47) Prat, I.; Gómez, L.; Canta, M.; Ribas, X.; Costas, M. *Chem. Eur. J.* **2013**, *19*, 1908.
- (48) Liu, P.; Liu, Y.; Wong, E.; Xiang, S.; Che, C.-M. *Chem. Sci* **2011**, *2*, 2187.
- (49) Costas, M.; Que Jr., L. *Angew Chem. Int. Ed.* **2002**, *41*, 2179.
- (50) Okuno, T.; Ito, S.; Ohba, S.; Nishida, Y. *J. Chem. Soc., Dalton Trans.* **1997**, 3547.
- (51) Clemente-Tejeda, D.; López-Moreno, A.; Bermejo, F. A. *Tetrahedron* **2012**, *68*, 9249.
- (52) White, M. C.; Doyle, A. G.; Jacobsen, E. N. *J. Am. Chem. Soc.* **2001**, *123*, 7194.
- (53) Mas-Balleste, R.; Que Jr., L. *J. Am. Chem. Soc.* **2007**, *129*, 15964.
- (54) Lyankin, O. Y.; Ottenbacher, R. V.; Byankov, K. P.; Talsi, E. P. *ACS Catal.* **2012**, *2*, 1196.
- (55) Shul'pin, G. B.; Kozlov, Y. N.; Shul'pina, L. S.; Petrovskiy, P. V. *Appl. Organomet. Chem.* **2010**, *24*, 464.
- (56) Shul'pin, G. B.; Kozlov, Y. N.; Shul'pina, L. S.; Kudinov, A. R.; Mandelli, D. *Inorg. Chem.* **2009**, *48*, 10480.
- (57) Shul'pin, G. B. *J. Mol. Catal. A Chem.* **2002**, *189*, 39.
- (58) Zhang, Y. Y.; Yang, L. *Expert Opin. Drug Metab. Toxicol.* **2009**, *5*, 621.
- (59) K. Monostory, Z. D. *Curr. Drug Metab.* **2011**, *12*, 154.
- (60) Salvador, J. A. R.; Silvestre, S. M.; Moreira, V. M. *Curr. Org. Chem* **2012**, *16*, 1243.
- (61) Kille, S.; Zilli, F. E.; Acevedo, J. P.; Reetz, M. T. *Nat. Chem.* **2011**, *3*, 738.
- (62) Cano, A.; Ramírez-Apan, M. T.; Delgado, G. J. *Braz. Chem. Soc.* **2011**, *22*, 1177.
- (63) Kim, C.; Dong, Y.; Que Jr., L. *J. Am. Chem. Soc.* **1997**, *119*, 3635.
- (64) Choudhary, M. I.; Musharraf, S. G.; Sami, A.; Atta ur, R. *Helv. Chim. Acta* **2004**, *87*, 2685.
- (65) Bazin, M.-A.; Kihel, L. El; Boulouard, M.; Bouët, V.; Rault, S. *Steroids* **2009**, *74*, 931.
- (66) Doller, D.; Gros, E. G. *Steroids* **1991**, *56*, 168.
- (67) Baldessari, A.; Bruttomesso, A. C.; Gros, E. G. *Helv. Chim. Acta* **1996**, *79*, 999.
- (68) Marwah, P.; Marwah, A.; Lardy, H. A. *Tetrahedron* **2003**, *59*, 2273.
- (69) Al-Awadi, S.; Afzal, M.; Oommen, S. *Steroids* **2005**, *70*, 327.
- (70) Boynton, J.; Hanson, J. R.; Hunter, A. C. *Phytochemistry* **1997**, *45*, 951.

A NEW FAMILY OF IRON CATALYSTS INCORPORATING BULKY SILYL GROUPS FOR
EFFICIENT AND REGIOSELECTIVE OXIDATION OF ALKANES



V.1 INTRODUCTION

The selective functionalization of aliphatic C—H groups stands as one of the main challenges for modern synthetic organic chemistry.^{1–4} Recent advances have been achieved in predictable and selective tertiary C—H group oxidations using non-heme iron catalysts and hydrogen peroxide as oxidant.^{5–7} Although secondary sites can be efficiently oxidized with iron-based catalysts (Figure V.1),^{8–10} the selective oxidation of methylenic sites in a predictable manner that is catalyst-dependent is still a non-resolved issue.

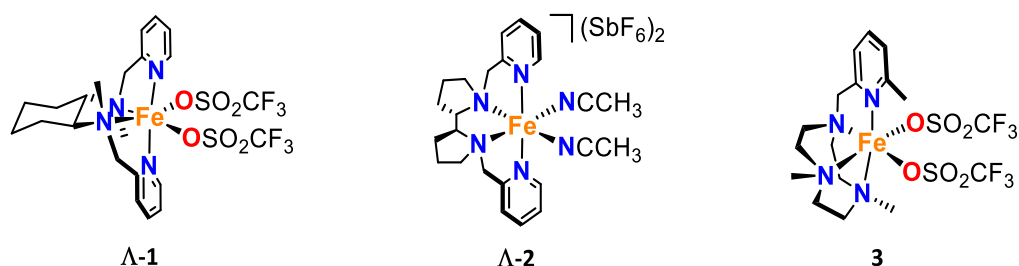


Figure V.1. Recently reported non-heme iron catalysts for the effective oxidation of methylenic sites.^{8–10}

Bioinspired by the exquisite selectivity exhibited by enzymes, catalysts have been developed by following the strategy of hindering the iron site by the use of bulky ligands.^{5,11} A very illustrative example reported by our group was the introduction of bulky pinene groups at the pyridine moieties to achieve remarkable regioselectivity in C—H group oxidation reactions (Figure V.2).⁶ In addition, tacn-based complex **3** also proved to exhibit a notable trend for preferentially oxidizing secondary over tertiary C—H bond, and this selectivity was traced to a sterically congested iron active site. Along the same track, very recently, White and coworkers reported an iron pdp-based catalyst modified with aryl-CF₃ moieties at the pyridine rings that restricted the approaching trajectories of the substrate at the surroundings of the metal center, thus offering enhanced selectivity toward the oxidation of methylenic sites (Figure V.2).¹²

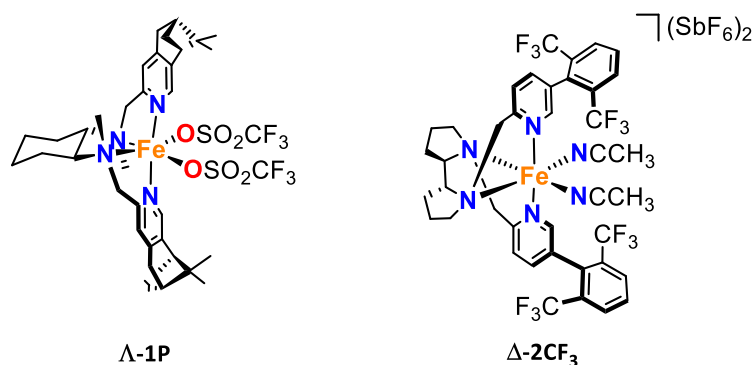


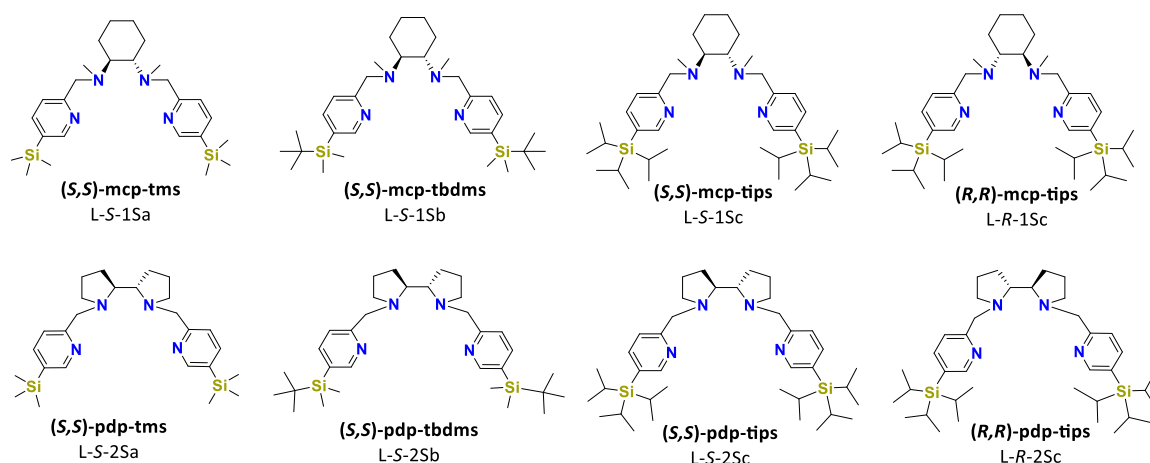
Figure V.2. Recently reported non-heme catalysts bearing bulky ligand architectures.^{6,12}

From these precedents, we sought to systematically study the steric influence of the ligand in the regioselectivity of C—H group oxidation reactions. In this work we present a new family of catalysts bearing bulky silyl-based groups at the 5th position of the pyridine rings, which present predictable selectivity toward the preferential oxidation of methylenic over tertiary sites.

V.2 RESULTS AND DISCUSSION

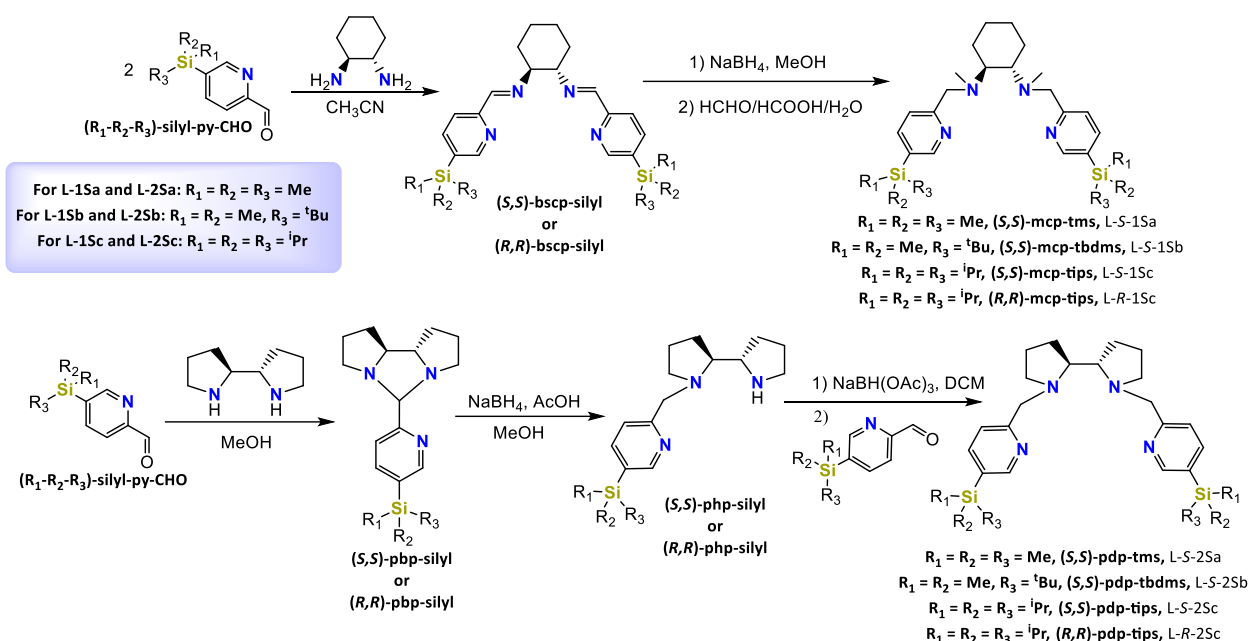
V.2.1 SYNTHESIS OF LIGANDS AND IRON COMPLEXES

A new family of tetradentate ligands (L-S-1Sa, L-S-1Sb, L-S-1Sc, L-R-1Sc, L-S-2Sa, L-S-2Sb, L-S-2Sc, and L-R-2Sc, Scheme V.1) that contain two aliphatic amino groups from the diamine backbone and two pyridines substituted with different silyl moieties at the 5th position was prepared. The introduction of the silyl groups allows for the systematic introduction of steric impediment at the proximity at the iron center, without perturbing catalyst stability. Following this strategy, related iron catalysts have been described to be more efficient and robust, mainly due to the protection at the catalytic center conferred by the bulky moieties in the pyridine groups.^{5,6,11} Moreover, we envisioned that the steric influence of the bulk in the proximity of the iron center would enable the selective oxidation of more exposed secondary sites in presence of weaker tertiary C—H bonds. From a practical point of view, the silyl derivatization of the catalysts offers a simple synthetic strategy to obtain modular scaffolds in order to systematically increase their bulkiness. Furthermore, in combination with different chiral diamine backbones, a whole family of iron complexes that will be used as catalysts in the oxidation of alkanes can be easily obtained.



Scheme V.1. Representation of the new family of silyl-derived ligands.

L-S-1Sa – L-R-1Sc were synthesized following a three-step synthetic method involving aldehyde-diamine condensation, hydrogenation, and permethylation with good yields (Scheme V.2). The addition of two equiv of 5-(trimethyl-silyl)-2-picolylaldehyde, 5-(*tert*-butyl-dimethyl-silyl)-2-picolylaldehyde, or 5-(triisopropyl-silyl)-2-picolylaldehyde ((R₁-R₂-R₃)-silyl-py-CHO) to a solution of chiral *trans*-1,2-diaminocyclohexane (1*S*,2*S* or 1*R*,2*R*) in acetonitrile afforded Schiff base ligands (*S,S*)-bscp-silyl and (*R,R*)-bscp-silyl. These Schiff base ligands were hydrogenated by treatment with NaBH₄ in methanol and subsequently reacted with HCHO/HCOOH/H₂O under reflux, which afforded methylated ligands (*S,S*)-mcp-tms, (*S,S*)-mcp-tbdms, (*S,S*)-mcp-tips and (*R,R*)-mcp-tips (L-S-1Sa, L-S-1Sb, L-S-1Sc, and L-R-1Sc, respectively; L stands for ligand, *S* and *R* refer to the chirality of the diamine backbone, 1 and 2 refer to mcp- and pdp-based ligands respectively, and Sa, Sb, and Sc describe the three different silyl-substituents at the ligand), which were purified by column chromatography.

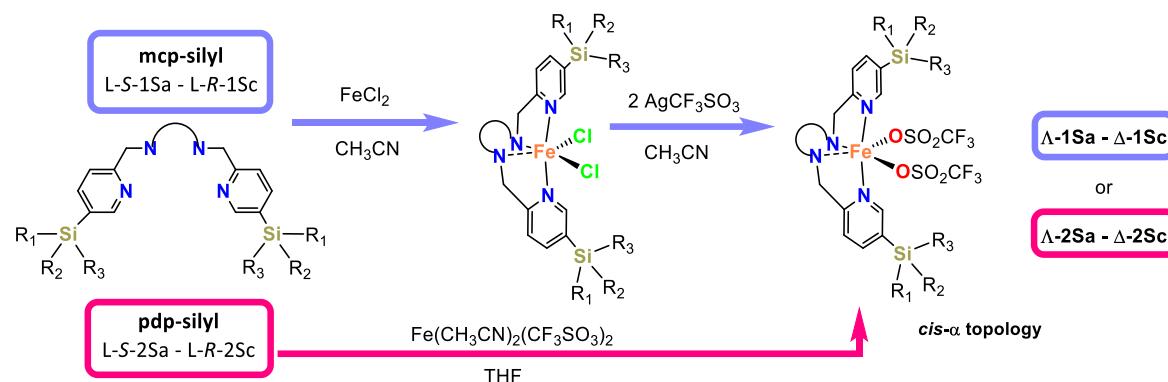


Scheme V.2. Synthesis of the silyl-based ligands employed in this work.

On the other hand, L-S-2Sa – L-R-2Sc were synthesized by reaction of 1 equiv of the corresponding $(R_1-R_2-R_3)$ -silyl-py-CHO with the appropriate chiral form of the diamine, (2*S*,2'*S*)-2,2'-bipyrrolidine or (2*R*,2'*R*)-2,2'-bipyrrolidine (Scheme V.2) in methanol, yielding (*S,S*)-pbp-silyl and (*R,R*)-pbp-silyl, respectively. These compounds were hydrogenated to afford (*S,S*)-php-silyl and (*R,R*)-php-silyl, respectively, by treatment with NaBH_4 and AcOH in methanol. After reaction with $\text{NaBH}(\text{OAc})_3$ in dichloromethane, a second equiv of $(R_1-R_2-R_3)$ -silyl-py-CHO was added, to yield the final ligands (*S,S*)-pdp-tms, (*S,S*)-pdp-tbdms, (*S,S*)-pdp-tips and (*R,R*)-pdp-tips (L-S-2Sa, L-S-2Sb, L-S-2Sc, and L-R-2Sc, respectively), which were purified by column chromatography.

In order to prepare the corresponding iron complexes in *cis-α* topology, which have proven to afford especially efficient oxidation catalysts,^{13–16} the mcp-based ligands L-S-1Sa – L-R-1Sc were submitted to a two-step route for the selective preparation of this isomer (Scheme V.3). Upon reaction of the tetradentate ligands L-S-1Sa – L-R-1Sc with FeCl_2 in acetonitrile, complexes $[\text{FeCl}_2(\text{L-S-1Sa})] - [\text{FeCl}_2(\text{L-R-1Sc})]$ (Cl-Λ-1Sa, Cl-Λ-1Sb, Cl-Λ-1Sc, and Cl-Δ-1Sc; Cl stands for chloride iron complex, Λ and Δ indicate the chirality at the metal center) were obtained. Subsequent addition of two equiv of AgOTf (OTf = trifluoromethanesulfonate anion) yielded the desired complexes $[\text{Fe}(\text{OTf})_2(\text{L-S-1Sa})] - [\text{Fe}(\text{OTf})_2(\text{L-R-1Sc})]$ (Λ-1Sa, Λ-1Sb, Λ-1Sc, and Δ-1Sc), which were obtained as crystalline

solids after diethyl ether diffusion. On the other hand, complexes $[\text{Fe}(\text{OTf})_2(\text{L-S-2Sa})]$ - $[\text{Fe}(\text{OTf})_2(\text{L-R-2Sc})]$ (Λ -**2Sa**, Λ -**2Sb**, Λ -**2Sc**, and Δ -**2Sc**) were obtained directly by reacting the corresponding pdp-based ligands with $\text{Fe}(\text{OTf})_2(\text{CH}_3\text{CN})_2$ as iron source in acetonitrile.^{6,17,18}



Scheme V.3. Preparation of complexes Λ -1Sa – Δ -2Sc.

V.2.2 CHARACTERIZATION OF COMPLEXES

Metal complexes have been characterized by elemental analysis, HRMS (ESI-TOF) spectrometry, $^1\text{H-NMR}$ spectroscopy and X-Ray diffraction (XRD) analysis.

V.2.2.1 Solid state structures

The solid state structure of complexes Λ -1Sa, Λ -1Sb, Λ -1Sc, Λ -2Sa, Λ -2Sb, and Λ -2Sc could be established by XDR analysis. Figure V.3 shows the structure diagrams of the complexes) and Table V.1 and Table V.2 (mcp-based and pdp-based complexes, respectively) gather selected bond lengths and angles for the six crystallographically determined structures.

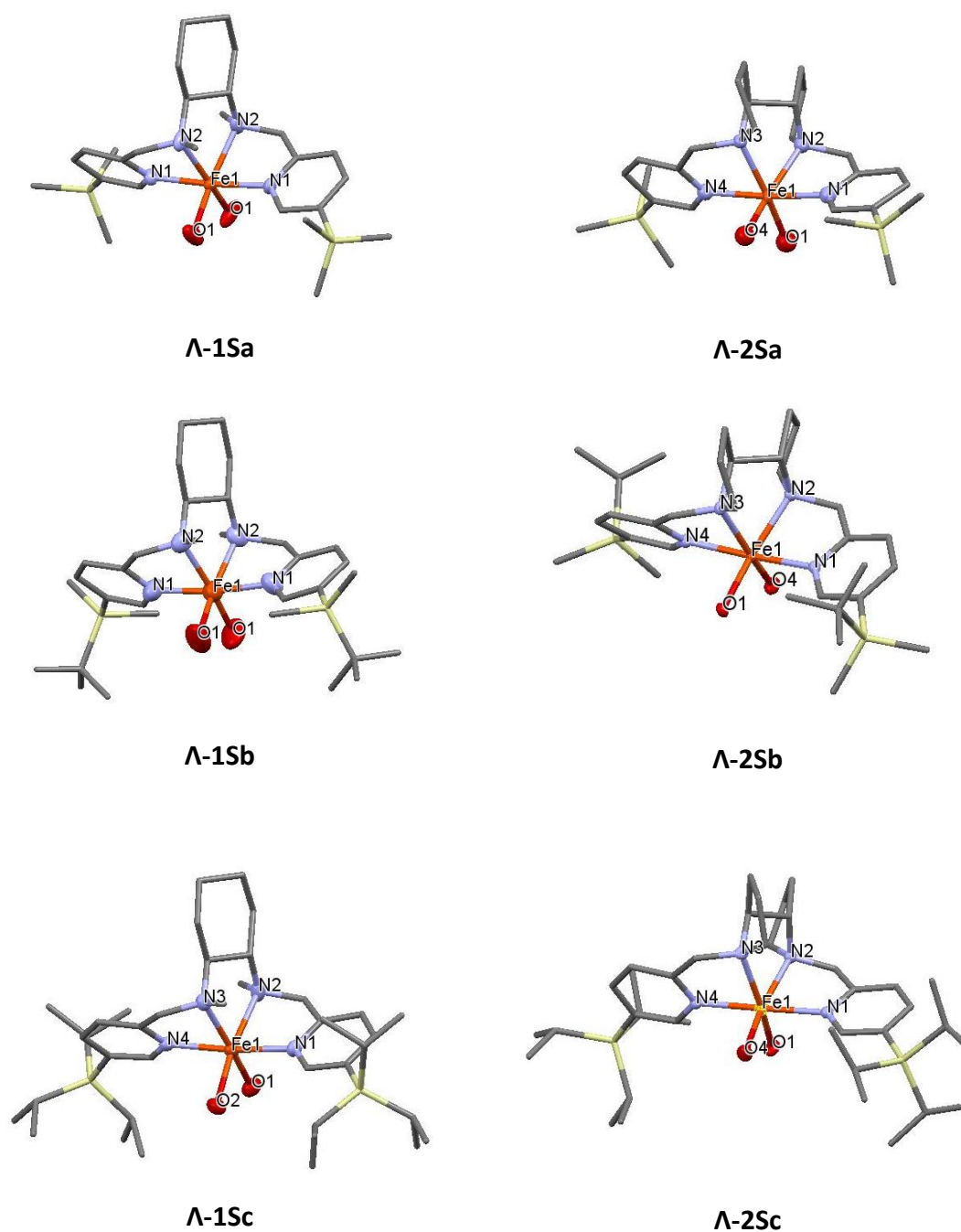


Figure V.3. X-Ray structures of Λ -1Sa, Λ -1Sb, Λ -1Sc, Λ -2Sa, Λ -2Sb, and Λ -2Sc. Hydrogen atoms, triflate moieties (except for the atom directly bound to the iron center), and solvents of crystallization are omitted for clarity.

Table V.1. Selected bond lengths [Å] and angles [°] for mcp-based complexes **Λ-1Sa**, **Λ-1Sb**, and **Λ-1Sc**.

Λ-1Sa		Λ-1Sb		Λ-1Sc	
Fe-O(1)	2.122(5)	Fe-O(1)	2.084(8)	Fe-O(1)	2.157(5)
Fe-O(1)	2.122(5)	Fe-O(1)	2.084(8)	Fe-O(2)	2.123(5)
Fe-N(1)	2.152(4)	Fe-N(1)	2.138(9)	Fe-N(1)	2.154(5)
Fe-N(1)	2.152(4)	Fe-N(1)	2.138(9)	Fe-N(4)	2.171(5)
Fe-N(2)	2.226(5)	Fe-N(2)	2.222(9)	Fe-N(2)	2.223(6)
Fe-N(2)	2.226(5)	Fe-N(2)	2.222(9)	Fe-N(3)	2.247(6)
O(1)-Fe-O(1)	100.5(4)	O(1)-Fe-O(1)	92.2(6)	O(2)-Fe-O(1)	89.2(2)
O(1)-Fe-N(1)	93.70(18)	O(1)-Fe-N(1)	91.1(4)	O(2)-Fe-N(1)	92.2(2)
O(1)-Fe-N(1)	89.12(18)	O(1)-Fe-N(1)	94.6(3)	O(2)-Fe-N(4)	90.3(2)
O(1)-Fe-N(1)	89.12(18)	O(1)-Fe-N(1)	94.6(3)	N(1)-Fe-O(1)	92.9(2)
O(1)-Fe-N(1)	93.70(18)	O(1)-Fe-N(1)	91.1(4)	N(1)-Fe-N(4)	172.1(2)
N(1)-Fe-N(1)	175.6(3)	N(1)-Fe-N(1)	171.8(5)	O(1)-Fe-N(4)	94.6(2)
O(1)-Fe-N(2)	91.3(2)	O(1)-Fe-N(2)	95.1(4)	O(1)-Fe-N(2)	92.2(2)
O(1)-Fe-N(2)	163.33(19)	O(1)-Fe-N(2)	167.0(4)	O(2)-Fe-N(2)	170.0(2)
N(1)-Fe-N(2)	78.33(17)	N(1)-Fe-N(2)	96.0(3)	N(1)-Fe-N(2)	77.9(2)
N(1)-Fe-N(2)	98.24(18)	N(1)-Fe-N(2)	77.7(3)	N(4)-Fe-N(2)	99.4(2)
O(1)-Fe-N(2)	163.32(19)	O(1)-Fe-N(2)	167.0(4)	O(1)-Fe-N(3)	167.11(19)
O(1)-Fe-N(2)	91.3(2)	O(1)-Fe-N(2)	95.1(4)	O(2)-Fe-N(3)	99.76(19)
N(1)-Fe-N(2)	98.24(18)	N(1)-Fe-N(2)	77.7(3)	N(1)-Fe-N(3)	96.0(2)
N(1)-Fe-N(2)	78.33(17)	N(1)-Fe-N(2)	96.0(3)	N(4)-Fe-N(3)	76.27(19)
N(2)-Fe-N(2)	79.8(3)	N(2)-Fe-N(2)	79.8(5)	N(2)-Fe-N(3)	80.6(2)

The experimental details of the crystal structure determination of complexes are collected in Table V.8 and Table V.9 (section V.4.5). All complexes exhibit C_2 pseudo-symmetry about an axis that passes through the metal center and bisects the aliphatic diamine of the ligand, what ensures that the complex has two equivalent parts. Complexes **Λ-1Sa**, **Λ-1Sb**, **Λ-2Sa**, **Λ-2Sb**, and **Λ-2Sc** are neutral and the Fe^{II} coordination geometry is distorted octahedral. Four coordination sites are occupied by the N atoms of the ligand and the coordination environment is completed by two triflate dicationic ligands. On the other hand, **Λ-1Sc** crystalizes as a complex with two water molecules coordinated to the metal center and two triflate as counterions. X-ray analyses reveal that

all the complexes adopt a *cis-α* geometric topology. The two nitrogen atoms of the pyridine rings are mutually in *trans* configuration, while the two aliphatic nitrogen atoms are mutually in *cis*. Fe-N distances measured in all complexes are characteristic of high-spin Fe^{II} complexes (~ 2.1 - 2.2 Å).^{19,20}

Table V.2. Selected bond lengths [Å] and angles [°] for pdp-based complexes **Λ-2Sa**, **Λ-2Sb**, and **Λ-2Sc**.

Λ-2Sa		Λ-2Sb		Λ-2Sc	
Fe-O(1)	2.121(17)	Fe-O(1)	2.1322(15)	Fe-O(4)	2.100(3)
Fe-O(4)	2.095(16)	Fe-O(4)	2.0958(15)	Fe-O(1)	2.123(3)
Fe-N(1)	2.168(19)	Fe-N(1)	2.1544(17)	Fe-N(1)	2.145(3)
Fe-N(4)	2.19(2)	Fe-N(4)	2.1758(17)	Fe-N(4)	2.141(3)
Fe-N(3)	2.215(18)	Fe-N(3)	2.1959(17)	Fe-N(3)	2.204(3)
Fe-N(2)	2.24(2)	Fe-N(2)	2.2054(17)	Fe-N(2)	2.207(3)
O(4)-Fe-O(1)	100.4(7)	O(4)-Fe-O(1)	105.50(6)	O(4)-Fe-O(1)	101.02(11)
O(1)-Fe-N(1)	94.4(7)	O(1)-Fe-N(1)	88.29(6)	O(1)-Fe-N(1)	91.17(11)
O(4)-Fe-N(1)	88.2(7)	O(4)-Fe-N(1)	95.52(6)	O(4)-Fe-N(1)	90.80(11)
O(1)-Fe-N(4)	89.8(7)	O(1)-Fe-N(4)	91.33(6)	O(1)-Fe-N(4)	90.81(11)
O(4)-Fe-N(4)	93.6(7)	O(4)-Fe-N(4)	89.00(6)	O(4)-Fe-N(4)	88.75(11)
N(1)-Fe-N(4)	175.1(8)	N(1)-Fe-N(4)	175.40(7)	N(4)-Fe-N(1)	178.02(12)
O(4)-Fe-N(3)	90.3(7)	O(4)-Fe-N(3)	161.28(6)	O(4)-Fe-N(3)	94.46(12)
O(1)-Fe-N(3)	164.7(7)	O(1)-Fe-N(3)	87.88(6)	O(1)-Fe-N(3)	160.57(11)
N(1)-Fe-N(3)	96.9(7)	N(1)-Fe-N(3)	97.96(6)	N(1)-Fe-N(3)	100.37(11)
N(4)-Fe-N(3)	78.5(7)	N(4)-Fe-N(3)	77.45(6)	N(4)-Fe-N(3)	77.74(11)
O(4)-Fe-N(2)	160.9(7)	O(4)-Fe-N(2)	88.75(6)	O(4)-Fe-N(2)	166.56(11)
O(1)-Fe-N(2)	92.2(7)	O(1)-Fe-N(2)	161.12(6)	O(1)-Fe-N(2)	86.71(11)
N(1)-Fe-N(2)	76.5(8)	N(1)-Fe-N(2)	77.87(6)	N(1)-Fe-N(2)	77.96(11)
N(4)-Fe-N(2)	100.8(7)	N(4)-Fe-N(2)	101.43(6)	N(4)-Fe-N(2)	102.24(11)
N(3)-Fe-N(2)	80.5(7)	N(3)-Fe-N(2)	81.48(6)	N(3)-Fe-N(2)	80.56(11)

Comparison between the solid state structures of **Λ-1Sa** – **Λ-2Sc** and those of previously reported [Fe(CF₃SO₃)₂(mcp)]²¹, **1**, [Fe(CF₃SO₃)₂(pdp)]¹⁸, **2**, and their pinene-derivatives [Fe(CF₃SO₃)₂(mcpp)]⁵, **1P**, [Fe(CF₃SO₃)₂(pdpp)]⁶, **2P**, indicates only minor

differences between their respective structural parameters of the first coordination sphere.

The space-filling diagram of complexes Λ -1Sa – Λ -2Sc (Figure V.4) illustrates the effect of increasing the steric bulk of the ligand. A systematic introduction of steric hindrance at the proximity of the metal is achieved by using the three silyl groups: tms, tbdms and tips. Moving from the less sterically demanding trimethylsilyl group (complexes Λ -1Sa and Λ -2Sa) to the bulkiest triisopropyl (complexes Λ -1Sc and Λ -2Sc), well-defined cavity around the *cis* labile position of the iron center is created.

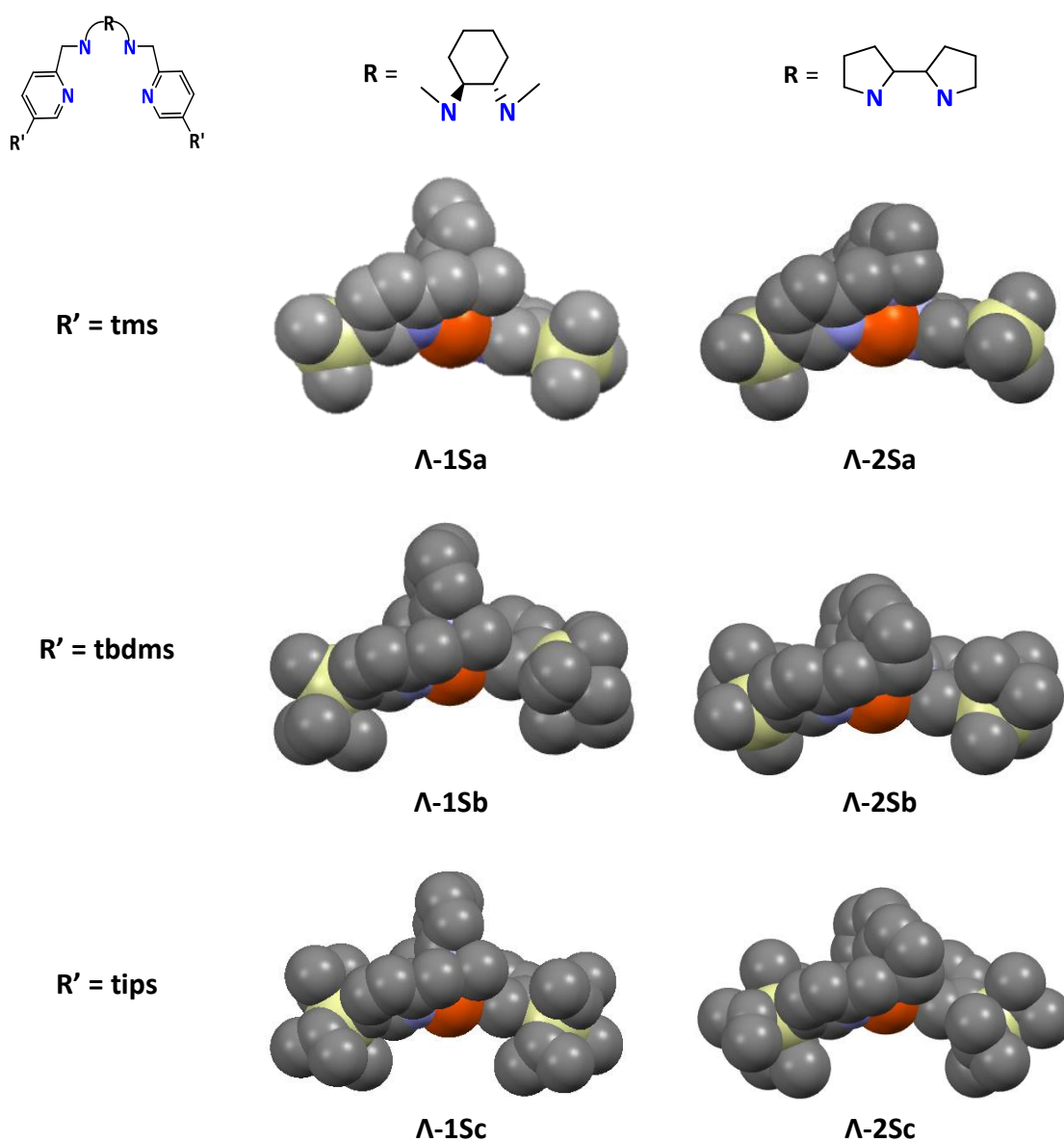


Figure V.4. Space-filling diagrams of Λ -1Sa – Λ -2Sc. Solvent of crystallization, hydrogen atoms and CF_3SO_3 molecules have been omitted for clarity.

V.2.2.2 Solution behavior

The structure of complexes **Λ -1Sa** – **Λ -2Sc** in solution was studied by means of ^1H -NMR spectroscopy. All complexes have high-spin Fe^{II} centers ($S = 2$) in CD_2Cl_2 , as indicated by the paramagnetically shifted ^1H -NMR signals (Figure V.5 for mcp-based complexes **Λ -1Sa** – **Λ -1Sc**; Figure V.6 for pdp-based complexes **Λ -2Sa** – **Λ -2Sc**). The spectrum of each complex only shows one set of signals for the two symmetric parts of the ligand, consistent with C_2 symmetry and indicative of the presence of unique species with *cis*- α conformation.

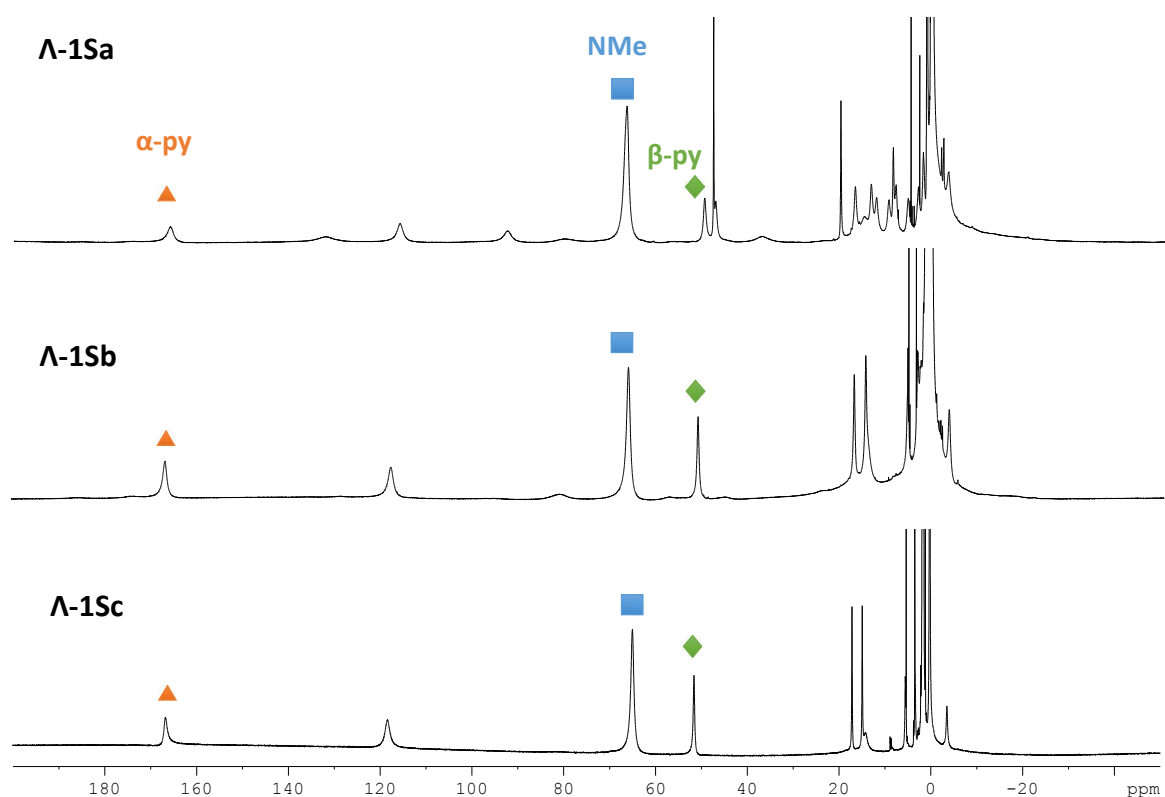


Figure V.5. ^1H -NMR spectra of mcp-based triflate complexes **Λ -1Sa** – **Λ -1Sc** in CD_2Cl_2 at 300 K.

Full assignment of the spectra was not possible, but the most characteristic peak could be assigned. The resonance at ~ 170 ppm for mcp-based complexes was assigned to the α -pyridine proton (orange triangle, Figure V.5) due to the large paramagnetic shift and relative integration (2H). On the other hand, this α -pyridine proton was slightly downfield shifted to ~ 180 ppm for pdp-based complexes (Figure V.6). For comparison with earlier reported complexes,²² the peak at ~ 50 ppm was assigned to β -pyridine protons (2H, green diamonds). The signal at ~ 65 ppm in the ^1H -NMR spectra of mcp-based complexes **Λ -1Sa** – **Λ -1Sc** was assigned to *N*-methyl protons based on its integration

(6H, blue squares). For pdp-based complexes **Λ -2Sa** – **Λ -2Sc**, the corresponding NCH₂ peak appears upshifted at ~ 80 ppm (4H, yellow circles).

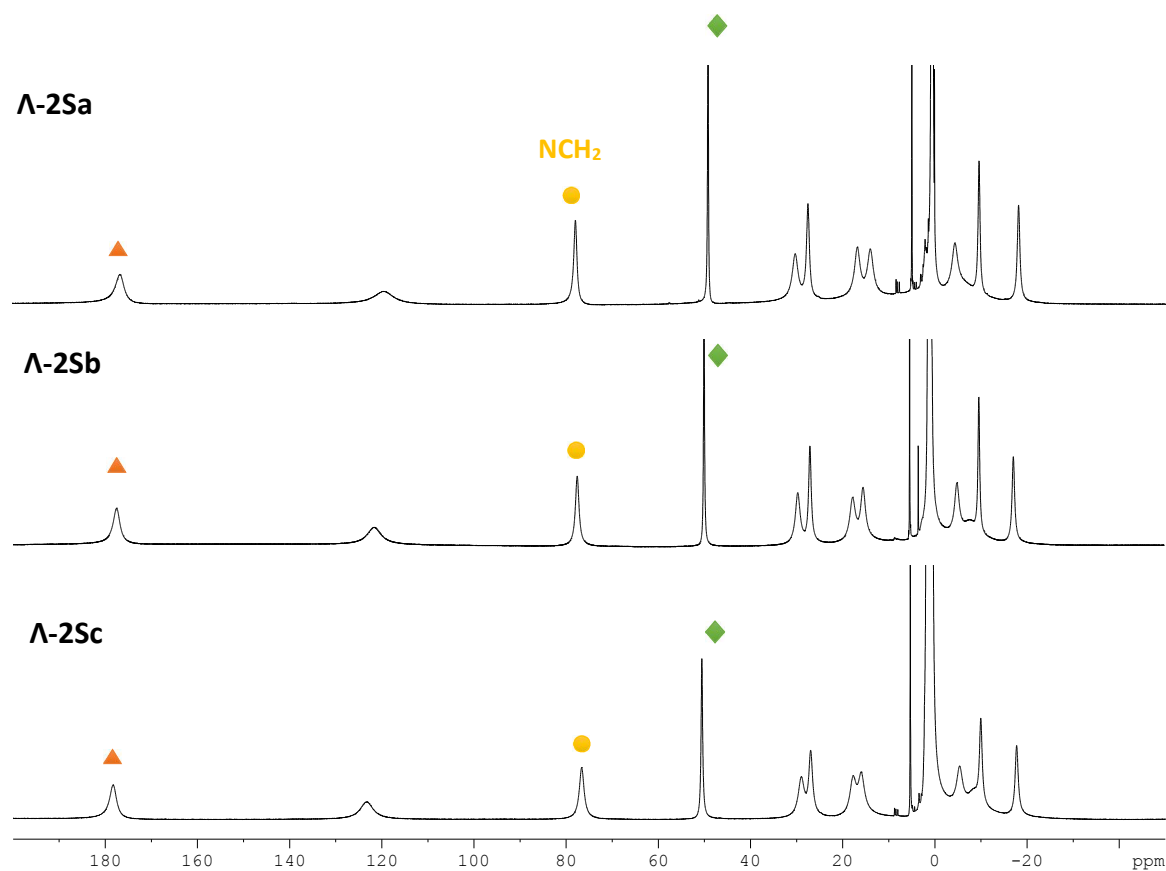


Figure V.6. ¹H-NMR spectra of pdp-based triflate complexes **Λ -2Sa** – **Λ -2Sc** in CD₂Cl₂ at 300 K.

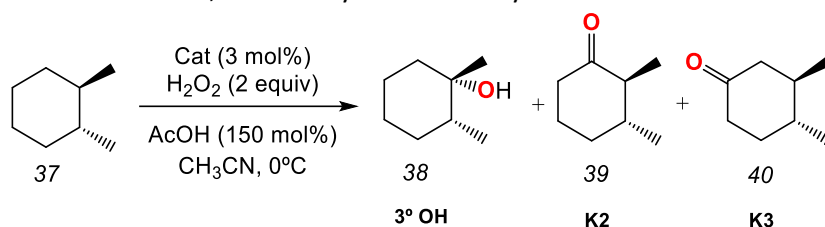
V.2.3 CATALYTIC STUDIES

V.2.3.1 *Establishing selectivity bases on simple substrates*

This new family of complexes was tested in the oxidation of simple substrates using hydrogen peroxide (H₂O₂) as oxidant and low catalyst loadings (3 mol%). Cyclohexane-based substrates were chosen as test platforms because they are ubiquitous scaffolds in natural products, and thus serve to study the selectivity bases of the catalysts avoiding the interference of multiple factors which can interplay in complex molecules. In this regard, *trans*-1,2-dimethylcyclohexane (**37**, *trans*-DMCH) and *trans*-decalin (**41**) were oxidized with the set of catalysts **Λ -1Sa** – **Λ -2Sc** (Table V.3), using 3 mol% catalyst, 2 equiv of H₂O₂ and 1.5 equiv of acetic acid (AcOH) as additive. Table V.3 presents the results of

the performance of catalysts **Λ -1Sa** – **Λ -2Sc** in the oxidation of *trans*-1,2-DMCH. For comparative purposes, catalysts **Λ -1**, **Λ -2** and **3** (Figure V.1) were also tested. A comparison between the mcp-based catalysts (entries 1-3, Table V.3) shows that when the size of the silyl group is increased, product yields are improved (from 39% using **Λ -1Sa** to 61% using **Λ -1Sc**). Moreover, discrimination between the two ketone products is enhanced (K3/K2 ratio from 1.4 with **Λ -1Sa** to 3.0 with **Λ -1Sc**), indicating a preference for the formation of the less sterically demanding ketone K3 upon increasing the bulk at the pyridine moiety of the ligand. According to this fact, secondary sites are more prone to be oxidized with bulkier catalysts ($2^\circ/3^\circ$ ratio from 1.8 using **Λ -1Sa** to 13.3 using **Λ -1Sc**).

Table V.3. Oxidation of *trans*-1,2-DMCH by various catalysts.



Entry	Catalyst	Conversion (%) ^a	Yield (%) ^a	3° OH/K2/K3 normalized ratio ^a	K3/K2 ^a	$2^\circ/3^\circ$ ^a
1	Λ-1Sa	77	39	35/27/38	1.4	1.9
2	Λ-1Sb	89	45	18/28/54	1.9	4.6
3	Λ-1Sc	83	61	7/23/70	3.0	13.3
4	Λ-2Sa	97	40	45/27/28	1.0	1.2
5	Λ-2Sb	91	49	36/26/38	1.5	1.8
6	Λ-2Sc	87	55	20/26/54	2.1	4.0
7	Λ-1	84	41	24/26/50	1.9	3.2
8	Λ-2	65	37	48/22/30	1.3	1.1
9	3 ^{8,b}	-	48	23/35/42	1.2	3.3

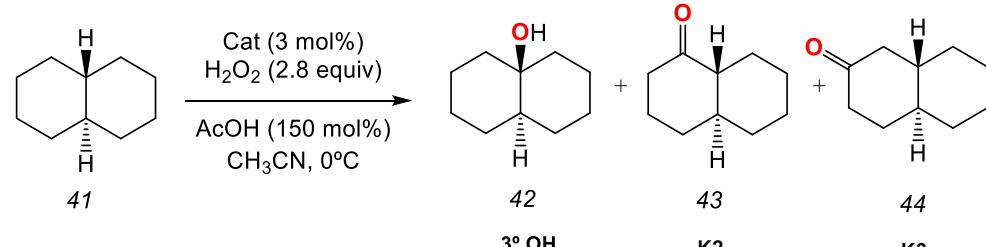
^a Based on GC analysis. ^b cat:H₂O₂:subst:AcOH 3:360:100:150.

The same trends are observed for the pdp-based catalysts **Λ -2Sa** – **Λ -2Sc** (entries 4-6, Table V.3). Product yields range from 40% (**Λ -2Sa**) to 55% (**Λ -2Sc**), selectivity between ketones is increased from K3/K2 = 1.0 (**Λ -2Sa**) to K3/K2 = 2.1 (**Λ -2Sc**), and $2^\circ/3^\circ$ site ratios from 1.2 (**Λ -2Sa**) to 4.0 (**Λ -2Sc**). Compared to their pdp-counterparts, mcp-based catalysts appear to be more active, more selective for secondary site oxidation and more able to discriminate among different secondary sites. These findings are in agreement with

previous studies which indicate that mcp-based iron catalysts are privileged structures for methylenic site oxidations.¹⁰

Comparison among silyl-derivative catalysts and the naked catalysts **Λ-1** and **Λ-2** under analogous reaction conditions indicates that the introduction of tms groups at the ligand architecture does not have a positive influence in terms of yield and selectivity (compare entry 1 vs entry 7 and entry 4 vs entry 8, Table V.3). On the other hand, the tbdms groups slightly increase the performance of the catalysts, while complexes bearing tips groups appear as much more active and selective catalysts than their naked counterparts. Interestingly, not only is catalyst **Λ-1Sc** the most active and selective, even compared to **3⁸** (entry 9, Table V.3), but also the one that offers a better mass balance.

Table V.4. Oxidation of *trans*-decalin by various catalysts.



Entry	Catalyst	Conversion (%) ^a	Yield (%) ^a	3° OH/K2/K3 normalized ratio ^a	K3/K2 ^a	2°/3° ^a
1	Λ-1Sa	88	54	5/48/47	1.0	19.0
2	Λ-1Sb	85	55	3/42/55	1.3	32.3
3	Λ-1Sc	68	58	1/34/65	1.9	99.0
4	Λ-2Sa	81	59	16/46/38	0.8	5.3
5	Λ-2Sb	82	54	9/43/49	1.1	10.2
6	Λ-2Sc	83	58	3/36/61	1.7	32.3
7	Λ-1	83	53	4/37/59	1.6	24.0
8	Λ-2	88	48	15/38/46	1.2	5.7
9	3^{8,b}	-	51	6/43/51	1.2	15.7

^a Based on GC analysis. Minor amounts of 2-ol and 3-ol are also considered. ^b cat:H₂O₂:subst:AcOH 3:360:100:150.

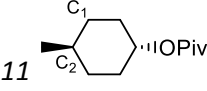
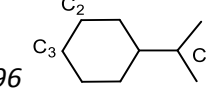
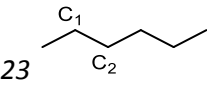
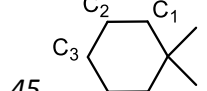
A similar analysis can be performed in the oxidation of *trans*-decalin (**41**) by the same set of catalysts (Table V.4). In this case, the increase of the steric bulk of the ligand does not have such an important impact in terms of yield as in the oxidation of *trans*-1,2-

DMCH. For the mcp-based catalysts (entries 1-3, Table V.4), product yields range from 54% to 58% (using **Λ -1Sa** and **Λ -1Sc**, respectively). Interestingly, the presence of the tips group in the ligand affords the most active and selective catalyst of the series ($K_3/K_2 = 1.9$, $2^\circ/3^\circ$ ratio = 99.0; entry 3, Table V.4). The robustness of **Λ -1Sc** is evidenced by the better mass balance obtained with this catalyst (entry 3, Table V.4). On the other hand, pdp-based catalysts afford yields from 54% to 59% (with **Λ -2Sb** and **Λ -2Sa**, respectively), and $2^\circ/3^\circ$ ratio ranges from 5.3 (for **Λ -2Sa**) to 32.3 (for **Λ -2Sc**).

When compared to their **Λ -1** analogue under the same reaction conditions, tms- and tbdms-derived catalysts present similar yields (compare entries 1, 2, and 7, Table V.4). Catalyst **Λ -1Sa** is less selective for secondary site oxidation than **Λ -1**, while **Λ -1Sb** is in line with the selectivity observed with the naked catalyst. However, the introduction of the tips moiety at the ligand is translated into moderately enhanced yield (5% increase, compare entry 3 and entry 7, Table V.4) and significantly improved selectivity toward methylenic site oxidation (from 24.0, entry 7, to 99.0, entry 3). In terms of yield, pdp-derived catalysts are more active than **Λ -2** (compare entries 4, 5, 6, and 8, Table V.4). **Λ -2Sa** is less selective in the oxidation of methylenic sites than **Λ -2**, slightly favoring the formation of the more sterically demanding ketone K2 ($K_3/K_2 = 0.8$, entry 4, Table V.4). However, the introduction of tbdms and tips groups at the pyridine moieties of the ligand increases the preference of such catalysts for oxidizing secondary sites (compare entries 5, 6, and 8, Table V.4). By using tips-modified catalysts, better yields and selectivity than the previously reported **3**⁸ can be obtained.

From the results of *trans*-1,2-DMCH and *trans*-decalin oxidation, it is clear that the introduction of triisopropylsilyl groups at the ligand architecture gives rise to unique catalysts with enhanced activity and selectivity toward the oxidation of methylenic sites. Therefore, **Λ -1Sc** and **Λ -2Sc** were the selected catalysts to further studied in a set of structurally simple substrates (*trans*-4-methylcyclohexyl pivalate (**11**), isopropylcyclohexane (**96**), *n*-hexane (**23**), and 1,1-dimethylcyclohexane (**45**)). For comparative purposes, **Λ -1** and **Λ -2** were also analyzed. The results obtained are shown in Table V.5.

Table V.5. Oxidation of simple substrates by various catalysts.

Substrate Cat:H ₂ O ₂ :subst:AcOH	Entry	Catalyst	Conversion (%) ^a	Yield (%) ^a	Selectivity ^a	
 11 3:200:100:150	1	Λ-1	43	40	C₁(2°)/C₂(3°) 0.43	
	2	Λ-1Sc	67	63	0.54	
	3	Λ-2	38	35	0.27	
	4	Λ-2Sc	66	61	0.46	
 96 3:200:100:150	5	Λ-1	75	48	C₁/C₂/C₃ 33/53/14	2°/3° 2.0
	6	Λ-1Sc	83	56	18/63/19	4.6
	7	Λ-2	64	38	50/40/10	1.0
	8	Λ-2Sc	65	42	34/51/15	1.9
 23 3:320:100:150	9	Λ-1	90	41	C₁/C₂ 1.6	
	10	Λ-1Sc	97	66	1.7	
	11	Λ-2	69	50	1.1	
	12	Λ-2Sc	75	69	1.1	
 45 3:280:100:150	13	Λ-1	64	49	C₁/C₂/C₃ 22/54/25	C₂/(C₁+C₃) 1.1
	14	Λ-1Sc	97	70	17/57/26	1.3
	15	Λ-2	68	58	36/43/21	0.8
	16	Λ-2Sc	96	69	26/50/24	1.0

^a Based on GC analysis.

In the oxidation of *trans*-4-methylcyclohexyl pivalate (**11**, entries 1-4, Table V.5), two products are formed: ketone at the secondary site C₁ and tertiary alcohol at C₂. The relative selectivities depend on the catalyst employed. Comparing the performance of **Λ-1** and **Λ-1Sc**, a slight preference for the formation of the ketone product at C₁ is observed for the latter (2°/3° = 0.43 for **Λ-1**, entry 1; 2°/3° = 0.54 for **Λ-1Sc**, entry 2, Table V.5). pdp-based catalysts are more selective for oxidizing the tertiary site C₂ than their mcp analogues, showing 2°/3° ratios of 0.27 and 0.46 for **Λ-2** and **Λ-2Sc**, respectively (entries 3-4, Table V.5). However, the ketone does not become the major product of the reaction in any case, probably due to the steric effect imposed by the pivalate group in the substrate, which hinders the C₂ site and prevents it from oxidation. A different behavior

is observed in the oxidation of isopropylcyclohexane (96, entries 5-8, Table V.5). In this case there is a competition between the formation of a tertiary alcohol at C₁, and ketones at C₂ and C₃.

In general, mcp-based catalysts are more prone to oxidize methylenic sites than their pdp analogues (compare entries 5-7 and 6-8, Table V.5). In addition, the introduction of tips groups in the ligand approximately doubles the 2°/3° ratio (compare entries 5-6 and 7-8, Table V.5), obtaining up to 4.6 selectivity for catalyst **Λ-1Sc** (entry 6, Table V.5). A more subtle case is the one of *n*-hexane (23, entries 9-12, Table V.5), where there is a competition between the formation of ketones at C₁ and C₂. The differentiation between them is only due to minor steric factors. The mcp-based catalysts are able to differentiate between them in a C₁/C₂ ratio of 1.6 and 1.7 (**Λ-1** and **Λ-1Sc**, respectively; entries 9 and 10, Table V.5), while **Λ-2** and **Λ-2Sc** afford virtually equal amounts of oxidation products at C₁ and C₂ (C₁/C₂ = 1.1, entries 11 and 12, Table V.5). Therefore, only in the former case there is actually an effect of the pyridine substituent, albeit modest. Finally, the oxidation of 1,1-dimethylcyclohexane (45) allows to interrogate competition among oxidation at three different methylenic sites (C₁, C₂, and C₃; entries 13-16, Table V.5). In all cases, oxidation at C₂ site is favored, mainly because of the steric effect imposed by the methyl groups which disfavor C₁ oxidation. C₂ normalized selectivity ranges between 43 and 57 (for **Λ-2** and **Λ-1Sc**, respectively; entries 15 and 14, Table V.5). The statistically expected ratio is 40/40/20, based on the number of C—H bonds of the substrate, which is virtually what is observed using **Λ-2**. Therefore, this catalyst is barely unable to discriminate among C₁, C₂ and C₃. In order to make this differentiation more clear, C₂/(C₁+C₃) is shown in Table V.5, where it is evidenced that only mcp-based catalysts are able to favor C₂ over the rest of secondary sites, and **Λ-1Sc** is the catalyst that offers the largest selectivity among the series for this less encumbered C—H group (entry 14, Table V.5).

Most importantly, as a general trend, product yields are ~ 20% improved by introducing tips groups in the catalysts (compare entries 1-2, 3-4, 5-6, 7-8, 9-10, 11-12, 13-14, and 15-16; Table V.5). This fact can be attributed to the robustness of the catalyst, imposed by the cavity-like space formed at the surrounding of the iron center formed by the bulky isopropyl groups present in the ligand architecture, as observed in the space-

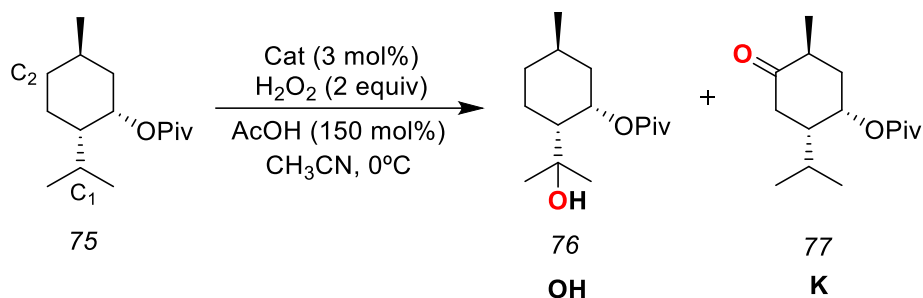
filling analysis (Figure V.4). This likely prevents the formation of dimers, which are postulated to be the major deactivation pathway of the catalysts.⁵

V.2.3.2 Application to natural product oxidations

Due to the potential of **Λ -1Sc** and **Λ -2Sc** observed in the selective oxidation of simple substrates, we sought to explore its performance in the oxidation of more complex molecules, such as natural products.

In the first place, we chose the terpene (+)-neomenthyl pivalate (**75**) as substrate platform, in which there is a competition for the formation of a tertiary alcohol at C₁ and a ketone at C₂ (Table V.6). Because this is a chiral substrate, different behavior is attained with catalysts in Λ and Δ relative configuration. Therefore the set of catalysts **Λ -1Sc**, **Δ -1Sc**, **Λ -2Sc**, and **Δ -2Sc** were evaluated (entries 3-4, 7-8, Table V.6). For comparative purposes, **Λ -1**, **Δ -1**, **Λ -2**, and **Δ -2** are also included in Table V.6 (entries 1-2, 5-6).

Table V.6. Oxidation of (+)-neomenthyl pivalate by various catalysts.



Entry	Catalyst	Conversion (%) ^a	Yield (%) ^a	K/OH ^a
1	Λ-1	37	32	0.9
2	Δ-1	31	26	1.9
3	Λ-1Sc	51	43	1.3
4	Δ-1Sc	45	38	1.1
5	Λ-2	50	38	1.5
6	Δ-2	43	34	1.9
7	Λ-2Sc	58	47	1.9
8	Δ-2Sc	43	39	1.1

^a Based on GC analysis.

Entries 1-4 in Table V.6 show the results with mcp-based catalysts. With the naked **Λ -1**, an improvement of the K/OH ratio occurs upon changing from the Λ configuration

catalyst to the Δ (from 0.9 to 1.9, entries 1-2, Table V.6). Moreover, a higher preference for the ketone product is also observed with Λ -**1Sc** with respect to Λ -**1** (0.9 vs 1.3; compare entries 1 and 3, Table V.6). Based on these results, one could expect that the corresponding Δ -**1Sc** complex, in Δ configuration, would be the most selective catalysts for secondary sites in the oxidation of (+)-neomenthyl pivalate. However, this is not the case observed in entry 4 (Table V.6), affording a K/OH ratio of 1.1. For the pdp-based catalysts, a similar trend is observed: the K/OH ratio increases from Λ to Δ for **2** (compare entries 5 and 6, Table V.6), but decreases from Λ -**2Sc** to Δ -**2Sc** (compare entries 7 and 8, Table V.6). In the case of Λ configuration catalysts, higher amounts of ketone are formed when tips groups are introduced in the catalyst structure (compare entries 5 and 7, Table V.6). These results evidence that multiple factors interplay in complex molecules, thus the trends observed in simple substrates are not directly translated into elaborated molecules. Therefore selectivity bases are not clearly understood and other factors besides sterics might influence in predicting site oxidation in complex molecules.

Although the reaction conditions are not optimized, yields are improved with catalysts decorated with the bulky tips groups (compare entries 1 and 3, 2 and 4, 5 and 7, and 6 and 8, Table V.6). The best performance in terms of yield and selectivity is achieved with Λ -**2Sc** (47% yield, K/OH ratio = 1.9, entry 6, Table V.6), and because of that the reaction of this particular catalyst with (+)-neomenthyl pivalate was tested using 4 equiv of oxidant (Figure V.7). Using this higher amount of H_2O_2 , 51% isolated yield of ketone is formed. The K/OH ratio increases to 3.2, but this result should be taken cautiously, since a part of the alcohol product might be converted to overoxidized products. However, the good yield of ketone achieved under these experimental conditions can be regarded as very useful from a synthetic point of view, especially taking into account that the best isolated yield described up to date was 30% using 3 mol% of catalyst **3**.⁸

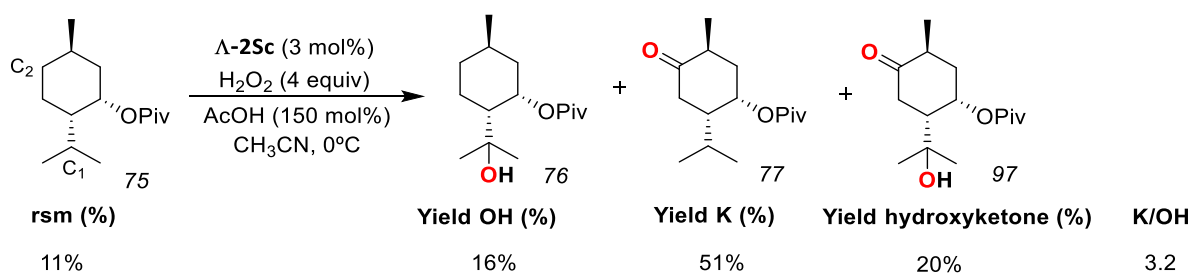
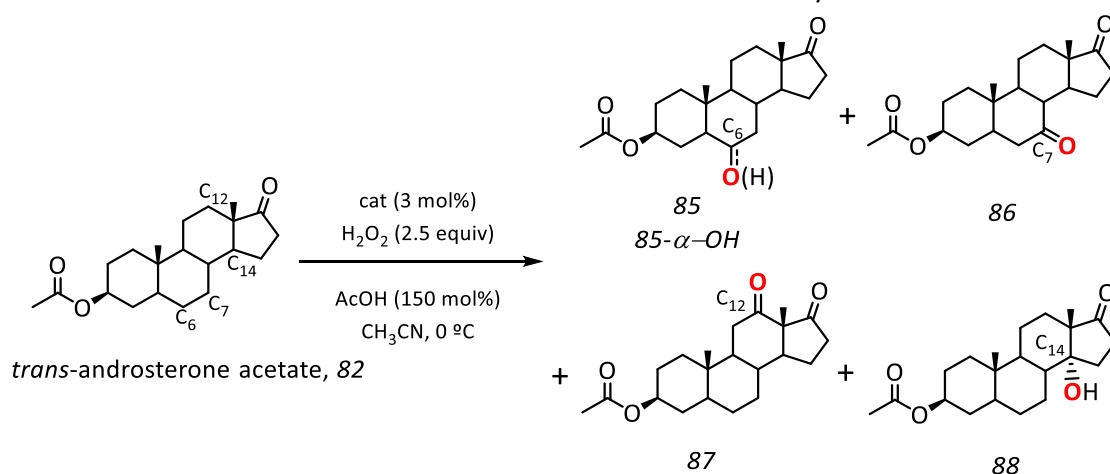


Figure V.7. Oxidation of (+)-neomenthyl pivalate using Λ -**2Sc** and 4 equiv of oxidant. Results indicate isolated yields.

Steroids are interesting substrate platforms because of their elaborated structure, with multiple and distinct C—H groups that hint at the possibility of studying the selectivity bases in C—H oxidation.²³ Moreover, steroids are also of biological relevance,²⁴ since their oxidation mediated by P450 enzymes is known to occur in living systems in the biosynthesis and biological degradation of steroidal hormones.^{25,26} The oxidation of *trans*-androsterone acetate (**82**) with the set of catalysts **Λ -1Sa** – **Δ -2Sc** was evaluated (Table V.7). From these results it is established that there is a systematic improvement in terms of yield when the size of the silyl group increases in both Λ -mcp-based (compare entries 1-3, Table V.7) and Λ -pdp-based catalysts (compare entries 5-7, Table V.7). A particularly very good yield is attained with **Δ -1Sc** (80%, entry 4, Table V.7), which appears to be the most active catalyst of the series, affording a good mass balance (86% conversion).

Table V.7. Oxidation of *trans*-androsterone acetate with various catalysts.



Entry	Catalyst	Conversion (%) ^a	Yield (%) ^a	Normalized selectivity ^a
				C ₆ ^b /C ₇ /C ₁₂ /C ₁₄
1	Λ-1Sa	70	52	56/14/30/-
2	Λ-1Sb	77	55	69/10/21/-
3	Λ-1Sc	85	70	72/5/23/-
4	Δ-1Sc	86	80	11/1/88/-
5	Λ-2Sa	81	50	51/21/13/15
6	Λ-2Sb	71	57	63/18/11/8
7	Λ-2Sc	83	60	82/12/3/3
8	Δ-2Sc	50	48	22/6/69/3

^a Based on GC analysis. ^b Sum of ketone and α -alcohol.

In terms of selectivity, it is important to notice that, as previously reported,¹⁰ only pdp-based catalysts present oxidation at C₁₄ to form the corresponding alcohol, once more demonstrating the somewhat higher preference of these type of catalysts for oxidizing tertiary C—H groups. Moreover, it is observed that the bulkier the silyl group is, the higher is the preference for the less hindered site C₆ (compare entries 1-3, and 5-7, Table V.7). Moreover, S-based catalysts tend to favor the oxidation at C₆, and the extent of this selectivity is also dependent on the size of the bulk at the pyridine moiety of the ligand. The best selectivity is achieved using **Λ-2Sc**, which affords 82% normalized selectivity for oxidation at C₆ (entry 7, Table V.7). Interestingly, selective oxidation at C₆ was observed with similar *trans*-androsterone derivatives when utilizing manganese porphyrins.^{27,28} However, this procedure required a highly elaborated porphyrin structure plus protection/deprotection steps in the substrate. Thus, the good yield and excellent selectivity attained with **Λ-2Sc** point toward a more simple and direct strategy for performing steroid oxidations. In addition, in entries 1-8 (Table V.7) oxidation at C₆ derives from the formation of the corresponding ketone and the diastereoisomeric α-alcohol. More interestingly, in the particular case of **Λ-2Sc**, the 82% selectivity derives from 43% selectivity for the ketone and 39% selectivity for the corresponding α-alcohol. The formation of this alcohol in moderate selectivity implies that a diastereoisomeric oxidation of a non-activated C—H bond has been achieved, which is one of the most challenging transformations in organic synthesis. It is worth mentioning that no traces of the corresponding β-alcohol at C₆ were detected.

On the other hand, R-based catalysts **Δ-1Sc** and **Δ-2Sc** present a dramatically different selectivity pattern in the oxidation of *trans*-androsterone acetate (entries 4 and 8, Table V.7). In this case, the oxidation occurs preferentially at C₁₂ with good to excellent selectivity (88% selectivity for **Δ-1Sc**, entry 4; 69% selectivity for **Δ-2Sc**, entry 8, Table V.7). Therefore, the catalysts **Δ-1Sc** and **Λ-2Sc** raise as a powerful toolbox to oxidize different sites of *trans*-androsterone acetate (C₆ and C₁₂, respectively) in good to excellent yield and selectivity.

V.3 CONCLUDING REMARKS

We have synthesized and characterized a new family of non-heme iron catalysts that systematically introduce steric bulkiness at the ligand architecture, using *trans*-1,2-diaminocyclohexane and 2,2'-bipyrrrolidine as backbones. The catalysts bearing the more sterically crowded triisopropylsilyl groups **Λ -1Sc** and **Λ -2Sc** create a cavity-like space around the metal site. Moreover, these appear as the most active and selective of the series in the oxidation of simple substrates. Very interestingly, they show enhanced selectivity toward the oxidation of methylenic sites compared to their analogous complexes without any silyl substituent (**Λ -1** and **Λ -2**, respectively). This fact can be rationalized in terms of steric demand on the catalyst and on the substrate, since secondary C—H bonds are more exposed to the bulk. In addition, they are capable of discriminating among multiple methylenic sites, again exhibiting preference for the less sterically crowded C—H groups. Not only are these trends observed in the oxidation of simple alkanes, but also maintained in the oxidation of natural products. The terpene (+)-neomenthyl pivalate can be oxidized to its ketone product in synthetically amenable yield. On the other hand, the steroid *trans*-androsterone acetate can be selectively oxidized to obtain two different ketones as major products depending on the catalyst employed in excellent yield and selectivity.

It should be noted that the percentage conversion and percentage yield differ in some of the reactions. This fact might be due to the difficultness of this type of oxidations, where mass balance is not complete. Although the formation of significant amounts of a single nonidentified product is not observed, the formation of trace amount of multiple byproducts can not be excluded.

Their relatively easy accessibility and cost, plus the high activity and selectivity they present make this new family of catalysts for a powerful tool toward the oxidation of elaborated substrates, such as natural products.

V.4 EXPERIMENTAL SECTION

V.4.1 MATERIALS

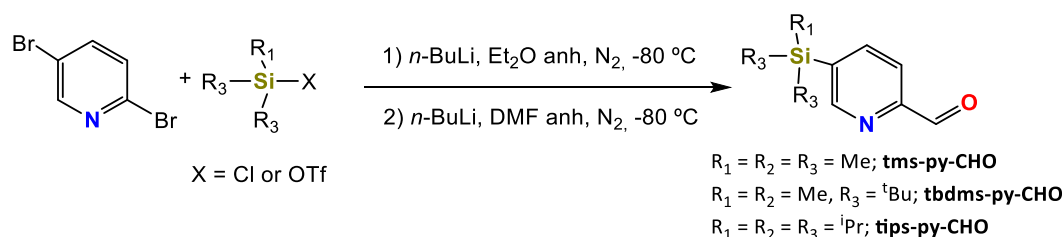
Reagents and solvents used were commercially available reagent quality unless otherwise stated. Acetonitrile for catalysis was HPLC grade. Preparation and handling of air-sensitive materials were carried out in a N₂ dry box (MBraun) with O₂ and H₂O concentrations < 1 ppm. [Fe(CF₃SO₃)₂-mcp)]²¹, **1**, and [Fe(CF₃SO₃)₂(pdp)]¹⁸, **2**, were prepared according to published procedures.

V.4.2 INSTRUMENTATION

NMR spectra were taken on a 300 or 400 MHz spectrometer (Bruker or Varian). ¹H-NMR spectra of paramagnetic compounds were performed with the following special parameters; relaxation delay = 0.03 s, acquisition time = 0.064 s, line broadening = 30 Hz, sweep width = 100-250 ppm. Spectra were referenced to the residual solvent peaks or TMS (tetramethylsilane) for ¹H. Elemental analyses were performed using a CHNS-O elemental analyzer. X-Ray diffraction analysis were carried out on a BRUKER SMART APEX CCD diffractometer using graphite-monochromated Mo K α radiation ($\lambda = 0.71073 \text{ \AA}$) from an X-Ray Tube. HRMS were performed on time-of-flight mass spectrometer with an ESI source using methanol as mobile phase. Product analyses were performed on a gas chromatograph (HP5 column, 30m or Cyclosil-B column, 30 m) and a flame ionization detector.

V.4.3 SYNTHESIS OF LIGANDS

Silyl-derived picolylaldehydes were synthesized by reacting 2,5-dibromopyridine with the corresponding silyl triflate in presence of *n*-butyllithium (*n*-BuLi) and DMF at low temperature (Scheme V.4).



Scheme V.4. Synthesis of silyl-derived picolylaldehydes tms-py-CHO, tbdms-py-CHO and tips-py-CHO.

tms-py-CHO. 2,5-dibromopyridine (2.4 g, 10 mmol) were dissolved in 30 mL of anhydrous diethyl ether under inert atmosphere at cooled to $-80\text{ }^{\circ}\text{C}$ in an ethyl acetate/liquid N_2 bath. Then 1 equiv of *n*-BuLi (1.6 M in hexanes, 6.2 mL, 10 mmol) were slowly added over 10 min, and the reaction mixture was let stir for 45 min. At that point, 1.1 equiv of trimethylsilyl chloride (1.4 mL, 11 mmol) was added all at once at $-80\text{ }^{\circ}\text{C}$, and stirred for another hour to form the 2-bromo-5-(trimethyl)-pyridine. 1.1 equiv of *n*-BuLi (1.6 M in hexanes, 6.8 mL, 11 mmol) was added over 10 min to the crude reaction at $-80\text{ }^{\circ}\text{C}$. After 45 min, 1.6 equiv of anhydrous DMF (1.3 mL, 16 mmol) were slowly added. The reaction was stirred for 2h, and the temperature was rised up to $-15\text{ }^{\circ}\text{C}$ after that time. At this point, the reaction was quenched with 10 mL of H_2O and extracted with diethyl ether (3 x 30 mL). The combined organic layers were washed with 30 mL of brine, dried over MgSO_4 , concentrated on a rotatory evaporator and purified by silica column chromatography eluting with hexane: ethyl acetate (10:1) to yield 1.13 g (6.29 mmol, 63%) of the pure product as a yellow oil. $^1\text{H-NMR}$ (CDCl_3 , 400 MHz, 300 K) δ , ppm: 10.06 (s, 1H), 8.83 (s, 1H), 7.96 (ddd, $J = 7.6, 1.6, 0.8$ Hz, 1H), 7.88 (dd, $J = 7.6, 1.0$ Hz, 1H), 0.32 (s, 9H). $^{13}\text{C-NMR}$ (CDCl_3 , 100 MHz, 300 K) δ , ppm: 193.8, 154.1, 152.7, 142.1, 141.5, 120.6, 1.53. HRMS (ESI-TOF, $[\text{M} + \text{Na}]^+$): m/z calcd for $\text{C}_9\text{H}_{14}\text{NOSi}$ 180.0845, found 180.0853.

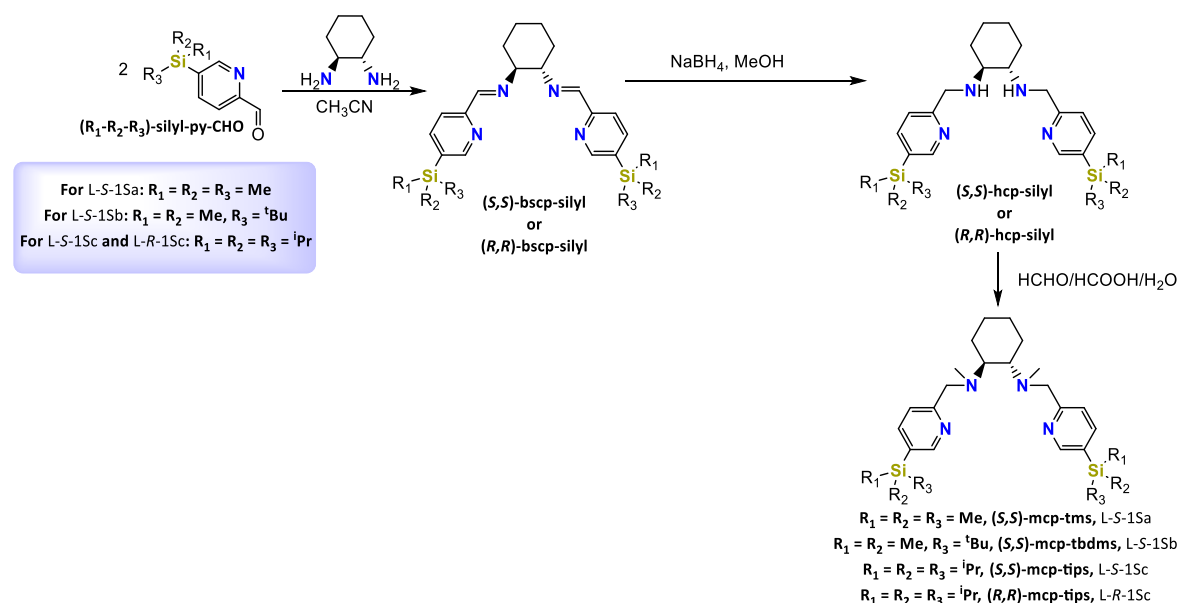
tbdms-py-CHO was prepared following a procedure analogous to **tms-py-CHO**, using 2,5-bromopyridine (2.8 g, 12 mmol) and 1 equiv of *tert*-butyl-dimethylsilyl triflate (2.8 mL, 12 mmol) to yield 0.7 g (3.2 mmol, 27%) of the desired product as a yellow solid after purification by silica colum chromatography eluting with hexane:diethyl ether (15:1). $^1\text{H-NMR}$ (CDCl_3 , 400 MHz, 300 K) δ , ppm: 10.06 (s, 1H), 8.82 (s, 1H), 7.95 (dd, $J = 7.6, 0.9$ Hz, 1H), 7.88 (d, $J = 7.6$ Hz, 1H), 1.17 (t, $J = 7.0$ Hz, 1H), 0.87 (s, 9H), 0.32 (s, 6H). $^{13}\text{C-NMR}$ (CDCl_3 , 100 MHz, 300 K) δ , ppm: 193.8, 154.8, 152.5, 143.2, 139.3, 120.4, 26.2, 16.8, 6.5.

tips-py-CHO was prepared following a procedure analogous to **tms-py-CHO**, using 2,5-bromopyridine (2.8 g, 12 mmol) and triisopropylsilyl triflate (3.4 mL, 12 mmol) to yield 2.9 g (11 mmol, 92%) of the pure product as a yellow solid after purification by silica column chromatography eluting with hexane: ethyl acetate (15:1). $^1\text{H-NMR}$ (CDCl_3 , 400 MHz, 300 K) δ , ppm: 10.10 (s, 1H), 8.86 (s, 1H), 7.95 (ddd, $J = 18.3, 7.6, 1.2$ Hz, 2H), 1.52-1.39 (m, 3H), 1.09 (d, $J = 7.5$ Hz, 18H). $^{13}\text{C-NMR}$ (CDCl_3 , 100 MHz, 300 K) δ , ppm: 193.9,

155.6, 152.5, 144.0, 137.0, 120.5, 18.4, 10.6. HRMS (ESI-TOF, $[M + Na]^+$): m/z calcd for $C_{15}H_{25}NOSi$ 264.1778, found 264.1768.

The corresponding picolyl aldehydes were reacted with the diamines to afford the final ligands. The procedure to obtain the mcp-based ligands (L-S-1Sa, L-S-1Sb, L-S-1Sc, L-R-1Sc) is represented in Scheme V.5.

(S,S)-bscp-tms. (1*S*,2*S*)-1,2-Diaminocyclohexane (350 mg, 3.05 mmol) were dissolved in 15 mL of dry acetonitrile and stirred. Then 2 equivalents of **tms-py-CHO** (1.1 g, 6.1 mmol) were added to the reaction mixture, and stirred for 4 h at rt. After high vacuum evaporation, 1.3 g (3.05 mmol, 99%) of the desired product were obtained as a white solid. 1H -NMR ($CDCl_3$, 400 MHz, 300 K) δ , ppm: 8.54 (dd, $J = 1.6, 1.0$ Hz, 2H), 8.24 (s, 2H), 7.76 (dd, $J = 7.8, 0.9$ Hz, 2H), 7.67 (dd, $J = 7.8, 1.7$ Hz, 2H), 3.48-3.46 (m, 2H), 1.81-1.75 (m, 6H), 1.44-1.43(m, 2H), 0.19 (s, 18H).



Scheme V.5. Schematic representation of the synthesis of the mcp-based ligands (L-S-1Sa – L-R-1Sc).

(S,S)-bscp-tbdms was synthesized following a procedure analogous to **(S,S)-bscp-tms** using (1*S*,2*S*)-1,2-diaminocyclohexane (195 mg, 1.7 mmol) and **tbdms-py-CHO** (750 mg, 3.4 mmol, 2 equiv). After solvent removal, 855 mg (1.7 mmol, 99%) of the desired product were obtained as a white solid. 1H -NMR ($CDCl_3$, 400 MHz, 300 K) δ , ppm: 8.58 (s, 2H), 8.28 (s, 2H), 7.80 (d, $J = 7.8$, 2H), 7.71 (dd, $J = 7.8, 1.5$ Hz, 2H), 3.52-3.50 (m, 2H), 1.85-

1.79 (m, 6H), 1.50-1.45(m, 2H), 1.39-1.34 (m, 2H), 0.81 (s, 18H), 0.23 (s, 12H).¹³C-NMR (CDCl₃, 100 MHz, 300 K) δ , ppm: 161.7, 154.6, 154.1, 142.5, 134.1, 120.3, 73.6, 32.7, 26.3, 24.3, 16.8, 6.5.

(S,S)-bscp-tips was synthesized following a procedure analogous to **(S,S)-bscp-tms** using (1*S*,2*S*)-1,2-diaminocyclohexane (220 mg, 1.9 mmol) and **tbdms-py-CHO** (1 g, 3.8 mmol, 2 equiv). After solvent removal, 1.1 g (1.9 mmol, 99%) of the desired product were obtained as a white solid. ¹H-NMR (CDCl₃, 300 MHz, 300 K) δ , ppm: 8.62 (s, 2H), 8.33 (s, 2H), 7.86 (d, *J* = 7.8 Hz, 2H), 7.75 (dd, *J* = 7.8, 1.5 Hz, 2H), 3.57-3.54 (m, 2H), 1.86-1.75 (m, 6H), 1.52-1.51(m, 2H), 1.38 (dt, *J* = 14.7, 7.5 Hz, 6H), 1.04 (d, *J* = 7.4 Hz, 36H).¹³C-NMR (CDCl₃, 75 MHz, 300 K) δ , ppm: 161.8, 154.8, 154.4, 143.5, 131.7, 120.5, 73.6, 32.8, 24.4, 18.4, 10.6. HRMS (ESI-TOF, [M + H]⁺): *m/z* calcd for C₃₆H₆₀N₄Si₂ 605.4429, found 605.4436.

(R,R)-bscp-tips was synthesized following a procedure analogous to **(S,S)-bscp-tms** using (1*R*,2*R*)-1,2-diaminocyclohexane (110 mg, 1 mmol) and **tbdms-py-CHO** (500 mg, 1.9 mmol, 2 equiv). After solvent removal, 600 mg (1 mmol, 99% yield) of the desired product were obtained as a white solid.

(S,S)-hcp-tms. **(S,S)-bscp-tms** (1.3 g, 3.0 mmol) was dissolved in anhydrous methanol (25 mL) and NaBH₄ (455 mg, 12 mmol, 4 equiv) was slowly added. After 4 h of reaction at rt, the crude was brought to dryness, then 15 mL of H₂O were added and it was extracted with CH₂Cl₂ (3 x 30 mL). The combined organic layers were dried with MgSO₄ and the solvent was removed under vacuum. The desired product was obtained as a yellow oil. ¹H-NMR (CDCl₃, 400 MHz, 300 K) δ , ppm: 8.56 (dd, *J* = 1.7, 1.0 Hz, 2H), 7.76 (dd, *J* = 7.7, 1.8 Hz, 2H), 7.34 (d, *J* = 7.6 Hz, 2H), 4.00 (d, *J* = 14.3 Hz, 2H), 3.81 (d, *J* = 14.3 Hz, 2H), 2.33-2.31 (m, 2H), 1.70-1.67 (m, 4H), 1.27-1.18 (m, 4H), 0.25 (s, 18H).¹³C-NMR (CDCl₃, 100 MHz, 300 K) δ , ppm: 160.7, 153.2, 141.5, 132.6, 121.7, 61.2, 52.3, 31.4, 24.9, -1.3. HRMS (ESI-TOF, [M + H]⁺): *m/z* calcd for C₂₄H₄₁N₄Si₂ 441.2870, found 441.2866.

(S,S)-hcp-tbdms was synthesized following a procedure analogous to **(S,S)-hcp-tms** using **(S,S)-bscp-tbdms** (885 mg, 1.7 mmol). The desired product (880 mg, 1.7 mmol, 99%) was obtained as a yellow oil. ¹H-NMR (CDCl₃, 400 MHz, 300 K) δ , ppm: 8.54 (s, 2H), 7.66 (d, *J* = 7.7, 1.8 Hz, 2H), 7.33 (d, *J* = 7.7 Hz, 2H), 3.98 (d, *J* = 14.3 Hz, 2H), 3.79 (d, *J* = 14.3 Hz, 2H), 2.31-2.29 (m, 2H), 2.11-2.08(m, 2H), 1.67-1.65 (m, 4H), 1.21-1.16 (m, 4H),

0.82 (d, $J = 1.7$ Hz, 18H), 0.22 (s, 12H). ^{13}C -NMR (CDCl_3 , 100 MHz, 300 K) δ , ppm: 160.7, 154.0, 142.5, 130.1, 121.5, 61.4, 52.4, 31.5, 26.3, 24.9, 16.7, -6.4.

(S,S)-hcp-tips was synthesized following a procedure analogous to **(S,S)-hcp-tms** using **(S,S)-bscp-tips** (1.1 g, 1.8 mmol). The desired product (1.1 g, 1.8 mmol, 99%) was obtained as a yellow oil. ^1H -NMR (CDCl_3 , 300 MHz, 300 K) δ , ppm: 8.60 (d, $J = 0.7$ Hz, 2H), 7.72 (dd, $J = 7.7, 1.8$ Hz, 2H), 7.41 (d, $J = 7.7$ Hz, 2H), 4.05 (d, $J = 14.2$ Hz, 2H), 3.85 (d, $J = 14.2$ Hz, 2H), 2.40-2.37 (m, 2H), 2.25-2.15 (m, 6H), 1.75-1.73 (m, 2H), 1.40 (dt, $J = 14.7, 7.5$ Hz, 6H), 1.07 (d, $J = 7.4$ Hz, 36H). ^{13}C -NMR (CDCl_3 , 75 MHz, 300 K) δ , ppm: 160.5, 154.7, 143.4, 127.4, 121.7, 61.6, 52.5, 31.6, 25.0, 18.4, 10.6. HRMS (ESI-TOF, $[\text{M} + \text{H}]^+$): m/z calcd for $\text{C}_{36}\text{H}_{64}\text{N}_4\text{Si}_2$ 609.4742, found 609.4763.

(R,R)-hcp-tips was synthesized following a procedure analogous to **(S,S)-hcp-tms** using **(R,R)-bscp-tips** (580 mg, 0.9 mmol). The desired product (570 mg, 0.9 mmol, 99%) was obtained as a yellow oil.

(S,S)-mcp-tms (L-S-1Sa). **(S,S)-hcp-tms** (1.7 g, 3.9 mmol) was mixed with H_2O (12 mL), HCHO (37%, 4.4 mL, 59 mmol, 15 equiv) and HCOOH (97%, 2.2 mL, 59 mmol, 15 equiv) and refluxed overnight. The solution was then cooled and an aqueous solution of NaOH 6M was added until $\text{pH} > 12$. The resulting suspension was extracted with CH_2Cl_2 (3 x 25 mL). The combined organic layers were dried over MgSO_4 and the solvent was evaporated to afford a yellow solid. The product was purified over an alumina chromatographic column eluting with hexane:ethyl acetate (30:70) followed by a silica chromatographic column eluting with CH_2Cl_2 : CH_3OH : NH_4OH (93:6:1) to give the desired pure product (1.2 g, 2.6 mmol, 65%) as a white foam. ^1H -NMR (CDCl_3 , 400 MHz, 300 K) δ , ppm: 8.52 (s, 2H), 7.68 (dd, $J = 7.7, 1.6$ Hz, 2H), 7.54 (d, $J = 7.6$ Hz, 2H), 3.94 (d, $J = 14.4$ Hz, 2H), 3.80 (d, $J = 14.4$ Hz, 2H), 2.72-2.69 (m, 2H), 2.30 (s, 6H), 2.01-1.98 (m, 2H), 1.76-1.74 (m, 2H), 1.28-1.15 (m, 4H), 0.26 (s, 18H). ^{13}C -NMR (CDCl_3 , 100 MHz, 300 K) δ , ppm: 161.3, 152.8, 141.4, 131.4, 122.5, 63.6, 40.3, 36.4, 25.7, 24.1, -1.29. HRMS (ESI-TOF, $[\text{M} + \text{H}]^+$): m/z calcd for $\text{C}_{26}\text{H}_{44}\text{N}_4\text{Si}_2$ 469.3177, found 469.3197.

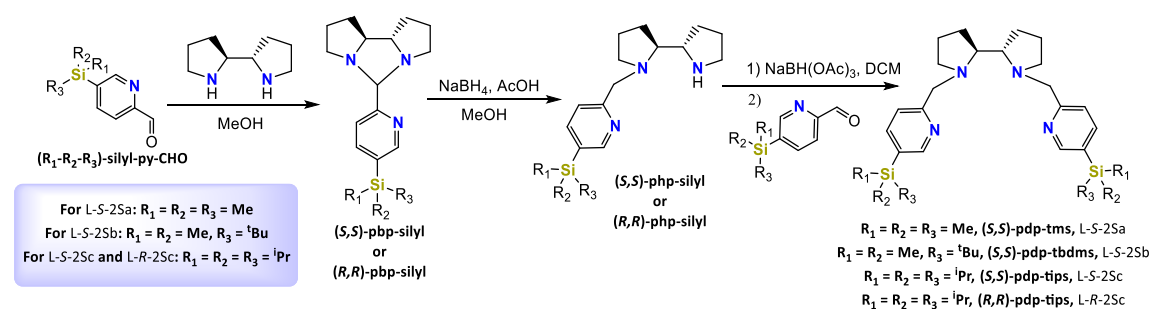
(S,S)-mcp-tbdms (L-S-1Sb) was synthesized following a procedure analogous to **(S,S)-mcp-tms** using **(S,S)-hcp-tbdms** (880 mg, 1.7 mmol). Purification was performed by alumina chromatographic column eluting with hexane:ethyl acetate (20:80) followed by

a silica chromatographic column eluting with CH₂Cl₂:CH₃OH:NH₄OH (91:8:1) to yield 490 mg (0.9 mmol, 55%) of the product as a white foam. ¹H-NMR (CDCl₃, 300 MHz, 300 K) δ, ppm: 8.56 (dd, J = 1.7, 0.9 Hz, 2H), 7.71 (dd, J = 7.7, 1.7 Hz, 2H), 7.58 (d, J = 7.6 Hz, 2H), 3.94 (d, J = 14.8 Hz, 2H), 3.81 (d, J = 14.8 Hz, 2H), 2.70-2.68 (m, 2H), 2.30 (s, 6H), 2.00-1.97 (m, 2H), 1.79-1.76 (m, 2H), 1.33-1.18 (m, 4H), 0.88 (s, 18H), 0.28 (d, J = 1.0 Hz, 12H). ¹³C-NMR (CDCl₃, 75 MHz, 300 K) δ, ppm: 161.7, 153.7, 142.5, 130.0, 122.1, 64.7, 60.5, 40.3, 36.8, 26.4, 25.8, 16.8, -6.3, -6.3. HRMS (ESI-TOF, [M + H]⁺): m/z calcd for C₃₂H₅₆N₄Si₂ 553.4116, found 553.4120.

(S,S)-mcp-tips (L-S-1Sc) was synthesized following a procedure analogous to **(S,S)-mcp-tms** using **(S,S)-hcp-tips** (1.1 g, 1.8 mmol). Purification was performed by alumina chromatographic column eluting with hexane:ethyl acetate (20:80) followed by a silica chromatographic column eluting with CH₂Cl₂:CH₃OH:NH₄OH (94:5:1) to yield 740 mg (1.3 mmol, 75%) of the product as a white foam. ¹H-NMR (CDCl₃, 300 MHz, 300 K) δ, ppm: 8.56 (s, 2H), 7.70 (dd, J = 7.8, 1.7 Hz, 2H), 7.560 (d, J = 7.7 Hz, 2H), 3.93 (d, J = 14.8 Hz, 2H), 3.81 (d, J = 14.8 Hz, 2H), 2.70-2.67 (m, 2H), 2.30 (s, 6H), 2.02-1.97 (m, 2H), 1.78-1.76 (m, 2H), 1.40 (dt, J = 14.7, 7.5 Hz, 6H), 1.28-1.15 (m, 4H), 1.08 (dd, J = 7.4, 0.7 Hz, 36H). ¹³C-NMR (CDCl₃, 75 MHz, 300 K) δ, ppm: 161.5, 154.4, 143.3, 127.4, 122.2, 64.7, 60.6, 36.8, 26.1, 25.8, 18.5, 10.7. HRMS (ESI-TOF, [M + H]⁺): m/z calcd for C₃₈H₆₈N₄Si₂ 637.5055, found 637.5040.

(R,R)-mcp-tips (L-R-1Sc) was synthesized following a procedure analogous to **(S,S)-mcp-tms** using **(R,R)-hcp-tips** (490 mg, 0.81 mmol) and the same purification protocol as for **(S,S)-mcp-tips** to yield 370 mg (0.58 mmol, 72%).

The pdp-based ligands (L-S-2Sa, L-S-2Sb, L-S-2Sc, L-R-2Sc) were synthesized as it follows (Scheme V.6).



Scheme V.6. Schematic representation of the synthesis of the pdp-based ligands (L-S-2Sa – L-R-2Sc).

(S,S)-pbp-tms. To an anhydrous methanol (15 mL) solution of (2*S*,2'*S*)-2,2'-bipyrrolide (420 mg, 3.0 mmol), 3 Å molecular sieves (500 mg) were added. **tms-py-CHO** (540 mg, 3.0 mmol) was then added to this mixture and stirred overnight under inert atmosphere. After that, the crude was diluted in CH₂Cl₂, filtered and concentrated in a rotatory evaporator to yield the desired product as a white solid (895 mg, 3 mmol, 99%). ¹H-NMR (CDCl₃, 400 MHz, 300 K) δ, ppm: 8.68 (dd, *J* = 1.6, 1.0 Hz, 1H), 7.78 (dd, *J* = 7.7, 1.8 Hz, 1H), 7.60 (d, *J* = 7.6 Hz, 1H), 4.91 (s, 1H), 3.54-3.42 (m, 2H), 3.04-2.99 (m, 1H), 2.66-2.59 (m, 2H), 2.42-2.39 (m, 1H), 2.16-2.12 (m, 1H), 2.0-1.62 (m, 7H), 0.28 (s, 9H). HRMS (ESI-TOF, [M + H]⁺): *m/z* calcd for C₁₇H₂₈N₃Si 302.2053, found 302.2046.

(S,S)-pbp-tbdms was synthesized following a procedure analogous to **(S,S)-pbp-tms** using **tbdms-py-CHO** (245 mg, 1.1 mmol) to yield 375 mg (1.1 mmol, 99%) of the desired product. ¹H-NMR (CDCl₃, 400 MHz, 300 K) δ, ppm: 8.62 (d, *J* = 0.9 Hz, 1H), 7.71 (dd, *J* = 7.7, 1.8 Hz, 1H), 7.53 (d, *J* = 7.7 Hz, 1H), 4.81 (s, 1H), 3.38-3.31 (m, 2H), 2.94-2.91 (m, 1H), 2.56-2.52 (m, 2H), 2.31-2.27 (m, 1H), 2.0.9-2.05 (m, 1H), 1.92-1.69 (m, 7H), 1.60-1.55 (m, 1H), 0.82 (s, 9H), 0.23 (d, *J* = 0.7 Hz, 6H).

(S,S)-pbp-tips was synthesized following a procedure analogous to **(S,S)-pbp-tms** using **tips-py-CHO** (420 mg, 1.6 mmol) to yield 550 mg (1.4 mmol, 89%) of the desired product. ¹H-NMR (CDCl₃, 300 MHz, 300 K) δ, ppm: 8.68 (s, 1H), 7.77 (dd, *J* = 7.7, 1.8 Hz, 1H), 7.60 (d, *J* = 7.7 Hz, 1H), 4.87 (s, 1H), 3.46-3.35 (m, 2H), 3.03-2.94 (m, 1H), 2.68-2.55 (m, 2H), 2.36-2.30 (m, 1H), 2.17-2.08 (m, 1H), 1.96-1.73 (m, 6H), 1.65-1.60 (m, 1H), 1.42 (dt, *J* = 14.8, 7.5 Hz, 3H), 1.08 (d, *J* = 7.4 Hz, 18H). ¹³C-NMR (CDCl₃, 75 MHz, 300 K) δ, ppm: 159.4, 155.1, 143.2, 128.4, 121.3, 88.3, 71.2, 70.8, 52.1, 47.4, 30.6, 28.8, 25.6, 24.9, 18.5, 10.6. HRMS (ESI-TOF, [M + H]⁺): *m/z* calcd for C₂₃H₃₉N₃Si 386.2986, found 386.2993.

(R,R)-pbp-tips was synthesized following a procedure analogous to **(S,S)-pbp-tms** using (2*R*,2'*R*)-2,2'-bipyrrolidine (135 mg, 1 mmol) **tips-py-CHO** (255 mg, 1 mmol) to yield 375 mg (1 mmol, 99%) of the desired product.

(S,S)-php-tms. **(S,S)-pbp-tms** (890 mg, 3 mmol) was dissolved in anhydrous methanol (15 mL) and cooled to 0 °C. At this point, 1.5 equiv of NaBH₄ (170 mg, 4.5 mmol) were slowly added. Afterwards, 4 equiv of AcOH (0.7 mL, 12 mmol) were added over 15 min. The mixture was stirred for 2 h at 0 °C, and then diluted with AcOEt (50 mL) and

hydrolyzed with 15 mL of NaOH 2 M. The aqueous layer was extracted with AcOEt (2 x 30 mL) and CH₂Cl₂ (2 x 30 mL). Finally, the combined organic layers were dried over MgSO₄ and brought to dryness. The desired product was obtained as a white solid (810 mg, 2.7 mmol, 90%). ¹H-NMR (CDCl₃, 400 MHz, 300 K) δ, ppm: 8.53 (s, 1H), 7.67 (dd, J = 7.6, 1.5 Hz, 1H), 7.30 (d, J = 7.7 Hz, 1H), 4.23 (d, J = 14.4 Hz, 1H), 3.57 (d, J = 14.4 Hz, 1H), 3.04-2.67 (m, 5H), 2.35-2.29 (m, 1H), 1.90-1.33 (m, 8H), 0.21 (s, 9H). ¹³C-NMR (CDCl₃, 100 MHz, 300 K) δ, ppm: 160.6, 153.2, 141.6, 132.7, 122.1, 67.9, 63.9, 62.5, 55.1, 46.3, 28.4, 24.8, 34.0, -1.3. HRMS (ESI-TOF, [M + H]⁺): m/z calcd for C₁₇H₃₀N₃Si 304.2209, found 304.2208.

(S,S)-php-tbdms was synthesized following a procedure analogous to **(S,S)-php-tms** using **(S,S)-pbp-tbdms** (375 mg, 1.1 mmol) to yield 275 mg (0.8 mmol, 73%) of the desired product. ¹H-NMR (CDCl₃, 400 MHz, 300 K) δ, ppm: 8.52 (d, J = 0.8 Hz, 1H), 7.67 (dd, J = 7.7, 1.7 Hz, 1H), 7.30 (d, J = 7.6 Hz, 1H), 4.23 (d, J = 14.3 Hz, 1H), 3.57 (d, J = 14.3 Hz, 1H), 3.02-2.68 (m, 5H), 2.34-2.32 (m, 1H), 1.87-1.46 (m, 8H), 0.81 (d, J = 1.6 Hz, 9H), 0.21 (d, J = 1.7 Hz, 6H). ¹³C-NMR (CDCl₃, 100 MHz, 300 K) δ, ppm: 160.5, 154.0, 142.6, 130.3, 122.0, 67.9, 63.9, 62.5, 55.2, 46.3, 28.3, 28.2, 26.3, 24.8, 23.9, 16.8, -6.4.

(S,S)-php-tips was synthesized following a procedure analogous to **(S,S)-php-tms** using **(S,S)-pbp-tips** (540 mg, 1.4 mmol) to yield 485 mg (1.25 mmol, 90%) of the desired product. ¹H-NMR (CDCl₃, 300 MHz, 300 K) δ, ppm: 8.57 (s, 1H), 7.75 (dd, J = 7.7, 1.7 Hz, 1H), 7.32 (d, J = 7.6 Hz, 1H), 4.22 (d, J = 14.6 Hz, 1H), 3.71 (d, J = 14.7 Hz, 1H), 3.26-3.21 (m, 1H), 3.11-2.98 (m, 3H), 2.86-2.79 (m, 1H), 2.55-2.47 (m, 1H), 2.02-1.73 (m, 7H), 1.63-1.51 (m, 1H), 1.41 (dt, J = 14.8, 7.4 Hz, 3H), 1.07 (d, J = 7.4 Hz, 18H). ¹³C-NMR (CDCl₃, 75 MHz, 300 K) δ, ppm: 159.8, 154.6, 143.7, 127.9, 122.2, 67.18, 63.4, 62.2, 45.6, 28.3, 28.2, 24.6, 24.1, 18.4, 10.6. HRMS (ESI-TOF, [M + H]⁺): m/z calcd for C₂₃H₄₁N₃Si 388.3143, found 388.3162.

(R,R)-php-tips was synthesized following a procedure analogous to **(S,S)-php-tms** using **(R,R)-pbp-tips** (375 mg, 1.0 mmol) to yield 350 mg (0.9 mmol, 90%) of the desired product.

(S,S)-pdp-tms (L-S-2Sa). **(S,S)-php-tms** (810 mg, 3 mmol) were dissolved in CH₂Cl₂ (50 mL) and cooled to 0 °C, and 1.3 equiv of NaB(AcO)₃ (827 mg, 3.9 mmol) were added to the reaction mixture, which was stirred for 30 min at 0 °C. **tms-silyl-py-CHO** (540 mg,

3.0 mmol) was added at this point, and the crude was stirred at room temperature overnight. It was then extracted with 40 mL of a NaHCO₃ aqueous saturated solution. The aqueous layer was washed with CH₂Cl₂ (2x 40 mL). The combined organic layers were dried over MgSO₄ and under vacuum. The product was purified by alumina column chromatography eluting with hexane:AcOEt (10:90) to afford 720 mg of a white solid (1.55 mmol, 52%). ¹H-NMR (CD₃OD, 300 MHz, 300 K) δ, ppm: 8.45 (dd, J = 7.7, 1.7 Hz, 2H), 7.88 (dd, J = 7.6, 1.7 Hz, 2H), 7.49 (d, J = 7.6 Hz, 2H), 4.25 (d, J = 14.4 Hz, 2H), 3.51 (d, J = 14.4 Hz, 2H), 3.00-2.98 (m, 2H), 2.81-2.77 (m, 2H), 2.27-2.24 (m, 2H), 1.97-1.74 (m, 8H), 0.31 (s, 18H). ¹³C-NMR (CD₃OD, 75 MHz, 300 K) δ, ppm: 160.1, 151.6, 142.3, 133.3, 122.6, 66.0, 60.4, 55.1, 26.2, 23.18, -2.73. HRMS (ESI-TOF, [M + H]⁺): m/z calcd for C₂₆H₄₂N₄Si₂ 467.3021, found 467.3022.

(S,S)-pdp-tbdms (L-S-2Sb) was synthesized following a procedure analogous to **(S,S)-pdp-tms** using **(S,S)-php-tbdms** (270 mg, 0.78 mmol), to yield 180 mg (0.33 mmol, 42%) of the desired product after purification by alumina column chromatography eluting with hexane:AcOEt (5:95). ¹H-NMR (CDCl₃, 400 MHz, 300 K) δ, ppm: 8.51 (s, 2H), 7.64 (d, J = 7.4 Hz, 2H), 7.30 (d, J = 7.4 Hz, 2H), 4.11 (d, J = 13.7 Hz, 2H), 3.41 (d, J = 13.7 Hz, 2H), 2.94-2.73 (m, 4H), 2.17-2.15 (m, 2H), 1.72-1.63 (m, 8H), 0.8 (s, 18H), 0.21 (s, 12H). ¹³C-NMR (CD₃OD, 75 MHz, 300 K) δ, ppm: 160.0, 152.5, 143.3, 130.9, 122.5, 66.0, 60.4, 55.1, 26.1, 25.4, 23.2, 16.2, -7.7. HRMS (ESI-TOF, [M + H]⁺): m/z calcd for C₃₂H₅₄N₄Si₂ 551.3960, found 551.3966.

(S,S)-pdp-tips (L-S-2Sc) was synthesized following a procedure analogous to **(S,S)-pdp-tms** using **(S,S)-php-tips** (485 mg, 1.25 mmol) to yield 470 mg (0.75 mmol, 60%) of the desired product after purification by alumina column chromatography eluting with hexane:AcOEt (50:50). ¹H-NMR (CD₃OD, 400 MHz, 300 K) δ, ppm: 8.47 (s, 2H), 7.88 (dd, J = 7.8, 1.7 Hz, 2H), 7.50 (d, J = 7.8 Hz, 2H), 4.15 (d, J = 14.2 Hz, 2H), 3.54 (d, J = 14.2 Hz, 2H), 2.99-2.97 (m, 2H), 2.71-2.69 (m, 2H), 2.27-2.25 (m, 2H), 1.74-1.66 (m, 8H), 1.44 (dt, J = 14.9, 7.5 Hz, 6H), 1.09 (dd, J = 7.5, 1.7 Hz, 36H). ¹³C-NMR (CD₃OD, 100 MHz, 300 K) δ, ppm: 159.9, 15.4, 144.2, 128.0, 122.8, 65.8, 60.5, 25.9, 23.1, 17.5, 10.4. HRMS (ESI-TOF, [M + H]⁺): m/z calcd for C₃₈H₆₆N₄Si₂ 635.4904, found 635.4904.

(R,R)-pdp-tips (L-R-2Sc) was synthesized following a procedure analogous to **(S,S)-pdp-tms** using **(R,R)-php-tips** (350 mg, 0.9 mmol) to yield 360 mg (0.6 mmol, 67%) of the

desired product after purification by alumina column chromatography eluting with hexane:AcOEt (50:50).

V.4.4 SYNTHESIS OF COMPLEXES

The iron complexes were obtained by two different procedures depending on the diamine backbone of the ligand. Their synthesis was performed as it follows.

[FeCl₂(L-S-1Sa)] (Cl-Λ-1Sa). Under N₂ atmosphere, FeCl₂ (57 mg, 0.45 mmol) was slowly added to a **(S,S)-mcp-tms** (L-S-1Sa) (210 mg, 0.45 mmol) solution in CH₃CN (3 mL). After overnight stirring, the desired product appeared as an orange solid, which was washed with CH₃CN (2 x 3 mL). HRMS (ESI-TOF, [M - Cl]⁺): m/z calcd for C₂₆H₄₄ClFeN₄Si₂ 559.2138, found 559.2148.

[Fe(CF₃SO₃)₂(L-S-1Sa)] (Λ-1Sa). AgCF₃SO₃ (231 mg, 0.90 mmol) was added to a stirring suspension of **Cl-Λ-1Sa** (0.45 mmol) in CH₃CN (3 mL) under inert atmosphere. The reaction mixture was stirred overnight, filtered through Celite® and evaporated to dryness. The solid was then redissolved in CH₂Cl₂ and crystallized by slow diethyl ether diffusion to yield the desired product as yellow crystals suitable for X-Ray diffraction (220 mg, 0.27 mmol, 60%). Anal. Calcd. for C₂₈H₄₄F₆FeN₄O₆S₂Si₂ (MW = 822.81 g/mol): N, 6.81; C, 40.87; H 5.39%. Found: N, 6.31; C, 41.18; H 5.15%. ¹H-NMR (400 MHz, CD₂Cl₂, 300K) δ, ppm: 166 (s), 116 (s), 67 (s), 50 (s), 48 (s), 20 (s), 17–(-3) (m). HRMS (ESI-TOF, [M - 2OTf]⁺): m/z calcd for C₂₆H₄₄FeN₄Si₂ 262.1227, found 262.1224.

[FeCl₂(L-S-1Sb)] (Cl-Λ-1Sb) was synthesized following a procedure analogous to **1Cl** using **(S,S)-mcp-tbdms** (L2) (143 mg, 0.26 mmol). HRMS (ESI-TOF, [M - Cl]⁺): m/z calcd for C₃₂H₅₆ClFeN₄Si₂ 643.3077, found 643.3087.

[Fe(CF₃SO₃)₂(L-S-1Sb)] (Λ-1Sb) was synthesized following a procedure analogous to **Λ-1Sa** using the suspension of **Cl-Λ-1Sb** (0.26 mmol). Yellow crystals suitable for X-Ray analysis were obtained after crystallization with THF/diethyl ether (155 mg, 0.17 mmol, 65%). ¹H-NMR (400 MHz, CD₂Cl₂, 300K) δ, ppm: 167 (s), 118 (s), 66 (s), 51 (s), 17 (s), 15 (s), 5.6–(-3.4) (m). HRMS (ESI-TOF, [M - 2OTf]⁺): m/z calcd for C₃₂H₅₆FeN₄Si₂ 304.1697, found 304.1723.

[Fe(Cl₂)(L-S-1Sc)] (Cl-Λ-1Sc) was synthesized following a procedure analogous to **Cl-Λ-1Sa** using **(S,S)-mcp-tips** (L-S-1Sc) (560 mg, 0.89 mmol). HRMS (ESI-TOF, [M - Cl]⁺): m/z calcd for C₃₈H₆₈ClFeN₄Si₂ 727.4016, found 727.4043.

[Fe(CF₃SO₃)₂(L-S-1Sc)] (Λ-1Sc) was synthesized following a procedure analogous to **Λ-1Sa** using the suspension of **Cl-Λ-1Sc** (0.89 mmol). Yellow crystals suitable for X-Ray diffraction were obtained after crystallization with CH₂Cl₂/hexane (510 mg, 0.52 mmol, 58%). Anal. Calcd. for C₂₈H₄₂F₆FeN₄O₆S₂Si₂ (MW = 820.79 g/mol): N, 5.65; C, 48.47; H 6.02%. Found: N, 5.78; C, 48.23; H 6.81%. ¹H-NMR (400 MHz, CD₂Cl₂, 300K) δ, ppm: 167 (s), 118 (s), 65 (s), 52 (s), 17 (s), 15 (s), 5.6 (s), 5.5 (s), 3.5–(-3.5) (m). HRMS (ESI-TOF, [M - 2OTf]⁺): m/z calcd for C₃₈H₆₈FeN₄Si₂ 346.2161, found 346.2197.

[Fe(Cl₂)(L-R-1Sc)] (Cl-Δ-1Sc) was synthesized following a procedure analogous to **Cl-Λ-1Sa** using **(R,R)-mcp-tips** (L-S-1Sc) (312 mg, 0.49 mmol).

[Fe(CF₃SO₃)₂(L-R-1Sc)] (Δ-1Sc) was synthesized following a procedure analogous to **Λ-1Sa** using a suspension of **Cl-Δ-1Sc** (0.49 mmol) to yield the desired product as yellow crystals after CH₂Cl₂/hexane crystallization (237 mg, 0.26 mmol, 53%).

[Fe(CF₃SO₃)₂(L-S-2Sa)] (Λ-2Sa). Under nitrogen atmosphere, a suspension of Fe(CH₃CN)₂(CF₃SO₃)₂ (140 mg, 0.32 mmol) in THF (2 mL) was added dropwise to a vigorously stirred solution of **(S,S)-pdp-tms** (L-S-2Sa) (150 mg, 0.32 mmol) in THF (3 mL). After overnight stirring, a yellow precipitate was formed. The mother liquor was separated, and the solid was dried, redissolved in CH₂Cl₂, filtered through Celite® and crystallized by slow diethyl ether diffusion to afford bright yellow crystals suitable for X-Ray diffraction (175 mg, 0.21 mmol, 67%). Anal. Calcd. for C₂₈H₄₂F₆FeN₄O₆S₂Si₂ (MW = 820.79 g/mol): N, 6.83; C, 40.97; H 5.16%. Found: N, 6.75; C, 40.94; H 4.89%. ¹H-NMR (400 MHz, CD₂Cl₂, 300K) δ, ppm: 177 (s), 120 (s), 78 (s), 49 (s), 30.6 (s), 27.8 (s), 17.1–14.4 (m), 3.6–(-4.0) (m), -9.2 (s), -17.8 (s). HRMS (ESI-TOF, [M - 2OTf]⁺): m/z calcd for C₂₆H₄₂FeN₄Si₂ 261.1143, found 261.1148.

[Fe(CF₃SO₃)₂(L-S-2Sb)] (Λ-2Sb) was synthesized following a procedure analogous to **Λ-2Sa** using **(S,S)-pdp-tbdms** (L-S-2Sb) (124 mg, 0.23 mmol). Yellow crystals suitable for X-Ray analysis were obtained (132 mg, 0.15 mmol, 65%). Anal. Calcd. for C₃₄H₅₄F₆FeN₄O₆S₂Si₂·(MW = 923.49 g/mol): N, 6.19; C, 45.13; H 6.01%. Found: N, 6.19; C,

45.06; H 5.76%. $^1\text{H-NMR}$ (400 MHz, CD_2Cl_2 , 300K) δ , ppm: 178 (s), 122 (s), 78 (s), 50 (s), 29.6 (s), 27.0 (s), 17.7-15.5 (m), 3.5-(-4.9) (m), -9.7 (s), -17.2 (s). HRMS (ESI-TOF, $[\text{M} - 2\text{OTf}]^+$): m/z calcd for $\text{C}_{32}\text{H}_{54}\text{FeN}_4\text{Si}_2$ 303.1619, found 303.1638.

$[\text{Fe}(\text{CF}_3\text{SO}_3)_2(\text{L-S-2Sc})]$ (Λ -2Sc) was synthesized following a procedure analogous to **Λ -2Sa** using **(S,S)-pdp-tips** (L-S-2Sc) (150 mg, 0.24 mmol). Yellow crystals suitable for X-Ray diffraction were obtained (148 mg, 0.15 mmol, 63%). Anal. Calcd. for $\text{C}_{40}\text{H}_{66}\text{F}_6\text{FeN}_4\text{O}_6\text{S}_2\text{Si}_2$ (MW = 989.11 g/mol): N, 5.66; C, 48.57; H 6.73%. Found: N, 5.64; C, 48.61; H 6.79%. $^1\text{H-NMR}$ (400 MHz, CD_2Cl_2 , 300K) δ , ppm: 178 (s), 123 (s), 77 (s), 51 (s), 29.0 (s), 27.0 (s), 17.8-16.0 (m), 2.1-0.73 (m), -9.9 (s), -17.7 (s). HRMS (ESI-TOF, $[\text{M} - 2\text{OTf}]^+$): m/z calcd for $\text{C}_{38}\text{H}_{66}\text{FeN}_4\text{Si}_2$ 345.2088, found 345.2095.

$[\text{Fe}(\text{CF}_3\text{SO}_3)_2(\text{L-R-2Sc})]$ (Δ -2Sc) was synthesized following a procedure analogous to **Λ -2Sa** using **(R,R)-pdp-tips** (L-R-2Sc) (260 mg, 0.41 mmol). The desired product was obtained as yellow crystals after CH_2Cl_2 /diethyl ether crystallization (285 mg, 0.29 mmol, 71%).

V.4.5 CRYSTAL DATA

The solid state structure of Λ -complexes and could be established by X-Ray diffraction analysis. Crystal data and refinement details are given in Table V.8 for mcp-based catalysts (**Λ -1Sa – Λ -1Sc**), and in Table V.9 for pdp-based complexes (**Λ -2Sa – Λ -2Sc**).

Table V.8. Crystal data and structure refinement details for complexes **Λ -1Sa – Λ -1Sc**.

Compound	Λ -1Sa	Λ -1Sb	Λ -1Sc
Empirical formula	C ₂₈ H ₄₄ F ₆ FeN ₄ O ₆ S ₂ Si ₂	C ₃₄ H ₅₆ F ₆ FeN ₄ O ₆ S ₂ Si ₂	C ₄₀ H ₇₂ F ₆ FeN ₄ O ₈ S ₂ Si ₂
Formula weight	822.82	906.98	1027.16
Temperature	100(2) K	100(2) K	100(2) K
Wavelength	0.71073 Å	0.71073 Å	0.71073 Å
Crystal system	Monoclinic	Orthorhombic	Orthorhombic
Space group	C2	P2(1)2(1)2	P 21 21 21
Unit cell dimensions	a = 21.164(8) Å α = 90° b = 13.532(5) Å β = 90.194(6)° c = 13.907(5) Å γ = 90°	a = 14.162(6) Å α = 90° b = 22.293(9) Å β = 90° c = 13.916(6) Å γ = 90°	a = 9.1671(10) Å α = 90° b = 17.5551(19) Å β = 90° c = 31.595(3) Å γ = 90°
Volume	3983(2) Å ³	4393(3) Å ³	5084.5(9) Å ³
Z	4	4	4
Density (calculated)	1.372 Mg/m ³	1.371 Mg/m ³	1.342 Mg/m ³
Absorption coefficient	0.613 mm ⁻¹	0.563 mm ⁻¹	0.498 mm ⁻¹
F(000)	1712	1904	2176
Reflections collected	30581	26795	31487
Independent reflections	9844 [R(int) = 0.0641]	10042 [R(int) = 0.1909]	11583 [R(int) = 0.0508]
Final R indices	R1 = 0.0593	R1 = 0.0884	R1 = 0.0704
[I > 2 σ (I)]	wR2 = 0.1170	wR2 = 0.1865	wR2 = 0.1704
R indices (all data)	R1 = 0.0868 wR2 = 0.1294	R1 = 0.3254 wR2 = 0.2890	R1 = 0.0946 wR2 = 0.1842

Table V.9. Crystal data and structure refinement details for complexes **Λ -2Sa** – **Λ -2Sc**.

Compound	Λ -2Sa	Λ -2Sb	Λ -2Sc
Empirical formula	C ₂₈ H ₄₂ F ₆ FeN ₄ O ₆ S ₂ Si ₂	C ₃₄ H ₅₄ F ₆ FeN ₄ O ₆ S ₂ Si ₂	C ₄₄ H ₇₆ F ₆ FeN ₄ O ₇ S ₂ Si ₂
Formula weight	820.80	904.96	1063.23
Temperature	100(2) K	100(2) K	100(2) K
Wavelength	0.71073 Å	0.71073 Å	0.71073 Å
Crystal system	Monoclinic	Orthorhombic	Orthorhombic
Space group	P 21	P2(1)2(1)2(1)	P 21 21 21
Unit cell dimensions	a = 10.705(19) Å α = 90° b = 15.26(3) Å β = 97.42(3)° c = 25.05(4) Å γ = 90°	a = 10.7624(14) Å α = 90° b = 14.9710(19) Å β = 90° c = 27.761(4) Å γ = 90°	a = 17.1929(8) Å α = 90° b = 17.8669(8) Å β = 90° c = 17.9032(8) Å γ = 90°
Volume	4056(13) Å ³	4472.9(10) Å ³	5499.6(4) Å ³
Z	4	4	4
Density (calculated)	1.344 Mg/m ³	1.344 Mg/m ³	1.284 Mg/m ³
Absorption coefficient	0.602 mm ⁻¹	0.553 mm ⁻¹	0.461 mm ⁻¹
F(000)	1704	1896	2256
Reflections collected	18424	70379	87970
Independent reflections	13630 [R(int) = 0.2182]	11068 [R(int) = 0.0535]	13622 [R(int) = 0.1038]
Final R indices	R1 = 0.1209	R1 = 0.0363	R1 = 0.0485
[I>2sigma(I)]	wR2 = 0.2339	wR2 = 0.0797	wR2 = 0.0846
R indices (all data)	R1 = 0.3548 wR2 = 0.3316	R1 = 0.0433 wR2 = 0.0831	R1 = 0.0763 wR2 = 0.0941

V.4.6 SYNTHESIS OF SUBSTRATES

trans-1,2-Dimethylcyclohexane (37), *trans*-decalin (41), 1,1-dimethylcyclohexane (45), *n*-heptane (26), and isopropylcyclohexane (96) were purchased from Aldrich or TCI America. *trans*-4-methyl-cyclohexanol, (+)-neomenthol, and *trans*-androsterone were

purchased from Aldrich or TCI America. All liquid substrates were passed through an alumina plug before being used.

trans-4-methylcyclohexyl pivalate (**11**), (+)-neomethyl pivalate (**75**), and *trans*-androsterone acetate (**82**) were synthesized according to published procedures.^{5,6,10}

V.4.7 REACTION CONDITIONS FOR CATALYSIS

V.4.7.1 *Sample analysis*

GC analysis of the catalysis provided substrate conversions and product yields relative to the internal standard integration. Calibration curves were obtained from commercial products when available or from pure isolated products obtained from a catalytic reaction.

n-heptanones, 1-decalone, 2-decalone, isopropylcyclohexanones, 2-cyclohexyl-2-propanol, and 1,1-dimethylcyclohexanones were purchased from Aldrich or TCI America. For non-commercially available products, pure samples were synthesized, isolated and characterized following the experimental procedures described in the literature.^{5,6,10}

V.4.7.2 *Reaction protocol for catalysis*

A 5 mL vial was charged with: Catalyst (1.2 μmol , 3 mol%), substrate (40 μmol , 1 equiv.), CH_3CN (0.8 mL) and a magnetic stir bar. A 1.74 M $\text{CH}_3\text{CO}_2\text{H}$ solution in CH_3CN was added (35 μL , 60 μmol , 150 mol%) and the vial was placed on an ice bath and stirred. The necessary amount of a 1.5 M (X equiv, see Table V.10) H_2O_2 solution (diluted from a 35% H_2O_2 aqueous solution) was delivered by syringe pump over 17 min at 0 °C. After syringe pump addition, the resulting solution was stirred for another 10 min. Biphenyl was added at this point as internal standard. The iron complex was removed by passing the solution through a short path of silica followed by elution with 2 mL of AcOEt. Finally, the solution was subjected to GC analysis.

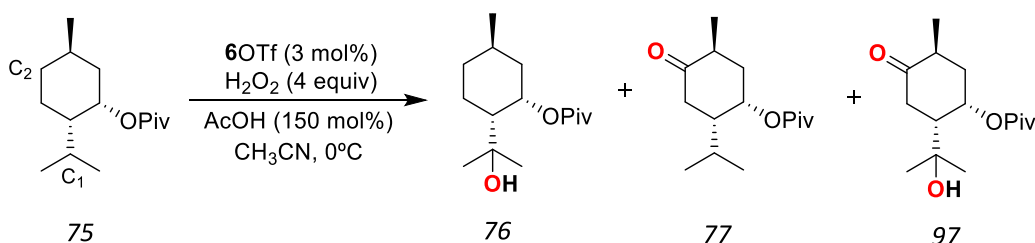
Table V.10. Conditions for the oxidation of substrates.

cat:H ₂ O ₂ :Substrate:AcOH (equiv of H ₂ O ₂)	Substrates
3:200:100:150 (2)	11, 37, 75, 96
3:250:100:150 (2.5)	82
3:280:100:150 (2.8)	41, 45
3:320:100:150 (3.2)	26

V.4.8 PROCEDURE FOR PRODUCT ISOLATION

Here we describe the oxidation catalysis protocol of (+)-neomenthyl pivalate (75, see Scheme V.7).

A 25 mL round bottom flask was charged with: Catalyst (12 μ mol, 3 mol%), (+)-neomenthyl pivalate (75) (0.4 mmol, 1 equiv), CH₃CN (8 mL) and a magnetic stir bar. A 1.74 M CH₃CO₂H solution in CH₃CN was added (0.35 mL, 0.6 mmol, 150 mol%) and the mixture was placed on an ice bath and stirred. 1.6 mmol (4 equiv) of a H₂O₂ solution (diluted from a 35% H₂O₂ aqueous solution) were delivered by syringe pump over 17 min at 0°C. After syringe pump addition, the solution was stirred for 10 min at 0°C. The iron complex was removed by passing the solution through a short path of silica followed by elution with 2 mL of AcOEt. Solvent was removed under reduced pressure and the resulting residue was purified by flash chromatography on silica gel over hexane:AcOEt (9:1). Purity of obtained products was checked by ¹H-NMR and GC, and yields corrected based on this results.

**Scheme V.7.** Catalytic oxidation of 75.

76. ¹H-NMR (400 MHz, CDCl₃, 300 K) δ , ppm: 5.36-5.35 (m, 1H), 1.95-1.89 (m, 1H), 1.87-1.81 (m, 1H), 1.78-1.60 (m, 3H), 1.44-1.39 (m, 1H), 1.22 (s, 9H), 1.20 (s, 3H), 1.16 (s,

3H), 1.11-0.91 (m, 2H), 0.88 (d, $J = 6.6$ Hz, 3H). In agreement with that reported in the literature.⁶

77. ¹H-NMR (400 MHz, CDCl₃, 300 K) δ , ppm: 5.27 (m, 1H), 2.62-2.49 (m, 2H), 2.44-2.30 (m, 2H), 1.60-1.50 (m, 3H), 1.25 (s, 9H), 1.01 (d, $J = 6.6$ Hz, 3H), 0.92 (d, $J = 6.9$ Hz, 3H), 0.88 (d, $J = 6.5$ Hz, 3H). In agreement with that reported in the literature.⁶

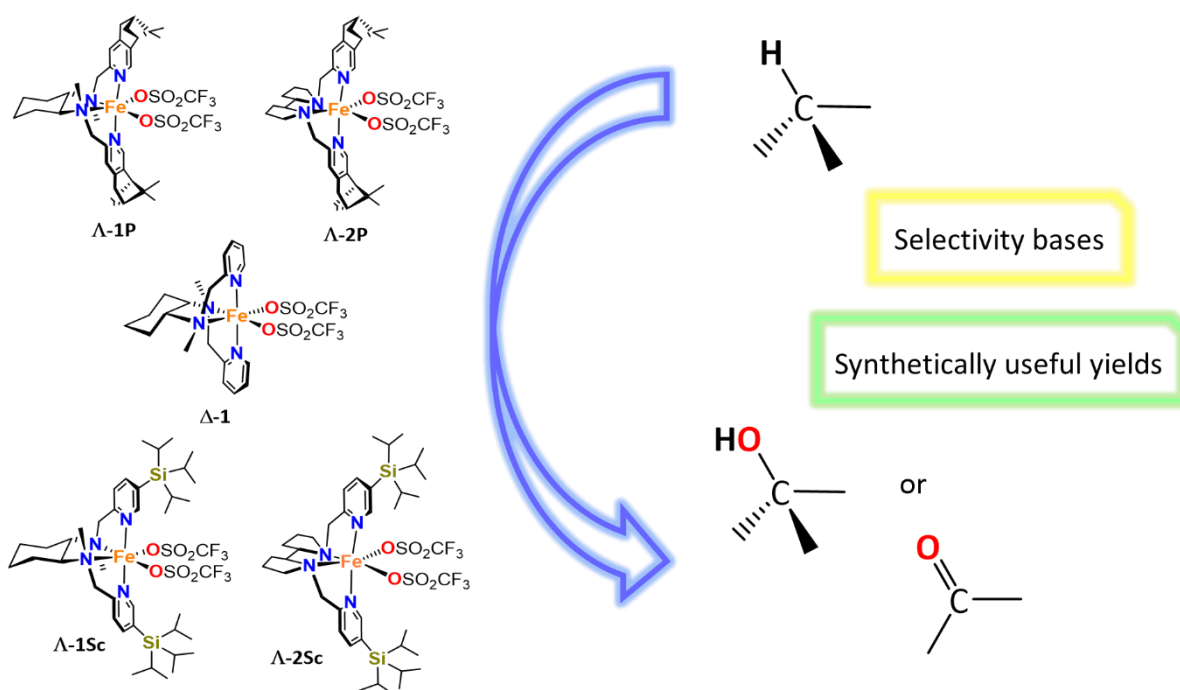
97. ¹H-NMR (400 MHz, CDCl₃, 300 K) δ , ppm: 5.49-5.48 (m, 1H), 2.77 (dt, $J = 13.9$, 0.9 Hz, 1H), 2.67-2.60 (m, 1H), 5.52 (ddd, $J = 13.8$, 4.1, 1.3 Hz, 1H), 2.52 (ddd, $J = 14.6$, 6.0, 3.4 Hz, 1H), 1.96 (ddd, $J = 14.1$, 4.0, 2.1 Hz, 1H), 1.56-1.48 (m, 2H), 1.27 (s, 9H), 1.26 (s, 3H), 1.19 (s, 3H), 1.04 (d, $J = 1.04$ Hz, 3H). ¹³C-NMR (75 MHz, CDCl₃, 300 K) δ , ppm: 211.1, 177.0, 70.75, 68.6, 50.6, 38.3, 37.8, 30.8, 29.4, 28.0, 26.8, 26.5, 13.2. HRMS (ESI-TOF, [M + Na]⁺): m/z calc for C₁₅H₂₆O₄Na 293.1723, found 293.1731.

V.5 REFERENCES

- (1) Dyker, G. *Handbook of C-H Transformations*; Wiley-VCH: Weinheim, 2005; Vol. 1-2.
- (2) Davies, H. M. L.; Manning, J. R. *Nature* **2008**, *451*, 417.
- (3) Gutekunst, W. R.; Baran, P. S. *Chem. Soc. Rev.* **2011**, *40*, 196.
- (4) Sun, C.-L.; Li, B.-J.; Shi, Z.-J. *Chem. Rev.* **2011**, *111*, 1293.
- (5) Gómez, L.; Garcia-Bosch, I.; Company, A.; Benet-Buchholz, J.; Polo, A.; Sala, X.; Ribas, X.; Costas, M. *Angew. Chem. Int. Ed.* **2009**, *48*, 5720.
- (6) Gómez, L.; Canta, M.; Font, D.; Prat, I.; Ribas, X.; Costas, M. *J. Org. Chem.* **2013**, *78*, 1421.
- (7) Chen, M. S.; White, M. C. *Science*, **2007**, *318*, 783.
- (8) Prat, I.; Gómez, L.; Canta, M.; Ribas, X.; Costas, M. *Chem. Eur. J.* **2013**, *19*, 1908.
- (9) Chen, M. S.; White, M. C. *Science*. **2010**, *327*, 566.
- (10) Canta, M.; Font, D.; Gómez, L.; Ribas, X.; Costas, M. *Adv. Synth. Catal.* **2014**, *356*, 818.
- (11) Meunier, B. *Chem. Rev.* **1992**, *92*, 1411.
- (12) Gormisky, P. E.; White, M. C. *J. Am. Chem. Soc.* **2013**, *135*, 14052.
- (13) White, M. C.; Doyle, A. G.; Jacobsen, E. N. *J. Am. Chem. Soc.* **2001**, *123*, 7194.
- (14) England, J.; Britovsek, G. J. P.; Rabadia, N.; White, A. J. P. *Inorg. Chem.* **2007**, *46*, 3752.

-
- (15) Mas-Ballesté, R.; Costas, M.; Berg, T. v. d.; Que Jr., L. *Chem. Eur. J.* **2006**, *12*, 7489.
- (16) Ryu, J. Y.; Kim, J.; Costas, M.; Chen, K.; Nam, W.; Que Jr., L. *Chem. Commun.* **2002**, *12*, 1288.
- (17) Chen, K.; Que Jr., L. *Chem. Commun.* **1999**, *38*, 2227.
- (18) Suzuki, K.; Oldenburg, P. D.; Que Jr., L. *Angew. Chem. Int. Ed.* **2008**, *47*, 1887.
- (19) Hagen, K. S. *Inorg. Chem.* **2000**, *39*, 5867.
- (20) Chen, K.; Que Jr., L. *J. Am. Chem. Soc.* **2001**, *123*, 6327.
- (21) Costas, M.; Tipton, A. K.; Chen, K.; Jo, D.-H.; Que Jr., L. *J. Am. Chem. Soc.* **2001**, *123*, 6722.
- (22) Zang, Y.; Kim, J.; Dong, Y.; Wilkinson, E. C.; Appelman, E. H.; Que Jr., L. *J. Am. Chem. Soc.* **1997**, *119*, 4197.
- (23) Kille, S.; Zilli, F. E.; Acevedo, J. P.; Reetz, M. T. *Nat. Chem.* **2011**, *3*, 738.
- (24) Salvador, J. A. R.; Silvestre, S. M.; Moreira, V. M. *Curr. Org. Chem* **2012**, *16*, 1243.
- (25) Zhang, Y. Y.; Yang, L. *Expert Opin. Drug Metab. Toxicol.* **2009**, *5*, 621.
- (26) K. Monostory, Z. D. *Curr. Drug Metab.* **2011**, *12*, 154.
- (27) Breslow, R.; Huang, Y.; Zhang, X.; Yang, J. *Proc. Acad. Sci. USA* **1997**, *94*, 11156.
- (28) Breslow, R.; Zhang, X.; Huang, Y. *J. Am. Chem. Soc.* **1997**, *7863*, 11648.

GENERAL DISCUSSION



VI. GENERAL DISCUSSION

The oxidation of hydrocarbons in a selective manner is one of the most important reactions for organic synthesis in chemical and pharmaceutical industry, as well as in academic research. It is so because this transformation converts alkanes, which are rather inert compounds, into functionalized molecules that serve as relevant scaffolds and intermediates for elaborated chemical syntheses.¹ In contrast to traditional methodologies which rely in harsh conditions and, stoichiometric processes, current approaches involve the development of strategies based on green oxidants and first row transition metal-based catalysts that operate under mild conditions, while retaining analogous or even improved efficiency and selectivity.²

Toward this end, the bioinspired approach in the development of oxidation catalysts offers an interesting alternative. It involves the design of synthetic complexes of biologically relevant metals that mimic structural characteristics of the enzyme to reproduce the basic aspects of its reactivity. However, literature precedents indicate that it is not necessary to closely mimic the enzyme active site, and simple coordination complexes can engage in oxidation reactions characteristic of enzymes. In order to develop simple and synthetically useful oxidation catalysts, the minimum structural aspects that enable this reactivity should be identified.³ Even though several iron complexes have been studied in catalytic C—H group oxidation reactions, only few examples exhibiting good efficiency and selectivity without the involvement of Fenton-type free diffusing radicals have been described up to date.⁴ Early work by Que and co-workers showed that non-heme iron coordination complexes ligated to oxygen and nitrogen based ligands, and with two labile coordination sites, appear to be capable of reproducing metal based oxidation activity when reacting with H₂O₂.² Consequently, coordination complexes that fulfill these rather simple structural motives have been explored as potential oxidation catalysts.⁵

In this PhD thesis we have explored two novel families of N-based tetradentate iron catalysts that involve bulky substituents at the ligand architecture, creating sterically demanding active sites. These complexes are shown to exhibit enhanced

catalytic activity in C—H oxidation reactions, and also exhibit remarkable C—H regioselectivity. In parallel, a related but structurally simpler iron complex has been identified as a very convenient tool capable of efficiently oxidizing tertiary and secondary C—H groups, in product yields amenable for synthetic purposes. The latter is an important aspect. While C—H oxidation with iron complexes have been explored for decades, they have been usually employed under conditions of large excess of substrate. Therefore, these reactions have very little synthetic utility. The challenge of the work is to find catalyst that operate in a selective manner and provide product yields that could be amenable for organic synthesis purposes.

VI.1 REGIOSELECTIVE OXIDATION OF NONACTIVATED ALKYL C—H GROUPS USING HIGHLY STRUCTURED NON-HEME IRON CATALYSTS

In Chapter III, a family of complexes based on linear N₄-tetradentate pinene-substituted ligands has been presented (Figure VI.1).

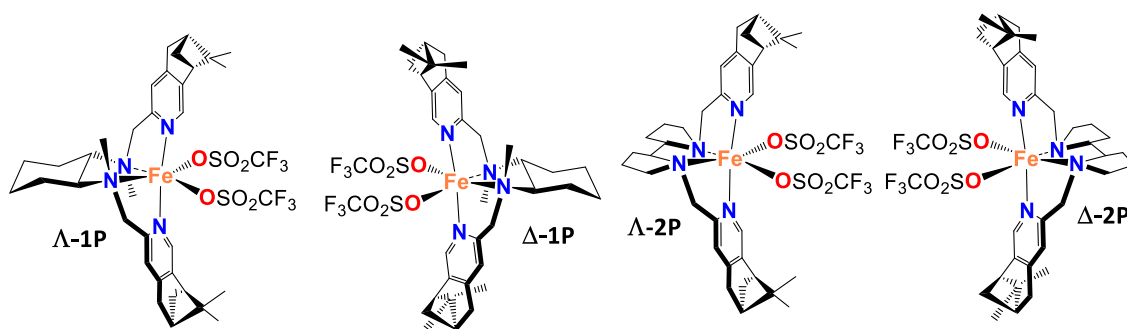


Figure VI.1. Pinene-substituted catalysts employed in Chapter III

VI.1.1 CATALYST DESIGN AND CATALYST HIGHLY ORDERED STRUCTURES

The ligand architecture has been modified with pinene groups attached at the 4th and 5th position of the pyridine, with the purpose of creating sterically hindering ligands that can protect the iron center without compromising catalyst stability, as occurs when 6th position of the pyridine are derivatized.^{6,7} This class of linear tetradentate ligands forms octahedral complexes that present chirality at the metal (Λ and Δ). The catalysts present a *cis-α* topological geometry; the two nitrogen atoms of the pyridine rings are mutually in *trans* configuration, while the two aliphatic nitrogen atoms are mutually in *cis*. This analysis also shows that the chirality at the metal is

determined by the chirality of the chiral diamine backbone; (*S,S*)-*trans*-diaminocyclohexane and (*S,S*)-2,2'-bipyrrrolidine give rise to Λ complexes, while Δ complexes are formed with tetradentate ligands based in the analogous (*R,R*) diamines.

Space filling diagrams of the crystal structures of the full set of catalysts show that the chirality at the metal also dictates the relative orientation of the methyl groups at the pinene moiety. In Λ catalysts the methyl groups are pointing toward the iron labile sites, creating a well-defined cavity around the metal active site. This cavity was envisioned to be important for preventing deactivation pathways that usually involve dimerization *via* formation of oxo-bridged diferric species. Inhibition or limitation of this pathway was planned to give rise to more robust and efficient catalysts for C—H oxidation reactions. Moreover, the combination of steric hindrance at the metal center and the chirality of the catalysts (Λ or Δ) along with the nature of the diamine backbone (*trans*-1,2-diaminocyclohexane or 2,2'-bipyrrrolidine) was envisioned to provide structurally rich iron sites, that will translate in structural bias in defining the C—H selectivity exhibited by these oxidants.

VI.1.2 OPTIMIZATION OF THE CATALYTIC REACTIONS

This set of complexes was studied in C—H oxidation reactions. The experimental conditions reported by Gómez and coworkers involved several additions of catalyst and H₂O₂.⁸ For convenience, in this work a simpler protocol was evaluated, which involved a single addition of H₂O₂ over an acetonitrile solution of 3 mol% catalyst, acetic acid and substrate at 0 °C. In the oxidation of *cis*-4-methyl-cyclohexylpivalate (**7**) and cyclohexane (**9**), it has been shown that this simpler set of conditions provides preparative useful yields based on product converted into oxidation products (51-75%). In the oxidation of **7**, the tertiary alcohol is exclusively obtained, while the oxidation of **9** affords cyclohexanone as the sole oxidation product, presumably *via* a 2-step oxidation (see Table III.1 for results).

Comparative analysis of the performance of the different catalysts show that Λ complexes, which contain structurally better defined active sites, provide better product yields and selectivities. These catalysts also retain their activity when reacted with a second addition of oxidant (H₂O₂) demonstrating that deactivation pathways are

limited, as initially planned (see Figure III.3 and Figure III.4 for results). In contrast, this is not observed for the Δ related complexes nor for the simpler Λ complexes lacking the pinene rings (Figure VI.2).

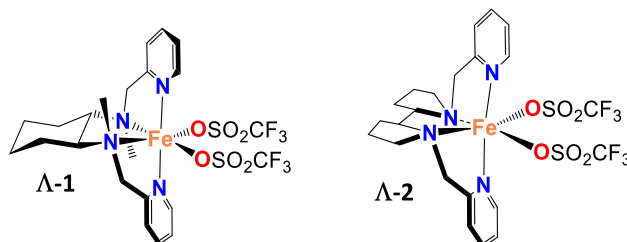


Figure VI.2. Related complexes lacking the pinene rings utilized in Chapter III.

Product yields are dependent on the catalyst employed, but in order to focus the comparison among catalysts on the basis of selectivities, standard conditions that could provide comparable product yields for all catalysts have been initially investigated. The amount of oxidant (hydrogen peroxide, added via syringe pump over 17 min) used is dependent on the substrate to be oxidized. Some substrates require milder conditions in order to avoid the formation of overoxidized products and therefore only 1 mol% catalyst has been used (see Table III.1-Table III.4 for specific cases). More interestingly, the new protocol is not only operationally more simple than the previously described by Gómez et al,⁸ but also most catalysts exhibit an improved performance when subjected to this method.

VI.1.3 INVESTIGATION ON THE FACTORS GOVERNING SELECTIVITY IN C—H OXIDATIONS

The factors governing site selectivity in the C—H oxidation of simple substrates was investigated. It is shown that the oxidizing species have electrophilic character and, when confronted with structurally similar sites, they oxidize preferentially the electronically richer C—H bond. In addition, the active species appear to oxidize preferentially tertiary over secondary C—H groups, presumably responding to the lower bond dissociation energy (DBE) exhibited by the former C—H sites when compared to the latter. Reaction patterns also rule out the involvement of long-lived carbon-centered radicals, since reactions are stereospecific. Moreover, ketone products can also be formed via a two-step oxidation of the C—H groups into their corresponding alcohols, which are further oxidized to the ketone products. In cyclohexane derivatives, the

orientation of the C—H group to be oxidized turns out to be determinant for the regioselectivity of the process: since a strain release of the 1,3-diaxial interactions occurs in the rate determining C—H bond-breaking step, thus tertiary C—H groups in equatorial position are more prone to oxidation than axial groups (Figure VI.3). Therefore, tertiary alcohols can be obtained in high selectivity when a tertiary C—H group is in equatorial position, while when they are positioned in axial orientation oxidation occurs preferentially at secondary sites (see Table III.4 and Table III.5 for results).

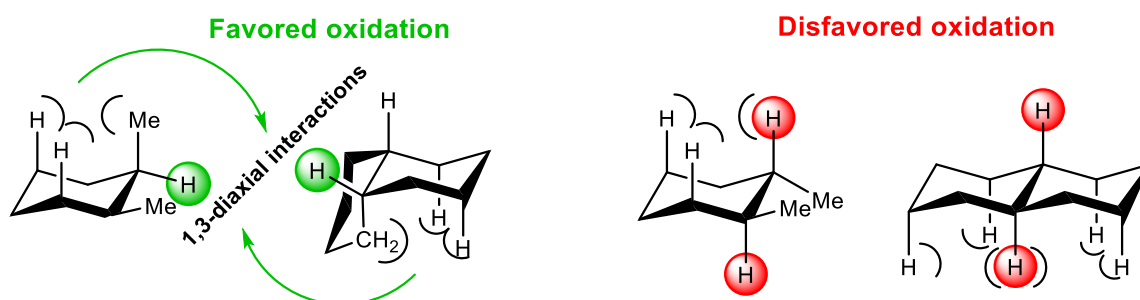


Figure VI.3. Influence of chair conformation orientation in C—H group oxidations of cyclohexane-based substrates.

On the other hand, the steric constraint imposed by the substrate also plays a crucial role in defining the C—H regioselectivity exhibited by the complexes: shielding of the tertiary sites is translated in an enhanced preference for oxidizing secondary C—H groups. More interestingly, the selectivity appears to be dependent on the structure of the catalysts, and diaminocyclohexane-based catalysts (**1P**) show the best selectivities toward methylenic sites. Moreover, **1P** catalysts exhibit remarkable discrimination among methylenic sites, favoring oxidation at the least hindered position. This trend is not observed with the related catalysts **2P** or **2** (see Table III.3, substrates **23** and **26**, and Table III.5 and Table III.6). We attribute this fact to the more effective steric constraints imposed by cyclohexyl *N*-methyl groups staying in close proximity to the iron center than those exerted by the bipyrrolidine backbone.

VI.1.4 CATALYTIC APPLICATION TO THE OXIDATION OF COMPLEX ORGANIC MOLECULES

The high efficiency and selectivity of such catalysts highlights their potential utility in the oxidation of structurally complex organic molecules. In this regard, the oxidation of sesquiterpenes **49** and **51** (Figure VI.4) occurred with exquisite selectivity, affording a single oxidation product (**50** and **52**, respectively) regardless of the catalyst

employed (see Table III.7 and Table III.8 for results). This fact can be rationalized on the basis of the nature of the substrates, by hyperconjugative effect of the ether moiety in 49, and by the deactivating character of the acetate group plus the rigid nature of the tricycle in 51.

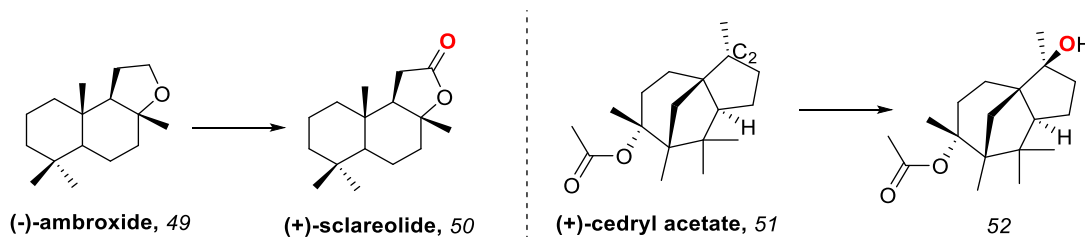


Figure VI.4. Structure of sesquiterpenes 49 and 51 oxidized in Chapter III.

In contrast to the substrate-based regioselectivity observed in the previously described cases, a more interesting approach is to utilize this family of catalysts to divert the selectivity in C—H group oxidation reactions. This is especially relevant in molecules where different factors are in competition: sterics, activating/deactivating effects, and chirality on the substrate. When combined with different steric and chiral features on the catalysts, it is shown that catalysts give rise to diverse selectivity based on the catalyst architecture. Two relevant examples are the oxidation of menthyl derivative 75 and sesquiterpene 50 (Figure VI.5). In the former case, only by changing the chirality of the catalyst (Λ -1P or Δ -1P) alcohol 76 or ketone 77 can be selectively obtained in moderate yields (see Table III.12). On the latter case, ketones 78, 79, and 80 can be selectively obtained in moderate yields using Λ -2P, Δ -1P and Λ -2P, respectively, under appropriate experimental conditions (see Table III.15 for results). Although individual yields could be regarded as modest, they are suitable for synthetic purposes and, more interestingly, their value becomes most evident when considering that 78 had only previously been synthesized by biological methods.⁹ Moreover, this switch in selectivity among secondary sites with nonenzymatic systems finds exclusive precedent in sterically hindered metalloporphyrins.^{10,11}

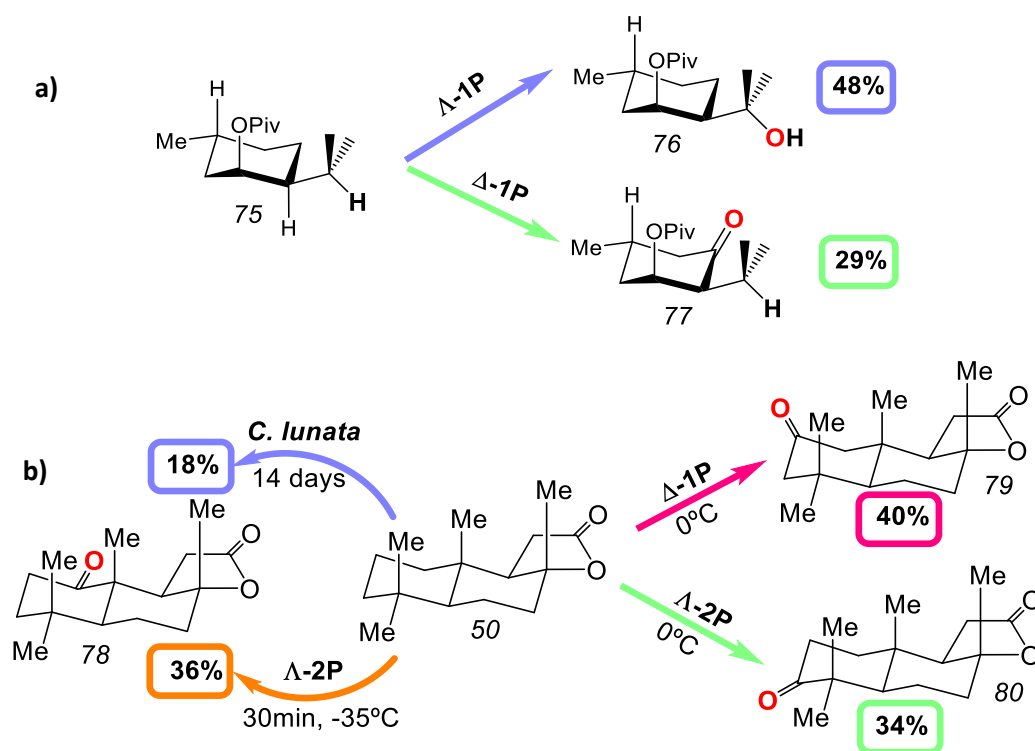


Figure VI.5. Catalyst-based diverted selectivity. **a)** Oxidation of 75. **b)** Oxidation of 50.

VI.2 THE IRON(II) COMPLEX $[\text{Fe}(\text{CF}_3\text{SO}_3)_2(\text{MCP})]$ AS A CONVENIENT, READILY AVAILABLE CATALYST FOR THE SELECTIVE OXIDATION OF METHYLENIC SITES IN ALKANES

In Chapter III we have shown that the nature of the diamine backbone in the catalyst architectures is determinant in defining the C—H selectivity of the oxidation reactions. **1P** catalysts (Λ and Δ) are pinene-derived complexes based on *trans*-1,2-diaminocyclohexane that show enhanced selectivity towards the oxidation of methylenic sites in comparison with their analogous 2,2'-bipyrrrolidine-based catalysts **2P**. Focusing in these findings, in Chapter IV we have studied the performance of a structurally simpler catalyst **1** (Λ and Δ), which lacks the pinene rings, in the oxidation of methylenic sites in synthetically useful conditions. Moreover, we have compared it with other previously described catalysts Λ -**2SbF₆**¹² and **3**¹³, showing an enhanced preference of **1** for secondary site oxidations (Figure VI.6).

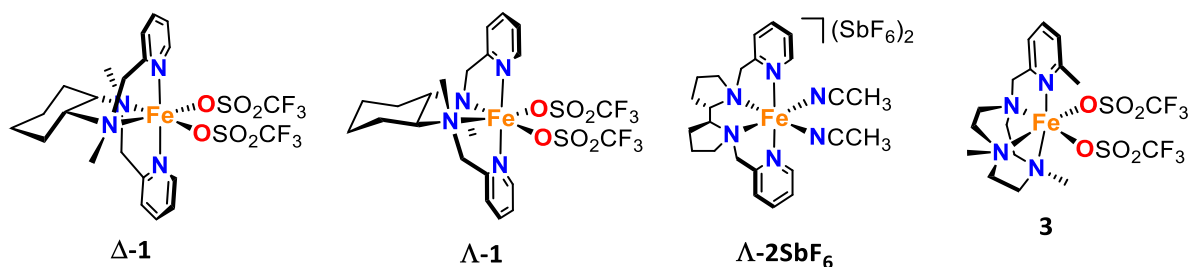


Figure VI.6. Structurally simple catalysts for efficient oxidation of methylenic sites.

The remarkable feature of catalyst **Λ-1** is its simplicity, which allows it to be obtained on a multigram scale. This fact is particularly interesting since oxidation reactions can be performed on a gram scale with low loadings of a non-expensive catalyst, contrary to **Λ-2SbF₆**.¹² Herein we have shown that we can obtain more than 4 g of **Λ-1** in good to excellent yield.

VI.2.1 OPTIMIZATION OF THE CATALYTIC PROTOCOL FOR OXIDATION REACTIONS

The optimized conditions for the oxidation of tertiary and secondary sites were found to be two additions of 3 mol% catalyst, hydrogen peroxide (amount dependent on substrate) and 5 equiv of AcOH (see Section IV.4.5.3 for details). In addition, we discarded any effect of the catalyst anion on the outcome of the reaction, since virtually identical catalytic performance was obtained in terms of yield and selectivity when using triflate (**1**) and SbF₆⁻ (**1SbF₆**) anions in the catalyst structure (see Table IV.1 and Table IV.2, entries 10 and 11). Comparative studies also demonstrated higher efficiency and selectivity of **Λ-1** when compared to **2** and **5** ([Fe(CF₃SO₃)₂(mep)] mep = *N,N'*-dimethyl-*N,N'*-bis(2-pyridylmethyl) ethylenediamine)^{14,15} under the same experimental conditions (see Table IV.1 and Table IV.2, entries 10-12 and 10-13, respectively).

VI.2.2 SUBSTRATE SCOPE AND SELECTIVITY BASES IN C—H OXIDATIONS

Catalysts **Λ-1** and **Δ-1** were tested in the oxidation of several substrates bearing tertiary and secondary C—H bonds. The selectivity bases observed were in concordance with those established in Chapter III for pinene-based catalysts, and similar albeit slightly lower yields were obtained. In order to compare the regioselectivity among different iron catalysts in C—H oxidation reactions, the oxidation of *trans*-1,2-dimethylcyclohexane (**37**) and *trans*-decalin (**41**) were analyzed under the same experimental conditions. It was shown that, irrespective of the catalyst employed,

oxidation occurred preferentially at secondary sites. This trend was most enhanced with catalysts **Λ-1** and **3**. However, the most interesting observation was that discrimination between the two secondary sites in **37** and **41** was highly dependent on the nature of the catalyst: only diaminocyclohexane-based catalysts **Λ-1** and **Λ-1P**¹⁶ oxidized preferentially the least sterically congested C—H groups, while **Λ-2** and **3** showed basically no preference for any of the two secondary sites. Therefore, the structurally simple catalyst **Λ-1** is capable of oxidizing alkanes in good yields and notable regioselectivity among multiple methylenic sites on the basis of steric arguments.

VI.2.3 OXIDATION OF NATURAL PRODUCTS AND MULTIGRAM-SCALE OXIDATIONS

In order to further substantiate these results, we tested the performance of catalysts **Λ-1**, **Δ-1** and *rac-1* in the oxidation of androsterone derivatives, which oxidation presents biological interest.¹⁷ Good yields were obtained in these oxidations, in contrast to the more moderate yields afforded by **Λ-2**, **Δ-2** and **5**. Selectivity appeared to be dependent on the chirality of the catalyst, on the nature of the diamine backbone and on the chirality of the substrate. The best selectivity for the least sterically hindered position (see Table IV.6, entry 6) was achieved using **Λ-1** and *cis*-androsterone acetate. This results will be further discussed in section VI.3 of this chapter, along with the results afforded by their related silyl-based catalysts presented in Chapter V.

Moreover, in order to show the synthetic value of this methodology, a sesquiterpene, **50**, and a steroid, **82**, were oxidized in multigram scale using **Λ-1** as catalyst. In these two cases, product yields and selectivity can be reasonably inferred from small scale reactions, which emphasizes the convenience of this protocol for the large-scale C—H oxidation reactions of natural products.

VI.3 A NEW FAMILY OF IRON CATALYSTS INCORPORATING BULKY SILYL GROUPS FOR EFFICIENT AND REGIOSELECTIVE OXIDATION OF ALKANES

In order to get further insight on how the steric control of the catalysts affects C—H selectivity, we have designed a new family of N₄-tetradentate iron complexes that introduce systematically bulkier substituents at the pyridine 5th position (Figure VI.7).

Interestingly, such catalysts can be relatively easily obtained in comparison to their pinene counterparts.^{8,16}

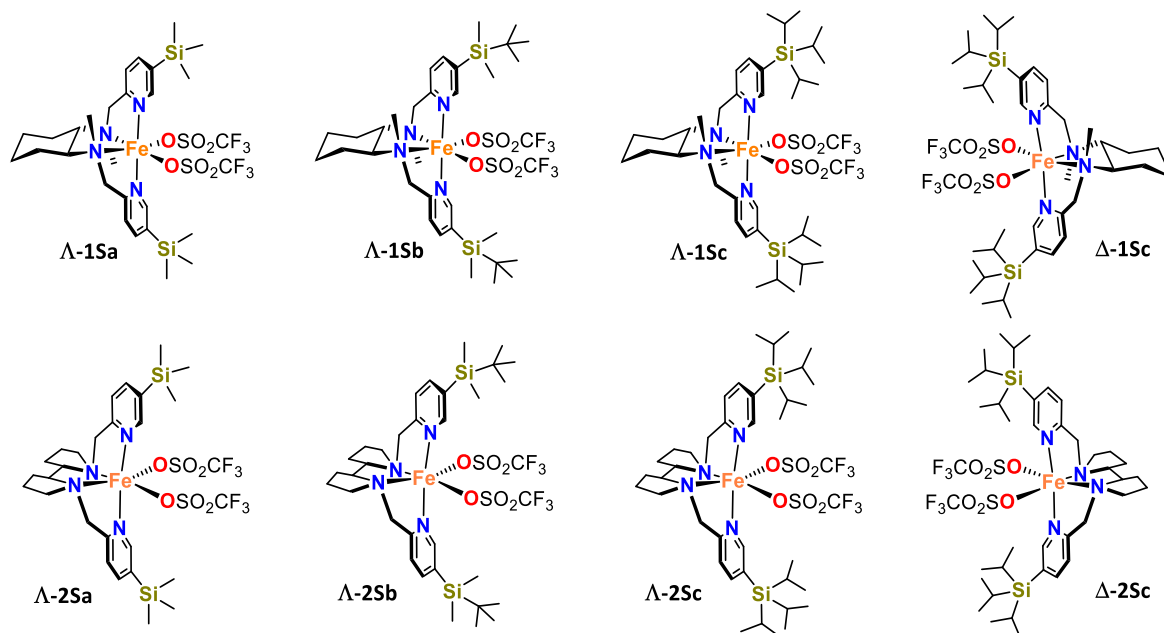


Figure VI.7. New family of silyl-based catalysts employed in Chapter V.

VI.3.1 LIGAND SYNTHESSES AND COMPLEX CHARACTERIZATION

For the synthesis of the ligands, two different types of diamine backbones have been used: *trans*-1,2-diaminocyclohexane and 2,2'-bipyrrrolidine. In combination with that, three different silyl-substituents (trimethylsilyl (tms), tert-butyldimethylsilyl (tbdms) and triisopropylsilyl (tips)) at the 5th position of the pyridine give rise to 6 different ligands. In addition, for the particular case of tips-derived ligands, the corresponding enantiomers using (*R,R*)-diamines have also been synthesized.

Diaminocyclohexane-based ligands were reacted with FeCl₂ and AgOTf (OTf = triflate) to afford the corresponding iron(II) triflate complexes. On the other hand, bipyrrrolidine-based ligands were transformed into their corresponding iron (II) triflate complexes by direct reaction with FeOTf₂. In all cases, C₂ pseudo-symmetry complexes were obtained, as confirmed by X-Ray diffraction (XRD) analysis. In addition, they adopt *cis-α* geometrical topology, with the two nitrogen atoms of the pyridine rings in mutually *trans* configuration and the two aliphatic nitrogen atoms mutually in *cis*. Measured Fe-N distances were indicative of high-spin Fe^{II} complexes.

Very interestingly, the space-filling analyses of such complexes (see Figure V.4) reveal the more sterically demanding silyl groups (tms < tbdms < tips) create a more well-defined cavity at the proximity of the metal center.

VI.3.2 COMPARATIVE OXIDATION CATALYSIS WITH SIMPLE SUBSTRATES

Steric hindrance in the catalysts appears to have an impact on the outcome of C—H oxidation reactions using hydrogen peroxide, affording more efficient catalysts (~20% yield increase comparing **A-1Sc** to **1**, and **A-2Sc** to **2**), presumably by preventing degradation of the catalyst *via* dimerization. Besides, it does also affect the regioselectivity of the processes. In general, mcp-based (mcp = *N,N'*-dimethyl-*N,N'*-bis(2-pyridylmethyl) cyclohexane-*trans*-1,2-diamine) catalysts are more prone to oxidize methylenic sites than their 2,2'-bipyrrolidine analogues. In addition, the introduction of bulky silyl groups (tips) in the ligand further strengthens the preference for methylenic site oxidation, and higher discrimination among them, favoring the oxidation of the least sterically encumbered C—H group (see Table V.3, Table V.4 and Table V.5). A particularly remarking result arises from the oxidation of *trans*-decalin with catalyst **A-1Sc**, which shows a secondary site vs tertiary site oxidation ratio of 99.0, in contrast to the 20.0 ratio observed with catalyst **A-1Sa**.

VI.3.3 APPLICATION TO THE OXIDATION OF COMPLEX MOLECULES

Do to the potential of **A-1Sc** and **A-2Sc** observed in the selective oxidation of simple substrates we sought to explore its performance in the oxidation of more complex molecules, such as natural products. Particularly interesting is the oxidation of (+)-neomenthyl pivalate **75** with catalyst **A-2Sc** (see Figure V.7), which can give the ketone product **77** in 51% isolated yield using 4 equiv of hydrogen peroxide. Albeit the moderate yield, this oxidation can be regarded as very significant from a synthetic point of view since, to our knowledge, the best isolated yield reported up to date was 30% using **3** as catalyst.

On the other hand, as previously discussed, steroids are particularly interesting substrate platforms. In order to investigate the performance of this new family of catalysts, we studied the oxidation of *trans*-androsterone acetate **82** (Figure VI.8). From

the results presented in Chapter IV (see Table IV.6), we know that, in terms of selectivity, mcp-based catalysts favor the oxidation at C₆, while pdp-based (pdp = *N,N'*-bis(2-pyridylmethyl)-2,2'-bipyrrrolidine) catalysts show almost no discrimination between C₆ and C₇, which are the preferred oxidation sites. Moreover, differences arise also from the chirality of the catalyst. While for **Λ-1** C₇ is the second most oxidized site, for **Δ-1** catalyst C₁₂ is preferred over C₇. Moreover, only pdp-based catalysts show oxidation at C₁₄, this position being preferred over C₁₂ in the case of **Λ-2**. When silyl-modified catalysts were tested in the oxidation of **82**, the same basic selectivity rules exhibited by the simpler catalysts were maintained. Very interestingly, the effect of the bulky silyl group was very significant in favoring oxidation at the least sterically hindered position C₆, which was gradually favored from **Λ-1Sa** to **Λ-1Sc**, and from **Λ-2Sa** to **Λ-2Sc** (see Table V.7). Particularly remarkable is the 82% normalized selectivity toward C₆ exhibited by **Λ-2Sc**. However, in tips-based catalysts there is a dramatic effect of the chirality of the complexes, not observed with simpler catalysts **1** and **2**: **Δ-1Sc** and **Δ-2Sc** strongly favor oxidation at C₁₂ with up to 88% normalized selectivity.

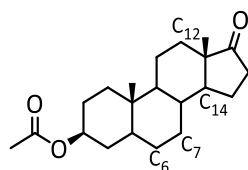


Figure VI.8. Structure of substrate **82** (*trans*-androsterone acetate)

As previously observed with simpler substrates, tips-based catalysts afford significantly higher yields than their naked and their smaller silyl counterparts, reaching up to 80% combined yield in the oxidation of an elaborated molecule such as steroid **82**.

In summary, three different groups of N₄-tetradentate iron catalysts have been studied in the oxidation of simple and elaborated substrates in order to establish the selectivity based of such catalysts and evaluate their performance. Highly structured pinene-based catalysts arise as very robust and selective, with privileged structures capable of modifying to some extent the substrate-based imposed by inherent C—H properties. Part of the selectivity observed is due to the diamine backbone, as corroborated in the study performed with the related, structurally simpler and readily available catalyst **1**. This catalyst has shown enhanced preference toward the oxidation

of methylenic sites. Although **1** had been regarded as a relatively poor catalyst for C-H oxidation, a new experimental protocol has been developed and shown to be capable of oxidizing natural products in synthetically amenable yields. Further exploration of the steric control in the catalysts architecture has been performed with silyl-based catalysts, which have proven especially valuable in the oxidation of methylenic sites of simple and elaborated substrates with high efficiency and exquisite selectivity.

VI.4 REFERENCES

- (1) Punniyamurthy, T.; Velusamy, S.; Iqbal, J. *Chem. Rev.* **2005**, *105*, 2329.
- (2) Que Jr., L.; Tolman, W. B. *Nature* **2008**, *455*, 333.
- (3) Bruijninx, P. C. A.; van Koten, G.; Klein Gebbink, R. J. M. *Chem. Soc. Rev.* **2008**, *37*, 2716.
- (4) Sun, C.-L.; Li, B.-J.; Shi, Z.-J. *Chem. Rev.* **2011**, *111*, 1293.
- (5) Company, A.; Gómez, L.; Costas, M. S. P de Visser, D. K., Ed.; RSC: Cambridge, 2011.
- (6) Chen, K.; Que Jr., L. *J. Am. Chem. Soc.* **2001**, *123*, 6327.
- (7) Chen, K.; Costas, M.; Kim, J.; Tipton, A. K.; Que Jr., L. *J. Am. Chem. Soc.* **2002**, *124*, 3026.
- (8) Gómez, L.; Garcia-Bosch, I.; Company, A.; Benet-Buchholz, J.; Polo, A.; Sala, X.; Ribas, X.; Costas, M. *Angew. Chem. Int. Ed.* **2009**, *48*, 5720.
- (9) Cano, A.; Ramírez-Apan, M. T.; Delgado, G. *J. Braz. Chem. Soc.* **2011**, *22*, 1177.
- (10) Bartoli, J. F.; Brigaud, O.; Battioni, P.; Mansuy, D. *J. Chem. Soc. Chem. Commun.* **1991**, 440.
- (11) Cook, B. R. ; Reinert, T. J.; Suslick, K. S. *J. Am Chem. Soc.* **1986**, *108*, 7281.
- (12) Chen, M. S.; White, M. C. *Science* **2010**, *327*, 566.
- (13) Prat, I.; Gómez, L.; Canta, M.; Ribas, X.; Costas, M. *Chem. Eur. J.* **2013**, *19*, 1908.
- (14) Okuno, T.; Ito, S.; Ohba, S.; Nishida, Y. *J. Chem. Soc., Dalt. Trans.* **1997**, 3547.
- (15) Clemente-Tejeda, D.; López-Moreno, A.; Bermejo, F. A. *Tetrahedron* **2012**, *68*, 9249.

- (16) Gómez, L.; Canta, M.; Font, D.; Prat, I.; Ribas, X.; Costas, M. *J. Org. Chem.* **2013**, 78, 1421.
- (17) Salvador, J. A. R.; Silvestre, S. M.; Moreira, V. M. *Curr. Org. Chem* **2012**, 16, 1243.

CHAPTER VII

GENERAL CONCLUSIONS

VII. GENERAL CONCLUSIONS

- A family of pinene-containing non-heme iron catalysts **Λ -1P**, **Δ -1P**, **Λ -2P** and **Δ -2P** has been studied in the oxidation of alkanes. These complexes have been found to mediate the fast oxidation of nonactivated tertiary and secondary alkyl moieties under mild experimental conditions in synthetically amenable yields, using hydrogen peroxide as oxidant and substrate limiting conditions.
- The steric hindrance offered by the (+)-pinene scaffolds at the proximity of the iron active site in catalysts with **Λ** chirality confers stability toward catalyst degradation pathways, which allows using low catalyst loadings maintaining high efficiencies.
- Complex organic molecules are oxidized in good yield and selectivity. Simple rules previously established for alkyl C—H functionalization with electrophilic reagents can be used to predict which C—H groups may be prone to oxidation.
- Unlike most synthetic reagents, these catalysts are highly structured. This feature allows for modulating or even altering selectivity without the use of covalent or strong supramolecular substrate—oxidant interactions.
- The final selectivity outcome depends on the combination of more subtle aspects, mainly affecting the spatial structure of the iron active site. The chirality of the catalysts, the nature of the diamine backbone, and the presence of a cavity-like site surrounding the metal center have been identified as structural aspects that translate into C—H site selectivity.
- The percentage conversion and percentage yield differ in some of the reactions. This fact might be due to the difficulty of this type of oxidations, where mass balance is not complete. Although the formation of significant amounts of a single nonidentified product is not observed, the formation of trace amounts of multiple byproducts can not be excluded.
- **Λ -1** is a very convenient catalyst for C—H oxidation reactions employing hydrogen peroxide as terminal oxidant, since it operates at low catalyst loadings at 0 °C and short reaction times. It leads to the oxidation of nonactivated tertiary

- and secondary alkyl C—H bonds of organic molecules in preparative useful yields.
- Preparation of **Λ-1** in multigram scale can be done from simple and inexpensive reagents, which constitutes an important advantage with regard to other C—H oxidation reagents described so far, including Fe-based catalysts.
 - This catalyst exhibits predictable site-selectivity. It generates electrophilic species upon reaction with H₂O₂ that appear sensitive to the structural properties of the substrate. This aspect results in remarkable site-selectivity properties that can be used to direct oxidation in substrates where multiple methylene sites are available, obtaining remarkable selectivity for oxidation products of the less sterically hindered methylenic sites, as demonstrated in the oxidation of natural products.
 - Site-selectivity in these reactions is distinct from that attained with other iron catalysts previously described, offering new alternatives for selective C—H functionalization.
 - Given the easy access to large amounts of catalysts and the simplicity of the methodology, multigram scale oxidation of natural products can be conveniently performed in short reaction times, and product yields and selectivities are reliably predicted from small scale reactions.
 - A new family of non-heme iron catalysts (**Λ-1Sa**, **Λ-1Sb**, **Λ-1Sc**, **Λ-2Sa**, **Λ-2Sb**, and **Λ-2Sc**) has been synthesized and fully characterized. 2,2'-bipirrolidine and *trans*-1,2-diaminocyclohexane have been used as backbones, and they introduce systematic steric bulkiness at the ligand architecture.
 - The catalysts bearing the more sterically crowded triisopropylsilyl groups **Λ-1Sc** and **Λ-2Sc** create a cavity-like space around the metal site. These appear as the most active and selective of the series in the oxidation of simple substrates and they show enhanced selectivity toward the oxidation of methylenic sites compared to their analogous complexes without any silyl substituent (**Λ-1** and **Λ-2**, respectively). This reactivity trend can be rationalized in terms of steric demand on the catalyst and on the substrate, since secondary C—H bonds are more exposed to the bulk.

- These catalysts are capable of discriminating among multiple methylenic sites, exhibiting preference for the less sterically crowded C—H groups.
- These trends are maintained in the oxidation of natural products, which can be oxidized in synthetically amenable yields in a very selective manner. The major products obtained are dependent on the catalyst employed, and chirality of the catalyst appears to be a key aspect.
- The relatively easy accessibility and cost of these catalysts, plus the high activity and selectivity they present make this new family of catalysts a powerful tool toward for the oxidation of elaborated substrates.

APPENDIX

Contribution to other publications not included in this thesis:

- Observation and mechanistic study of facile C–O bond formation between a well-defined aryl-copper(III) complex and oxygen nucleophiles. L. M. Huffman, A. Casitas, M. Font, M. Canta, M. Costas, X. Ribas, S. S. Stahl. *Chem. Eur. J.* **2011**, 17, 10643-10650.
- Nucleophilic aryl fluorination and aryl halide exchange mediated by a Cu^I/Cu^{III} catalytic cycle. A. Casitas, M. Canta, M. Solà, M. Costas, Xavi Ribas. *J. Am. Chem. Soc.* **2011**, 133, 19386–19392.
- An iron catalyst for oxidation of alkyl C–H bonds showing enhanced selectivity for methylenic sites. I. Prat, L. Gómez, M. Canta, X. Ribas, M. Costas. *Chem. Eur. J.*, **2013**, 19, 1908 – 1913.

All these papers have been published in journals that belong to the first quartile according to JRC.

Manuscripts in preparation derived from this thesis:

Chapter I

- Selective alkane oxidation reactions with mononuclear non-heme iron catalysts: recent advances and future challenges. M. Canta, L. Que Jr., M. Costas. (Review article)

Chapter V

- A new family of iron catalysts incorporating bulky silyl groups for efficient and regioselective oxidation of alkanes. M. Canta, D. Font, O. Cussó, X. Ribas, M. Costas.

Other manuscripts in preparation:

- Kinetic analysis of activation barriers for Hydrogen Atom Transfer and Oxygen Atom Transfer of non-heme oxoiron(IV) complexes. M. Canta, G. Sabeña, X. Ribas, L. Que Jr., M. Costas.
- Mechanistic study on high valent Pytacn iron species involved in water oxidation catalysis with Ce(IV): forming the O—O bond. M. Canta, Z. Codolà, X. Ribas, J. Lloret, L. Que Jr., M. Costas.
- A new family of iron and manganese complexes with aryl-substituted ligands for enantioselective epoxidation catalysis. M. Canta, I. Garcia-Bosch, L. Gómez, X. Ribas, M. Costas.